



ICEBE
IMAGINEERING
NATURE

Reaction Modeling in Computational Fluid Dynamics with Special Focus on the Blast Furnace Raceway Zone

by Eva-Maria Wartha

A thesis for the degree of
Doctor technicae

In the
**Doctoral programme in Engineering Sciences – Chemical and
Process Engineering**

At the
Faculty of Mechanical and Industrial Engineering, TU Wien

Under the supervision of
Michael Harasek, TU Wien
and co-supervision of
Markus Bösenhofer, TU Wien

Reviewed by
Terese Løvås, NTNU
and
Franz Winter, TU Wien

This work was supported by COMET (Competence Center for Excellent Technologies), the Austrian program for competence centers contracted under the FFG (Austrian Research Promotion Agency) grant no. 844607 and 869295.

Author

Eva-Maria Wartha
Matr.Nr.: 01208963

Supervisor

Michael Harasek
TU Wien
Institute of Chemical, Environmental
and Bioscience Engineering
Getreidemarkt 9/E166
1060 Wien, Austria

Co-Supervisor

Markus Bösenhofer
TU Wien
Institute of Chemical, Environmental
and Bioscience Engineering
Getreidemarkt 9/E166
1060 Wien, Austria

Reviewers

Terese Løvås
Norwegian University of Science and
Technology
Departement of Energy and Process
Engineering
Kolbjørn Hejes vei 1A
7034 Trondheim, Norway

Franz Winter
TU Wien
Institute of Chemical, Environmental
and Bioscience Engineering
Getreidemarkt 9/E166
1060 Wien, Austria

Going to press

I confirm that going to press of this thesis needs the confirmation of the examination committee.

Affidavit

I declare in lieu of oath, that I wrote this thesis and performed the associated research myself, using only literature cited in this volume. If text passages from sources are used literally, they are marked as such.

I confirm that this work is original and has not been submitted elsewhere for any examination, nor is it currently under consideration for a thesis elsewhere.

I acknowledge that the submitted work will be checked electronically-technically using suitable and state-of-the-art means(plagiarism detection software). On the one hand, this ensures that the submitted work adheres to the high-quality standards of the current rules for ensuring good scientific practice "Code of Conduct" at the TU Wien. On the other hand, a comparison with other students' theses avoids violations of my personal copyright.

Vienna, August 2022

Eva-Maria Wartha

Kurzfassung

Durch Strömungssimulation (CFD) kann der Übergang zu einer nachhaltigen Industrie mittels digitaler Prozessänderungen und Anpassungen unterstützt werden. Digitale Einblicke in nicht-messbare Zustände helfen den Prozess besser zu verstehen und ihn dadurch zu verbessern. Für solche Untersuchungen sind Modelle notwendig, die alle relevanten Phänomene abbilden. In der Verfahrenstechnik sind Reaktionen fundamentale Bestandteile vieler Prozesse, deshalb müssen auch diese in den Modellen Eingang finden. Diese Dissertation beschäftigt sich mit der Entwicklung und Verbesserung von Modellen reaktiver Strömungen.

Ein wichtiger Industriesektor in Europa ist die Stahlindustrie, welche einen großen Anteil der Emissionen verantwortet. Die Hauptprozessroute über den Hochofen ist von chemischen Reaktionen bestimmt. Deshalb steht die CFD dieses Prozesses im Fokus dieser Dissertation.

Generell können Herausforderungen in der Modellierung in zwei Rubriken unterteilt werden: Einerseits müssen Modelle die wichtigsten Effekte abbilden. Andererseits soll der numerische Aufwand gering gehalten werden, um deren Anwendbarkeit zu erlauben. Deshalb ist das Ziel dieser Arbeit Verbesserungen in beiderlei Hinsicht zu entwickeln, um die Anwendung von CFD für verfahrenstechnische Prozesse mit Reaktionen zu ermöglichen.

Basierend auf der Wirbelzone im Hochofen wurden Verbesserungen für homogene und heterogene reaktive Strömungen entwickelt. Der numerische Aufwand zur Berechnung von Gasphasenreaktionen wurde reduziert, indem passende Splitting- und Tabulationsmethoden identifiziert wurden. Für heterogene reaktive Strömungen wurden algorithmische Verbesserungen für das Zweiphasenmodell erarbeitet.

In Bezug auf die Modellgenauigkeit wurde die Anwendbarkeit eines erweiterten Modells ermöglicht, in dem passende Abschätzungen der charakteristischen chemischen Zeitskala präsentiert wurden. Weiters wurde ein Verfahren zur verbesserten Kinetikidentifikation für Gas-Feststoff-Reaktionen präsentiert.

Für heterogene reaktive Strömungen wurden sowohl Modelle für niedrige (Lagrange) als auch für hohe Feststoffkonzentrationen (Euler) bearbeitet. Der Einfluss turbulenter Strömung auf die thermochemische Umsetzung kleiner Partikel wurde modelliert und dessen Effekt auf die Hochofensimulation gezeigt. Im Eulerschen Bereich wurden passende Modelle für die Wirbelzonenströmung analysiert und deren Effekte auf die Reaktionen betrachtet.

Die entwickelten Modelle erlauben nicht nur die digitale, genaue und schnelle Analyse der Wirbelzone im Hochofen, sondern können auch auf andere verfahrenstechnische Prozesse angewandt werden. Deshalb hilft die vorliegende Arbeit nicht nur den Hochofenprozess zu verbessern, sondern kann auch den Übergang zu einer emissionsfreien Stahlindustrie unterstützen. Zum Beispiel kann die Direktreduktion von Eisen mittels Wasserstoff untersucht werden.

Abstract

Computational fluid dynamics (CFD) can empower the transition to a sustainable industry through digitally testing process changes and adaptations. Digital insight into non-measurable states helps to understand the process better and consequently improve it. These investigations require models to capture the essential phenomena of the process. In chemical engineering, reactions are fundamental to many processes, therefore, they need to be incorporated in the model. This work is concerned with the development and improvement of models for reactive fluids.

The steel industry is an important industry sector in Europe and causes a large share of the overall emissions. The main process route over the blast furnace is largely governed by chemical reactions. Therefore, CFD of this process is in focus of this thesis.

Generally, challenges in modeling are two-fold: On the one hand, models need to capture the essential effects. On the other hand, the computational burden to solve the models needs to be low enough to allow CFD simulations. Therefore, the aim of this thesis is to develop improvements in both regards to enable the application of CFD for chemical engineering processes incorporating reactions.

Based on the blast furnace raceway zone improvements for homogeneous reactive flows and heterogeneous reactive flows were targeted, with a focus on gas phase and gas-solid reactions.

The computational burden of gas phase reaction modeling was reduced by identifying appropriate operator splitting and tabulation techniques, and establishing strategies for efficient partitioning. For heterogeneous reactive flows, algorithmic improvements for two-fluid modeling were developed.

In terms of modeling accuracy, the application of an extended model was enabled through appropriate chemical time scale approximation. Furthermore, an approach to enhance kinetic model identification for gas-solid reactions was presented.

For heterogeneous reactive flows, modeling improvements for the Lagrangian framework – applied to low solid’s concentrations – and for the Eulerian framework – applied to higher solid’s concentrations were developed. The influence of turbulent clustering in the Lagrangian particle conversion model was incorporated and the model effects on the raceway prediction and reactions in the Eulerian framework were evaluated.

The developed models not only enable a digital, accurate and fast analysis of the blast furnace raceway, but can be also applied to other chemical engineering processes. Therefore, the work does not only help to improve the blast furnace process, but can also boost the transition to a net-zero emission steel industry. For example direct reduction of iron ore with hydrogen – also in this process reactions need to be modeled.

Danksagung

Auch wenn eine Seite nie darstellen kann, was all die Menschen zu dieser Arbeit beigetragen haben...

Zu Beginn geht der Dank natürlich an meinen Betreuer Michael Harasek, der mich für dieses Thema begeistert hat, mir die Möglichkeit gegeben hat in seiner Forschungsgruppe zu arbeiten und mich bei der Bearbeitung fortwährend unterstützt hat. Gleich anschließend ist natürlich Markus Bösenhofer zu nennen, der mich durch die Betreuung meiner Diplomarbeit an das Thema herangeführt hat, mich während meiner Dissertation unterstützt hat und ohne dessen Vorarbeiten ich nie an diesen Punkt gekommen wäre.

Vielen Dank auch an meine Kollegen - stellvertretend hier besonders all jene aus unserem Büro im Geniegebäude: Florian, Diana, Johannes, Matthias und Thomas. Ohne die netten Gespräche und Mittagspausen wäre die Hitze in unserem Büro, aber auch OpenFOAM nie auszuhalten gewesen.

Mein Dank gilt auch an alle Projektpartner außerhalb der TU Wien bei K1-Met, JKU, voestalpine und Primetals, die mit ihrer Expertise und kritischen Fragen die Arbeit sehr bereichert haben.

Ein sehr bereichernder Teil meiner Dissertation war der Aufenthalt bei der ComKin-Gruppe in Norwegen. Vielen Dank für die Möglichkeit bei euch mitzuarbeiten, die herzliche Aufnahme und die Unterstützung. Tusen takk til alle fra ComKin-gruppe, Nils og Eva.

Neben all der fachlichen und kollegialen Unterstützung möchte ich ganz besonders bei meinen Freunden bedanken. Ohne die Ablenkung oder ein offenes Ohr für meine Jammerei, hätte ich das nicht geschafft. Ganz speziell darunter natürlich an die Bierdienstagscrew. In der Felix nicht nur als Freund, sondern immer auch als fachlicher Coach fungiert hat.

Das Beste kommt natürlich zum Schluss – die Familie. Meine Eltern, die mich auf all meinen Wegen unterstützt haben und die ich jederzeit um Rat fragen kann. Danke Schwesterherz! Und danke Flo, du hast gerade noch gefehlt.

Für meine Großmütter...

Contents

Research summary	1
1 Introduction and Motivation	2
2 State-of-the-Art	4
2.1 Homogeneous reactive flows	4
2.2 Heterogeneous reactive flows	8
3 Problem Statement	14
4 Research Approach	16
4.1 Homogeneous reactive flows	17
4.2 Heterogeneous reactive flows	18
5 Results - Summary of Publications	21
5.1 Homogeneous reactive flows	21
5.2 Heterogeneous reactive flows	22
6 Conclusions and Outlook	24
References	26
List of Figures	41
Nomenclature	41
Publications	45
Paper 1	46
<i>Characteristic Chemical Time Scales for Reactive Flow Modeling</i>	
Paper 2	74
<i>Importance of considering interstitial fluid effects in the kinetic theory of granular flow for raceway formation prediction</i>	
Paper 3	88
<i>Enhanced kinetic model identification for gas–solid reactions through Computational Fluid Dynamics</i>	
Paper 4	98
<i>The Effect of Turbulence on the Conversion of Coal under Blast Furnace Raceway Conditions</i>	
Conference Publications	123
Co-Author Publications	167

Research summary

This introductory chapter provides the context and synopsis of the publications that constitute this thesis. A general introduction and motivation of the work is given at the start, which is embedded in the climate challenges we face today. Based on this global perspective, the motivation is narrowed down to the industry sector and the special role of the steel industry in Section 1. Based on the mentioned benefits of employing computational fluid dynamics (CFD) for process improvements and design, the need for reaction modeling is emphasized. Because of the blast furnace's importance in steel production it serves as an example process, based on which concrete deficiencies in reaction modeling are illustrated. The different reactions occurring in the blast furnace are discussed and based on those, a general distinction in modeling homogeneous and heterogeneous reactive flow is made, Section 2. This distinction helps to synthesize state-of-the-art modeling strategies. With the knowledge of the state-of-the-art and the general motivation behind the application of CFD, the hindering factors in the application can be formulated, Section 3. This boils down to two main points: insufficient modeling accuracy and too high computational cost. Guided by those general problems, specific points were targeted in this thesis: speed-up through tabulation techniques and algorithmic improvements, and modeling improvements through validated model adaptations summarized in Section 4. The main results were published in journal and conference publications and are recapped in Section 5. As an overall conclusion, the presented results help to simulate the raceway zone in a blast furnace faster and more accurately. Consequently, they enable to test alternative process conditions to aim for a more sustainable blast furnace operation and reduced emissions. These concluding remarks are condensed in Section 6 and enriched with an outlook on future pathways in terms of on-line CFD and zero-emission steel production.

1 Introduction and Motivation

We have only one earth. One of the slogans of the Friday's for Future initiative shows us that we should act now to save our planet. It is our and our children's future which is at stake due to the human induced climate change. But how can each and everyone of us support the transition to a sustainable world? For one, we have to change our behavior. Use the resources our planet provides efficiently. A lot of small individual actions will contribute to an overall transition – take public transportation instead of taking the car, repair electric devices instead of buying new ones, or buy clothes produced nearby instead of clothes shipped from the other side of the world. Just to name a few small things. Our small actions feel useless – but they take a share. Looking for example on our mobility in Austria: the transportation sector took a 35% share in the overall energy consumption in 2015 (Krutzler et al. 2017) or 25% in European Union (EU) (Eurostat n.d.).

How does this relate to this thesis? Well, similarly as we should reconsider and change the behavior in our personal life, we can devote our work to the same goal – combat climate change. How can this small piece of work contribute to reduce global warming? – Truly it will not stop climate change on its own, but it can be a small piece. It aims to help the transition to reduced emissions and a carbon free industry.

To combat climate change policy makers signed a legally binding agreement to reduce global warming well below 2 degrees – the Paris Agreement (United Nations n.d.). To achieve this goal the EU has developed a strategy to meet net-zero emissions 2050 – called the European Green Deal (European Commission 2019).

A strong focus in the strategy is also the transformation of the european industry, which contributed to 775 Mt green house gas (GHG) emissions in 2021 (European Environment Agency 2022). A special focus there is the steel production in EU. It accounts for 221 Mt GHG emissions, which corresponds to 5.7% of the total EU emissions (Commission of the European Communities 2021). The two main routes for steel production in the EU are the blast furnace / basic oxygen furnace route and the electric arc furnace route (Commission of the European Communities 2021), producing 60% and 40% of the steel in the EU respectively.

Guevara Opinska et al. (2021) discusses different scenarios on the way to a net zero-emission steel industry. They highlight, that for a transition until 2050 several concepts will play a role: novel technologies, such as hydrogen direct reduction, as well as improved state-of-the-art technologies, possibly combined with carbon capture approaches.

To support the transition and improve current processes, computational fluid dynamics (CFD) can be a precious tool. Runchal (2012) discuss the future of CFD and emphasize, that it will be embedded in solving engineering design problems.

This can be done in numerous ways: We can use CFD to estimate not measurable parameters inside an industrial device and get a virtual view inside. This information helps to improve the process – for example, by estimating the end time of batch processes, or increasing mass flow rates for less wear of the apparatus. Thus, CFD can help to continuously improve processes, test process variations or fasten the design of new ones.

To use CFD for chemical engineering processes, we need well suited models to obtain an accurate estimation in the CFD simulation. A special challenge in many industrial processes are the reactions and the modeling of these. The reaction modeling challenges in the blast furnace process – one of the most important processes in european steel industry today – guide through the work in this thesis.

2 State-of-the-Art

Reaction modeling in CFD is a wide topic and the work presented here focuses on aspects relevant for chemical engineering devices. Even though my research dealt with reaction modeling in general, the use case that guided this research were blast furnaces in steel production, due to their importance in the steel industry (Commission of the European Communities 2021). The blast furnace will guide this work to showcase relevant aspects in reaction modeling for CFD. First, I want to introduce the most important features of the blast furnace process. Figure 1 shows a schematic drawing of the blast furnace with its main parts. The in- and outflows in the blast furnace are: iron ore, burden, and coke provided from the top; hot blast and reducing agents through the tuyeres; the top gas leaving above the throat; and slag and pig iron flowing out from the hearth.

The main reactions occurring in the blast furnace are the iron ore reduction, the coke conversion and the reducing agents conversion. In the stack, the iron ore is reduced by reducing gases (e.g. CO, H₂) provided through conversion reactions with the hot blast (O₂, N₂, H₂O) entering through the tuyeres. The hot blast reacts with the coke supplied from the top and reducing agents added through the tuyeres. In front of the tuyeres, a cavity forms, which is called the raceway cavity. The supplied reducing agents react mainly within this cavity. For a good description of the blast furnace see (Cameron et al. 2019).

In general, one can classify homogeneous and heterogeneous flows – comprised of one or two different phases, respectively. Similarly, chemical reactions are categorized into homogeneous and heterogeneous reactions – occurring within one phase or two different phases, respectively. Within the blast furnace heterogeneous reactions (iron ore reduction, coke conversion, conversion of solid/liquid reducing agents) as well as homogeneous reactions (reactions of the hot blast, gaseous reducing agents and reaction products) play a role. Because of their inherent difference, current modeling strategies will be discussed in the following sections separately for the two types:

2.1 Homogeneous reactive flows

Homogeneous reactive flows are flows with one phase and reactions therein. In blast furnaces only homogeneous reactions in the gas phase are relevant. For this reason, I will focus the discussion in this section on this type. A lot of research is devoted to combustion reactions and the reactions occurring within the blast furnace can also be considered as combustion reactions – be it combustion of gaseous reducing agents, combustion of volatiles released from solids or combustion of vaporized liquids.

Before coming to the reaction modeling itself, the motion and energy of the

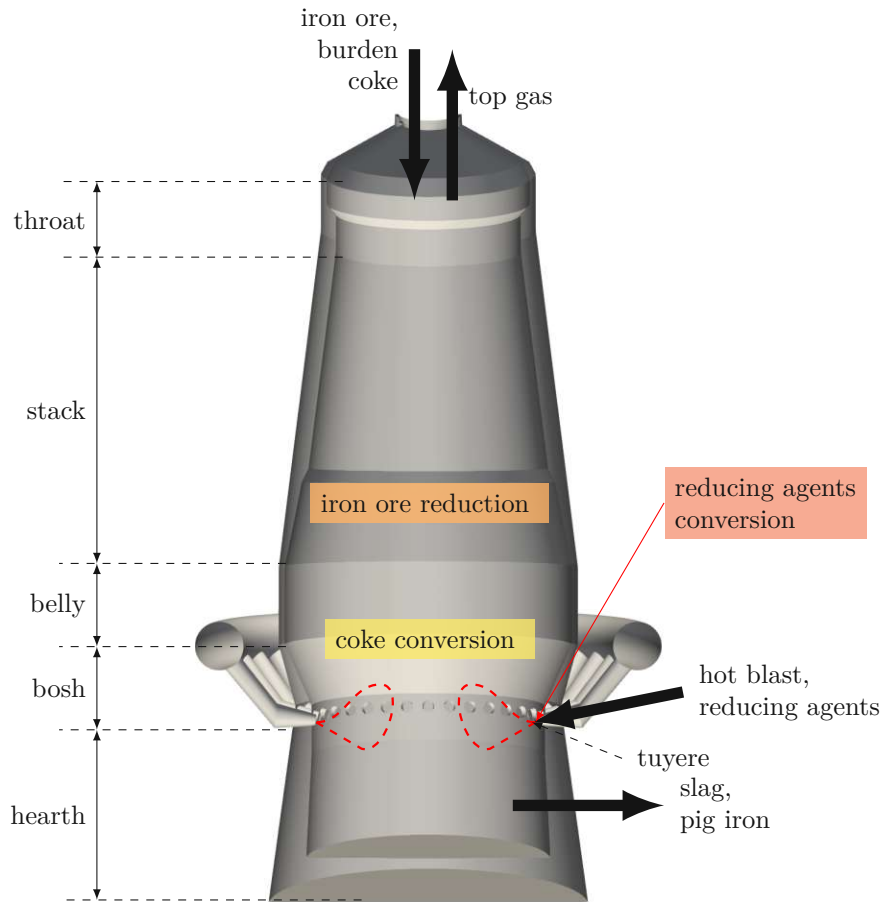


Figure 1: Schematic drawing of the blast furnace marking the different sections, the in- and outflows, and the main reactions in the blast furnace

gaseous phase have to be modeled to predict its properties. The governing equations are the continuity equation and the Navier-Stokes equations. They can be solved analytically only for a few simple, laminar flows (Versteeg et al. 2007). Using the finite-volume method they are usually attempted to be solved numerically. In general, it is possible to compute all the velocity fluctuations – not only the mean values. This approach is called Direct Numerical Simulation (DNS), but it requires the resolution of the finest scales and is computationally very demanding. Therefore, it is usually only used for small scales or laminar flow configurations. More commonly for turbulent flows, only the mean quantities are computed and the turbulent fluctuations are modeled. Those techniques can be categorized as Large-Eddy Simulation (LES) – resolving up to larger unsteady scales – or Reynolds-averaged Navier-Stokes (RANS) equations – resolving only the average

flow scale. A detailed description of modeling approaches in the finite volume method (FVM) framework is given by Versteeg et al. (2007) and an overview on general turbulence modeling by Pope (2000).

In this thesis the RANS-approach is used, because it requires less computational effort than LES. Despite increasing computational powers, it is still important to keep that in mind when targeting engineering applications. Therefore, reaction modeling for this framework will be discussed in the following, although many statements and reaction models are also applicable for LES. Special differences in combustion modeling between LES and RANS have been addressed by Pitsch (2006).

As mentioned, a model for the turbulence needs to be applied in conjunction with RANS. Here, a two-equation model, the k-epsilon model (Jones et al. 1972; Launder et al. 1974) was chosen. However, the reaction modeling techniques are not limited to this specific turbulence model (Veynante et al. 2002).

When the turbulent mixing of the reactants is not resolved, the turbulence effect of this mixing and the interchange with the chemical reactions needs to be modeled as well. Different approaches to model turbulence-chemistry interactions exist. According to Poinso et al. (2012) and Veynante et al. (2002) they can be distinguished based on their physical approaches into: geometrical analysis, turbulent mixing and one-point statistics. However, Poinso et al. (2012) mentions that no approach is superior to the others.

Some models are based on the assumption that the chemical kinetics are considerably faster than the mixing process, defining the mixing process as the rate limiting and decisive step, e.g. the eddy-break-up model (Spalding 1971). However, the possibility to handle finite-rate chemistry is essential if the reactions are not purely mixing dominated. Additionally, the coupling with source terms is necessary, when applied to multi-phase processes, such as the blast furnace. For example gases released from coal, coke, biomass are participating in the gas phase reactions.

A model satisfying these requirements, is the Eddy Dissipation Concept (EDC) (Magnussen 1981). It models the interactions between turbulence and chemistry, taking the mixing as well as finite-rate chemistry into account – using global one-step chemical mechanisms or detailed mechanisms with several thousand species. The details of the model and later adaptations have been presented by Magnussen and his co-authors Magnussen (1989), Gran et al. (1996a), Gran et al. (1996b), and Magnussen (2005). A detailed derivation of the energy cascade model, which is the basis of the EDC, was presented by Ertesvåg et al. (1999).

The model derivation is based on highly turbulent phenomena (high Reynolds and Damköhler number) (Veynante et al. 2002). In the recent years the model has also been extended to fields with broadened reaction fronts and regimes with

lower Damköhler and Reynolds numbers in the range of unity (Parente et al. 2016; Bao 2017; Lewandowski et al. 2020b; Lewandowski et al. 2020a; Romero-Anton et al. 2020). Mainly because moderate or intense low oxygen dilution (MILD) combustion (Cavaliere et al. 2004) has become increasingly interesting due to its reduced emissions. A detailed and critical discussion of those recently proposed changes was presented by Ertesvåg (2020) and Ertesvåg (2022).

Since the blast furnace process was chosen to showcase reaction modeling techniques within CFD for chemical engineering applications, the approaches for gas phase modeling in blast furnace simulations were reviewed. Many different approaches have been used for blast furnace simulations.

Du et al. (2006), Du et al. (2015), and Yeh et al. (2012) applied the probability density function (PDF) method in simulation studies related to the blast furnace. They simulated pulverized coal injection (PCI) combustion, assuming only mixing controlled reactions. Similarly, Andahazy et al. (2006) investigated gas and oil injection in raceways and their combustion. However, Andahazy et al. (2006) did not take any solid source terms from solid reducing agents or the coke bed into account. Therefore, it is not clear, if this approach can be applied when the coke bed in the blast furnace shall be modeled as well. Vuokila et al. (2017) compared the EDC and a PDF method for the prediction of heavy oil combustion in a raceway. They concluded that the EDC model performed better than the PDF in this application. Additionally, Liu et al. (2021b) stated that the equilibrium chemistry model – a pdf method – is not suitable to model pulverized biomass injection. Consequently, the application of the equilibrium chemistry model would limit the injection studies in a blast furnace and suggests that the EDC would be a better choice.

The Eddy Dissipation Model (EDM) (Magnussen et al. 1977), a predecessor of the EDC, is used in many blast furnace studies, e.g. by Nogami et al. (2004), Zhou (2008), Gu et al. (2010), Shen et al. (2011), Wijayanta et al. (2014b), Majeski et al. (2015), Wu et al. (2019), Barros des Souza (2020), Liu et al. (2020a), Liu et al. (2020b), Zhang et al. (2020a), Liu et al. (2020c), Peng et al. (2021), Liu et al. (2021a), and Wang et al. (2022). The EDM takes a simplified approach to account for finite-rate chemistry – limiting the overall reaction rate minimum of the mixing term and reaction term. The main benefit of the EDM is its reduced computational cost. However, the simplified approach also leads to deficiencies in the predictions.

The EDM and EDC have been compared for the prediction capabilities for oxy-fuel combustion by Andersen et al. (2009) and Galletti et al. (2013), who concluded that the EDM has too many deficiencies to be applied in oxy-fuel combustion. The similarities to the blast furnace process – the high temperature and consequently importance of CO₂ decomposition reactions – suggest, that also here the supri-

urity of the EDC predictions is important. For co-firing of biomass Tabet et al. (2015) evaluate different turbulence-chemistry interaction models. They conclude that the EDM is not as good as the EDC, and that PDF/mixture fraction are only applicable for high Damköhler numbers, which are not generally ensured within the blast furnace raceway zone.

The EDC was applied for blast furnace simulation in the following publications (Maier 2015; Vuokila 2017; Vuokila et al. 2016; Vuokila et al. 2017; Bösenhofer 2020) and showed good performance in the predictions. To sum up, the reviewed literature suggests that in terms of accurate predictions and flexibility, the EDC should be used for blast furnace simulations. Its main downside is the increased computational cost. Consequently it should be used, if computationally affordable.

2.2 Heterogeneous reactive flows

Multiple phases are present in the blast furnace: iron ore, iron, slag, coke, blast and reducing agents. The heterogeneous reactions of those phases are iron ore reduction, coke conversion and reducing agents conversion. Iron ore, iron, and slag are present in solid and liquid phase, coke in solid and blast in gaseous phase. The reducing agents, can be either solid, liquid or gaseous. For liquid reducing agents, the modeling can be reduced to homogeneous reaction modeling, by assuming vaporisation and consecutive combustion as by Maier (2015). For gas-solid reactions this simplification can not be done. Therefore, we focus on gas-solid reaction modeling within the group of heterogeneous reactive flows. In contrast to homogeneous reactions the reactants in heterogeneous reactions are not mixed on a molecular level. Therefore, the modeling of the overall, macroscopic conversion process in gas-solid reactions will be discussed.

In general, one can distinguish between two approaches in gas-solid reaction modeling: First, a mechanistic modeling approach based on the important physical processes (e.g. mass transfer through boundary layer, mass transfer in pores and intrinsic kinetic) contributing to the overall conversion (Szekely et al. 1976). Second, the single step approximation – modeling the rate determining step.

The mechanistic based conversion models can be based on a resistance model of the physical processes contributing to the overall conversion: the reactant diffusion through the boundary layer, the diffusion of the reactant through the pores/porous structure and the intrinsic reaction kinetics. Probably the first model of this type was the shrinking core model presented by Yagi et al. (1955).

The kinetic contribution to the overall conversion is often modeled by the Arrhenius expression, but could be also modeled based on a Langmuir-Hinshelwood description if adsorption and desorption play a major role for the conversion at the reaction site, as discussed by Murphy et al. (2006). The bulk diffusion is often modeled based on a Sherwood correlation for mass transfer, e.g. (Ranz et al.

1952), and the probably most common model for the diffusion through the porous solid is based on the work from Thiele (1939).

On the other hand, the single-step approximation, is based on the assumption that only one step is rate-limiting and therefore decisive for the reaction. This is the probably most widely used approach in solid-state kinetics (Vyazovkin et al. 2011), which can be described as following:

$$\frac{d\alpha}{dt} = k(T)f(\alpha)h(p, p_{eq}) \quad (1)$$

It combines the temperature effect $k(T)$, geometrical effects $f(\alpha)$, and the driving force $h(p, p^{eq})$. The temperature effect is – as in the mechanistic model – usually modeled based on the Arrhenius equation, which was originally derived for gas phase reactions. A critical discussion reviewing the concepts from homogeneous reaction kinetics for gas-solid reactions was presented by Galwey (2004).

The geometrical effects in the single step approximation are often attempted to be modeled based on physical relations, for example the volume reaction model, grain model (Szekely et al. 1970), random pore model (Bhatia et al. 1980) – further developed as flexibility enhanced random pore model (Lisandy et al. 2017). A good overview of available models for the geometrical contribution to the single step approximation was given by Khawam et al. (2006) and Deutsch (2017).

Often, the driving force term $h(p, p_{eq})$ is ignored (Vyazovkin et al. 2011) – may it be due to its problematic identification or controllability in experiments or the lack in model identification techniques. A profound discussion on its effects, its importance and different modeling strategies was presented by Birkelbach et al. (2020) and Vyazovkin (2020).

Besides the general perspective of reaction models, the modeling of the phases in heterogeneous reactive flows also needs to be covered. In gas-solid flows, the gas phase can in principal be modeled in the same way as discussed for the homogeneous reactive flows in the previous sections. The modeling of the solid phase should be discussed specifically, because different approaches exist here.

The focus in this thesis lies on chemical engineering applications, therefore models resolving the solid are not considered due to their high computational demand. However, they can provide useful insights in mechanistic effects or help derive simplified models. That is why, the most important recent approaches in resolved particle modeling are mentioned here: the SKIPPY code used by Hecht et al. (2012), Shaddix et al. (2013), and Shaddix et al. (2019), the work from Tufano et al. (2019) resolving the solid particle as a porous medium, or the approach by Gómez et al. (2018) and Kiss et al. (2021) describing the solid particle as an Eulerian phase.

Disregarding the resolved solid models, the solid can be either modeled as discrete particles – modeled with a Lagrangian description – or as a continuous phase

– with the Eulerian description. Since those modeling techniques are inherently different and pose restrictions and implications on the reaction modeling, they will be discussed separately in the following subsections.

Lagrangian description

When the solid phase is treated as discrete particles, it is called a Lagrangian description. In this case, their movement is described by Newton's laws of motion. When the fluid phase is modeled as Eulerian and the solid as Lagrangian phase, one can generally distinguish approaches based on their complexity. First, one-way coupling methods, where the transport of the Lagrangian particles is passive. Second, two-way coupling, where the interaction between the two phases is resolved. Third, four-way coupling, where the interaction between the phases, as well as particle-particle interactions are resolved. For further information, see (Jakobsen 2008).

It is commonly agreed, that for low solid concentrations, one-way coupling is sufficiently accurate, but for larger concentrations, the interactions should be modeled (Jakobsen 2008). For dense particle flows, often a four-way coupling scheme – probably the most common being the discrete element method (DEM) – is employed. Insights and a good overview of CFD-DEM modeling are given by Norouzi et al. (2016).

To avoid the computational expensive four-way coupling, resolving the particle-particle interactions, an approach to combine the benefits of Eulerian and Lagrangian modeling has been developed: the multiphase particle-in-cell (MPPIC) method (Andrews et al. 1996; Snider 2001; O'Rourke et al. 2009; O'Rourke et al. 2012). There, the particle-particle interactions are not solved directly, but are modeled by solving the solid stresses in an Eulerian frame. The method has also been applied to heterogeneous reaction by Snider et al. (2011). A similar approach has been presented and implemented by Klimanek et al. (2015) for coal gasification.

The computational demand increases naturally with increased coupling. Nonetheless, also with one- or two-way coupling the computational demand is often prohibitive if a large number of particles needs to be tracked in the system. Then, the particles can be grouped and only representative parcels – comprised of numerous particles having the same features – are tracked and solved for (Jakobsen 2008).

The treatment of single particles or parcels, offers the possibility to track distinct properties. Although the distinct shape of the particles can be tracked, modeling non-spherical particles poses challenges. An established approach within DEM modeling is to approximate non-spherical particles by multiple spheres (Norouzi et al. 2016).

However, within one- or two-way coupling approaches, the particles are often

approximated as spheres. The simplest approaches to account for non-sphericity are drag model modifications, e.g. the correlation from Haider et al. (1989). Those do usually not take into account the particle orientation. Some recent work accounting for spheroidal particles and their orientation has been presented by Guo et al. (2019) and Guo et al. (2020) for biomass combustion.

In addition to the increased computational demand with increased coupling or increased number of particles, a special challenge with larger reacting particles is the source term coupling. Additionally to the momentum and heat transfer coupling, coupling source terms from the heterogeneous reactions arise. Conventionally – so for example in OpenFOAM or Fluent (ANSYS 2016) – the coupling is realized on a point basis, called the particle centroid method (PCM) (Zhang et al. 2020b). However, this should only be done when the particles are significantly smaller than the grid cell. For larger particles, other coupling strategies should be employed. A profound evaluation of different coupling strategies, their benefits and drawbacks, has been studied for biomass combustion by Zhang et al. (2020b).

An important topic in blast furnace operation is the application of alternative reducing agents in the raceway zone. Because the iron ore reduction happens above this zone, it is usually not investigated in those studies (Maier 2015). The volume fraction of the reducing agents is usually low, therefore, Lagrangian modeling without resolving particle-particle interaction is appropriate for those studies.

To study the reducing agents the simulations are often simplified by ignoring the coke bed (Shen et al. 2008; Shen et al. 2009a; Shen et al. 2009b; Shen et al. 2009c; Yeh et al. 2012; Wijayanta et al. 2014b; Wijayanta et al. 2014a; Majeski et al. 2015; Du et al. 2015; Vuokila et al. 2016; Zhang et al. 2020a; Zhou et al. 2021). This is suitable, when laboratory equipment for reducing agents is studied, e.g. by Shen et al. (2008) and Shen et al. (2009b). A closer step to the actual blast furnace is made, when the coke bed is included. For simplification, it is often modeled as a porous, stationary media (Shen et al. 2011; Shen et al. 2015; Shen et al. 2012; Shiozawa 2013; Liu et al. 2020c; Liu et al. 2021a; Wang et al. 2022) or not directly coupled to the gas phase (Wu et al. 2019; Maier 2015). The incorporation of non-spherical effects for the reducing agents becomes important when studying biochar as reducing agent. Liu et al. (2020c) and Wang et al. (2022) have studied its application and accounted for non-sphericity by shape factors.

When modeling the denser region of the blast furnace – the coke bed – usually particle-particle interactions should be modeled as well. Full scale studies of the blast furnace with CFD-DEM, do usually not account for reactions, because they are already at the limit in terms of computational cost (Nie et al. 2021). Several full-scale studies of the blast furnace, considering only the flow exist, e.g. (Allert et al. 2009; Geleta et al. 2018; Bambauer et al. 2018).

The CFD-DEM simulations of the raceway incorporating heterogeneous reac-

tions are often simplified in other aspects. Cui et al. (2020) study the raceway zone, but ignore any gas phase reactions, while several other works are limited to lab-scale raceways, (Wang et al. 2021; E et al. 2021; Nogami et al. 2004), or lab-scale studies on iron-ore reduction (Kinaci et al. 2020; E 2020).

However, CFD-DEM simulations of other processes including heterogeneous reactions (Scherer et al. 2017) have been presented: e.g. waste incineration (Wissing et al. 2017), or lime stone calcination (Krause et al. 2015).

Eulerian description

Compared to point modeling, modeling the solid phase as a continuous phase is better in terms of computational effort (Zhou et al. 2016; Jakobsen 2008). In this case, the two phases are treated as interpenetrating continua, including the phase volume fraction in the continuity, momentum and energy equation (Gidaspow 1994). This is called a two-fluid model (TFM), but can easily be extended to a multi-fluid model, by adding additional coupling terms. In general, the coupling is realized by source terms in the continuity equation stemming from phase transformation or reactions, source terms in the momentum equation coming for example from drag and lift forces, and in the energy equation from reactions, phase transformation and/or heat transfer.

For a solid Eulerian phase a closure relation for the solid stress is required. Based on the kinetic theory of granular gases, the velocity fluctuations of the solid can be related to a granular temperature and an additional equation for this granular temperature can be constructed. This approach is called the kinetic theory of granular flows and has been developed by Lun et al. (1984), Lun et al. (1986), and Savage (1998). In the past decades different approaches to model the closure terms of this equation have been developed. A good overview was published by Van Wachem (2000).

When treating the solid phase as a continuous phase, no discrete particles are tracked and consequently no distinct properties of the individual particles are available. The phase properties are averaged values per grid cell and are often constant, for example the particle diameter of a phase, used to model the drag force.

This inherent feature of (averaged) values per grid cell leads unavoidably to the question of how to average the solid phase properties, especially when the phase mixes. For example, if we model the thermochemical conversion as consecutive steps, consisting of drying, devolatilization and char conversion: How do moist particles mix with already partly devolatilized ones? Also the mixing in combination with the single step approximation Eq. (1) is unclear – is an average conversion state of mixed solids conceptually correct?

Therefore, all models requiring individual particle features, or requiring consecu-

tive conversion steps, can not be treated within the Eulerian modeling framework. For example Luo et al. 2022 discuss the biomass pyrolysis modeling in fluidized beds, emphasizing that the progressive conversion model and the interface based model can not be applied within this framework.

A trick to circumvent this problem, was proposed by Gerber et al. (2010). They use a multi fluid approach to model wood gasification (drying, devolatilization, char conversion) – treating each conversion stage as a separate phase: wood before devolatilization is one phase, char is one phase and the reacted products are one phase. However, this increases the computational demand because all the constitutive equations need to be solved for all the phases, requiring coupling terms between the different phases.

Some problems are resolved, if the solid coke phase is considered stationary. Then, no solid mixing occurs and the solid properties can be tracked consistently in each cell, for example for blast furnace modeling by Bösenhofer (2020). There, the coke is already dried and devolatilized, so only char conversion needs to be modeled.

Other Eulerian examples in blast furnace modeling are given by Liu et al. (2021a) and Jiao (2020) considering coke reactions and iron ore reduction, where solids are treated as an incompressible fluid. Jiao (2020) included additionally the coke and sinter particle size by correlating it to the conversion degree.

The reducing agents in the blast furnace are mostly modeled as Lagrangian particles, as discussed in the previous section. However, some studies consider also those as continuous phase (Okosun et al. 2020; Gu et al. 2010).

3 Problem Statement

The previous chapter introduced the state-of-the-art in reaction modeling for CFD. The special focus is lying on modeling the blast furnace, therefore, the focus was laid on gas phase and gas-solid reaction modeling.

The application of CFD to analyze and improve chemical engineering processes is increasing, but there are still limitations. The modeling and simulation of reactions in these systems brings an additional complexity and is also influenced by the underlying modeling choices. The hindering aspects can be categorized in two main groups:

First, the computational **time** of the CFD simulation. To optimize a running process and investigate operational changes a-priori, it is prohibitive if the CFD simulation takes several days, weeks or even months. The process operator is not willing, or simply can not wait to obtain the CFD results. The incorporation of the reactions into CFD modeling increase those challenges.

Second, the **accuracy** of the simulation results. A simulation will never identically reflect the reality, but it is necessary that the predictions are accurate enough to help improve or design a process. The essential effects need to be captured and the error needs to be limited to an acceptable tolerance. E.g. if the peak temperature shall be analyzed to estimate the influence on the material wear, the error of the predicted temperature has to be in a tolerable range.

Often it is a trade of between computational performance and accuracy. But it is not as simple as that. On the one hand, applying speed-up techniques can be applied, modifying algorithmic structures or changing solution techniques can fasten the computation without any loss in accuracy. And on the other hand, models can be reparameterized, modified, or changed – generally speaking improved – without increasing the computational effort. The question remains how to accomplish this?

fast & accurate models?

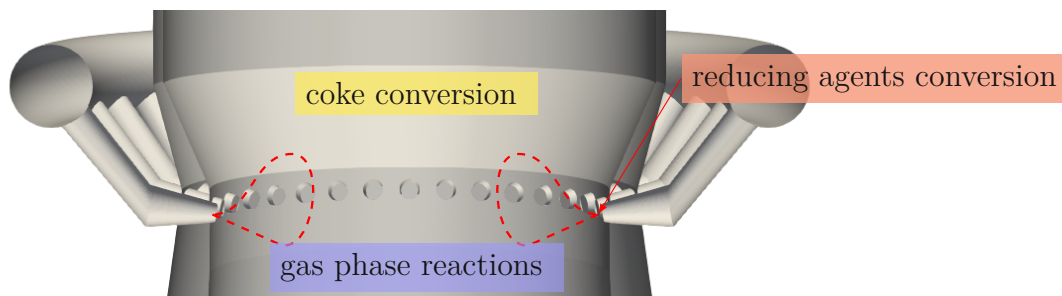


Figure 2: The problem of fast and accurate models related to the reactions occurring in the blast furnace raceway zone

To recap the important reactions to be modeled in the blast furnace, Figure 2 shows the raceway zone of a blast furnace with its main reactions. Based on those two objectives the state-of-the-art in reaction modeling has been analyzed with focus on the blast furnace raceway zone. The methodology to improve the modeling of the homogeneous reactive flow with its gas phase reactions and gaseous reducing agents and the heterogeneous reactive flow with the coke conversion is discussed in the next section.

4 Research Approach

Based on the example of the blast furnace raceway, modeling approaches for the reaction types occurring there are analyzed. Important bottlenecks – based on the two main hindering factors computational time and modeling accuracy – were identified. The approach was to first investigate homogeneous – gas-phase reactions – reactive flows and then heterogeneous – gas-solid reactions – reactive flows. The details of the identified limitations and the improvement strategies are discussed in the following section, first for homogeneous reactive flows, second for heterogeneous reactive flows and categorized into the improvements regarding either time or accuracy, see Figure 3.

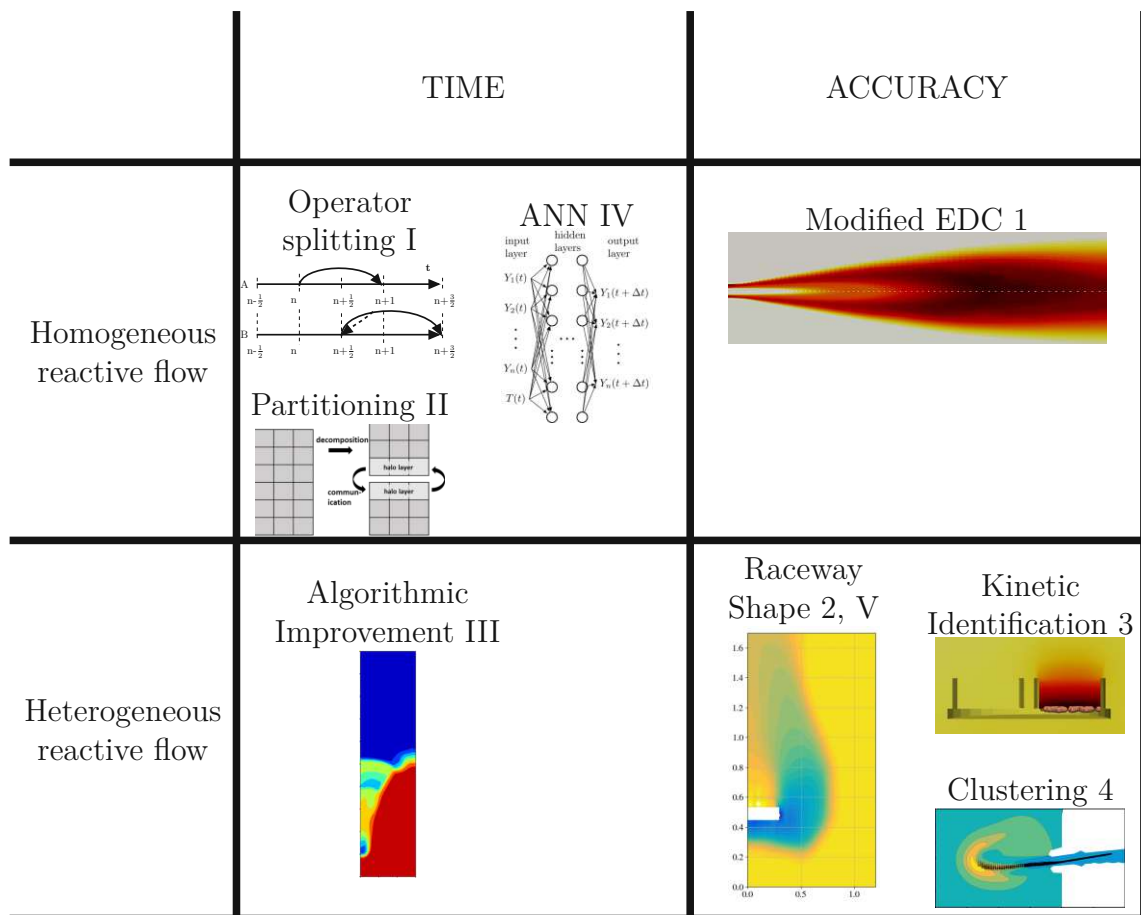


Figure 3: Publication work categorized into improvements for time or accuracy and the reaction type heterogeneous or homogeneous

4.1 Homogeneous reactive flows

Generally, the modeling effort in homogeneous flows should be kept low when simulating large scale applications. Therefore, usually RANS modeling is chosen and the turbulence fluctuations are not resolved. The chemical reactions introduce additional complexity, since not only the transport of all the species needs to be modeled, but also their reaction and interaction with the turbulent flow.

Based on the state-of-the-art, section 2.1, the EDC model was chosen as the most suitable to model the reactions in the blast furnace. Related to the general problem statement, it was analyzed – first, in terms of computational time and second, in terms of modeling accuracy.

A computationally intensive part of the EDC is the solution of a set of coupled ordinary differential equations (ODEs) for the species evolution. To speed-up those calculations, several strategies have been suggested. For example, the tabulation of the solution as in-situ adaptive tabulation (ISAT) (Pope 1997). To make use of this tabulation methodology in conjunction with the original EDC formulation, operator splitting techniques should be applied (Rehm 2010). Therefore, different operator splitting techniques and their performance with the EDC were analyzed and the results were presented in **Conference Paper I**.

Large scale simulations are usually carried out on multiple processors to reduce the calculation time. The speed-up, is however not unlimited and does not scale linearly with the number of processors. The computational resources should therefore be used efficiently. For non-reactive flow simulations using the open-source platform OpenFOAM partitioning strategies have been reviewed in literature (Haddadi et al. 2017). The increased computational demand per cell due to the solution of the reactions, might change those results. Because the calculation demand in each cell increases and the communication between processors contributes to a smaller part to the overall calculation time. Efficient partitioning strategies for reactive flows were investigated and the results for optimal partitioning were presented in **Conference Paper II**.

The increasing application of machine learning in all kinds of engineering applications lead to the idea to make use of this technique to speed-up and improve the solution of the chemical reactions as well. First approaches to apply neural networks for the solution of ODEs in combustion simulations have been presented by Blasco et al. 1998; Cerri et al. 2003; Laubscher 2017. The application in conjunction with the EDC in OpenFOAM was investigated in collaboration with a master student (Cabrera Ormazá 2021) and joint results were published in **Conference Paper IV**.

After the improvements in terms of computational time, the model accuracy of the model was targeted. A very common simplification in the EDC model is the approximation of the fine structures, in which the chemical species react, as plug

flow reactors (PFRs) instead of perfectly stirred reactors (PSRs). The treatment of these fine structures and the effect on the results was assessed for classical combustion in detail by my colleague and me in **Co-Author Paper A**.

Besides this modeling choice, studies under MILD combustion regimes have shown deficiencies of the EDC. The EDC has originally been derived for highly turbulent flames and its basis relies on high Damköhler number regimes. MILD conditions are less turbulent and can be characterized by lower Damköhler numbers. To overcome the deficiencies of the EDC under these conditions, modifications have been proposed by Parente et al. (2016), Bao (2017), Lewandowski et al. (2018), Lewandowski et al. (2020b), and Lewandowski et al. (2020a).

The problems with the EDC were first revealed when applying to MILD combustion, but are true for all combustion regimes characterized by lower Damköhler numbers. This is also the case for other applications, e.g. gasification as shown by Rehm et al. (2009). Therefore, we investigated the reaction regime in the raceway zone of the blast furnace and showed, that the conditions also show regions with lower Damköhler number in **Co-Author Paper C**. These results suggested, that the modified EDC parameters would be beneficial for predicting the gas phase reactions in the blast furnace raceway zone.

Although, modifications have been proposed in literature, open questions remained with there application. The modified correlations require the Damköhler number calculation – hence the characteristic chemical time scale calculation. The approximation and estimation of a characteristic chemical time scale in a multi-reaction system is not straightforward. Therefore, different strategies to approximate the characteristic time scales have been assessed and their influence on predictions has been compared to experimental flame results from Flame D (Barlow et al. 1998; Masri et al. 1996) and Adelaide Jet-in-hot-coflow, (Dally et al. 2002). The results were presented in **Paper 1**.

4.2 Heterogeneous reactive flows

The gas-solid reaction modeling was investigated based on the same structure as introduced in the section 2.2. First, the general reaction modeling was investigated. This can not be directly related to simulation details, therefore it was studied in terms of model accuracy only. In section 2.2 it was summarized, that gas-solid reaction models mostly describe the overall conversion process, including not only intrinsic kinetics, but also transport effects. Therefore, the identified mechanisms are usually tailored for specific properties, e.g. porosity and heating rate.

When modeling kinetic reactions, e.g. within CFD, the mechanism should be related to the conditions in the actual application. Meaning, that the experiments used to derive the kinetic mechanism should closely resemble the actual reaction conditions in the application. This issue was extensively discussed for PCI kinetic

identification for the blast furnace by Bösenhofer et al. (2020a) and Bösenhofer (2020).

Of course aiming for closer representation of the actual conditions will improve the specific models. But aiming for more generalizable models – by abstracting the essential influential factors – can also lead to better kinetic models. Therefore, work on improving kinetic model identification can be useful to obtain better kinetic models which can then be used for modeling in CFD.

Therefore, improvements for model identification based on the most widely used gas-solid reaction model (Vyazovkin et al. 2011) – the single-step approximation – were investigated. With the single-step approximation, temperature, conversion and distance to equilibrium are taken into account. Birkelbach (2020) has developed a mathematical methodology to compute those three effects separately, in contrast to many other models assuming the distance to equilibrium to be negligible. However, within the experimental device, those parameters should be tightly controlled and measured, which is often not possible. Therefore, we developed a strategy to combine CFD – without making any modeling assumptions for the simulation – with the kinetic model identification. Through the CFD simulation, the deviations from set-points can be estimated and taken into account without using any a-priori assumption on the kinetic model. This combination improves the derived models. The methodology was presented and show-cased in **Paper 3**.

Models based on the single step approximation Eq. (1) are also used for coal conversion modeling (Jess et al. 2010) or for studying blast furnace injection (Ye et al. 2022). Therefore, this improved methodology could also be used for improved blast furnace raceway simulations.

Lagrangian description

For the gas-solid reaction modeling using the Lagrangian solid treatment, the computational time was only targeted by choosing the model framework. A two-way coupling approach, grouping several particles into parcels, as discussed in section 2.2 is the method of choice, because it offers a good balance between computational time and level of detail.

The Lagrangian description is mostly used for modeling the reducing agents in a blast furnace. There, diffusion and kinetic effects in the conversion play a role. The raceway zone in a blast furnace is highly turbulent. DNS studies from Krüger et al. 2017; Haugen et al. 2018 revealed that small particles – e.g. coal – cluster under turbulent flow conditions in the turbulent eddies. This influences the mass transfer to the particles, hence the diffusional contribution to the conversion.

Therefore, the question arose, if this effect might be essential when simulating the reducing agents conversion in the blast furnace raceway zone. An investigation on the important scales in PCI combustion **Co-Author Paper B** suggested,

that the Damköhler numbers are in a range, where these effects are important. Therefore, the model has been implemented in OpenFOAM to carry out a detailed investigation. The results showed, that the turbulent clustering is influential in this regime and should be taken into account. The detailed results are summarized in the submitted publication **Paper 4**.

Eulerian description

For gas-solid reaction modeling within a Eulerian-Eulerian modeling framework the modeling of the solid in densely packed regions is challenging. However, the reaction and conversion can only be correctly modeled, if the motion is predicted accurately. In section 2.2 we showed, that the dense bed in blast furnace models is often modeled as Eulerian phase, when the reaction is computed. Therefore, the general modeling of the solid phase as Eulerian phase and possible improvements in terms of computational time and model accuracy were investigated.

For two-fluid models, the discretization and solution of the continuity equations is challenging. Rusche (2002) and Oliveira et al. (2003) discussed different approaches to conservatively and boundedly solve the phase-averaged continuity equations in a TFM. In OpenFOAM this is done by the algorithm called multi-dimensional universal limiter with explicit solution (MULES). The explicit solution brings some deficiencies, for example a small time-step requirement (Wardle et al. 2013). Therefore, a new algorithm combining an implicit and explicit solution step for the phase-averaged continuity equations was proposed, implemented and evaluated. The details can be found in **Conference Paper III**.

Besides the computational aspect, also the model accuracy of the TFM was investigated. The usage of the KTGF to model the motion of the solid phase was especially investigated for the blast furnace raceway by Mondal et al. (2005) and Rangarajan et al. (2014). This work was extended by investigating the effect of different closure models for the KTGF. The study revealed that the choice of closure models is important for the prediction of the raceway shape. The detailed results were communicated in **Paper 2**.

Furthermore, we showed that the prediction of the raceway shape significantly affects the gas-solid reactions. Consequently also the predictions on the species concentration profiles in the blast furnace, see **Conference Paper V**.

5 Results - Summary of Publications

The research approach to target improvements for reaction modeling in CFD has been discussed in the previous section. There, the methodology and context of the publications contributing to the objectives of this thesis has been established. Figure 4 contextualizes the publications based on the different reactions in the blast furnace. In the following, a short summary and the most important results of each paper are presented. My contribution to each publication is stated in the second part of this thesis and the abstracts of relevant publications as co-author are added there as well.

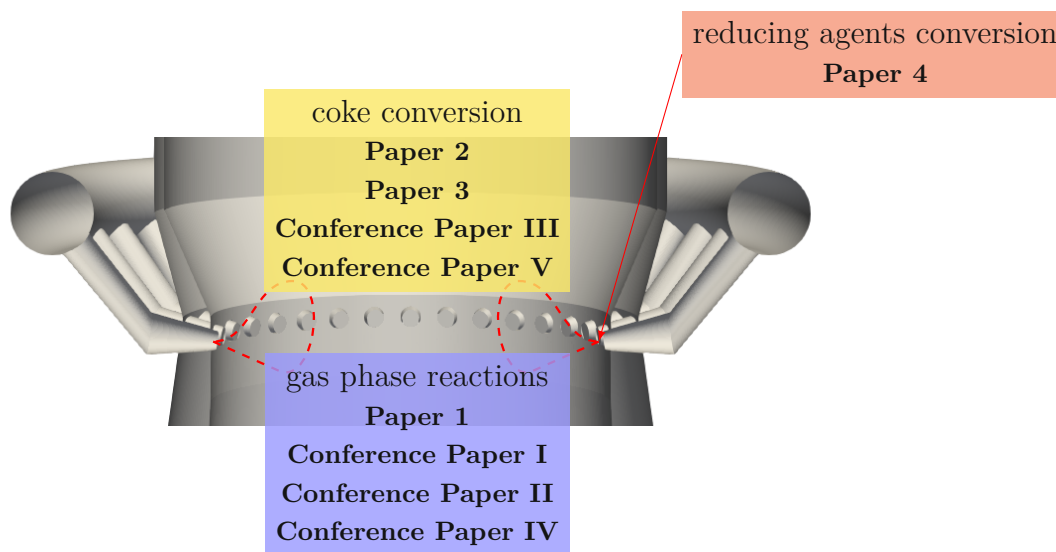


Figure 4: Context of the publications contributing to this thesis within the blast furnace raceway modeling associate to the different reaction types

5.1 Homogeneous reactive flows

Conference Paper I This paper covers improvements for the EDC to reduce the computational demand. The model is needed to model the turbulence-chemistry interactions in turbulent unresolved simulations. It requires the solution of a set of ODEs for the chemical reactions. To reduce the computational demand, tabulation methods exist, e.g. ISAT. To apply them for the original EDC, it is necessary to use operator splitting. Two operator splitting techniques from literature were investigated and applied with the EDC. To evaluate their performance, the simulation results were compared to experimental results from a laboratory-scale flame, Sandia Flame D. The investigated staggered splitting scheme gave the best results in terms of computational time and accuracy.

Conference Paper II This paper deals with the efficient partitioning of combustion simulations on multiple processors. The CFD simulation can be split up on multiple processors to reduce the computational time. However, the speed-up does not scale linearly with increasing processors. Therefore, it is important to use the computational resources efficiently and partition the CFD domain most effectively on the different processors. The existing guidelines for partitioning can not be directly applied for reactive flows. This has been revealed and studied in this publication by examining the partitioning of combustion simulations with the open-source software OpenFOAM.

Conference Paper IV In this publication the usage of machine learning to speed-up CFD simulations was presented. The demanding problem of solving the ODEs resulting from the EDC should be reduced by substituting the solver with an ANN. Based on previous results from literature and the results from a master thesis, a trained ANN was used to predict the results of the ODEs, instead of solving them numerically. The results for single-cell simulations, were accurate and very promising. The application to flame simulation still showed some deficiencies. The investigations in this paper showed future directions for our work in this field.

Paper 1 In this paper the determination of characteristic chemical time scales for combustion simulations was targeted. To use extended EDC models, which employ relationships depending on dimensionless numbers a good estimate of those dimensionless numbers in each computational cell is needed. Especially the Damköhler number is needed to characterize the relation between mixing and kinetics in the system. Therefore, the characteristic chemical time scale is needed to describe the system. Since the formulation of a single characteristic chemical time scale is not straightforward in a reaction system, different approaches to approximate this characteristic chemical time scale were analyzed in this paper. Those time scales were analyzed based on a simple test problem and flame simulations. The results show, which of those are capable to correctly characterize the system and are easy enough to not slow down the simulation significantly.

5.2 Heterogeneous reactive flows

Paper 3 This paper covers improved model identification for gas-solid reactions based on the single-step approximation. Deficiencies in existing kinetic experiments are shown and their influence on the model identification are discussed. The implementation of a CFD framework, which does not need any kinetic model to simulate the experimental conditions in the device enables the estimation of the reaction conditions. These details can be used to derive enhanced kinetic models

with the TensorNPK method. The application was showcased with the example of a $\text{CuO}/\text{Cu}_2\text{O}$ reaction system.

Lagrangian description

Paper 4 The effect of clustering on small particles under blast furnace conditions was analyzed in this paper. A turbulent clustering model which depicts the reduction of mass transfer to small particles and consequently the effect on conversion was implemented and test. For the pulverized coal conversion under blast furnace conditions a reduction of the conversion rate was observed. The results revealed that the effects are important under blast furnace conditions. Furthermore, it was shown, that a global a-priori estimation of the turbulence effect is difficult. To capture does clustering effects, the model should be taken into account in raceway simulations.

Eulerian description

Conference Paper III In this paper a novel algorithm to solve the phase-averaged continuity equations in a two-fluid model was presented. A novel algorithm, which combines an implicit solution step with (an) explicit corrector step(s) was proposed. The details of the implementation in OpenFOAM were discussed and the differences to the current – explicit – approach. The performance was tested on different test cases, showing its accurate predictions and its improvement for larger time steps, which can additionally lead to faster simulations.

Paper 2 This paper targets the modeling of solid flows in the blast furnace raceway. For this densely packed bed, the KTGF can be used to model the solid motion. Different closure models are assessed – one accounting for interstitial fluid effects and one not accounting for them. The comparison with experiments, DEM simulations and another established TFM code showed, that the incorporation of interstitial fluid effects in the closure models is essential to predict the raceway shape in a blast furnace raceway.

Conference Paper V This paper uses the results of the closure model investigation for the raceway formation and extends it to simulations including coke reactions. A lab-scale raceway was simulated and compared to detailed measurement of the species concentration from literature. This showed, that the correct prediction of the raceway shape significantly influences the species concentration profiles.

6 Conclusions and Outlook

The obstacles when applying computational fluid dynamics (CFD) to chemical engineering problems, are on the one hand high computational demand and on the other hand insufficient model accuracy. Based on the blast furnace raceway zone current reaction modeling techniques in CFD were reviewed and suitable modeling techniques were analyzed with respect to these two objectives. The analysis of the modeling strategies for gas phase and gas-solid reactions – both occurring in the blast furnace – revealed deficiencies and lead to the work presented in this thesis.

For gas phase reactions the eddy dissipation concept (EDC) was investigated, which is a suitable model for Reynolds-averaged Navier-Stokes (RANS) simulations. The main share of computational cost is the solution of the ordinary differential equation (ODE) system. Improvements through operator splitting, tabulation, and efficient partitioning were analyzed and the best performing approaches were presented in conference publications. They can now be applied in the blast furnace modeling framework and enable a faster solution of the EDC. Further, investigations to substitute the ODE solver with an artificial neural network (ANN) showed promising results and open an interesting topic for further research. In terms of modeling accuracy, the applicability of an extended EDC for low Damköhler number regimes is now ensured through appropriate chemical time scale approximations. This is necessary, because low Damköhler regimes exist in the blast furnace, where the standard EDC has deficiencies in the predictions.

The presented improved kinetic identification methodology enables enhanced reaction mechanism extraction from experiments. Thereby the identification of kinetic models for gas-solid reactions is improved. The method overcomes some of the deficiencies resulting from set-point deviations in experiments through exothermic reactions and reactant depletion. The identified enhanced mechanism can be applied in CFD, where one-step approximations are appropriate. However, not only the intrinsic kinetics are relevant in modeling gas-solid reactions with RANS, but also the turbulence effects the mass transport and consequently the overall conversion of small (Lagrangian) solid particles. The importance of this effect for the blast furnace was shown in this thesis and a suitable model incorporating those effects was implemented. This permits the consideration of turbulent clustering effects in the conversion of small particles in the blast furnace, or other devices featuring the thermo-chemical conversion of small particles.

Densely packed solids –like coke in the blast furnace – are usually modeled as Eulerian phase. A solution algorithm for Eulerian phases was implemented to improve the accuracy and speed-up the simulations. The algorithm can be applied in blast furnace simulations with a dynamic raceway, or to other two-fluid model (TFM) simulations. Furthermore, the closure models for the coke motion were evaluated to find a suitable model, which predicts the raceway shape correctly.

Thereby, the accuracy of species predictions in the raceway zone is improved.

These developments improve estimations in the blast furnace raceway zone and permit the a-priori testing of alternative reducing agents. An accurate estimation of the raceway shape, temperature levels and reactions is essential to predict the applicability of different reducing agents and estimate the possible coke substitution rates. This enables a reduction of the CO₂ emissions and supports the transition to a carbon neutral steel production.

The general applicability of the models was always considered during the method development. Therefore, beside the benefits in the steel production, the methods can be utilized for other chemical engineering applications. As an example, the modified EDC enables improved predictions for all low Damköhler number regimes, e.g. for moderate or intense low oxygen dilution (MILD) combustion. Further, the algorithmic improvement for the TFM can be used to improve fluidized bed predictions of any kind, if modeled in the Eulerian-Eulerian framework.

To conclude, several improvements in terms of computational time and modeling accuracy have been suggested, successfully implemented and tested in the course of this thesis. Naturally, the presented developments have resolved only some challenges for reaction modeling in CFD, and there is still room for further research. The incorporation of the iron reduction in the blast furnace raceway model – possibly as further Eulerian phase – requires suitable coupling strategies, and is hindered by the increased computational time. Another point, is the conversion modeling of reducing agents: the approximation of uniform temperature particles leads to errors for larger reducing agents and should be taken into account in those cases.

A general future perspective is the utilization of CFD models including reactions for process control or the coupling with flow sheeting methodologies. To achieve such on-line simulations, additional speed-up will be necessary.

With respect to the steel production on the way to reach the climate goals, intermediately, reduced emissions in blast furnaces are necessary, followed by their substitution through net-zero-emission technologies. A possible technology could be the direct reduction of iron ores with hydrogen. The developed method for the EDC to model gas phase reactions or the model for turbulence effects on gas-solid conversion can enhance the advancement of this technology.

To conclude, there are definitely interesting times ahead and I hope the work presented here, can help to enforce the transition to a sustainable industry.

References

- Allert, A., Y. Yongxiang, and B. Rob (2009). “Coupled DEM - CFD modelling of the iron-making blast furnace”. In: *Seventh International Conference on CFD in the Minerals and Process Industries*, pp. 1081–1085.
- Andahazy, D., S. Slaby, G. Löffler, F. Winter, C. Feilmayr, and T. Bürgler (2006). “Governing processes of gas and oil injection into the blast furnace”. In: *ISIJ International* 46.4, pp. 496–502. ISSN: 09151559. DOI: 10.2355/isijinternational.46.496.
- Andersen, J., C. L. Rasmussen, T. Giselsson, and P. Glarborg (2009). “Global combustion mechanisms for use in CFD modeling under oxy-fuel conditions”. In: *Energy and Fuels* 23.3, pp. 1379–1389. ISSN: 08870624. DOI: 10.1021/ef8003619.
- Andrews, M. J. and P. J. O’Rourke (1996). “The multiphase particle-in-cell (MP-PIC) method for dense particulate flows”. In: *International Journal of Multiphase Flow* 22.2, pp. 379–402. ISSN: 03019322. DOI: 10.1016/0301-9322(95)00072-0.
- ANSYS (2016). *ANSYS Fluent - CFD Software | ANSYS*. URL: <http://www.ansys.com/products/fluids/ansys-fluent>.
- Bambauer, F., S. Wirtz, V. Scherer, and H. Bartusch (2018). “Transient DEM-CFD simulation of solid and fluid flow in a three dimensional blast furnace model”. In: *Powder Technology* 334, pp. 53–64. ISSN: 1873328X. DOI: 10.1016/j.powtec.2018.04.062.
- Bao, H. (2017). “Development and Validation of a New Eddy Dissipation Concept (EDC) Model for MILD Combustion”. MSc. Delft University of Technology. URL: <http://resolver.tudelft.nl/uuid:45fdb951-408f-404f-8b9a-71f2eda6540b>.
- Barlow, R. S. and J. H. Frank (1998). “Effects of turbulence on specific mass fractions in methane/air jet flames”. In: *Twenty-Seventh Symposium (International) on Combustion* 27, pp. 1087–1095.
- Barros des Souza, E. E. (2020). “Modelling and Simulation of Coke and PCI Combustion in an Industrial Blast Furnace Raceway”. MSc. Universidade Federal Do Ceará.
- Bhatia, S. and D. Perlmutter (1980). “A Random Pore Model for Fluid-Solid Reactions: I. Isothermal, Kinetic Control”. In: *AIChE Journal* 26.3, pp. 379–386. DOI: 10.1002/aic.690270211.
- Birkelbach, F. (2020). “Non-parametric kinetic modeling of gas-solid reactions for thermochemical energy storage”. Dissertation. Technische Universität Wien. DOI: 10.34726/hss.2020.82863.
- Birkelbach, F., M. Deutsch, and A. Werner (2020). “The effect of the reaction equilibrium on the kinetics of gas-solid reactions — A non-parametric modeling

-
- study". In: *Renewable Energy* 152, pp. 300–307. ISSN: 0960-1481. DOI: 10.1016/j.renene.2020.01.033.
- Blasco, J. A., N. Fueyo, C. Dopazo, and J. Ballester (1998). "Modelling the temporal evolution of a reduced combustion chemical system with an artificial neural network". In: *Combustion and Flame* 113.1-2, pp. 38–52. ISSN: 00102180. DOI: 10.1016/S0010-2180(97)00211-3.
- Bösenhofer, M., E. Wartha, C. Jordan, M. Harasek, C. Feilmayr, and F. Hauzenberger (2018a). "Characterization of gas phase reaction regime in the raceway zone". In: *AISTech - Iron and Steel Technology Conference Proceedings*, pp. 441–454. ISBN: 978-193511772-8.
- Bösenhofer, M., E.-M. Wartha, C. Jordan, and M. Harasek (2018b). "The eddy dissipation concept-analysis of different fine structure treatments for classical combustion". In: *Energies* 11.7. ISSN: 19961073. DOI: 10.3390/en11071902.
- Bösenhofer, M. (2020). "On the modeling of multi-phase reactive flows: Thermochemical conversion in the raceway zone of blast furnaces". Dissertation. Technische Universität Wien. DOI: 10.34726/hss.2020.58548.
- Bösenhofer, M., E. M. Wartha, C. Jordan, C. Feilmayr, H. Stocker, F. Hauzenberger, J. Rieger, S. Tjaden, A. Walk, and M. Harasek (2020a). "Suitability of pulverised coal testing facilities for blast furnace applications". In: *Ironmaking and Steelmaking* 47.5, pp. 574–585. ISSN: 17432812. DOI: 10.1080/03019233.2019.1565152.
- Bösenhofer, M., E.-M. Wartha, C. Jordan, F. Hauzenberger, C. Feilmayr, H. Stocker, J. Rieger, B. König, and M. Harasek (2020b). "Pulverized Coal Conversion in Blast Furnaces – Analysis of Involved Scales". In: *AISTech - Iron and Steel Technology Conference Proceedings*.
- Cabrera Ormazá, M. D. (2021). "Artificial Neural Networks for the Application to Reactive Flow Simulations". Master Thesis. Technische Universität Wien. DOI: 10.34726/hss.2021.58068.
- Cameron, I., M. Sukhram, K. Lefebvre, and W. Davenport (2019). *Blast furnace ironmaking*. Elsevier, pp. 1–802. ISBN: 978-0-12-814227-1. DOI: <https://doi.org/10.1016/C2017-0-00007-1>.
- Cavaliere, A. and M. D. Joannon (2004). "Mild Combustion". In: *Progress in Energy and Combustion Science* 30, pp. 329–366. DOI: 10.1016/j.pecs.2004.02.003.
- Cerri, G., V. Michelassi, S. Monacchia, and S. Pica (2003). "Kinetic combustion neural modelling integrated into computational fluid dynamics". In: *Proceedings of the Institution of Mechanical Engineers, Part A: Journal of Power and Energy* 217.2, pp. 185–192. ISSN: 09576509. DOI: 10.1243/09576500360611218.

- Commission of the European Communities (2021). *Commission Staff Working Document: Towards competitive and clean European steel*. Tech. rep. Commission of the European Communities.
- Cui, J., Q. Hou, and Y. Shen (2020). “CFD-DEM study of coke combustion in the raceway cavity of an ironmaking blast furnace”. In: *Powder Technology* 362, pp. 539–549. ISSN: 1873328X. DOI: 10.1016/j.powtec.2019.12.012.
- Dally, B. B., A. N. Karpetis, and R. S. Barlow (2002). “Structure of Turbulent Non-Premixed Jet Flames in a Diluted Hot Coflow”. In: *Proceedings of the Combustion Institute* 29, pp. 1147–1154.
- Deutsch, M. (2017). “A systematic approach to identify new thermochemical energy storage systems”. Dissertation. Technische Universität Wien. DOI: 10.34726/hss.2017.32280.
- Du, S. W. and W. H. Chen (2006). “Numerical prediction and practical improvement of pulverized coal combustion in blast furnace”. In: *International Communications in Heat and Mass Transfer* 33.3, pp. 327–334. ISSN: 07351933. DOI: 10.1016/j.icheatmasstransfer.2005.10.015.
- Du, S. W., C. P. Yeh, W. H. Chen, C. H. Tsai, and J. A. Lucas (2015). “Burning characteristics of pulverized coal within blast furnace raceway at various injection operations and ways of oxygen enrichment”. In: *Fuel* 143, pp. 98–106. ISSN: 00162361. DOI: 10.1016/j.fuel.2014.11.038.
- E, D. (2020). “Validation of CFD-DEM model for iron ore reduction at particle level and parametric study”. In: *Particuology* 51, pp. 163–172. ISSN: 22104291. DOI: 10.1016/j.partic.2019.10.008.
- E, D., P. Zhou, S. Guo, J. Zeng, Q. Xu, L. Guo, Q. Hou, and A. Yu (2021). “Particle-scale study of coke combustion in the raceway of an ironmaking blast furnace”. In: *Fuel* October, p. 122490. ISSN: 00162361. DOI: 10.1016/j.fuel.2021.122490.
- Ertesvåg, I. S. (2020). “Analysis of Some Recently Proposed Modifications to the Eddy Dissipation Concept (EDC)”. In: *Combustion Science and Technology* 192.6, pp. 1108–1136. ISSN: 0010-2202. DOI: 10.1080/00102202.2019.1611565.
- Ertesvåg, I. S. and B. F. Magnussen (1999). “The Eddy Dissipation Turbulence Energy Cascade Model”. In: *Combustion Science and Technology* 159.1, pp. 213–235. DOI: 10.1080/00102200008935784.
- Ertesvåg, I. S. (2022). “Scrutinizing proposed extensions to the Eddy Dissipation Concept (EDC) at low turbulence Reynolds numbers and low Damköhler numbers”. In: *Fuel* 309. October 2021, p. 122032. ISSN: 00162361. DOI: 10.1016/j.fuel.2021.122032.
- European Commission (2019). *The European Green Deal - Communication from the commission to the European Parliament, the European Council, the European*

Economic and Social Committee and the Committee of the Regions. Tech. rep.
URL: https://ec.europa.eu/info/strategy/priorities-2019-2024/european-green-deal_en.

European Environment Agency (2022). <https://www.eea.europa.eu/>. DOI: 35963ca1e37145df933067593

Eurostat (n.d.). *Shedding light on energy in the EU - A guided tour of energy statistics*. DOI: 10.2785/551213.

Galletti, C., G. Coraggio, and L. Tognotti (2013). “Numerical investigation of oxy-natural-gas combustion in a semi-industrial furnace: Validation of CFD sub-models”. In: *Fuel* 109, pp. 445–460. ISSN: 00162361. DOI: 10.1016/j.fuel.2013.02.061.

Galwey, A. K. (2004). “Is the science of thermal analysis kinetics based on solid foundations?: A literature appraisal”. In: *Thermochimica Acta* 413.1-2, pp. 139–183. ISSN: 00406031. DOI: 10.1016/j.tca.2003.10.013.

Geleta, D. D. and J. Lee (2018). “Effects of Particle Diameter and Coke Layer Thickness on Solid Flow and Stress Distribution in BF by 3D Discrete Element Method”. In: *Metallurgical and Materials Transactions B: Process Metallurgy and Materials Processing Science* 49.6, pp. 3594–3602. ISSN: 10735615. DOI: 10.1007/s11663-018-1368-7.

Gerber, S., F. Behrendt, and M. Oevermann (2010). “An Eulerian modeling approach of wood gasification in a bubbling fluidized bed reactor using char as bed material”. In: *Fuel* 89.10, pp. 2903–2917. ISSN: 00162361. DOI: 10.1016/j.fuel.2010.03.034.

Gidaspow, D. (1994). *Multiphase Flow and Fluidization . - Continuum and Kinetic Theory Descriptions*. Academic Press, Inc. ISBN: 0-12-395783-4.

Gómez, M. A., J. Porteiro, S. Chapela, and J. L. Míguez (2018). “An Eulerian model for the simulation of the thermal conversion of a single large biomass particle”. In: *Fuel* 220. February, pp. 671–681. ISSN: 00162361. DOI: 10.1016/j.fuel.2018.02.063.

Gran, I. R. and B. F. Magnussen (1996a). “A Numerical Study of a Bluff-body Stabilized Diffusion Flame . Part 1 . Influence of Turbulence Modeling and Boundary Conditions”. In: *Combustion Science and Technology*, pp. 171–190. DOI: 10.1080/00102209608951998.

— (1996b). “A Numerical Study of a Bluff-Body Stabilized Diffusion Flame . Part 2 . Influence of Combustion Modeling And Finite-Rate Chemistry”. In: *Combustion Science and Technology* 119, pp. 191–217. DOI: 10.1080/00102209608951999.

Gu, M., G. Chen, M. Zhang, D. Huang, P. Chaubal, and C. Q. Zhou (2010). “Three-dimensional simulation of the pulverized coal combustion inside blast furnace tuyere”. In: *Applied Mathematical Modelling* 34.11, pp. 3536–3546. ISSN: 0307904X. DOI: 10.1016/j.apm.2010.03.004.

- Guevara Opinska, L., M. Mahmoud, C. Bene, and K. Rademaekers (2021). *Moving towards Zero-Emission Steel: Technologies Available, Prospects, Timeline and Costs*. Tech. rep. European Parliament's committee on Industry, Research and Energy.
- Guo, N., Á. D. García Llamas, T. Li, K. Umeki, R. Gebart, and T. Løvås (2020). "Computational fluid dynamic simulations of thermochemical conversion of pulverized biomass in a dilute flow using spheroidal approximation". In: *Fuel* 271.November 2019, p. 117495. ISSN: 00162361. DOI: 10.1016/j.fuel.2020.117495.
- Guo, N., T. Li, L. Zhao, and T. Løvås (2019). "Eulerian-Lagrangian simulation of pulverized biomass jet using spheroidal particle approximation". In: *Fuel* 239.June 2018, pp. 636–651. ISSN: 00162361. DOI: 10.1016/j.fuel.2018.10.137.
- Haddadi, B., C. Jordan, and M. Harasek (2017). "Cost efficient CFD simulations: Proper selection of domain partitioning strategies". In: *Computer Physics Communications* 219, pp. 121–134. ISSN: 00104655. DOI: 10.1016/j.cpc.2017.05.014.
- Haider, A. and O. Levenspiel (1989). "Drag Coefficient and Terminal Velocity of Spherical and Nonspherical Particles". In: *Powder Technology* 58, pp. 63–70.
- Haugen, N. E. L., J. Krüger, D. Mitra, and T. Løvås (2018). "The effect of turbulence on mass transfer rates of small inertial particles with surface reactions". In: *Journal of Fluid Mechanics* 836, pp. 932–951. ISSN: 14697645. DOI: 10.1017/jfm.2017.820.
- Hecht, E. S., C. R. Shaddix, M. Geier, A. Molina, and B. S. Haynes (2012). "Effect of CO₂ and steam gasification reactions on the oxy-combustion of pulverized coal char". In: *Combustion and Flame* 159.11, pp. 3437–3447. ISSN: 00102180. DOI: 10.1016/j.combustflame.2012.06.009.
- Jakobsen, H. A. (2008). *Chemical Reactor Modeling*. ISBN: 9783540251972.
- Jess, A. and A. K. Andresen (2010). "Influence of mass transfer on thermogravimetric analysis of combustion and gasification reactivity of coke". In: *Fuel* 89.7, pp. 1541–1548. ISSN: 00162361. DOI: 10.1016/j.fuel.2009.09.002.
- Jiao, L. (2020). "Development and Applications of a Comprehensive Three-Dimensional (3D) Blast Furnace Process Model". PhD thesis. Monash University. DOI: 10.26180/5f50c286aa226.
- Jones, W. P. and B. E. Launder (1972). "The prediction of laminarization with a two-equation model of turbulence". In: *International Journal of Heat and Mass Transfer* 15, pp. 301–314. DOI: 10.1016/0017-9310(72)90076-2.
- Khawam, A. and D. R. Flanagan (2006). "Solid-state kinetic models: Basics and mathematical fundamentals". In: *Journal of Physical Chemistry B* 110.35, pp. 17315–17328. ISSN: 15206106. DOI: 10.1021/jp062746a.

-
- Kinaci, M. E., T. Lichtenegger, and S. Schneiderbauer (2020). “A CFD-DEM model for the simulation of direct reduction of iron-ore in fluidized beds”. In: *Chemical Engineering Science* 227, p. 115858. ISSN: 00092509. DOI: 10.1016/j.ces.2020.115858.
- Kiss, M., M. Bösenhofer, M. Schatzl, and M. Harasek (2021). “Particle Resolved Thermo-Chemical Conversion of Pulverized Coal Clusters”. In: *VII International Conference on Particle-Based Methods PARTICLES 2021*.
- Klimanek, A., W. Adamczyk, A. Katelbach-Woźniak, G. Węcel, and A. Szłęk (2015). “Towards a hybrid Eulerian-Lagrangian CFD modeling of coal gasification in a circulating fluidized bed reactor”. In: *Fuel* 152, pp. 131–137. ISSN: 00162361. DOI: 10.1016/j.fuel.2014.10.058.
- Krause, B., B. Liedmann, J. Wiese, S. Wirtz, and V. Scherer (2015). “Coupled three dimensional DEM-CFD simulation of a lime shaft kiln-Calcination, particle movement and gas phase flow field”. In: *Chemical Engineering Science* 134, pp. 834–849. ISSN: 00092509. DOI: 10.1016/j.ces.2015.06.002.
- Krüger, J., N. E. L. Haugen, and T. Løvås (2017). “Correlation effects between turbulence and the conversion rate of pulverized char particles”. In: *Combustion and Flame* 185, pp. 160–172. ISSN: 15562921. DOI: 10.1016/j.combustflame.2017.07.008.
- Krutzler, T., A. Zechmeister, G. Stranner, H. Wiesenberger, T. Gallauner, M. Gössl, C. Heller, H. Heinfellner, N. Ibesich, G. Lichtblau, W. Schieder, J. Schneider, I. Schindler, A. Storch, and R. Winter (2017). *Energie- und Treibhausgas-Szenarien im Hinblick auf 2030 und 2050*. Tech. rep. Umweltbundesamt.
- Laubscher, R. (2017). “Utilization of artificial neural networks to resolve chemical kinetics in turbulent fine structures of an advanced CFD combustion model”. Dissertation. Stellenbosch University. URL: <http://hdl.handle.net/10019.1/101104>.
- Lauder, B. E. and D. B. Spalding (1974). “The numerical computation of turbulent flows”. In: *Computer Methods in Applied Mechanics and Engineering* 3, pp. 269–289. DOI: 10.1016/0045-7825(74)90029-2.
- Lewandowski, M. T. and I. S. Ertesvåg (2018). “Analysis of the Eddy Dissipation Concept formulation for MILD combustion modelling”. In: *Fuel* 224, pp. 687–700. ISSN: 00162361. DOI: 10.1016/j.fuel.2018.03.110.
- Lewandowski, M. T., Z. Li, A. Parente, and J. Pozorski (2020a). “Generalised Eddy Dissipation Concept for MILD combustion regime at low local Reynolds and Damköhler numbers . Part 2 : Validation of the model”. In: *Fuel* April, p. 117773. ISSN: 0016-2361. DOI: 10.1016/j.fuel.2020.117773.
- Lewandowski, M. T., A. Parente, and J. Pozorski (2020b). “Generalised Eddy Dissipation Concept for MILD combustion regime at low local Reynolds and

- Damköhler numbers . Part 1 : Model framework development”. In: *Fuel* March, p. 117743. ISSN: 0016-2361. DOI: 10.1016/j.fuel.2020.117743.
- Lisandy, K. Y., G. M. Kim, J. H. Kim, G. B. Kim, and C. H. Jeon (2017). “Enhanced Accuracy of the Reaction Rate Prediction Model for Carbonaceous Solid Fuel Combustion”. In: *Energy and Fuels* 31.5, pp. 5135–5144. ISSN: 15205029. DOI: 10.1021/acs.energyfuels.7b00159.
- Liu, L., B. Guo, S. Kuang, and A. Yu (2020a). “An Integrated Mathematical Model for Ironmaking Blast Furnace”. In: *Metallurgical and Materials Transactions B: Process Metallurgy and Materials Processing Science* 51.5, pp. 2211–2229. DOI: 10.1007/s11663-020-01905-w.
- Liu, L., S. Kuang, L. Jiao, B. Guo, and A. Yu (2021a). “Optimization of pulverized coal injection (PCI) rate in an ironmaking blast furnace by an integrated process model”. In: *Fuel* October, p. 122832. ISSN: 00162361. DOI: 10.1016/j.fuel.2021.122832.
- Liu, Y., J. Curtis, and Y. Shen (2020b). “Computational fluid dynamics study of re-blowin operation in an ironmaking blast furnace”. In: *Powder Technology* 361, pp. 145–159. ISSN: 1873328X. DOI: 10.1016/j.powtec.2019.09.061.
- Liu, Y. and Y. Shen (2020c). “Combined Experimental and Numerical Study of Charcoal Injection in a Blast Furnace: Effect of Biomass Pretreatment”. In: *Energy and Fuels* 34.1, pp. 827–841. ISSN: 15205029. DOI: 10.1021/acs.energyfuels.9b02949.
- (2021b). “Modelling and optimisation of biomass injection in ironmaking blast furnaces”. In: *Progress in Energy and Combustion Science* 87.March, p. 100952. ISSN: 03601285. DOI: 10.1016/j.pecs.2021.100952.
- Lun, C. K. and S. B. Savage (1986). “The effects of an impact velocity dependent coefficient of restitution on stresses developed by sheared granular materials”. In: *Acta Mechanica* 63.1-4, pp. 15–44. ISSN: 00015970. DOI: 10.1007/BF01182538.
- Lun, C. K., S. B. Savage, D. J. Jeffrey, and N. Chepurniy (1984). “Kinetic theories for granular flow: Inelastic particles in Couette flow and slightly inelastic particles in a general flowfield”. In: *Journal of Fluid Mechanics* 140, pp. 223–256. ISSN: 14697645. DOI: 10.1017/S0022112084000586.
- Luo, H., X. Wang, X. Liu, X. Wu, X. Shi, and Q. Xiong (2022). “A review on CFD simulation of biomass pyrolysis in fluidized bed reactors with emphasis on particle-scale models”. In: *Journal of Analytical and Applied Pyrolysis* 162.January, p. 105433. ISSN: 01652370. DOI: 10.1016/j.jaap.2022.105433.
- Magnussen, B. (1981). “On the structure of turbulence and a generalized eddy dissipation concept for chemical reaction in turbulent flow”. In: *19th American Institute of Aeronautics and Astronautics Aerospace Science Meeting*. St. Louis, p. 6.

-
- (1989). “Modeling of NO_x and Soot Formation by the Eddy Dissipation Concept”. In: *International Flame Research Foundation First Topic Oriented Technical Meeting*. Amsterdam.
 - (2005). “The Eddy Dissipation Concept a Bridge between science and technology”. In: *ECCOMAS Thematic Conference on Computational Combustion*.
 - Magnussen, B. and B. Hjertager (1977). “On mathematical modeling of turbulent combustion with special emphasis on soot formation and combustion”. In: *16th Symposium (International) on Combustion*. Vol. 16. 1. The Combustion Institute, pp. 719–729. DOI: 10.1016/S0082-0784(77)80366-4.
 - Maier, C. (2015). “Numerical Modeling of the Blast Furnace Process Injection of Auxiliary Reducing Agents Into the Raceway”. Dissertation. Technische Universität Wien. DOI: 10.34726/hss.2015.14843.
 - Majeski, A., A. Runstedtler, J. D’Alessio, and N. Macfadyen (2015). “Injection of pulverized coal and natural gas into blast furnaces for iron-making: Lance positioning and design”. In: *ISIJ International* 55.7, pp. 1377–1383. ISSN: 09151559. DOI: 10.2355/isijinternational.55.1377.
 - Masri, A. R., R. W. Dibble, and R. S. Barlow (1996). “The Structure of turbulent nonpremixed Flames revealed by Raman-Rayleigh-LIF Measurements”. In: *Progress in Energy and Combustion Science* 22, pp. 307–362. DOI: 10.1016/S0360-1285(96)00009-3.
 - Mondal, S. S., S. K. Som, and S. K. Dash (2005). “Numerical predictions on the influences of the air blast velocity, initial bed porosity and bed height on the shape and size of raceway zone in a blast furnace”. In: *Journal of Physics D: Applied Physics* 38.8, pp. 1301–1307. ISSN: 00223727. DOI: 10.1088/0022-3727/38/8/030.
 - Murphy, J. J. and C. R. Shaddix (2006). “Combustion kinetics of coal chars in oxygen-enriched environments”. In: *Combustion and Flame* 144.4, pp. 710–729. ISSN: 0010-2180. DOI: <https://doi.org/10.1016/j.combustflame.2005.08.039>.
 - Nie, H., Z. Li, S. Kuang, L. Yan, W. Zhong, A. Yu, X. Mao, and H. Xu (2021). “Numerical investigation of oxygen-enriched operations in blast furnace iron-making”. In: *Fuel* 296. March, p. 120662. ISSN: 00162361. DOI: 10.1016/j.fuel.2021.120662.
 - Nogami, H., H. Yamaoka, and K. Takatani (2004). “Raceway design for the innovative blast furnace”. In: *ISIJ International* 44.12, pp. 2150–2158. ISSN: 09151559. DOI: 10.2355/isijinternational.44.2150.
 - Norouzi, H. R., R. Zarghami, R. Sotuddeh-Gharebagh, and N. Mostoufi (2016). *Coupled CFD-DEM Modeling*. ISBN: 9781119005131.

- O'Rourke, P. J. and D. M. Snider (2012). "Inclusion of collisional return-to-isotropy in the MP-PIC method". In: *Chemical Engineering Science* 80, pp. 39–54. ISSN: 00092509. DOI: 10.1016/j.ces.2012.05.047.
- O'Rourke, P. J., P. (Zhao, and D. Snider (2009). "A model for collisional exchange in gas/liquid/solid fluidized beds". In: *Chemical Engineering Science* 64.8, pp. 1784–1797. ISSN: 00092509. DOI: 10.1016/j.ces.2008.12.014.
- Okosun, T., S. Nielson, J. D'Alessio, S. Ray, S. Street, and C. Zhou (2020). "On the impacts of pre-heated natural gas injection in blast furnaces". In: *Processes* 8.7. ISSN: 22279717. DOI: 10.3390/PR8070771.
- Oliveira, P. J. and R. I. Issa (2003). "Numerical aspects of an algorithm for the Eulerian simulation of two-phase flows". In: *International Journal for Numerical Methods in Fluids* 43.10-11, pp. 1177–1198. ISSN: 02712091. DOI: 10.1002/flid.508.
- Parente, A., M. Rafi, F. Contino, A. Cuoci, and B. B. Dally (2016). "Extension of the Eddy Dissipation Concept for turbulence / chemistry interactions to MILD combustion". In: *Fuel* 163, pp. 98–111. ISSN: 0016-2361. DOI: 10.1016/j.fuel.2015.09.020.
- Peng, X., J. Wang, C. Li, H. Zuo, G. Wang, X. She, and Q. Xue (2021). "Influence of Reducing Gas Injection Methods on Pulverized Coal Combustion in a Medium Oxygen-Enriched Blast Furnace". In: *Computational Modeling in Pyrometallurgy*. ISSN: 15431851. DOI: 10.1007/s11837-021-04812-w.
- Pitsch, H. (2006). "Large-eddy simulation of turbulent combustion". In: *Annual Review of Fluid Mechanics* 38, pp. 453–482. ISSN: 00664189. DOI: 10.1146/annurev.fluid.38.050304.092133.
- Poinsot, T. and D. Veynante (2012). *Theoretical and Numerical Combustion*, pp. 1–588.
- Pope, S. B. (1997). "Computationally efficient implementation of combustion chemistry using in situ adaptive tabulation". In: *Combustion Theory and Modelling* 1, pp. 41–63. ISSN: 1364-7830. DOI: 10.1080/713665229.
- Pope, S. B. (2000). *Turbulent Flows*. Cambridge: Cambridge University Press. ISBN: 0 521 59886 9.
- Rangarajan, D., T. Shiozawa, Y. Shen, J. S. Curtis, and A. Yu (2014). "Influence of operating parameters on raceway properties in a model blast furnace using a two-fluid model". In: *Industrial and Engineering Chemistry Research* 53.13, pp. 4983–4990. ISSN: 15205045. DOI: 10.1021/ie301936r.
- Ranz, W. E. and W. R. J. Marshall (1952). "Evaporation from drops: Part II". In: *Chemical Engineering Progress* 48.4, pp. 173–180.
- Rehm, M. (2010). "Numerische Strömungssimulation der Hochdruckvergasung unter Berücksichtigung detaillierter Reaktionsmechanismen". Dissertation. Technis-

che Universität Bergakademie Freiberg. URL: <https://nbn-resolving.org/urn:nbn:de:bsz:105-qucosa-66695>.

- Rehm, M., P. Seifert, and B. Meyer (2009). “Theoretical and numerical investigation on the EDC-model for turbulence-chemistry interaction at gasification conditions”. In: *Computers and Chemical Engineering* 33.2, pp. 402–407. ISSN: 00981354. DOI: 10.1016/j.compchemeng.2008.11.006.
- Romero-Anton, N., X. Huang, H. Bao, K. Martin-Eskudero, E. Salazar-Herran, and D. Roekaerts (2020). “New extended eddy dissipation concept model for flameless combustion in furnaces”. In: *Combustion and Flame* 220, pp. 49–62. ISSN: 15562921. DOI: 10.1016/j.combustflame.2020.06.025.
- Runchal, A. K. (2012). “The future of CFD and the CFD of the future”. In: *International Symposium on Advances in Computational Heat Transfer* 4.6, pp. 1–10. ISSN: 25785486. DOI: 10.1615/ICHMT.2012.CHT-12.10.
- Rusche, H. (2002). “Computational Fluid Dynamics of Dispersed Two-Phase Flows at High Phase Fractions”. Dissertation. Imperial College of Science, Technology & Medicine. URL: <http://hdl.handle.net/10044/1/8110>.
- Savage, S. B. (1998). “Analyses of slow high-concentration flows of granular materials”. In: *Journal of Fluid Mechanics* 377, pp. 1–26. ISSN: 00221120. DOI: 10.1017/S0022112098002936.
- Scherer, V., S. Wirtz, B. Krause, and F. Wissing (2017). “Simulation of Reacting Moving Granular Material in Furnaces and Boilers An Overview on the Capabilities of the Discrete Element Method”. In: *Energy Procedia* 120, pp. 41–61. ISSN: 18766102. DOI: 10.1016/j.egypro.2017.07.154.
- Shaddix, C. R., E. S. Hecht, C. Gonzalo-Tirado, and B. S. Haynes (2019). “The effect of bulk gas diffusivity on apparent pulverized coal char combustion kinetics”. In: *Proceedings of the Combustion Institute* 37.3, pp. 3071–3079. ISSN: 15407489. DOI: 10.1016/j.proci.2018.07.060.
- Shaddix, C. R., F. Holzleithner, M. Geier, and B. S. Haynes (2013). “Numerical assessment of Tognotti determination of CO₂/CO production ratio during char oxidation”. In: *Combustion and Flame* 160.9, pp. 1827–1834. ISSN: 00102180. DOI: 10.1016/j.combustflame.2013.03.019.
- Shen, Y. S., B. Y. Guo, A. B. Yu, P. R. Austin, and P. Zulli (2011). “Three-dimensional modelling of in-furnace coal/coke combustion in a blast furnace”. In: *Fuel* 90.2, pp. 728–738. ISSN: 00162361. DOI: 10.1016/j.fuel.2010.08.030.
- Shen, Y. S., B. Y. Guo, A. B. Yu, and P. Zulli (2009a). “A three-dimensional numerical study of the combustion of coal blends in blast furnace”. In: *Fuel* 88.2, pp. 255–263. ISSN: 00162361. DOI: 10.1016/j.fuel.2008.08.013.
- Shen, Y. S., D. Maldonado, B. Y. Guo, A. B. Yu, P. Austin, and P. Zulli (2009b). “Computational fluid dynamics study of pulverized coal combustion in blast

- furnace raceway”. In: *Industrial and Engineering Chemistry Research* 48.23, pp. 10314–10323. ISSN: 08885885. DOI: 10.1021/ie900853d.
- Shen, Y., B. Guo, A. Yu, D. Maldonado, P. Austin, and P. Zulli (2008). “Three-dimensional modelling of coal combustion in blast furnace”. In: *ISIJ International* 48.6, pp. 777–786. ISSN: 09151559. DOI: 10.2355/isijinternational.48.777.
- Shen, Y., B. Guo, A. Yu, and P. Zulli (2009c). “Model study of the effects of coal properties and blast conditions on pulverized coal combustion”. In: *ISIJ International* 49.6, pp. 819–826. ISSN: 09151559. DOI: 10.2355/isijinternational.49.819.
- Shen, Y. and A. Yu (2015). “Characterization of Coal Burnout in the Raceway of an Ironmaking Blast Furnace”. In: *Steel Research International* 86.6, pp. 604–611. ISSN: 16113683. DOI: 10.1002/srin.201400333.
- Shen, Y., A. Yu, P. Austin, and P. Zulli (2012). “Modelling in-furnace phenomena of pulverized coal injection in ironmaking blast furnace: Effect of coke bed porosities”. In: *Minerals Engineering* 33, pp. 54–65. ISSN: 08926875. DOI: 10.1016/j.mineng.2011.10.014.
- Shiozawa, T. (2013). “Numerical Modelling of Multiphase Flow in Raceway of Ironmaking Blast Furnace”. Dissertation. The University of New South Wales. DOI: 10.26190/unsworks/2456.
- Snider, D. M. (2001). “An Incompressible Three-Dimensional Multiphase Particle-in-Cell Model for Dense Particle Flows”. In: *Journal of Computational Physics* 170, pp. 523–549. DOI: 10.1006/jcph.2001.6747.
- Snider, D. M., S. M. Clark, and P. J. O. Rourke (2011). “Eulerian – Lagrangian method for three-dimensional thermal reacting flow with application to coal gasifiers”. In: *Chemical Engineering Science* 66.6, pp. 1285–1295. ISSN: 0009-2509. DOI: 10.1016/j.ces.2010.12.042.
- Spalding, D. B. (1971). “Mixing and chemical reaction in steady confined turbulent flames”. In: *Symposium (International) on Combustion* 13.1, pp. 649–657. ISSN: 00820784. DOI: 10.1016/S0082-0784(71)80067-X.
- Szekely, J. and J. W. Evans (1970). “A structural model for gas-solid reactions with a moving boundary”. In: *Chemical Engineering Science* 25.6, pp. 1091–1107. ISSN: 00092509. DOI: 10.1016/0009-2509(70)85053-9.
- Szekely, J., J. W. Evans, and H. Y. Sohn (1976). *GAS-SOLID REACTIONS*. Academic Press, Inc.
- Tabet, F. and I. Gökalp (2015). “Review on CFD based models for co-firing coal and biomass”. In: *Renewable and Sustainable Energy Reviews* 51, pp. 1101–1114. ISSN: 18790690. DOI: 10.1016/j.rser.2015.07.045.

-
- Thiele, E. W. (1939). “Relation between Catalytic Activity and Size of Particle”. In: *Industrial and Engineering Chemistry* 31.7, pp. 916–920. ISSN: 00197866. DOI: 10.1021/ie50355a027.
- Tufano, G. L., O. T. Stein, A. Kronenburg, G. Gentile, A. Stagni, A. Frassoldati, T. Faravelli, A. M. Kempf, M. Vascellari, and C. Hasse (2019). “Fully-resolved simulations of coal particle combustion using a detailed multi-step approach for heterogeneous kinetics”. In: *Fuel* 240.November 2018, pp. 75–83. ISSN: 00162361. DOI: 10.1016/j.fuel.2018.11.139.
- United Nations (n.d.). *The Paris Agreement*. URL: <https://unfccc.int/process-and-meetings/the-paris-agreement/the-paris-agreement>.
- Van Wachem, B. G. M. (2000). “Derivation, Implementation, and Validation of Computer Simulation Models for Gas-Solid Fluidized Beds”. PhD thesis. Delft University of Technology.
- Versteeg, H. K. and W. Malalasekera (2007). *An Introduction to Computational Fluid Dynamics - The Finite Volume Method*. 0. ISBN: 9780131274983.
- Veynante, D. and L. Vervisch (2002). “Turbulent combustion modeling”. In: *Progress in Energy and Combustion Science* 28.3, pp. 193–266. ISSN: 03601285. DOI: 10.1016/S0360-1285(01)00017-X.
- Vuokila, A. (2017). *CFD modeling of auxiliary fuel injections in the blast furnace tuyere-raceway area*. ISBN: 9789526217697.
- Vuokila, A., O. Mattila, R. L. Keiski, and E. Muurinen (2016). “CFD modelling of pulverized coal combustion in a blast furnace test rig”. In: *Industrial Combustion* 2016.1, pp. 1–16. ISSN: 20753071.
- Vuokila, A., O. Mattila, R. L. Keiski, and E. Muurinen (2017). “CFD study on the heavy oil lance positioning in the blast furnace tuyere to improve combustion”. In: *ISIJ International* 57.11, pp. 1911–1920. ISSN: 09151559. DOI: 10.2355/isijinternational.ISIJINT-2017-213.
- Vyazovkin, S. (2020). “Kinetic effects of pressure on decomposition of solids”. In: *International Reviews in Physical Chemistry* 39.1, pp. 35–66. ISSN: 1366591X. DOI: 10.1080/0144235X.2019.1691319.
- Vyazovkin, S., A. K. Burnham, J. M. Criado, L. A. Pérez-Maqueda, C. Popescu, and N. Sbirrazzuoli (2011). “ICTAC Kinetics Committee recommendations for performing kinetic computations on thermal analysis data”. In: *Thermochimica Acta* 520, pp. 1–19. ISSN: 0040-6031. DOI: 10.1016/j.tca.2011.03.034.
- Wang, Q. and E. Wang (2022). “Numerical investigation of the influence of particle shape, pretreatment temperature, and coal blending on biochar combustion in a blast furnace”. In: *Fuel* 313.December 2021, p. 123016. ISSN: 00162361. DOI: 10.1016/j.fuel.2021.123016.

- Wang, S. and Y. Shen (2021). “CFD-DEM modelling of raceway dynamics and coke combustion in an ironmaking blast furnace”. In: *Fuel* 302, April, p. 121167. ISSN: 0016-2361. DOI: 10.1016/j.fuel.2021.121167.
- Wardle, K. E. and H. G. Weller (2013). “Hybrid multiphase CFD solver for coupled dispersed/segregated flows in liquid-liquid extraction”. In: *International Journal of Chemical Engineering* 2013.1. ISSN: 1687806X. DOI: 10.1155/2013/128936.
- Wartha, E. M., F. Birkelbach, M. Bösenhofer, and M. Harasek (2022a). “Enhanced kinetic model identification for gas–solid reactions through Computational Fluid Dynamics”. In: *Chemical Engineering Journal* 430.P2, p. 132850. ISSN: 13858947. DOI: 10.1016/j.cej.2021.132850.
- Wartha, E. M., M. Bösenhofer, and M. Harasek (2018). “Computational Improvements for the Eddy Dissipation Concept by Operator Splitting and Tabulation”. In: *Proceedings of the 28th European Symposium on Computer Aided Process Engineering*. Vol. 43. 2010, pp. 1687–1692. ISBN: 9780444642356. DOI: 10.1016/B978-0-444-64235-6.50294-1.
- (2022b). “Importance of considering interstitial fluid effects in the kinetic theory of granular flow for raceway formation prediction”. In: *Chemical Engineering Science* 247, p. 117026. ISSN: 00092509. DOI: 10.1016/j.ces.2021.117026.
- Wartha, E.-M., M. Bösenhofer, and M. Harasek (2020a). “Characteristic Chemical Time Scales for Reactive Flow Modeling Characteristic Chemical Time Scales for Reactive Flow”. In: *Combustion Science and Technology* 00.00, pp. 1–26. ISSN: 0010-2202. DOI: 10.1080/00102202.2020.1760257.
- (2020b). “Combining an implicit solution with an explicit corrector step for the solution of the continuity equations in a two-fluid solver”. In: *14th International Conference on CFD in Oil & Gas, Metallurgical and Process Industries*. Trondheim, pp. 123–131.
- Wartha, E.-M., M. Bösenhofer, F. Hauzenberger, H. Stocker, C. Feilmayr, and M. Harasek (2022c). “Influence of Raceway Shape on Species Concentration”. In: *AISTech - Iron and Steel Technology Conference Proceedings*. Pittsburgh.
- Wartha, E.-M., M. Bösenhofer, C. Jordan, and M. Harasek (2019). “Mesh Partitioning of Reactive Flow Simulations – Speed-up and Other Side Effects”. In: *9th European Combustion Meeting*. Lisboa.
- Wartha, E.-M., M. D. Cabrera Ormaza, M. Bösenhofer, and M. Harasek (2021). “Artificial Neural Networks for the Application to Reactive Flow Simulations”. In: *10th European Combustion Meeting*. 4, pp. 266–271.
- Wijayanta, A. T., M. S. Alam, K. Nakaso, J. Fukai, K. Kunitomo, and M. Shimizu (2014a). “Combustibility of biochar injected into the raceway of a blast fur-

-
- nace". In: *Fuel Processing Technology* 117, pp. 53–59. ISSN: 03783820. DOI: 10.1016/j.fuproc.2013.01.012.
- (2014b). "Numerical study on pulverized biochar injection in blast furnace". In: *ISIJ International* 54.7, pp. 1521–1529. ISSN: 09151559. DOI: 10.2355/isijinternational.54.1521.
- Wissing, F., S. Wirtz, and V. Scherer (2017). "Simulating municipal solid waste incineration with a DEM/CFD method – Influences of waste properties, grate and furnace design". In: *Fuel* 206, pp. 638–656. ISSN: 00162361. DOI: 10.1016/j.fuel.2017.06.037.
- Wu, D., P. Zhou, H. Yan, P. Shi, and C. Q. Zhou (2019). "Numerical investigation of the effects of size segregation on pulverized coal combustion in a blast furnace". In: *Powder Technology* 342, pp. 41–53. ISSN: 1873328X. DOI: 10.1016/j.powtec.2018.09.067.
- Yagi, S. and D. Kunii (1955). "Studies on combustion of carbon particles in flames and fluidized beds". In: *Symposium (International) on Combustion* 5.1, pp. 231–244. ISSN: 00820784. DOI: 10.1016/S0082-0784(55)80033-1.
- Ye, L., J. Zhang, R. Xu, X. Ning, N. Zhang, C. Wang, X. Mao, J. Li, G. Wang, and C. Wang (2022). "Co-combustion kinetic analysis of biomass hydrochar and anthracite in blast furnace injection". In: *Fuel* 316. January, p. 123299. ISSN: 00162361. DOI: 10.1016/j.fuel.2022.123299.
- Yeh, C. P., S. W. Du, C. H. Tsai, and R. J. Yang (2012). "Numerical analysis of flow and combustion behavior in tuyere and raceway of blast furnace fueled with pulverized coal and recycled top gas". In: *Energy* 42.1, pp. 233–240. ISSN: 03605442. DOI: 10.1016/j.energy.2012.03.065.
- Zhang, C., G. Wang, X. Ning, J. Zhang, and C. Wang (2020a). "Numerical simulation of combustion behaviors of hydrochar derived from low-rank coal in the raceway of blast furnace". In: *Fuel* 278. February, p. 118267. ISSN: 00162361. DOI: 10.1016/j.fuel.2020.118267.
- Zhang, J., T. Li, H. Ström, and T. Løvås (2020b). "Grid-independent Eulerian-Lagrangian approaches for simulations of solid fuel particle combustion". In: *Chemical Engineering Journal* 387. October 2019, p. 123964. ISSN: 13858947. DOI: 10.1016/j.cej.2019.123964.
- Zhou, C., G. Tang, J. Wang, D. Fu, T. Okosun, A. Silaen, and B. Wu (2016). "Comprehensive Numerical Modeling of the Blast Furnace Ironmaking Process". In: *JOM* 68.5, pp. 1353–1362. ISSN: 15431851. DOI: 10.1007/s11837-016-1891-4.
- Zhou, C. Q. (2008). *CFD Modeling for high rate pulverized Coal injection (PCI) to blast furnaces*. Tech. rep. U.S. Department of Energy.

Zhou, Z., R. Wang, Q. Yi, G. Wang, and C. Ma (2021). “Combustion enhancement of pulverized coal with targeted oxygen-enrichment in an ironmaking blast furnace”. In: *Processes* 9.3, pp. 1–17. ISSN: 22279717. DOI: 10.3390/pr9030440.

List of Figures

1	Schematic drawing of the blast furnace	5
2	The problem of fast and accurate models in the blast furnace raceway	14
3	Publication work categorized into time and accuracy	16
4	Context of the publications in the blast furnace	21

Nomenclature

Acronyms

ANN	artificial neural networks
CFD	computational fluid dynamics
DEM	discrete element method
DNS	direct numerical simulation
EDC	eddy dissipation concept
EDM	eddy dissipation model
EU	European Union
FVM	finite volume method
GHG	green house gas emissions
ISAT	in-situ adaptive tabulation
KTGF	kinetic theory of granular flows
LES	large eddy simulation
MILD	moderate or intense low oxygen dilution
MPPIC	multiphase particle-in-cell
MULES	multi dimensional universal limiter with explicit solution
NPK	non-parametric kinetics
ODE	ordinary differential equation
PCI	pulverised coal injection

PCM particle centroid method

PDF probability density function

PFR plug flow reactor

PSR perfectly stirred reactor

RANS Reynolds-averaged Navier-Stokes

TFM two-fluid model

Subscripts

eq equilibrium

Symbols

α conversion

f conversion function

h equilibrium function

k temperature function

p pressure

T temperature

t time

Publications

In this chapter all publications that are relevant for this thesis are presented. The core of this thesis are the journal publications and the conference publications. Additionally, relevant publications as a co-author are listed. The summary of the core publications, showing the main results is given in the introductory chapter of this thesis. In the following section, the reference of each publication is given and the core publications are appended in full-length when possible according to copyright. For the other publications, the abstract is provided.

Papers

- 1 Characteristic Chemical Time Scales for Reactive Flow Modeling . 46
- 2 Importance of considering interstitial fluid effects in the kinetic theory of granular flow for raceway formation prediction 74
- 3 Enhanced kinetic model identification for gas–solid reactions through Computational Fluid Dynamics 88
- 4 The Effect of Turbulence on the Conversion of Coal under Blast Furnace Raceway Conditions 98

Conference Publications 123

- I Computational Improvements for the Eddy Dissipation Concept by Operator Splitting and Tabulation 123
- II Mesh Partitioning of Reactive Flow Simulations – Speed-up and Other Side Effects 131
- III Combining and Implicit Solution with an Explicit Corrector Step for the Solution of the Continuity Equations in a Two-Fluid Solver 139
- IV Artificial Neural Networks to Substitute the ODE Solver in Reactive Flow Simulations 150
- V Influence of Raceway Shape on Species Concentrations 157

Co-Author Publications 167

- A The eddy dissipation concept – analysis of different fine structure treatments for classical combustion 167
- B Pulverized Coal Conversion in Blast Furnaces – Analysis of Involved Scales 168
- C Characterization of Gas Phase Reaction Regime in the Raceway Zone 168

Paper 1

Characteristic Chemical Time Scales for Reactive Flow Modeling

published in *Combustion Science and Technology* in collaboration with Markus Bösenhofer and Michael Harasek.

My contribution: Initial investigation of chemical time scale approximations. Implementation of the simulation models for the simple test cases. Theoretical analysis of the EDC. Simulation of the flame, analysis of the results. Conceptualization and writing the original draft.

E.-M. Wartha, M. Bösenhofer, and M. Harasek (2020a). “Characteristic Chemical Time Scales for Reactive Flow Modeling Characteristic Chemical Time Scales for Reactive Flow”. In: *Combustion Science and Technology* 00.00, pp. 1–26. ISSN: 0010-2202. DOI: 10.1080/00102202.2020.1760257

Characteristic Chemical Time Scales for Reactive Flow Modeling

Eva-Maria Wartha ^a, Markus Bösenhofer ^{a,b}, and Michael Harasek ^a

^aInstitute of Chemical, Environmental & Bioscience Engineering, Technische Universität Wien, Vienna, Austria;

^bK1-MET GmbH, Linz, Austria

ABSTRACT

The chemical time scale can be used to characterize a reactive system (‘s behavior). In addition, various dimensionless numbers (e.g. Damköhler number) rely on a characteristic chemical time scale. The inverse eigenvalues of a system are regarded as the system’s time scales. This means, the number of time scales is equal the numbers of eigenvalues. A formulation for a single characteristic time scale is required for the system characterization and to calculate dimensionless numbers. Recently proposed modifications of the Eddy Dissipation Concept (a turbulence-chemistry interaction model) also incorporate the Damköhler number in their formulation. Besides accuracy, the numerical efficiency is important, since the chemical time scale needs to be computed in each cell at every time step. We present different chemical time scale definitions found in literature, evaluate them on simple test problems and use them for flame simulations in conjunction with the modified Eddy Dissipation Concept. For the simple test case, most formulations give satisfactory results. The complexity of the chemical reaction mechanism greatly impacts the calculated time scale values. Therefore, we suggest to use a simple global mechanism for the calculation of chemical time scales to ensure reproducibility and consistency of the results.

ARTICLE HISTORY

Received 27 December 2019

Revised 30 March 2020

Accepted 21 April 2020

KEYWORDS

Reactive flows; chemical time scales; eddy dissipation concept

Introduction

Time scales characterize a system and its behavior. Many dimensionless numbers (e.g. Damköhler, Karlovitz, Stokes number) incorporate time scales and are reported to describe a system(‘s behavior) or are used to design scale-up of plants. Many engineering processes incorporate reactive flows. In these cases, it is of particular interest to characterize those flows with time scales.

For reactive flows, the flow itself as well as the reaction determines the overall characteristics. The issue with reaction systems is that their chemical time scale is not inherently defined. Many different time scale definitions or time scale approximations exist in literature. Especially for the calculation of dimensionless numbers a characteristic and representative time scale of the system is needed.

Computational Fluid Dynamics (CFD) can provide detailed information of flows, to determine, for example, flow time scales. But time scale definitions are also used to develop and tailor CFD models. For example, the Eddy Dissipation Concept (EDC) is

CONTACT Eva-Maria Wartha  eva-maria.wartha@tuwien.ac.at  Institute of Chemical, Environmental & Bioscience Engineering, Technische Universität Wien, Getreidemarkt 9/166-2, Vienna, Austria

© 2020 The Author(s). Published with license by Taylor & Francis Group, LLC.

This is an Open Access article distributed under the terms of the Creative Commons Attribution License (<http://creativecommons.org/licenses/by/4.0/>), which permits unrestricted use, distribution, and reproduction in any medium, provided the original work is properly cited.

widely used for the simulation of reactive flows. A recent proposition for its modification incorporates the Damköhler number. This poses the need for a numerically efficient chemical time scale definition to calculate the Damköhler number and apply the suggested modifications in CFD.

Therefore, we discuss the theoretical background of chemical time scales and test proposed definitions for a characteristic chemical time scale, possibly suitable for the application to CFD. These are discussed and applied to simplified test cases, where they can be compared to an analytical solution.

Furthermore, we apply the most suitable chemical time scale formulations to simulations using the modified Eddy Dissipation Concepts and compare them to available flame measurement data. This investigates the practical applicability of the formulations.

Chemical time scales of a system

A chemical reaction system can be described by the following set of Ordinary Differential Equations (ODEs):

$$\frac{dY}{dt} = \dot{\omega} \quad \text{with} \quad Y(0) = Y_0 \quad (1)$$

where Y denotes the mass fractions of species and $\dot{\omega}$ denotes the net production/consumption rates. If the system is disturbed with a small perturbation in its initial value (Equation (2)), the change of the ODE can be approximated by the Jacobian J multiplied by ΔY (Equation (3)), see (Nagy and Turányi 2009; Tomlin, Whitehouse, Pilling 2002).

$$Y(0) = Y_0 + \Delta Y_0 \quad (2)$$

$$\frac{d\Delta Y}{dt} = J\Delta t \quad (3)$$

The Jacobian matrix is defined in the following way and assumed to be independent of time for sufficiently small time intervals:

$$J = \frac{\partial \dot{\omega}}{\partial Y} \quad (4)$$

Therefore, the time evolution of perturbations of the system is assumed to depend on the eigenvalues of the Jacobian, which consequently represent the characteristic time scales of the system. For a more thorough discussion of the connection between time scales and eigenvalues we refer to (Nagy and Turányi 2009; Tomlin et al. 2002).

For complex reaction mechanisms this leads to large Jacobian matrices and a time scale for each species. These time scales describe the chemical system. In the next section we present formulations to derive one characteristic time scale for chemical reaction systems, which is necessary for the calculation of dimensionless numbers.

Characteristic chemical time scale definitions

Different definitions of the characteristic chemical time scale have been proposed in literature (Caudal et al. 2013; Evans et al. 2019; Golovitchev and Chomiak 2001; Golovitchev and Nordin 2001; Isaac et al. 2013; Lam and Goussis 1991; Li et al. 2017; Løvås et al. 2002; Prüfert et al. 2014; Ren and Goldin 2011). Some of them were derived for the purpose of mechanism reduction and are based on the separation of the chemical system into a slow and a fast reacting subspace to identify the dominating system time scales. Others are based on eigenvalue approximations or simple ones only incorporate the reaction rates.

The main objective for the in-situ application to CFD is to obtain a characteristic chemical time scale which describes the chemical system with sufficient accuracy. The complexity of existing definitions varies greatly from simple algebraic expressions to complex eigenvalue problems or principle component analysis (PCA) (Isaac 2014; Parente et al. 2011). Some of them, for example computational singular perturbation (Lam and Goussis 1991) or intrinsic-low dimensional manifold (Glassmaker 1999), have also been developed for a different purpose and have only been recently adapted to determine a characteristic time scale.

The existing expressions for chemical time scale characterization can be divided into algebraic and eigenvalue based definitions. Typically the algebraic expressions employ combinations of species concentrations, chemical reaction rates and/or species consumption/destruction rates. Eigenvalue based formulations require the calculation or approximation of the Jacobian matrix and its decomposition.

Within this wide variety of definitions, the eigenvalue based, for example the CSP theory, have a solid theoretical foundation, while others try to approximate the characteristic scales of the system. The aim of this study is to identify sufficiently accurate, but numerically efficient, characteristic chemical time scale definitions, which can be applied within CFD. Therefore, selected time scale approximations suitable for in-situ determination from literature are discussed in the following sections. They are compared to an analytical solution of a simple reaction system and are employed within simulations of a “classical” turbulent and a moderate or intense low oxygen dilution (MILD) combustion flame.

Inverse Reaction Rate Time Scale (IRRTS)

The probably simplest time scale definition is the reciprocal of the chemical reaction rate (k_r):

$$\tau_{IRRTS} = \min_{r \in N_R} \left(\frac{1}{|k_r|} \right) \quad (5)$$

where N_R is the number of reactions.

For a global single-step reaction this definition is a good choice, since the chemical time scale is unambiguously defined. However, for more complex mechanisms, as many time scales as reactions exist. In this case, the fastest reaction is assumed to dominate the system, thus, defining the characteristic time scale. A drawback of this approach is that all reactions are considered equally important, although some might be of minor importance due to insignificant educt and/or product concentrations.

Ren Time Scale (RTS)

Ren and Goldin (2011) proposed the minimum ratio of the fuel species mass fraction (Y_i) and the corresponding species consumption rates ($\dot{\omega}_i$) as time scale (Equation (6)). Instead of defining a user-defined set of fuel species, in this work all species with a negative net production rate are taken into account. Additionally, Ren and Goldin (2011) introduced an empirical constant C_e to adapt the time scale. Since the numerical value of C_e was not defined, it is set to unity in this work. However, this definition also assumes that the fastest time scale is the dominant one.

$$\tau_{RTS} = C_e \min_{\substack{i \in N_s \\ \dot{\omega}_i < 0}} \left(\frac{Y_i}{\dot{\omega}_i} \right) \quad (6)$$

Ren Product Time Scale (RPTS)

In analogy to RTS, (section 3.2) the Ren Product Time Scale (RPTS) is defined for the product species (Equation (7)). This means all species with a positive net production rate are considered.

$$\tau_{RPTS} = C_e \min_{\substack{i \in N_s \\ \dot{\omega}_i > 0}} \left(\frac{Y_i}{\dot{\omega}_i} \right) \quad (7)$$

OpenFOAM Time Scale (OFTS)

Golovitchev and Nordin (2001) defined the chemical time scale as the ratio of the total species concentration c_{tot} and the sum of the production rate $k_{f,r}$ times the stoichiometric coefficient ν of the product species $N_{s,RHS}$. For mechanisms consisting of more than one reaction n_R , the ratios of all reactions are summed up, as follows (Li et al. 2018):

$$\tau_{OFTS} = \sum_{r=1}^{n_R} \frac{c_{\text{tot}}}{\sum_{n=1}^{N_{s,RHS}} \nu_{n,r} k_{f,r}} \quad (8)$$

Evans Time Scale (ETS)

Evans et al. (2019) suggests to use the major species N_{maj} (for example CH_4 , H_2 , O_2 , CO and CO_2) for the time scale definition shown in Equation (9). To avoid using non-reacting species for the calculation, species with a reaction rate $\dot{\omega}_i < 10^{-16}$ are neglected.

$$\tau_{ETS} = \max_{i \in N_{\text{maj}}} \left[\frac{Y_i}{|\dot{\omega}_i|/\rho} \right] \quad (9)$$

Inverse Jacobian Time Scale (IJTS)

The inverse Jacobian time scale requires the numerically expensive calculation of the species rate Jacobian (Equation (4)). Since most chemistry solvers need the Jacobian anyway, the increased numerical effort is negligible. Prüfert et al. (2014) and Caudal

et al. (2013) interpreted the diagonal elements of the Jacobian as approximation of the system's eigenvalues. For diagonal dominant matrices this approximation is valid, see Gerschgorin's circle theorem (Gerschgorin 1931). However, if the off-diagonal elements are relevant, this approximation can give bad results, since oscillating behavior indicated by complex eigenvalues is not covered. Further information on the quality of the eigenvalue approximation by the Jacobian diagonal can be found elsewhere, e.g. (Prüfert et al. 2014).

One way to get the characteristic time scale is to assume that the inverse of the smallest absolute diagonal element is the dominating time scale (Equation (10)). However, this approach does not check the significance of the individual time scales.

$$\tau_{IJTS} = \min\left(\frac{1}{\mathcal{J}_{ii}}\right) \quad (10)$$

Prüfert et al. (2014) defined a relevant sub set of time scales ($i \in \mathcal{I}$) by comparing the sub set reaction rate $\dot{\omega}e_i$ and the total absolute rate $\dot{\omega}$ (Equation (11)), where e_i is the i^{th} canonical basis vector.

$$\left\| \left(\sum_{i \in \mathcal{I}} \dot{\omega}e_i \right) - \dot{\omega} \right\| < \epsilon \quad (11)$$

The smallest sub set time scale is then assumed to be the characteristic system time scale.

System Progress Time Scale (SPTS)

Prüfert et al. (2014) also defined a chemical time scale based on the inverse norm of the Jacobian matrix multiplied by a weighting factor. The normalized species consumption rates are employed as weighting factor:

$$\tau_{SPTS} = \left(\left\| \mathbf{J} \frac{\dot{\omega}(t_0)}{\|\dot{\omega}(t_0)\|} \right\| \right)^{-1} \quad (12)$$

The SPTS represents the time evolution of the whole system, because τ_{SPTS} approximates $\|\mathbf{J}\|^{-1}$. Using the von Mises iteration it can be shown that τ^{-2} converges toward $\|\mathbf{J}\|^2$ (Prüfert et al. 2014). This method incorporates the significance of the different reactions by considering their contribution to the overall progress.

Inverse Eigenvalue Time Scale (IETS)

The simplest eigenvalue based time scale is the Inverse Eigenvalue Time Scale (IETS), which assumes that the largest eigenvalue (λ_i) defines the characteristic chemical time scale:

$$\tau_{IETS} = \min_{i \in N_s} \left(\frac{1}{|\lambda_i|} \right) \quad (13)$$

Using the importance criterion γ_i , all time scales greater than a threshold value ϵ are considered to be important. The characteristic chemical time scale of the system is then the smallest of the remaining (important) time scales.

Simple test cases

Single-step reaction

The chemical time scale definitions from section 3 are tested on a simple one-step carbon monoxide (CO) oxidation reaction:



According to Westbrook and Dryer (1981) the reaction is reversible; the forward rate (k_f) depends on the CO, H₂O, and O₂ concentrations (Equation (22)) while the reverse reaction rate (k_r) is a function of the CO₂ concentration (Equation (23)). (Units are cm³/s/mol/K)

$$k_f = \underbrace{3.98 \cdot 10^{14} e^{-\frac{20129}{T}}}_k [\text{CO}][\text{H}_2\text{O}]^{0.5}[\text{O}_2]^{0.25} \quad (22)$$

$$k_r = 5.0 \cdot 10^8 e^{-\frac{20129}{T}} [\text{CO}_2] \quad (23)$$

The reverse reaction rate is neglected for this test case. Further simplifying the rate dependency by removing H₂O, a 3 × 3 matrix is obtained for calculating the eigenvalues of the reaction system:

$$\det(\mathcal{J} - \lambda) = \begin{vmatrix} -2k[\text{O}_2]^{0.25} - \lambda_1 & -0.25k[\text{CO}][\text{O}_2]^{-0.75} & 0 \\ -2k[\text{O}_2]^{0.25} & -0.25k[\text{CO}][\text{O}_2]^{-0.75} - \lambda_2 & 0 \\ 2k[\text{O}_2]^{0.25} & 0.25k[\text{CO}][\text{O}_2]^{-0.75} & -\lambda_3 \end{vmatrix} \quad (24)$$

The eigenvalues of this matrix can be easily calculated analytically. Only one non zero eigenvalue exists:

$$\lambda_1 = -k[\text{O}_2]^{0.25} - 0.25k[\text{CO}][\text{O}_2]^{-0.75} \quad (25)$$

This analytic eigenvalue solution and the resulting chemical time scale is compared to the previously discussed time scale definitions. The conversion of a stoichiometric CO and O₂ mixture at 1500 K and 1 bar is modeled in a plug flow reactor (PFR) with Cantera (Goodwin, Moffat, Speth 2017). Chemical time scales were calculated at each output time step using a threshold value of $\epsilon = 0.00001$ where necessary. Figure 1 shows the species concentration and the species consumption profiles versus time. Obviously, under these conditions, the CO oxidation is a fast reaction reaching full conversion after around 10⁻⁷ seconds.

Figure 2 shows the corresponding time scales during the conversion. At the beginning, the different definitions span a range between 10⁻⁸ and 10⁻⁷ seconds, except for RTS. After around 10⁻⁸ second reaction time, different expressions form two groups: one giving

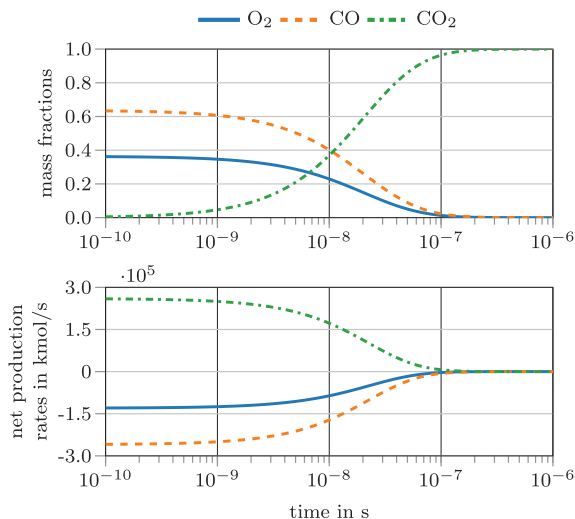


Figure 1. Species concentration (top) and species rates (bottom) for the simplified, one-step three species carbon monoxide oxidation.

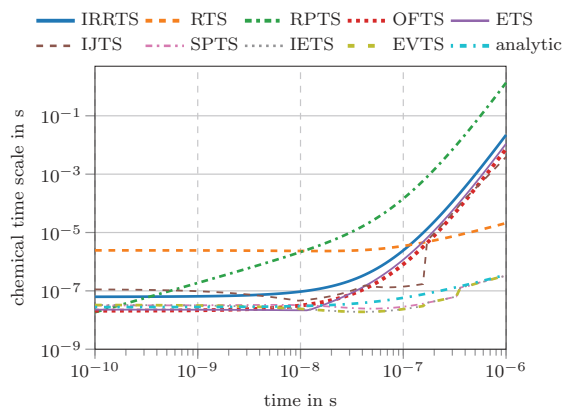


Figure 2. Chemical time scales for the simplified, one-step three species carbon monoxide oxidation.

a steep decrease in chemical time scales reaching values of more than 10^{-3} seconds, while the other reaches values around 10^{-6} seconds, only RTS and RPTS can not clearly be added to those groups. The analytic eigenvalue time scale is part of the latter group. The time scale definitions predicting higher values are the IRRTS, ETS, OFTS and IJTS. One might conclude that the system possesses two distinct time scales. However, since only a single reaction is considered, there should be a clearly defined system time scale. Therefore, the deviations between these two groups can be considered inherent to their definition. A different interpretation could be that the first group represents the current characteristic system velocity, since the time scales increase at a similar rate as the species

consumption and production rates (compare Figs. 1 and 2). Contrary, the second group might represent the ability to react on perturbations, meaning that the chemical system compensates disturbances quickly at high temperatures.

Comprehensive reaction mechanism

Comprehensive reaction mechanisms consist of multiple reactions and complex reaction rate dependencies of concentrations and pressure, e.g. Three-Body reactions, SRI, TROE or TSA fall-off (Gilbert et al. 1983; Lindemann et al. 1922; Stewart et al. 1989; Troe 1983; Tsang and Herron 1991). Thus, the calculation of chemical time scales, the Jacobian and eigenvalues becomes numerically more expensive than for an one-step reaction mechanism. Furthermore, identifying the relevant time scales is essential to obtain the characteristic ones. The same initial conditions are employed in combination with the well-known methane combustion mechanism GRI 3.0 (Smith et al. 2018). Figure 3 shows species concentration and species consumption/production rates for the involved main species (CO, CO₂, H₂O, O₂) and radical species (H, O, OH). The CO oxidation process takes longer when employing the detailed mechanism (10⁻³ compared to 10⁻⁷ seconds). This is caused by an incubation time necessary for the formation of a radical pool which enables the overall oxidation reaction. In this test case, water vapor acts as a reaction promoter, since it forms the radical pool by dissociation. This is clearly visible in the species and consumption rate profiles. However, Figure 4 shows, that not all chemical time scale definitions depict these incubation effects. The IRRTS, ETS and OFTS clearly feature a time scale decrease followed by an increase due to the reaction progress. The SPTS definition indicates a slight decrease, while the IJTS, and IETS predict almost constant chemical time scales around 10⁻⁸ seconds.

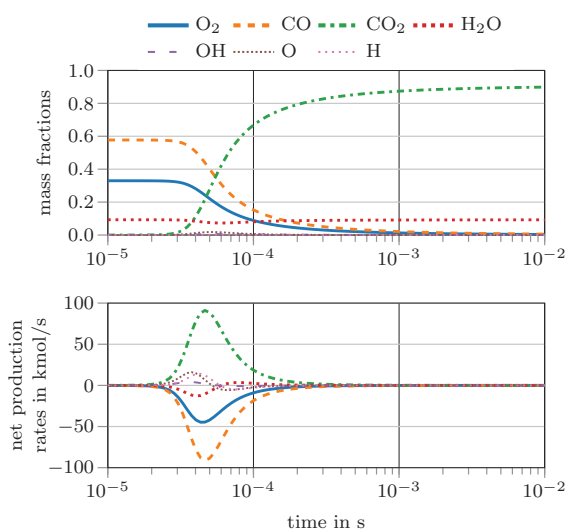


Figure 3. Species concentration (top) and species rates (bottom) for the carbon monoxide oxidation according to the GRI3.0 mechanism (Smith et al. 2018).

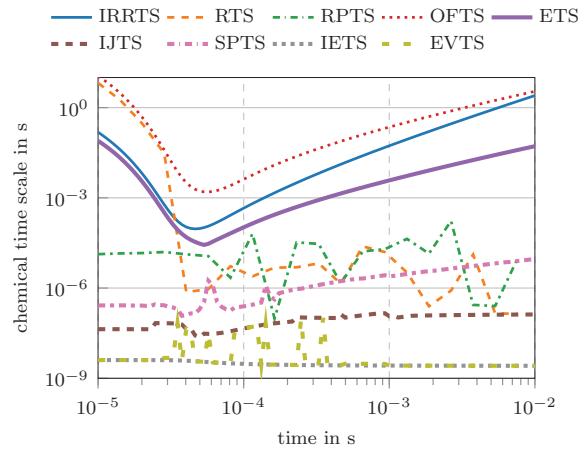


Figure 4. Chemical time scales for the carbon monoxide oxidation based on the GRI3.0 mechanism.

The RTS and RPTS definitions have quite strong fluctuations, caused by the fast changing net production and consumption rates of some radical species.

Methods for computational fluid dynamics

A characteristic chemical time scale can also be necessary for CFD models. Recently, adaptations of the EDC have been proposed, which need a characteristic chemical time scale (Bao 2017; Parente et al. 2016). Therefore, the EDC is described shortly in the next section and its modifications are discussed.

Eddy dissipation concept

The physical foundation of the EDC is the assumption that educts react only in the fine structures (denoted by *), since they are mixed on a molecular level there (Magnussen 1981). Based on the turbulent energy cascade, the fine structure length scale γ_L and the fine structure mass fraction γ^* can be calculated (Equation (26)) using the molecular viscosity ν , the dissipation rate ϵ , the turbulent kinetic energy k and a constant C_γ .

$$\gamma_L = C_\gamma \left(\frac{\epsilon \nu}{k^2} \right)^{1/4} = (\gamma^*)^{(1/3)} \quad (26)$$

The mass transfer rate between the fine structures and the surrounding divided by the fine-structure mass is also calculated based on ϵ , ν and a constant C_τ , which was derived from the turbulence energy cascade (Ertesvåg and Magnussen 1999):

$$\dot{m}^* = \frac{1}{C_\tau} \left(\frac{\epsilon}{\nu} \right)^{1/2} = \frac{1}{\tau^*} \quad (27)$$

The mass transfer rate per unit volume of species i in the mean cell is calculated based on the introduced quantities, the concentrations of species i in the fine structures Y_i^* and the mean cell \bar{Y}_i , and the reacting fraction χ (Equation (28)). This formulation is an adaptation of the original version by (Gran and Magnussen 1996). The different versions of the EDC and their development over time can be reviewed for example in (Bösenhofer et al. 2018; Ertesvåg 2019).

$$\bar{R}_i = \frac{\bar{\rho} \dot{m}^* \gamma_L^2 \chi}{1 - \gamma_L^3 \chi} (\bar{Y}_i - Y_i^*) \quad (28)$$

The reacting fraction χ is often set to unity (Gran and Magnussen 1996). Although this practice recently lead to some discussion (Ertesvåg 2019; Lewandowski et al. 2017), we follow this suggestion in our calculations.

The general relation for a quantity Ψ in the fine structures ($*$), surroundings (\circ) and mean cell values ($\bar{}$) is given as:

$$\bar{\Psi} = \gamma^* \chi \Psi^* + (1 - \gamma^* \chi) \Psi^\circ \quad (29)$$

A perfectly stirred reactor model can describe the actual reaction in the fine structures. The change in species concentration depends on the reaction term $\dot{\omega}_i$ and the mixing term $\frac{1}{\tau^*} (Y_i^\circ - Y_i^*)$:

$$\frac{dY_i}{dt} = \dot{\omega}_i + \frac{1}{\tau^*} (Y_i^\circ - Y_i^*) \quad (30)$$

This leads to a set of ordinary differential equations with as many equations as number of species in the employed reaction mechanism, which has to be solved to steady-state. This system can become computationally very expensive to solve. Therefore, many CFD codes simplify the model to a plug flow reactor model, e.g. in Ansys Fluent (Ansys-Inc., n.d.) or OpenFoam® (Weller et al. 1998), by dropping the second term on the right-hand side in Equation (30). The plug-flow reactor simplification is also used within this work.

Parente's formulation

MILD combustion has been under investigation to reduce emissions in combustion devices. The reaction zone in MILD combustion is more distributed (Cavaliere and de Joannon 2004) and differs from the "classical" turbulent combustion, which was the basis of original EDC (Magnussen 1981) and the turbulent energy cascade model (Ertesvåg and Magnussen 1999). Many authors suggested to modify the constants C_γ and C_τ when simulating MILD combustion conditions, for example (De et al. 2011; Evans et al. 2015; Farokhi and Birouk 2016; Rehm et al. 2009). Parente et al. (2016) proposed, that for thickened and distributed flame structures in MILD combustion regimes, the speed of the fine structures u^* could be approximated by the turbulent flame speed S_{turb} . Furthermore, the length scale of the fine structures L^* can be related to the laminar flame speed S_L . Those assumptions are used for the derivation of EDC constants and yield relations depending on the turbulent Damköhler (Equation (33)) and Reynolds number (Equation (34)):

$$C_\tau \propto \frac{1}{\text{Da}_\eta \sqrt{\text{Re}_{\text{turb}} + 1}} \quad (31)$$

$$C_y \propto (\text{Da}_\eta)^{\frac{1}{2}} (\text{Re}_{\text{turb}} + 1)^{\frac{1}{2}} \quad (32)$$

$$\text{Da}_\eta = \frac{\tau_\eta}{\tau_{\text{chem}}} \quad (33)$$

$$\text{Re}_{\text{turb}} = \frac{k^2}{\nu \epsilon} \quad (34)$$

$$\tau_\eta = \sqrt{\frac{\nu}{\epsilon}} \quad (35)$$

The relations were further developed by the authors (Evans et al. 2019), introducing the factor $1/2$ in **Equation 31** and $(2/3)^{1/2}$ in **Equation 32**. The formulation of C_τ is then equal to Bao's formulation in the next section, therefore, the original modification was used in this study.

Bao's formulation

Bao (2017) used a similar approach as Parente to derive relationships for the EDC constants. The main difference is, that he derived a quantitative formulation by eliminating the laminar flame speed:

$$C_\tau = \frac{1}{2 \text{Da}_\eta \sqrt{\text{Re}_{\text{turb}} + 1}} \quad (36)$$

$$C_y = (\text{Da}_\eta)^{\frac{3}{4}} \sqrt{\frac{3}{2} (\text{Re}_{\text{turb}} + 1)} \quad (37)$$

Limits of the modified model constants

The model constants C_y and C_τ are calculated based on the relations given by Bao and Parente, but are limited to their original values, as suggested by both. Therefore, the maximum of C_y is its original value of 2.13 and the minimum of C_τ is 0.4082. To avoid unreasonable small or large values of C_y and C_τ and to ensure stability of the simulations also the Damköhler number was limited between 0.01 and 1000.

Figure 5 shows the model constants depending on the turbulent Reynolds number and the Damköhler number. The upper limit of the Damköhler number has virtually no effect on the model constants since they are always in the limit of the classical constant values in this range.

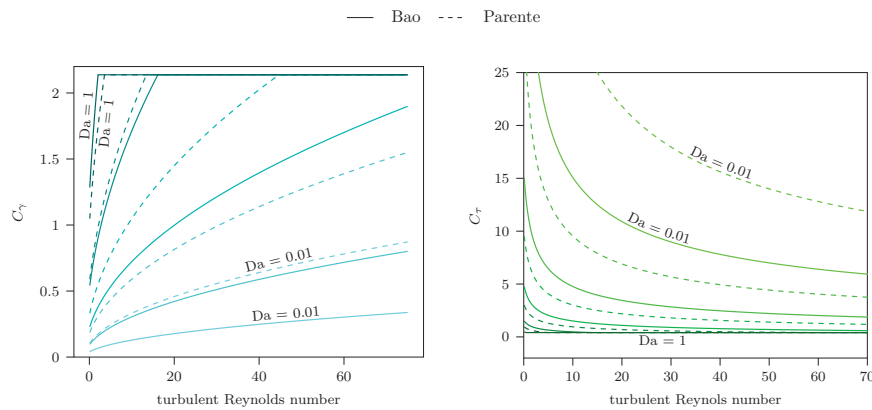


Figure 5. EDC Constants depending on Re_{turb} and Damköhler number Da_{η} ; Da_{η} is ranging from 0.01 (lightest color) to 1 (darkest color) and plots are logarithmically spaced between.

Numerical eigenvalue and eigenvector computation

For the chemical time scale definitions IETS and EVTS (see sections 3.8 and 3.9) the eigenvalues, and for EVTS also the eigenvectors, for a real nonsymmetric matrix have to be computed. The Jacobian matrix of the reaction system is in general neither sparse nor symmetric. The numerical calculation is usually done by first transforming the matrix into Hessenberg form and applying the eigenvalue search to this simplified matrix. The transformation can be conducted by a sequence of Householder transformations or by an elimination method analogous to Gaussian elimination with pivoting. Algorithmic details are presented in (Press et al. 2007; Wilkinson and Reinsch 1971). This algorithm needs approximately $5(N^3/3)$ operations (Press et al. 2007).

For the application in conjunction with the EDC, these operations need to be conducted at each time step and in each cell of the computational grid. This leads to long computational times which hinder practical applications of those eigenvalue based time scale formulations. Therefore, the IETS and EVTS will not be used in the flame simulations. Furthermore, the simple test cases showed that also simpler formulations approximate the analytically calculated chemical time scale well, section 4.1 and 4.2.

Numerical characterization of flame D

Sandia Flame D, a turbulent jet flame, is used to compare the time scales. Barlow and Frank (1998), Masri et al. (1996) provided detailed measurement data for this flame.

Although the modifications of the EDC, section 5.1, were suggested to improve the predictions for MILD combustion, they are also tested for the “classical” turbulent combustion regime to ensure their generality. As section 5.2 shows, for high turbulent Reynolds numbers and high Damköhler numbers the EDC model constants fall into the limit of the original EDC (Magnussen 2005).

The Flame was simulated in OpenFoam-6.x with an in-house code extension, based on the reactingFoam solver. The solver was modified to use the EDC-models from Parente

and Bao. A wedge of the flame is simulated consisting of 5 170 cells. The $k - \epsilon$ turbulence model (Jones and Launder 1972; Launder and Spalding 1974) was used with its original constants (Tannehill et al. 1984).

The suggested time scale formulations were tested with both, Parente's and Bao's EDC modification. The flame was simulated with the global Jones-Lindstedt mechanism (Jones and Lindstedt 1988) (see Table 1) and the detailed GRI-3.0 mechanism (Smith et al. 2018). This was done to study the effects of the difference in chemical time scale prediction on the flame simulation, because we saw already in the simplified test cases in section 4 that we get different results using a single-step and a comprehensive reaction mechanism.

Results using Jones-Lindstedt mechanism

The simulations using the time scale formulations IJTS, IRRTS and ETS failed to ignite the flame. The calculated characteristic chemical time scales were large and therefore, the Damköhler number was at the limit of $Da = 0.01$, which leads to low C_γ and high C_τ values. This usually happens in MILD combustion and depicts a thickening of the flame front, (Parente et al. 2016), but is not known to occur in "classical" turbulent flames.

The simulations with the other time scale formulations (SPTS, RTS, RPTS and OFTS) gave results in line with the experimental data, see Figure 6. The results were also compared with the original EDC formulation. The original EDC results are not shown to avoid overlaps. They are very close to the modified ones.

Figure 7 shows the characteristic chemical time scales for the simulation domain. The profiles show a qualitative agreement of the different definitions. Only the RPTS method gives a time scale decrease in the flame zone. This is probably caused by a scarcity of product species/produced species in this region. The differences in the absolute values can be more clearly seen in Figure 8 and in the deviations of the Damköhler number.

Figure 8 shows selected profiles of the characteristic chemical time scale and the Damköhler number. In some regions, especially outside the reaction zone, the Damköhler number is also at the lower limit with these time scale definitions. Low Damköhler values occur within the reaction zone for some time scale definitions. OFTS and RPTS even give Damköhler numbers below unity in this region. However, Figure 5 shows, that C_τ and C_γ might reach their original values even with these low Damköhler numbers, when the turbulent Reynolds number is sufficiently large.

Table 1. Methane combustion mechanism from Jones and Lindstedt (1988). Units in cm, s, cal and mol.

reactions	A	β	E_0	reaction orders
$\text{CH}_4 + 0.5 \text{O}_2 \rightarrow \text{CO} + 2 \text{H}_2$	7.820e13	0	30e3	$[\text{CH}_4]^{0.5}[\text{O}_2]^{1.25}$
$\text{CH}_4 + \text{H}_2\text{O} \rightarrow \text{CO} + 3 \text{H}_2$	0.300e12	0	30e3	$[\text{CH}_4][\text{H}_2\text{O}]$
$\text{H}_2 + 0.5 \text{O}_2 \leftrightarrow \text{H}_2\text{O}$	1.209e18	-1	40e3	$[\text{H}_2]^{0.25}[\text{O}_2]^{1.5}$
$\text{CO} + \text{H}_2\text{O} \leftrightarrow \text{CO}_2 + \text{H}_2$	0.275e13	0	20e3	$[\text{CO}][\text{H}_2\text{O}]$

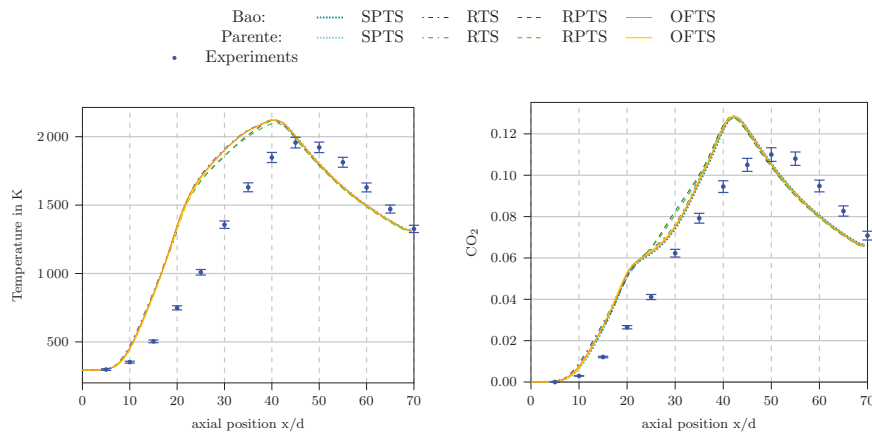


Figure 6. Temperature and CO_2 concentration profiles at the centerline of Flame D calculated using the Jones-Lindstedt mechanism.

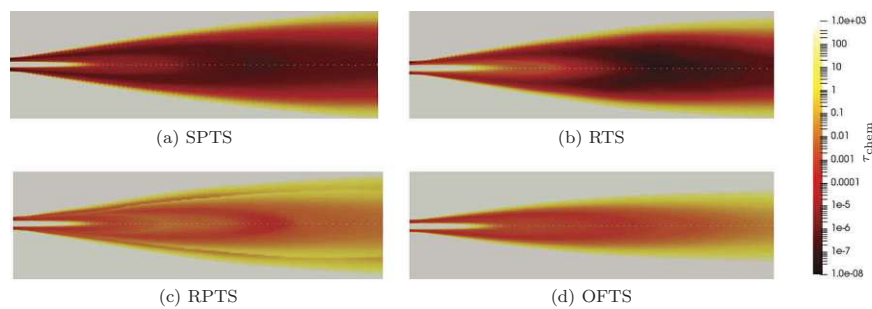


Figure 7. Characteristic chemical time scale in Flame D calculated with different methods using the Jones-Lindstedt mechanism. Upper half: Bao's formulation, lower half: Parente's formulation.

Results using GRI-3.0 mechanism

The OFTS, the IJTS, the IRRTS and ETS failed to ignite the flame also using the GRI-3.0 mechanism. Similar to the Jones and Lindstedt calculations (section 6.1) the Damköhler number was at its lower limit using those formulations.

Figure 9 shows the chemical time scales calculated with the methods SPTS, RTS and RPTS. The left half shows the simulation with Bao's formulation and the right half with Parente's.

The SPTS method gives lower chemical time scales in the reaction zone, whereas the other two methods give higher chemical time scale values in the reaction zone. This might seem unreasonable, since the reactions proceed faster in the reaction zone and, therefore, τ_{chem} should be lower than in the area surrounding the flame. It can be argued, that the characteristic chemical time scale can not be estimated properly outside the reaction zone because the reaction rate is close to zero. Therefore, τ_{chem} takes default values in these regions, which do not correspond to the state of the chemical system. In the actual "flame region", the SPTS method gives the lowest values inside the

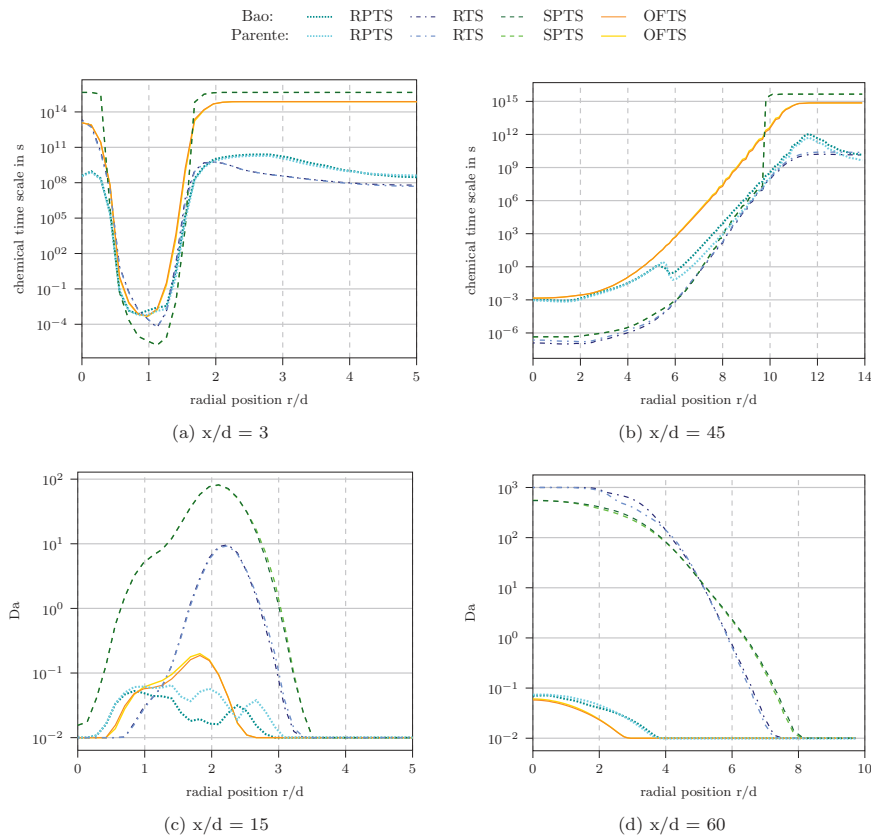


Figure 8. Profiles of the characteristic chemical time scale and the Damköhler number for Flame D simulated with the Jones-Lindstedt mechanism at different axial location.

flame and higher values at the flame fronts, where oxidizer and methane mix. For the RTS method, τ_{chem} is slower at the flame front, while the RPTS method gives low values in this region. The trends of SPTS and RTS are similar in the flame and at the flame fronts.

Figure 10 and Figure 11 underline these observations for certain radial and axial profiles. It has to be noted, that the SPTS method gives time scale values orders of magnitudes lower than the RTS and RPTS method. Therefore, SPTS is shown on the right axis.

In general, the time scale definitions SPTS, RTS and RPTS run into the limits for the original EDC values C_γ and C_τ with the complex reaction mechanism.

Comparison of the mechanisms

The difference between the formulation of Bao and Parente, section 5.1.1 and 5.1.2, are negligible compared to the differences induced by the different time scale formulations.

The IJTS, IRRTS and ETS methods modified the EDC constants in a way, that Flame D did not ignite in the simulation. The same holds true for the OFTS method in conjunction with

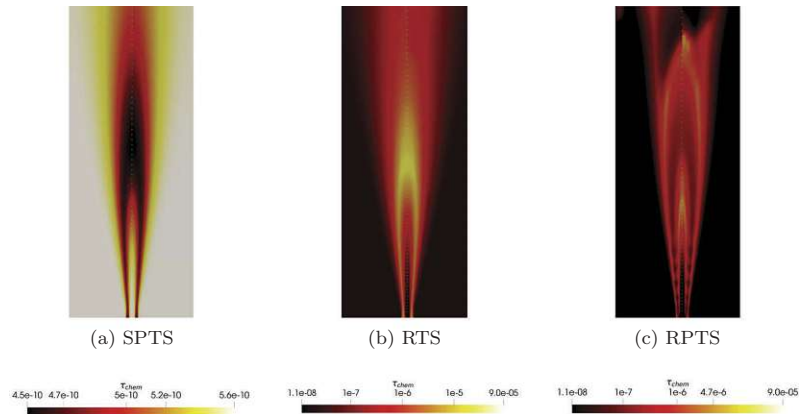


Figure 9. Characteristic chemical time scale in Flame D calculated with different methods (SPTS, RTS, RPTS). Left: Bao's formulation, Right: Parente's formulation.

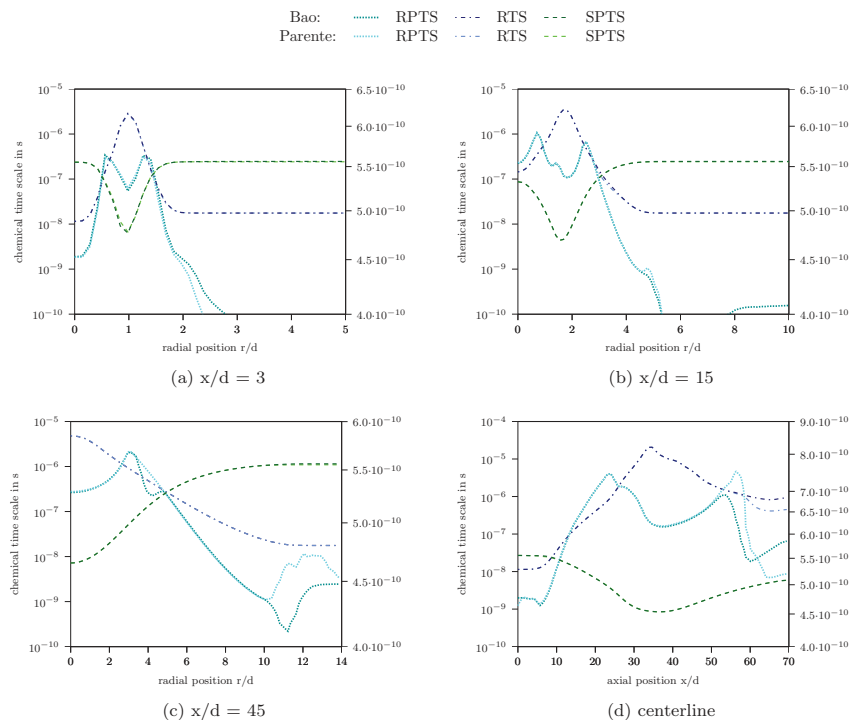


Figure 10. Profiles of the characteristic chemical time scale for Flame D simulated with GRI-3.0 at different radial and axial location(s). τ_{chem} calculated by the SPTS method is shown on the right axis in all the diagrams.

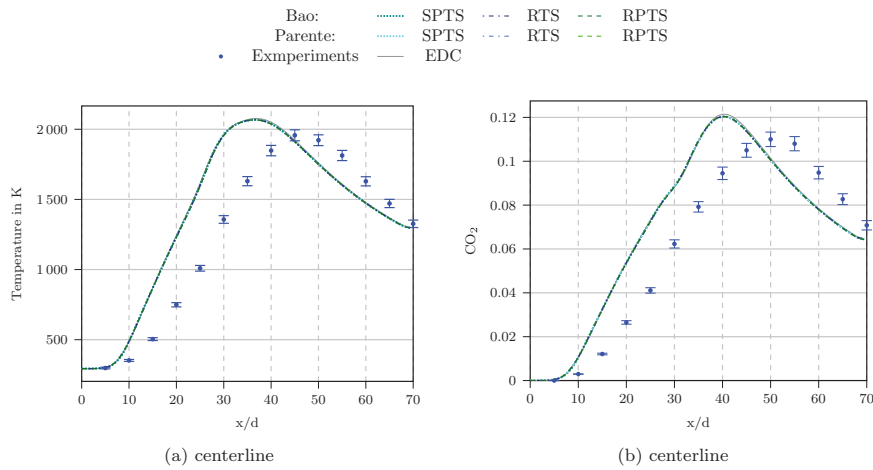


Figure 11. Temperature and CO₂ profiles at the centerline of Flame D calculated using GRI-3.0 mechanism.

the GRI-3.0 reaction mechanism. These time scale formulations should not be used in conjunction with the modified EDC, especially not for “classical” turbulent flames.

When comparing the definitions, which showed good results for Flame D, namely SPTS, RTS and RPTS, it has to be noted that they are strongly influenced by the reaction mechanism. Especially RTS and RPTS show different trends for the overall flame.

Numerical characterization of AJHC

To test the suggested EDC modifications for MILD conditions the Adelaide Jet in Hot Coflow (AJHC) Burner was chosen. It is a laboratory-scale burner, using methane and hydrogen. Dally, Karpetsis, and Barlow (2002) published extensive measurement data of the flame, with different levels of oxygen in the coflow (3, 6 and 9%). The cases are named HM1, HM2 and HM3. For this study HM1 was simulated as a wedge with 19 500 cells using the $k-\epsilon$ turbulence model with its original constants.

Compared to the Flame D simulations, a slightly different solver was used here to also account for differential diffusion effects. Christo and Dally (2005) showed that they play an essential role in MILD combustion simulations.

As for the classical combustion test case we employed two different reaction mechanisms, the Jones-Lindstedt mechanism (Jones and Lindstedt 1988) and the GRI-3.0 (Smith et al. 2018), as in section 6.1 and 6.2.

Results using Jones-Lindstedt mechanism

The Jones-Lindstedt mechanism (Table 1) was originally derived for methane oxidation, but it also incorporates hydrogen. It has already been used before for the simulation of hydrogen-methane flames, for example by Li et al. (2019).

The flame ignited only partially using the IRRTS formulation and extinction occurred, because the chemical time scales were large and lead to $Da = 0.01$ in the entire domain. This seems too low, even for a MILD combustion flame.

Also, the results using ETS were not very satisfactory. The high values of the chemical time scales lead to extinction of the flame, despite initial ignition. Damköhler numbers ranged from 0.01 to 1000. Therefore, the failure of this method could not be clearly related to an incorrect prediction of the Damköhler number.

The temperature profiles using the other characteristic chemical time scale formulations in conjunction with Bao's and Parente's EDC modification are shown in Figure 12. They all show reasonable agreement for the profiles at the $z = 4, 30$ and 60 mm locations. For $z = 120$ mm we see differences between the formulations. Bao's model in conjunction with IJTS underestimates the temperature. The flame in this simulation was not fully ignited. Using OFTS, the temperature peak was overestimated.

Figure 14 shows the Damköhler number for the flame simulations. The method, which overpredict the temperature peak the most (OFTS), have lower Damköhler numbers, especially compared to SPTS and RTS definition. OFTS might overestimate the characteristic chemical time scale leading to Damköhler numbers being too low.

The differences between the temperatures (Figure 12) are related to the chemical time scale definitions primarily and not to the EDC formulation (Bao vs. Parente). Only the IJTS method gives significantly different results for the two EDC constant formulations. Figure 13 reveals that those differences in temperature and other major scalars are caused by differences in γ^* and τ^* . The different γ^* and τ^* originate from the variable EDC constants C_τ and C_γ (Equation (26) and Equation (27)). The variation in those constants arises from the different chemical time scale approximations.

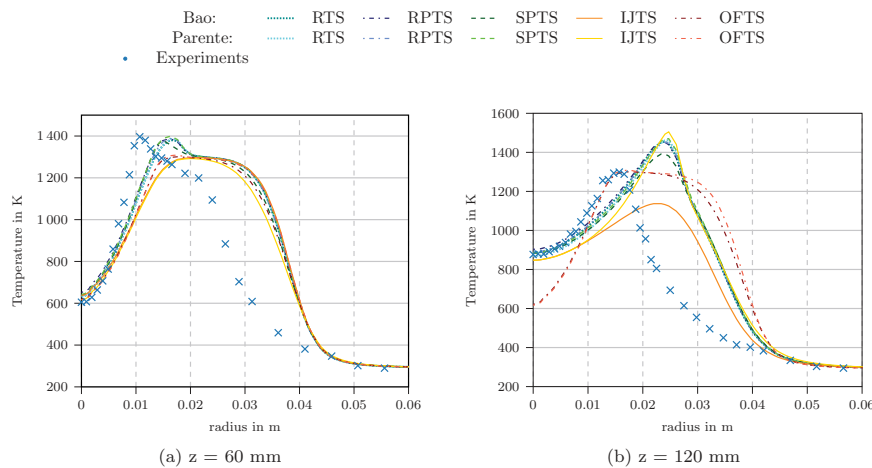


Figure 12. Radial temperature profiles at different locations for Adelaide Jet in Hot Coflow using the Jones-Lindstedt mechanism.

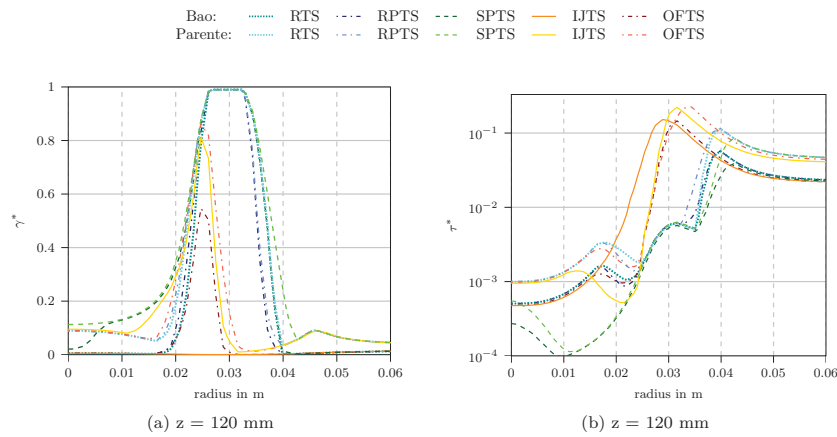


Figure 13. Radial profile for γ^* and τ^* at $z = 120$ mm for Adelaide Jet in Hot Coflow using the Jones-Lindstedt mechanism.

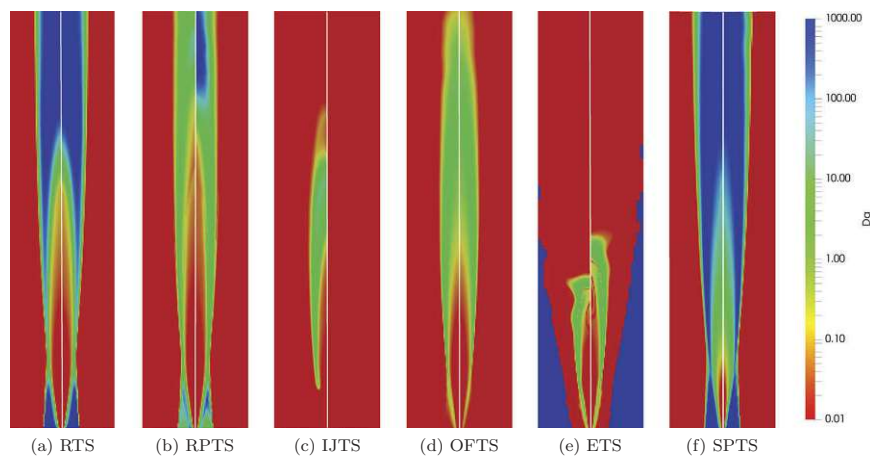


Figure 14. Damköhler numbers for the AJHC simulation domain ($r = 0-127$ mm, $z = 0-1$ m) using the Jones-Lindstedt mechanism; left: Parente's formulations, right = Bao's formulation.

Results using GRI-3.0 mechanism

Similarly to the simulation of Flame D using GRI-3.0 mechanism, only the RTS, RPTS and SPTS formulations show good results. The OFTS, LJTS, and IRRTS methods run into the limit of $Da = 0.01$ which lead to a failed ignition of the flame. Figure 15 shows the time scale methods which gave accurate results. For comparison, also the results using the original EDC model are shown. The modified models predict the temperature better for the profile at $z = 120$ mm (Figure 15b) but for the profile at $z = 60$ mm (Figure 15a) and $z = 30$ mm the modified models are superior.

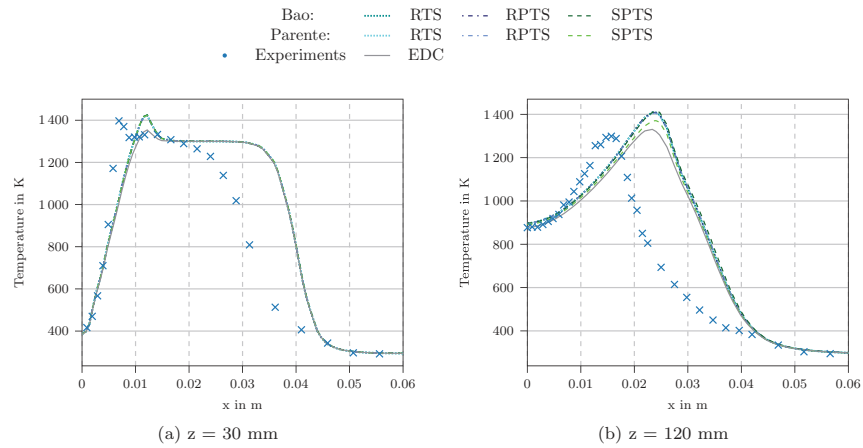


Figure 15. Radial temperature profiles at different locations for Adelaide Jet in Hot Coflow using GRI-3.0 mechanism.

Figure 16 shows selected chemical time scale profiles and the Damköhler number on the computational domain. The Damköhler number obtained with the SPTS method is not shown, since $Da = 1000$ in the whole domain. This seems unreasonable for a MILD combustion flame and suggests that the SPTS method underestimates the characteristic chemical time scale in combination with the GRI-3.0 mechanism.

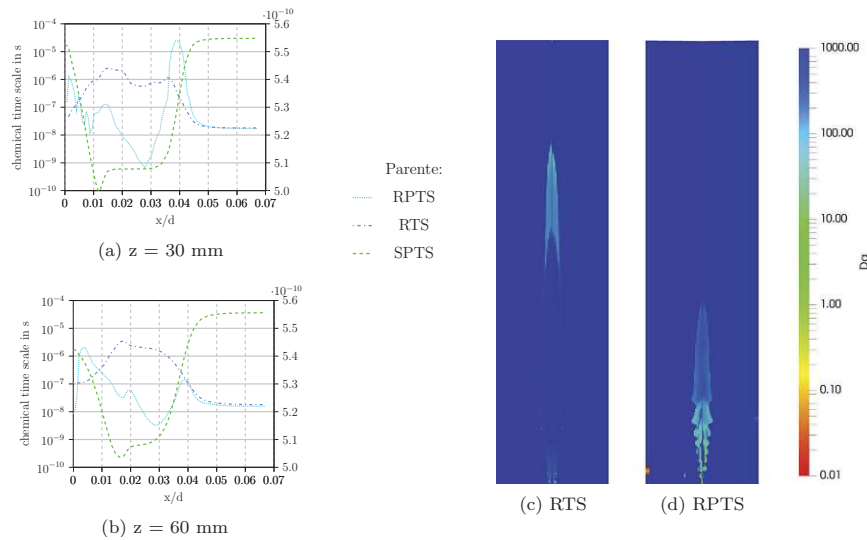


Figure 16. Chemical time scale profiles for AJHC using GRI-3.0 ((a) and (b) – SPTS on the right axis) and the Damköhler number ((c) and (d)) (left: Parente’s formulation, right plane: Bao’s formulation).

The characteristic chemical time scale profiles for $z = 30$ mm and $z = 60$ mm in Figure 16a and 16b (only the results with Parente's formulation are shown, since the results between the formulations do not differ significantly) show that SPTS gives values, which are orders of magnitudes lower than the others. This leads to the high Damköhler numbers. The other methods (RTS and RPTS) estimate lower characteristic chemical time scales and lead to Damköhler numbers, which seem high for a MILD combustion flame.

The differences between the original EDC formulation and the modified constants (Figure 15) is related to a difference in γ^* . The fine structure residence time values τ^* are nearly equivalent for all the cases. Figure 17 shows the differences in γ^* for selected profiles. (Only the results from Parente are depicted here, because Bao's formulation shows very similar results for γ^* .) The modified constants yield different results compared to the original EDC which agrees well with the differences seen in the temperature profiles (Figure 15).

Comparison of the mechanisms

Figure 18 compares the characteristic chemical time scales calculated with the Jones-Lindstedt and GRI-3.0 mechanism. For the definitions shown, the characteristic chemical time scales in conjunction with GRI-3.0 are orders of magnitudes lower than with the Jones-Lindstedt mechanism.

If we consider the chemical time scale as a value to characterize a flame, this depicts a problem with the available time scale approximations: They are highly dependent on the reaction mechanism. These variations could be eliminated by always using global mechanisms to approximate the characteristic chemical time scale.

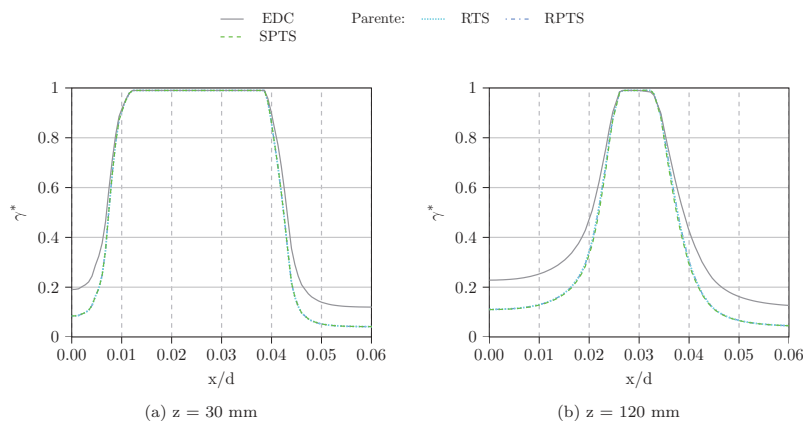


Figure 17. Radial profiles of γ^* at different locations for Adelaide Jet in Hot Coflow using GRI-3.0 mechanism.

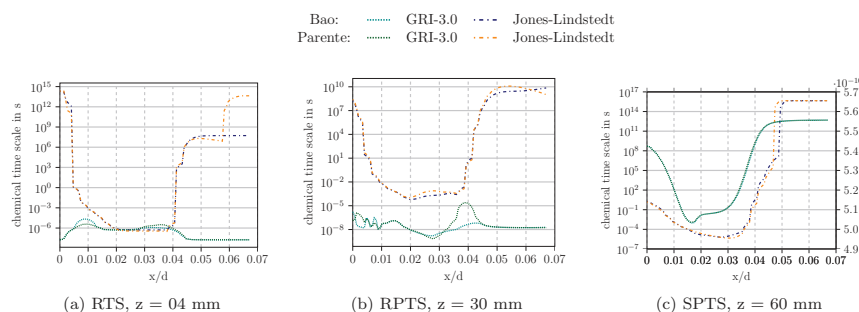


Figure 18. Comparison of chemical time scale profiles using Jones-Lindstedt and GRI-3.0 mechanism, In (c) the results from GRI-3.0 are shown on the right axis.

Conclusion

We presented various numerically efficient characteristic chemical time scale definitions – ranging from simple analytical expressions to complex eigenvalue based formulations. They were compared for a simple test case, where also an analytical eigenvalue can be computed. For this case, they all predict the trend of the time scales reasonably well. We see that, there are two groups, incorporating two different trends, though. One group, with the eigenvalue based methods approximate the analytic solution better.

Using a more complex reaction mechanism, the time scale predictions vary by several orders of magnitude and give different trends for the test case. Due to the lack of an analytical solution, the values can not be verified. Based on the simple test case, a good choice for the time scale approximation are the eigenvalue based definitions, for example EVTS, if fast computation of the time scale is not essential.

For CFD applications, such as the EDC model variations, the characteristic chemical time scale needs to be computed in every cell at every time step. In this case, eigenvalue based methods are not viable at the moment due to the numerical effort. Therefore, only the simpler formulations, without the need to compute eigenvalues, were tested for the flame simulations with the modified EDC.

The RTS, RPTS and SPTS seem to provide a suitable characteristic chemical time scale definition for combustion simulations. These formulations gave reasonable predictions for all test cases. Nevertheless, differences were observed and a great influence of the mechanism complexity on the chemical time scale was shown. This also leads to varying EDC model constants and consequently, differing simulation results.

Therefore, we suggest to use a simple, preferably one-step reaction mechanism, for the chemical time scale calculation, while using a complex chemical mechanism for the simulation. This enables comparable and consistent results, even when using chemical mechanisms with different levels of complexity. A detailed mechanism can be used to calculate temperatures and species concentrations, and a one step mechanism should be used to approximate the chemical time scale.

Parente et al. (2011) also used a single-step reaction mechanism for the determination of the chemical time scale and more complex ones for the calculation of the combustion

progress. Computational time was their reason for the global mechanism and no results using complex mechanisms were presented.

Within the tested time scale methods, the RTS, and SPTS gave the best results. The RPTS could also be a good choice, but shows some deficiencies since its formulation is only based on product species. Therefore, we recommend to use the RTS or SPTS formulation based on a single-step reaction mechanism for the modified EDC.

Disclosure statement

The authors declare no conflict of interest.

Funding

The authors gratefully acknowledge the funding support of K1-MET GmbH, metallurgical competence center. The research program of the competence center K1-MET is supported by COMET (Competence Center for Excellent Technologies), the Austrian program for competence centers. COMET is funded by the Federal Ministry for Transport, Innovation and Technology, the Federal Ministry for Digital and Economic Affairs, the province of Upper Austria, Tyrol, and Styria. Apart from funding, the project activities are financed by the industrial partners Primetals Technologies Austria, voestalpine Stahl and voestalpine Stahl Donawitz; Österreichische Forschungsförderungsgesellschaft [869295]. The authors acknowledge the TU Wien University Library for financial support through its Open Access Funding Program.

ORCID

Eva-Maria Wartha  <http://orcid.org/0000-0002-5564-8440>

Markus Bösenhofer  <http://orcid.org/0000-0003-3412-2113>

Michael Harasek  <http://orcid.org/0000-0002-6490-5840>

References

- Ansys-Inc. n.d.. *Ansys fluent theory guide release 17.0*. Canonsburg, PA, USA: Ansys Inc..
- Bao, H. (2017). *Development and validation of a new Eddy Dissipation Concept (EDC) model for MILD combustion*, Master's thesis, Delft University of Technology.
- Barlow, R. S., and J. H. Frank. 1998. Effects of turbulence on species mass fractions in methane/air jet flames. *Twenty-Seventh Symp. (Int.l) Combust.* 27:1087–95.
- Bösenhofer, M., E.-M. Wartha, C. Jordan, and M. Harasek. 2018. The eddy dissipation concept-analysis of different fine structure treatments for classical combustion. *Energies* 11:7.
- Caudal, J., B. Fiorina, M. Massot, B. Labégorre, N. Darabiha, and O. Gicquel. 2013. Characteristic chemical time scales identification in reactive flows. *Proc. Combust. Inst.* 34 (1):1357–64.
- Cavaliere, A., and M. de Joannon. 2004. MILD combustion. *Progr. Energy Combust. Sci.* 30 (4):329–66.
- Christo, F. C., and B. B. Dally. 2005. Modeling turbulent reacting jets issuing into a hot and diluted coflow. *Combust. Flame* 142 (1–2):117–29.
- Dally, B., A. Karpetsis, and R. Barlow. 2002. Structure of turbulent non-premixed jet flames in a diluted hot coflow. *Proc. Combust. Inst.* 29 (1):1147–54.
- De, A., E. Oldenhof, P. Sathiah, and D. Roekaerts. 2011. Numerical simulation of Delft- Jet-in-Hot-Coflow (DJHC) flames using the eddy dissipation concept model for turbulence- chemistry interaction. *Flow Turbul. Combust.* 87,4:537–67.

- Ertesvåg, I. S. 2019. Analysis of some recently proposed modifications to the Eddy Dissipation Concept (EDC) analysis of some recently proposed modifications to the Eddy Dissipation Concept (EDC). *Combust. Sci. Technol.* 1–29.
- Ertesvåg, I. S., and B. F. Magnussen. 1999. The eddy dissipation turbulence energy cascade model. *Combust. Sci. Technol.* 159 (1):213–35.
- Evans, M. J., P. R. Medwell, and Z. F. Tian. 2015. Modeling lifted jet flames in a heated coflow using an optimized Eddy Dissipation Concept model. *Combust. Sci. Technol.* 187 (7):1093–109.
- Evans, M. J., C. Petre, P. R. Medwell, and A. Parente. 2019. Generalisation of the eddy- dissipation concept for jet flames with low turbulence and low Damköhler number. *Proc. Combust. Inst.* 37:4497–505.
- Farokhi, M., and M. Birouk. 2016. Application of eddy dissipation concept for modelling biomass combustion, part 2: Gas-phase combustion modeling of a small-scale fixed bed furnace. *Energy Fuels* 30 (12):10800–08.
- Gerschgorin, S. 1931. Über die Abgrenzung der Eigenwerte einer Matrix. *Bulletin de l'Académie des Science de l'URSS. Classe des sciences mathématiques et na* 6:749–54.
- Gilbert, R. G., K. Luther, and J. Troe. 1983. Theory of thermal unimolecular reactions in the fall-off range. ii. weak collision rate constants. *Berichte der Bunsengesellschaft fr physikalische Chemie* 87 (2):169–77.
- Glassmaker, N. J. 1999. *Intrinsic low-dimensional manifold method for rational simplification of chemical kinetics*.
- Golovitchev, V. I., and J. Chomiak (2001). Numerical modeling of high temperature air "flameless" combustion, *The 4th International Symposium on High Temperature Air Combustion and Gasification, Rome, Italy*.
- Golovitchev, V. I., and N. Nordin. 2001. Detailed chemistry spray combustion model for the KIVA code by. *Int. Multidimension. Engine Model. User's Group Meeting SAE Congr.*
- Goodwin, D. G., H. K. Moffat, and R. L. Speth (2017). Cantera: An object-oriented software toolkit for chemical kinetics, thermodynamics, and transport processes, <http://www.cantera.org>. Version 2.3.0.
- Gran, I. R., and B. F. Magnussen. 1996. A numerical study of a bluff-body stabilized diffusion flame. Part 2. influence of combustion modeling and finite-rate chemistry. *Combust. Sci. Technol.* 119 (1–6):191–217.
- Isaac, B. J. (2014). *Principal component analysis-based combustion models*, PhD thesis, The University of Utah. <http://content.lib.utah.edu/cdm/singleitem/collection/etd3/id/2932/rec/1962>
- Isaac, B. J., A. Parente, C. Galletti, J. N. Thornock, P. J. Smith, and L. Tognotti. 2013. A novel methodology for chemical time scale evaluation with detailed chemical reaction kinetics. *Energy Fuels* 27 (4):2255–65.
- Jones, W., and R. Lindstedt. 1988. Global reaction schemes for hydrocarbon combustion. *Combust. Flame* 78:233–49.
- Jones, W. P., and B. E. Launder. 1972. The prediction of laminarization with a two-equation model of turbulence. *Int. J. Heat Mass Transfer* 15:301–14.
- Lam, S. H., and D. A. Goussis. 1991. Conventional asymptotics and computational singular perturbation for simplified kinetics modelling. In *Reduced kinetic mechanisms and asymptotic approximations for methane-air flames*, chapter 10. Berlin, Heidelberg: Springer Verlag.
- Launder, B. E., and D. B. Spalding. 1974. The numerical computation of turbulent flows. *Comput. Methods Appl. Mech. Eng.* 3:269–89.
- Lewandowski, M. T., I. S. Ertesvåg, and J. Pozorski (2017). Influence of the reactivity of the fine structures in modelling of the jet-in-hot-coflow flames with the eddy dissipation concept, *8th European Combustion Meeting, Dubrovnik, Croatia*.
- Li, Z., A. Cuoci, and A. Parente. 2019. Large eddy simulation of MILD combustion using finite rate chemistry: Effect of combustion sub-grid closure. *Proc. Combust. Inst.* 37:4519–29.
- Li, Z., A. Cuoci, A. Sadiki, and A. Parente. 2017. Comprehensive numerical study of the adelaide jet in hot-coflow burner by means of RANS and detailed chemistry. *Energy* 139:555–70.

- Li, Z., M. Ferrarotti, A. Cuoci, and A. Parente. 2018. Finite-rate chemistry modelling of non-conventional combustion regimes using a partially-stirred reactor closure: Combustion model formulation and implementation details. *Appl. Energy* 225:637–55.
- Lindemann, F. A., S. Arrhenius, I. Langmuir, N. R. Dhar, J. Perrin, and L. W. C. McC. 1922. Discussion on the radiation theory of chemical action. *Trans. Faraday Soc.* 17:598–606.
- Lövås, T., F. Mauss, C. Hasse, and N. Peters. 2002. Development of adaptive kinetics for application in combustion systems. *Proc. Combust. Inst.* 29:1403–10.
- Magnussen, B. F. (1981). On the structure of turbulence and a generalized eddy dissipation concept for chemical reaction in turbulent flow, *19th Aerospace Sciences Meeting, St. Louis, MO, USA*.
- Magnussen, B. F. (2005). The eddy dissipation concept—A bridge between science and technology, *ECCOMAS Thematic Conference on Computational Combustion, Lisbon, Portugal*.
- Masri, A. R., R. W. Dibble, and R. S. Barlow. 1996. The structure of turbulent nonpremixed flames revealed by Raman-Rayleigh-LIF measurements. *Progr. Energy Combust. Sci.* 22:307–62.
- Nagy, T., and T. Turányi. 2009. Relaxation of concentration perturbation in chemical kinetic systems. *React. Kinet. Catal. Lett.* 96 (2):269–78.
- Parente, A., M. R. Malik, F. Contino, A. Cuoci, and B. B. Dally. 2016. Extension of the eddy dissipation concept for turbulence/chemistry interactions to MILD combustion. *Fuel* 163:98–111.
- Parente, A., J. C. Sutherland, B. B. Dally, L. Tognotti, and P. J. Smith. 2011. Investigation of the MILD combustion regime via principal component analysis. *Proc. Combust. Inst.* 33 (2):3333–41.
- Press, W. H., S. A. Teukolsky, W. T. Vetterling, and B. P. Flannery. 2007. *Numerical recipes - the art of scientific computing*. Cambridge: Cambridge University Press.
- Prüfert, U., F. Hunger, and C. Hasse. 2014. The analysis of chemical time scales in a partial oxidation flame. *Combust. Flame* 161 (2):416–26.
- Rehm, M., P. Seifert, and B. Meyer. 2009. Theoretical and numerical investigation on the EDC-model for turbulence–chemistry interaction at gasification conditions. *Comput. Chem. Eng.* 33 (2):402–07.
- Ren, Z., and G. M. Goldin. 2011. An efficient time scale model with tabulation of chemical equilibrium. *Combust. Flame* 158 (10):1977–79.
- Smith, G. P., D. M. Golden, M. Frenklach, N. W. Moriarty, B. Eiteneer, M. Goldenberg, C. T. Bowman, R. K. Hanson, S. Song, W. C. Gardiner Jr., et al. (2018). GRI-Mech 3.0.
- Stewart, P., C. Larson, and D. Golden. 1989. Pressure and temperature dependence of reactions proceeding via a bound complex. 2. application to $2\text{CH}_3 + \text{C}_2\text{H}_5 + \text{H}$. *Combust. Flame* 75 (1):25–31.
- Tannehill, J. C., D. A. Anderson, and R. H. Pletcher. 1984. *Computational fluid mechanics and heat transfer. Second*. Boca Raton: CRC Press.
- Tomlin, A. S., L. Whitehouse, and M. J. Pilling. 2002. Low-dimensional manifolds in tropospheric chemical systems. *Faraday Discuss.* 120:125–46.
- Troe, J. 1983. Theory of thermal unimolecular reactions in the fall-off range. i. strong collision rate constants. *Berichte der Bunsengesellschaft für physikalische Chemie* 87 (2):161–69.
- Tsang, W., and J. T. Herron. 1991. Chemical kinetic data base for propellant combustion i. reactions involving NO , NO_2 , HNO , HNO_2 , HCN and N_2O . *J. Phys. Chem. Ref. Data* 20 (4):609–63.
- Weller, H., G. Tabor, H. Jasak, and C. Fureby. 1998. A tensorial approach to computational continuum mechanics using object-oriented techniques. *Comput. Phys.* 12:6.
- Westbrook, C. K., and F. L. Dryer. 1981. Simplified reaction mechanisms for the oxidation of hydrocarbon fuels in flames. *Combust. Sci. Technol.* 27 (1–2):31–43.
- Wilkinson, J., and C. Reinsch. 1971. *Handbook for automatic computation, vol. II, linear algebra*. Springer-Verlag Berlin Heidelberg, New York.

Paper 2

Importance of considering interstitial fluid effects in the kinetic theory of granular flow for raceway formation prediction

published in Chemical Engineering Science in collaboration with Markus Bösenhofer and Michael Harasek.

My contribution: Implementation and validation of the closure models in OpenFOAM. Formal analysis of the models. Carrying out the simulations and analyzing the results. Visualization of the results. Conceptualization and writing the original draft of the paper.

E. M. Wartha, M. Bösenhofer, and M. Harasek (2022b). “Importance of considering interstitial fluid effects in the kinetic theory of granular flow for raceway formation prediction”. In: *Chemical Engineering Science* 247, p. 117026. ISSN: 00092509. DOI: 10.1016/j.ces.2021.117026



Contents lists available at ScienceDirect

Chemical Engineering Science

journal homepage: www.elsevier.com/locate/ces

Importance of considering interstitial fluid effects in the kinetic theory of granular flow for raceway formation prediction

Eva-Maria Wartha^{a,*}, Markus Bösenhofer^{a,b}, Michael Harasek^a

^aTechnische Universität Wien, Institute of Chemical Environmental and Bioscience Engineering, Getreidemarkt 9/166, 1060 Wien, Austria

^bK1-Met GmbH, Area 4 - Simulation and Analyses, Stahlstrasse 14, BG88, 4020 Linz, Austria



HIGHLIGHTS

- Comparison between different closure models for the kinetic theory of granular flow.
- Influence of considering interstitial fluid effects in closure models.
- Improved raceway shape prediction when considering interstitial fluid effects.

ARTICLE INFO

Article history:

Received 10 June 2021

Received in revised form 23 July 2021

Accepted 13 August 2021

Available online 19 August 2021

Keywords:

Kinetic Theory of Granular Flow

Computational Fluid Dynamics

Interstitial Fluid Effects

Raceway Formation

Two-Fluid Model

ABSTRACT

Owing to its computational efficiency, the two-fluid model is widely used in computational fluid dynamics (CFD) to describe gas–solid flows in large-scale industrial processes. The motion of the solid phase is commonly modeled by the kinetic theory of granular flow (KTGF). The main conceptual difference between the two commonly used KTGF closure relations, namely the closure models by Lun et al. (1984) and Agrawal et al. (2001), is the treatment of the interstitial fluid. We theoretically compare both models and investigate their effects on simulation results. The interstitial fluid effects are essential during the raceway shape prediction but can be neglected in the fluidized bed regime. The correct prediction of the raceway size and shape is essential for predicting the processes in the raceway zone of ironmaking blast furnaces. Our results show that considering the interstitial fluid effects in the KTGF enables more accurate predictions in the raceway regime.

© 2021 The Author(s). Published by Elsevier Ltd. This is an open access article under the CC BY license (<http://creativecommons.org/licenses/by/4.0/>).

1. Introduction

Chemical engineering processes often involve gas–solid flows, such as the flow behaviors of fluidized beds in gasification processes, packed beds in adsorption columns, or slowly moving beds in blast furnaces or grate combustors. Computational fluid dynamics (CFD) can better clarify the intrinsic processes and predict flow structures and temperatures, pressure, and species concentration profiles, especially for processes where direct measurements are unfeasible owing to the conditions. Thus, CFD has become a vital tool for developing and optimizing complex processes by virtual experiments.

Different concepts for modeling gas–solid flows are available in the field of CFD: CFD-DEM (discrete element method), multiphase-particle-in-cell (MPPIC), or two-fluid models (TFMs). The main difference between these approaches is related to the solid-phase description. In CFD-DEM the particle–particle contacts are

resolved, which requires small time steps and leads to high computational demand, thus, the approach is unfavorable for large-scale applications (Almohammed et al., 2014; Chiesa et al., 2005; Lichtenegger and Pirker, 2018). The MPPIC method is an Eulerian–Lagrangian method that resolves the particle–particle interaction on an Eulerian grid (Snider et al., 1998), but tracking each parcel increases the computational cost. Contrary to the two above-mentioned modeling approaches, TFMs treat the solid and the fluid phase as interpenetrating continua. The kinetic theory of granular flow (KTGF) is often used to describe the solid rheology in this modeling approach. Within this framework, a granular temperature is used, which is related to the solid velocity fluctuations. The granular temperature equation requires closure models for the production and consumption terms (Gidaspow, 1994; Lun and Savage, 1986; Savage, 1998; Agrawal et al., 2001).

One conceptual difference among the available closure models is whether they consider the interstitial fluid effects (Agrawal et al., 2001) or not (Lun et al., 1984). The models by Agrawal et al. (2001) and Lun et al. (1984) have been widely used in the literature (Passalacqua and Marmo, 2009; Schneiderbauer et al.,

* Corresponding author.

E-mail address: eva-maria.wartha@tuwien.ac.at (E.-M. Wartha).

<https://doi.org/10.1016/j.ces.2021.117026>

0009-2509/© 2021 The Author(s). Published by Elsevier Ltd.

This is an open access article under the CC BY license (<http://creativecommons.org/licenses/by/4.0/>).

Nomenclature

Latin symbols Variable Name Unit

a	constant -
C_D	drag coefficient for a sphere -
e_p	restitution coefficient -
d	diameter m
g_o	radial distribution function -
\mathbf{g}	gravitational acceleration m s^{-2}
k	turbulent kinetic energy m^2s^{-2}
p	pressure $\text{kg m}^{-1}\text{s}^{-2}$
t	time s
U	circumference m
\mathbf{v}	velocity vector ms^{-1}

Greek symbols

α	volume fraction -
β	momentum exchange term $\text{kg m}^{-3} \text{s}^{-1}$
γ_s	collisional dissipation $\text{kg m}^{-1} \text{s}^{-3}$
ϵ	energy dissipation rate m^2s^{-3}
η	modified restitution coefficient -
Θ	granular temperature $\text{m}^2 \text{s}^{-2}$
κ_s	solid conductivity $\text{kg m}^{-1} \text{s}^{-1}$
λ	thermal conductivity $\text{kg m}^{-1} \text{s}^{-1}$
μ	viscosity Pas
ν	viscosity m^2s^{-1}
ρ	density kg m^{-3}

σ_s	solid stress Pa
Φ	angle of internal friction °
ϕ_s	sphericity coefficient -

Sub- and superscripts

s	solid
g	gas
b	bulk
*	modified (to account for interstitial gas effects)
fric	frictional
ktgf	kinetic theory of granular flow
min	minimum
max	maximum
rel	relative
RW	raceway

Abbreviations

RHS	right-hand side
LHS	left-hand side
CFD	computational fluid dynamics
KTGF	kinetic theory of granular flow
TFM	two-fluid model
DEM	discrete element method
MPPIC	multiphase particle in cell

2012; Zhao et al., 2020) and are implemented in simulation codes. For example, the model by Lun et al. (1984) is implemented in OpenFOAM, and that by Agrawal et al. (2001) is implemented in the MFIX code (Syamlal et al., 1993; Benyahia et al., 2012). The work by Agrawal et al. (2001) is considering the drag force calculated with the instantaneous fluid and gas velocities in the derivation of the KTGF closures, as suggested by Balzer et al. (1995); Ma and Ahmadi (1988). To our knowledge, no in-depth comparison of these models has been presented thus far. Therefore, we investigate the difference between these KTGF closure models and their effects on the simulation results for various applications.

A more extensive incorporation of interstitial fluid effects in the derivation of the KTGF was presented by Garzó et al. (2012). They also modeled the instantaneous particle acceleration and incorporated it in the derivation. The original model by Lun et al. (1984) is derived based on the inelastic particle assumption - as the Agrawal et al. (2001) model - whereas the solution by Garzó et al. (2012) is obtained by using the method for states near the local homogeneous cooling state. Therefore, we limit our study to the comparison between the Lun et al. (1984) and Agrawal et al. (2001) model.

We examine the differences between the models theoretically and practically by applying them to classical chemical engineering applications. A simple bubble formation case, a fluidized bed case, and raceway formation cases were evaluated. Lab-scale setups were chosen, where experimental data and DEM results were available. This work focuses on raceway formation because we aim to improve the predictive raceway modeling of our open-source model (Bösenhofer et al., 2019; Bösenhofer, 2020), to improve the economic efficiency and sustainability of blast furnaces (Kuang et al., 2018).

2. Model Description and Theoretical Discussion

In TFMs, both phases are treated as interpenetrating continua, so that we obtain averaged continuity and momentum equations, Eqs. (1)–(4), for both phases. In the equations, α refers to the phase fraction, ρ to the density, \mathbf{v} to the velocity, σ to the stress, \mathbf{g} to the

gravitational acceleration and t to the time. The subscripts s and g refer to solid and gas, respectively.

$$\frac{\partial}{\partial t} \alpha_g \rho_g + \nabla \cdot (\alpha_g \rho_g \mathbf{v}_g) = 0 \tag{1}$$

$$\frac{\partial}{\partial t} \alpha_s \rho_s + \nabla \cdot (\alpha_s \rho_s \mathbf{v}_s) = 0 \tag{2}$$

The continuity equations have to be reformulated to ensure the conservativeness as presented by Weller (2005) and Passalacqua and Fox (2011). We use a blended approach between an implicit solution and the multidimensional universal limiter with explicit solution (Tacconi, 2018) presented in (Wartha et al., 2020) to solve the reformulated phase continuity equations.

The momentum equations, Eqs. (3) and (4), are coupled through momentum exchange terms; here, the drag $\beta(\mathbf{v}_g - \mathbf{v}_s)$ and the virtual mass force (F_{VM}) terms are considered and other inter-phase forces are neglected.

$$\frac{\partial}{\partial t} (\alpha_g \rho_g \mathbf{v}_g) + \nabla \cdot (\alpha_g \rho_g \mathbf{v}_g \mathbf{v}_g) = -\alpha_g \nabla \cdot \sigma_g - \beta(\mathbf{v}_g - \mathbf{v}_s) + \rho_g \alpha_g \mathbf{g} + F_{VM} \tag{3}$$

$$\frac{\partial}{\partial t} (\alpha_s \rho_s \mathbf{v}_s) + \nabla \cdot (\alpha_s \rho_s \mathbf{v}_s \mathbf{v}_s) = -\alpha_s \nabla \cdot \sigma_s + \beta(\mathbf{v}_g - \mathbf{v}_s) + \rho_s \alpha_s \mathbf{g} + F_{VM} \tag{4}$$

In addition to the continuity, momentum, and energy equations, a closure relation for the solid stress is required. This can be the KTGF, whose development method is analogous to that of the kinetic theory of dense gases. Based on the KTGF, a granular temperature Θ is introduced, which is defined as one-third of the mean square of the particle velocity fluctuations. This pseudo-temperature is balanced as shown in Eq. (5) and is related to the solid stress σ_s .

$$\underbrace{\frac{3}{2} \left[\frac{\partial}{\partial t} (\alpha_s \rho_s \Theta) + \nabla \cdot (\alpha_s \rho_s \Theta \mathbf{v}_s) \right]}_{\text{Dissipation or Creation exerted by the gas}} = - \underbrace{\sigma_s : \nabla \mathbf{v}_s}_{\text{Creation due to shear}} + \underbrace{\nabla \cdot (\kappa_s \nabla \Theta)}_{\text{Diffusive Transport}} - \underbrace{\gamma_s}_{\text{Collisional Dissipation}} \tag{5}$$

Table 1
Overview of the employed models in this publication.

Variable	Compared Models	Section
Closure Models for the KTGF		
σ_s solid stress	With and without interstitial fluid effects (Lun et al., 1984) (Agrawal et al., 2001)	2.1.1
κ_s solid conductivity		2.1.2
γ_s collisional dissipation		2.1.3
J_s dissipation or creation exerted by the gas		2.1.4
g_0		(Carnahan and Starling, 1969)
Frictional Models		
p_s frictional pressure	(Srivastava and Sundaresan, 2003) (Schaeffer, 1987)	2.3
μ_s frictional viscosity		
Momentum Exchange Terms		
β momentum exchange term	(Gidaspow, 1994)	2.4

The terms on the right-hand side (RHS) in Eq. (5) represent the dissipation or creation exerted by the gas J_s , the creation of fluctuating energy due to shear, the diffusion of fluctuating energy, and the dissipation due to inelastic particle collisions γ_s (Agrawal et al., 2001); κ_s represents the diffusivity of the granular temperature.

Different closure relations exist for the terms on the RHS, but the most widely used are based on the work by Lun et al. (1984). They assume binary particle–particle interactions and nearly inelastic particles, while the role of the interstitial fluid was neglected. Hereafter, the model based on these assumptions will be referred to as the Lun model.

Agrawal et al. (2001) proposed modified closure relations for the equation of granular temperature. The relations are based on the findings of Balzer et al. (1995), Boelle et al. (1995), Koch and Sangani (1999), who showed that the effect of the interstitial fluid is essential in gas–solid flows. These closure relations are hereafter referred to as the Agrawal model.

In the classical derivation of the KTGF, only instantaneous and binary interactions between the particles are considered, however, frictional contacts between the particles also exist at high solid volume fractions. Frictional models have been developed to account for those effects above a certain solid volume fraction α_{\min} . The different frictional models considered in this paper are described in Section 2.3.

The main focus of this paper is to compare the Lun and Agrawal closure models for the KTGF. The Lun model neglects interstitial fluid effects, while the Agrawal model considers them. Additional models are required to simulate gas–solid flows: frictional models for high solid volume fractions, and gas–solid drag models for the momentum exchange. These models are introduced in the next section. Table 1 summarizes the employed models and indicates the section in which they are discussed. A general overview on models for the KTGF can be found in van Wachem (2000).

2.1. Closure Relations for the KTGF

The different terms for the closure of the KTGF from Lun et al. (1984) and Agrawal et al. (2001) are explained in the next section. Special emphasis is placed on the difference between the two formulations and how interstitial fluid effects are considered by the Agrawal model.

2.1.1. Solid Stress

Lun et al. (1984) proposed the following expression to model the solid stress σ_s for slightly inelastic particles:

$$\sigma_s = \left[\rho_s \alpha_s [1 + 2(1 + e_p) \alpha_s g_0] \text{granularpressurecoeff.} \Theta - \eta \mu_b (\nabla \cdot v_s) \right] \bar{\mathbb{I}} - \left[\frac{2\mu}{g_0 \eta (2 - \eta)} \left(1 + \frac{8}{5} \alpha_s \eta g_0 \right) \left(1 + \frac{8}{5} \eta (3\eta - 2) \alpha_s g_0 \right) + \frac{6}{5} \eta \mu_b \right] \text{solidviscosity} \bar{\mathbb{S}} \quad (6)$$

The first part of Eq. (6) represents the granular pressure, where η is a modified restitution coefficient, Eq. (7), and g_0 is the radial distribution function. Different expressions to model the radial distribution function are discussed in Section 2.2. Alternative closures for the granular pressure exist, see (van Wachem, 2000) for an overview.

The second part of Eq. (6) is also called the solid viscosity. The tensor $\bar{\mathbb{S}}$ is defined in Eq. (8). The expressions for the viscosity μ and the bulk viscosity μ_b are given by Eqs. (9) and (10), respectively.

$$\eta = \frac{1 + e_p}{2} \quad (7)$$

$$\bar{\mathbb{S}} = \frac{1}{2} (\nabla v_s + (\nabla v_s)^T) - \frac{1}{3} (\nabla v_s) \bar{\mathbb{I}} \quad (8)$$

$$\mu = \frac{5\rho_s d \sqrt{\pi} \Theta}{96} \quad (9)$$

$$\mu_b = \frac{256\mu\alpha_s^2 g_0}{5\pi} = \frac{8}{3} \rho_s d_s \alpha_s^2 g_0 \sqrt{\frac{\Theta}{\pi}} \quad (10)$$

Agrawal et al. (2001) used the same expression as Lun et al. (1984) for the granular pressure but substituted μ with μ^* , Eq. (12), in the expression for the solid viscosity to account for the effects of the interstitial fluid, Eq. (11). Additionally, a factor $\frac{2+a}{3}$ was added to the solid viscosity, which was introduced by Johnson and Jackson (1987). This leads to the following equation for the solid stress:

$$\sigma_s = \left[\rho_s \alpha_s [1 + 2(1 + e_p) \alpha_s g_0] \text{granularpressurecoeff.} \Theta - \eta \mu_b (\nabla \cdot v_s) \right] \bar{\mathbb{I}} - \left(\frac{2+a}{3} \right) \left[\frac{2\mu^*}{g_0 \eta (2 - \eta)} \left(1 + \frac{8}{5} \alpha_s \eta g_0 \right) \left(1 + \frac{8}{5} \eta (3\eta - 2) \alpha_s g_0 \right) + \frac{6}{5} \eta \mu_b \right] \text{solidviscosity} \bar{\mathbb{S}} \quad (11)$$

The modified viscosity μ^* incorporates the momentum exchange term β to account for the effects of the interstitial fluid, Eq. (12). Different drag models can be used to calculate β , however, we use the Gidaspow drag model in this work, which is discussed in Section 2.4.

$$\mu^* = \frac{\mu}{1 + \frac{2\beta\mu}{(\rho_s \alpha_s)^2 g_0 \Theta}} \quad (12)$$

For typical parameters (Table 2) in a gas–solid flow the dimensionless solid viscosities obtained from the two different closure models are compared in Fig. 1. At high solid volume fractions, there is only a slight difference between the solid viscosities, but the difference is significant at small solid volume fractions and high granular temperatures. The relative velocity U_{rel} does influence the drag, but has only a minor influence on the solid viscosity in this parameter space. The Agrawal model gives lower solid viscosities at these con-

Table 2
Typical values used to compare the solid viscosity and the solid conductivity.

e_p	ρ_s	μ_g	ρ_g	Θ	C_D	g_0
0.8	1200	10^{-5}	1.2	10^{-4} - 10^3	0.44	Carnahan Starling Model

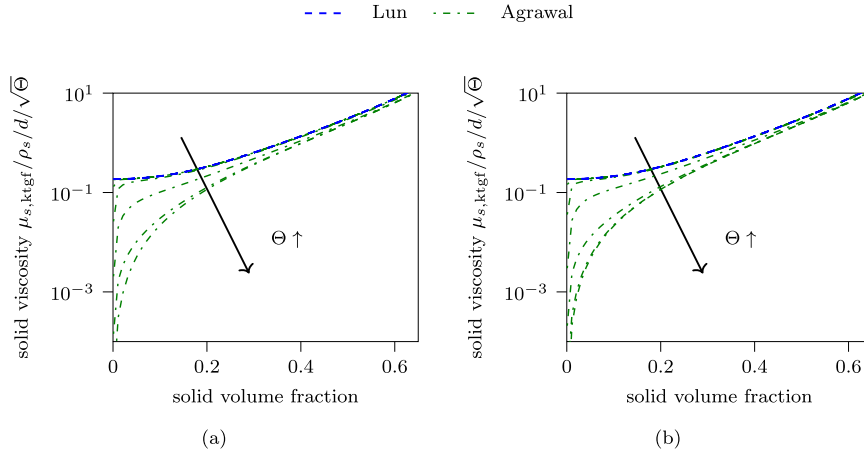


Fig. 1. Comparison of the dimensionless solid viscosity for (a) $U_{ref} = 10\text{ms}^{-1}$ and (b) $U_{ref} = 100\text{ms}^{-1}$ for typical conditions in Table 2.

ditions. The dimensionless Lun solid viscosity becomes independent of the granular temperature.

2.1.2. Solid Conductivity

The solid conductivity was modeled by Lun et al. (1984) as presented in Eq. (13). A second term occurs in the original publication, which is supposed to be small compared with the first one and therefore, is mostly neglected, as done here and in the work by van Wachem (2000).

$$\kappa_s = \frac{\lambda}{g_0} \left[\left(1 + \frac{12}{5} \eta \alpha_s g_0\right) \left(1 + \frac{12}{5} \eta^2 (4\eta - 3) \alpha_s g_0\right) + \frac{64}{25\pi} (41 - 33\eta) \eta^2 \alpha_s^2 g_0^2 \right] \quad (13)$$

$$\lambda = \frac{75 \rho_s d \sqrt{\pi \Theta}}{48 \eta (41 - 33 \eta)} \quad (14)$$

Agrawal et al. (2001) used a similar formulation for the solid conductivity. They replaced λ with a modified conductivity term (λ^*) to account for the interstitial fluid effects. Similar to the solid viscosity, the momentum exchange term β was incorporated to account for the interstitial fluid effects:

$$\lambda^* = \frac{\lambda}{1 + \frac{6\beta\lambda}{5(\rho_s \alpha_s)^2 g_0 \Theta}} \quad (15)$$

Several other solid conductivity models have been proposed in the literature, and a comprehensive review of common models can be found in the work by van Wachem (2000). Here, we compare the models by Agrawal et al. (2001) and Lun et al. (1984), since this paper focuses on the effect of the interstitial fluid in the KTGF on gas–solid flows.

Fig. 2 compares the normalized Agrawal and Lun solid conductivities for the same conditions as Fig. 1 does for the solid viscosity. Fig. 2 reveals that the differences between the models vanish at low granular temperatures but become significant at high granular temperatures and low solid volume fractions. The relative velocity clearly influences the solid conductivity with the Agrawal model, which can be seen comparing Fig. 2 (a) and (b).

2.1.3. Collisional Dissipation

The definition of the collisional dissipation rate in (Lun et al., 1984 and Agrawal et al., 2001) is the same and given by the following equation:

$$\gamma_s = 12 \left(1 - e_p^2\right) \frac{\alpha_s^2 \rho_s}{d_s \sqrt{\pi}} g_0 \Theta^{3/2} \quad (16)$$

2.1.4. Dissipation or Creation Exerted by the Gas

The following correlation is given by van Wachem (2000):

$$J_s = \beta \left(3\Theta - \frac{\beta d_s (\mathbf{v}_g - \mathbf{v}_s)^2}{4\alpha_s \rho_s \sqrt{\pi \Theta}} \right) \quad (17)$$

Agrawal et al. (2001) used the same closure relation but divided the second term by the radial distribution function. By introducing the drag after formulation and using the the drag coefficient relation ($C_D = 24/\text{Re}$), we obtain the following equation:

$$J_s = 3\beta\Theta - \frac{81\alpha_s \mu_g^2 (\mathbf{v}_g - \mathbf{v}_s)^2}{g_0 d_s^2 \rho_s \sqrt{\pi \Theta}} \quad (18)$$

2.2. Radial Model

Different models for the radial distribution function exist. For the simulations presented in this paper, the Carnahan–Starling model is used (Carnahan and Starling, 1969):

$$g_0 = \frac{1}{1 - \alpha} + \frac{3\alpha}{2(1 - \alpha)^2} + \frac{\alpha^2}{2(1 - \alpha)^3} \quad (19)$$

van Wachem (2000) provides a good overview of different radial models. A drawback of the Carnahan–Starling model is that it does not tend to the correct limit at the maximum solid volume fraction. In the next section, we show that close to the maximum packing limit the frictional contribution outweighs that from the kinetic theory by orders of magnitude. Therefore, the Carnahan–Starling

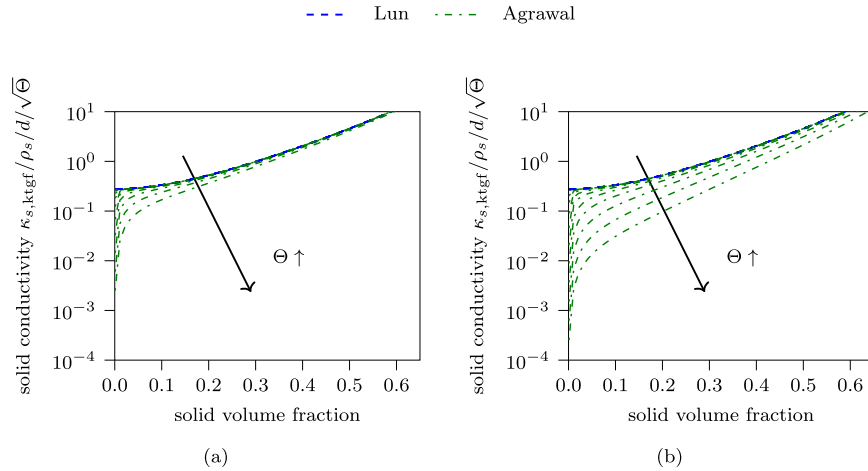


Fig. 2. Comparison of solid conductivity for (a) $U_{rel} = 10\text{ms}^{-1}$ and (b) $U_{rel} = 100\text{ms}^{-1}$ for typical conditions in Table 2.

model can be applied in conjunction with the chosen frictional models.

2.3. Frictional Models

At high solid volume fractions, besides instantaneous and binary interactions, frictional effects become important. A frictional pressure $p_{s,fric}$ and a frictional viscosity $\mu_{s,fric}$ are added to the solid pressure and viscosity above a solid volume fraction threshold α_{min} , Eqs. (20) and (21), to account for these frictional effects.

$$p_s = p_{s,ktgf} + p_{s,fric} \quad (20)$$

$$\mu_s = \mu_{s,ktgf} + \mu_{s,fric} \quad (21)$$

Different models describing the frictional pressure and viscosity have been proposed in the literature. In the following section, we discuss the frictional models used for the subsequent simulations. An extensive comparison of different frictional stress models can be found in (Venier et al., 2018; Passalacqua and Marmo, 2009).

2.3.1. Schaeffer Frictional Model

The Schaeffer frictional stress model (Schaeffer, 1987) defines the frictional pressure $p_{s,fric}$ and the frictional viscosity $\nu_{s,fric}$ as follows:

$$p_{s,fric} = 10^{25} (\alpha_s - \alpha_{min})^{10} \quad (22)$$

$$\mu_{s,fric} = 0.5 p_{s,fric} (I_{2D})^{-1/2} \sin(\Phi) \quad (23)$$

where $(I_{2D})^{-1/2}$ is the second-order deviatoric shear stress tensor and Φ is the angle of internal friction, which is usually set to 28° .

Fig. 3 compares the solid pressure given by the kinetic theory model and the frictional stress models. As shown, the frictional contribution is dominant above α_{min} , especially for the presented models. The Johnson and Jackson frictional stress model (Johnson et al., 1990) has a subtle increase and might lead to a smoother transition to the frictional regime. We found the use of the Johnson-Jackson model in combination with the Carnahan-Starling model does not necessarily ensure the packing limit when using an implicit solution algorithm for the continuity equation (Wartha et al., 2020); therefore, we chose to apply the Schaeffer model to cases close to the packing limit.

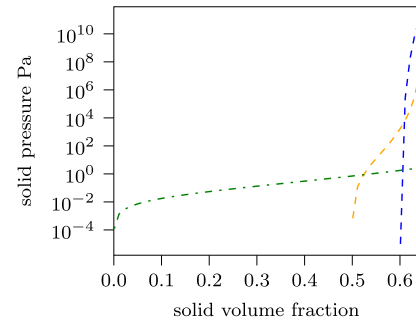


Fig. 3. Comparison of the pressure contributions from the kinetic theory and the frictional model for $\Theta = 10^{-4}$.

2.3.2. Srivastava-Sundaresan Frictional Model

Srivastava and Sundaresan (2003) derived a frictional stress model based on the work of Johnson et al. (1990). The model by Srivastava and Sundaresan (2003) considers the strain rate fluctuations for the frictional viscosity while the frictional pressure remains unchanged. The more robust and reasonably accurate simplification of the frictional stresses was taken here (Srivastava and Sundaresan, 2003). The frictional viscosity and pressure are given by

$$p_{s,fric} = Fr \frac{(\alpha_s - \alpha_{min})^\eta}{(\alpha_{max} - \alpha_s)^P} \quad (24)$$

$$\mu_{s,fric} = 0.5 p_{s,fric} \left(I_{2D} + \frac{\Theta}{d_p^2} \right)^{-1/2} \sqrt{2} \sin(\Phi) \quad (25)$$

with the constants $Fr = 0.05$, $\eta = 2$ and $P = 5$.

2.4. Drag Model

Although there are different momentum exchange models for the drag (the second term on the RHSs of Eqs. (3)), we use the drag correlation by Gidaspow (1994), Eq. (29), in this paper. This model combines the WenYu-model, Eq. (26), and the Ergun model, Eq. (28), based on the fluid volume fraction.

$$\beta_{\text{WenYu}} = \frac{3}{4} C_D \frac{\alpha_g \alpha_s |\mathbf{v}_s - \mathbf{v}_g| \rho_g}{d_p} \alpha_g^{-2.65} \quad (26)$$

$$C_D = \begin{cases} \frac{24}{\text{Re}} [1 + 0.15 \text{Re}^{0.687}] & \text{Re} < 1000 \\ 0.44 & \text{Re} \geq 1000 \end{cases} \quad (27)$$

$$\beta_{\text{Ergun}} = 150 \frac{\alpha_s^2 \mu_g}{\alpha_g (d_s)^2} + 1.75 \frac{\rho_g |\mathbf{v}_g - \mathbf{v}_s| \alpha_s}{d_s} \quad (28)$$

$$\beta_{\text{Gidaspow}} = \begin{cases} \beta_{\text{Ergun}} & \alpha_g \leq 0.8 \\ \beta_{\text{WenYu}} & \alpha_g > 0.8 \end{cases} \quad (29)$$

3. Simulation Studies and Results

A customized solver based on OpenFOAM, version 7, was used for all simulations. OpenFOAM is an open-source C++ CFD library employing the finite volume method (Weller et al., 1998).

The investigations focus on the influence of the kinetic theory model closures on the raceway prediction; nonetheless, for consistency, we also include two cases for the classical application of the KTGF, namely a 2D bubble formation (Section 3.1) and a 2D fluidized bed case (Section 3.2); these cases have been widely used to compare frictional stress models or radial models in conjunction with the KTGF (Venier et al., 2018; Passalacqua and Marmo, 2009).

To demonstrate the effect of the KTGF closure models on the raceway formation, we studied three raceway formation cases. The results of the closure models implemented in OpenFOAM are compared with DEM results (Section 3.3), another established TFM code - MFIX - (Syamlal et al., 1993; Benyahia et al., 2012) (Section 3.4) and experimental results (Section 3.5).

For all the cases, the gas phase turbulence was modeled by the $k-\epsilon$ model. The frictional effects for the solid phase were modeled using the Schaeffer model, except for the bubble formation case, where we used the Srivastava model. The wall boundary conditions were set to no-slip for the gas velocity and a Johnson-Jackson type boundary condition (Johnson and Jackson, 1987) for the particle velocity. Based on the results by Liu and Hinrichsen (2014) we used TVD differencing schemes in general and the vanLeer scheme for the phase fraction. A cell-based gradient scheme was chosen based on Liu and Hinrichsen (2014).

3.1. Bubble Formation

The first test case is a simple pseudo-2D bubble growth case, which was investigated experimentally by Kuipers et al. (1991) and numerically by Venier et al. (2018) and Patil et al. (2005). The domain is 0.57 m wide, 1 m high, and discretized by 112 x 200 cells. A single jet of 0.015 m width enters the domain in the middle. For the simulation, the frictional stress model of Srivastava and Sundaresan (2003) was used; this model has been determined to be appropriate for this case by Venier et al. (2018). The model was used with two different values for the onset of friction. Mostly a value of 0.5 is employed with this model, but Passalacqua and Marmo (2009) presented that a value of 0.6 gave more realistic results. Therefore, both were tested here. Additional simulation details are given in Table 3. No virtual mass effects were considered in this simulation and the Gidaspow drag model was used (Gidaspow, 1994) for the simulations.

Fig. 4 compares the bubble diameter ratio (ratio of the vertical to the horizontal bubble extension) of the simulation for the single bubble case. The simulation results agree well with the experimental results at the beginning of the bubble formation. After approximately 0.15 s, the bubble stretch was overpredicted by the

Table 3
Properties for the bubble formation simulation.

Description	Value	Unit
Gas density	1.225	kg m ⁻³
Gas viscosity	1.85 · 10 ⁻⁵	Pa s
Solid density	2660	kg m ⁻³
Particle diameter	500 · 10 ⁻⁶	m
Restitution coefficient	0.95	-
Initial bed height	0.5	m
Initial packing	0.598	-
Maximum packing	0.63	-
α_{min}	0.5/ 0.6	-
Jet inlet velocity	10	ms ⁻¹
Maximum time-step size	10 ⁻⁵	s
Maximum Courant number	0.25	-
Time discretization	First-order implicit	-

simulations compared with the experiment results, which was more profound for $\alpha_{\text{min}} = 0.5$. In this regime, no significant influence of the Agrawal and Lun models was seen. We showed in Sections 2.1.2 and 2.1.1 that the solid viscosity and solid conductivity deviate the most for small solid volume fractions between the two KTGF closure models. The region with small solid volume fractions is small, which might influence the results. Additionally, the relative velocity is small and consequently the difference between the calculated solid conductivities is small (Fig. 2).

The simulated bubble detachment time was well predicted by the simulations. Kuipers et al. (1991) reported a bubble detachment time of 0.188 s, while the simulations predicted 0.19 s bubble detachment time.

3.2. Fluidized Bed

The simulated fluidized bed was presented by Patil et al. (2005). The setup is similar to the bubble formation case from Section 3.1, except for an additional fluidization air stream of 0.25 ms⁻¹. The simulation was set up in the same way as the bubble formation case (Section 3.1).

The experimental results by Patil et al. (2005) were the average over 60 s. Here, we averaged the simulation results after an initial start-up time of 10 s over a period of 20 s, since no changes were observed even for smaller averaging windows.

Fig. 5 depicts time-averaged axial phase fraction profiles at two distinct vertical lines. The simulated profiles agree well with the experimental profile (Fig. 5 (a)) for regions close to the central jet and at the bottom of the fluidized bed. With increasing bed height, the phase fraction predictions deviate compared with the experiments. Fig. 5 (b) reveals that the bed expansion was well predicted but that the fluidization was underpredicted for the bed bottom.

The simulation results by Patil et al. (2005) agree better with the experimental results. They either used the Johnson and Jackson frictional stress model or neglected frictional stresses, which suggests that the Schaeffer frictional stress model overpredicted frictional stresses in the given fluidized bed.

Nevertheless, the main focus is to compare the effects of the KTGF closure models. The results show that interstitial fluid effects do not influence the simulation results in the fluidized bed regime. Similarly to the bubble formation case this seems to be related to the relatively low relative velocities and consequently small differences in the solid conductivity (Fig. 2).

3.3. Raceway - DEM Comparison

Lu et al. (2020) presented a novel methodology to analyze the void morphology in CFD-DEM simulations. DEM offers a possibility

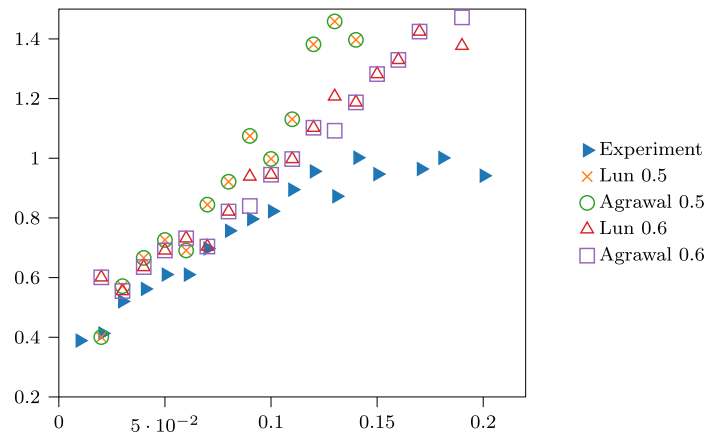


Fig. 4. Bubble diameter ratio obtained from experiment and simulation (using different KTGF closure models and radial distribution functions).

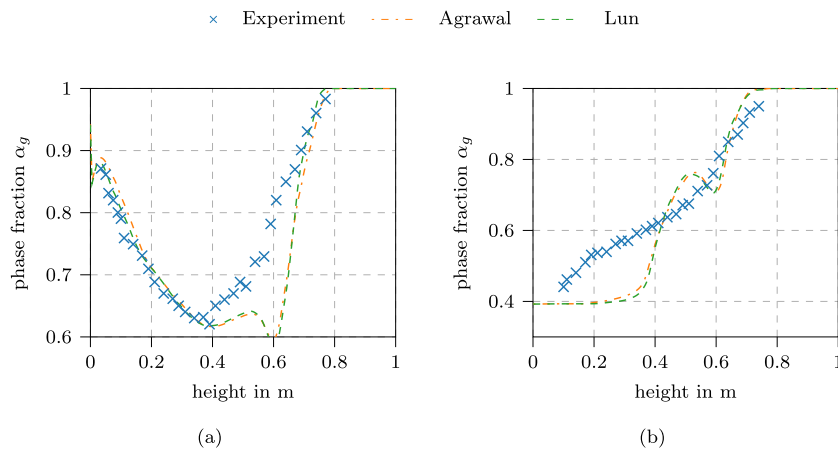


Fig. 5. Gas phase fraction from experiment and simulation using Agrawal and Lun models at (a) 0.375 cm from the center and (b) 9.375 cm from the center.

to study the void formation in more detail, since the particle–particle interactions are resolved. In this study, the investigated pseudo-2D domain was 2.6 m wide, 3.5 m high, and 88.6 mm deep. The middle of the gas inlet was positioned 0.4873 m above the bottom, was 88.6 mm times 88.6 mm large, and reached 0.300 m into the bed.

The used particles had a density of 1200 kg m^{-3} and a diameter of 40 μm , and the gas had a viscosity of $1.88 \cdot 10^{-5} \text{ Pa s}$ and a temperature of 1000 °C. Periodic boundary conditions were applied at the front and back patches, while a fixed pressure of 1 bar was applied at the top. The depth and height of the formed raceway were studied for inlet gas velocities ranging from 168 to 232 ms^{-1} .

The maximum packing limit was defined as 0.63 in the OpenFOAM simulations, while the volume fraction for the onset of friction was set to 0.61. The simulation using the KTGF was conducted as a transient simulation for 10 s, and the resulting raceway void was taken from the average phase fraction over 5 to 10 s.

Fig. 6 compares simulated and published (Lu et al., 2020) raceway depths and heights. The raceway boundary depth and height were calculated with $\alpha_{\text{particle}} = 0.3$ as the boundary. The comparison reveals significant differences in the raceway depth and height depending on the KTGF closure model. The Agrawal model predicts the raceway height well for high gas velocities, while the raceway depth was overpredicted for low gas velocities and underpredicted for high gas velocities. The Lun model underpredicted the raceway

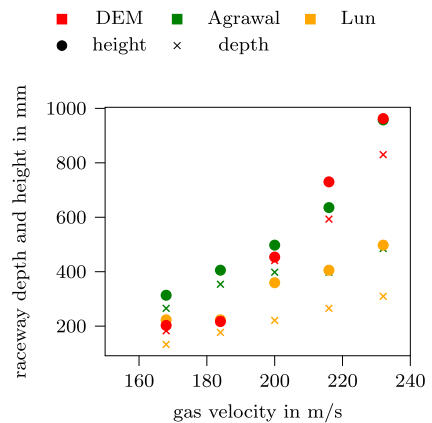


Fig. 6. Raceway depth (circle) and height (cross) for different gas inlet velocities; Comparison between Agrawal model (green), Lun model (orange), and DEM (red) results from Lu et al. (2020).

depth and height at high gas flow rates, while it gave reasonable predictions at low gas flow rates compared to the DEM results.

Fig. 7 gives averaged solid volume fraction contours of all cases. Comparing the results obtained from the Agrawal model and the Lun model. Although the raceways may look similar, the figure shows that a more pronounced raceway was formed using the Agrawal model. For all cases, the raceway showed a very high top extension, which was not seen in the results presented by Lu et al. (2020). This might be due to the averaging of the solid volume fraction. The high inlet velocities prevent stable-steady states and cause periodic bubble detachment from the raceway. These detached bubbles cause reduced solid volume fractions above the raceway cavity.

3.4. Raceway - TFM Comparison

For the second raceway case, we compared the results from an established, two-fluid model code - MFIX (Syamlal et al., 1993; Benyahia et al., 2012). According to Benyahia et al. (2012), MFIX also employs the Agrawal model. We chose a simple 2D raceway based on that presented by Feng et al. (2003). The geometry was 0.3 m wide and 1 m high and was discretized by 12000 cells. The inlet was positioned 0.1 m above the bottom of the bed with a height of 0.02 m. The bed was initially 0.5 m high with an initial solids volume fraction of 0.55. The maximum packing limit and α_{min} were both set to 0.63, which is in accordance with MFIX when the Schaeffer model is used. The time discretization was chosen in the same way for MFIX and OpenFOAM. Otherwise, the default schemes and under-relaxation factors in MFIX were taken (version 20.3.1). The gas phase was modeled as perfect gas with a constant viscosity of $1.8 \cdot 10^{-5}$ Pa s. The raceway formation was computed for three different inlet velocities: 20, 25 and 30 ms^{-1} , and 1 s of physical time was simulated.

Fig. 8 compares the raceway penetration depths obtained from the MFIX simulations and the OpenFOAM simulations (using $\alpha_{particle} = 0.3$ as boundary) with that presented by Feng et al. (2003). The correlation between the raceway size and inlet velocity was reproduced by all simulation models, but the exact depth deviated. The depth is underpredicted by the MFIX simulations and overpredicted in the OpenFOAM simulations. No clear raceway

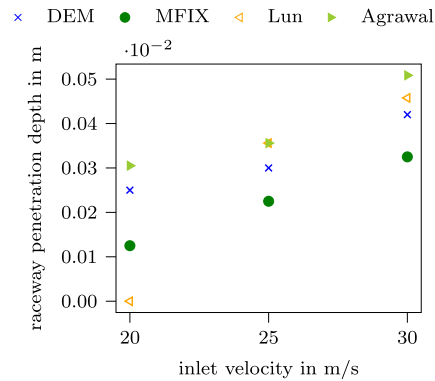


Fig. 8. Comparison of raceway penetration depth from MFIX code, DEM simulation (Feng et al., 2003), and OpenFOAM (using Agrawal and Lun models).

cavity was formed for the lowest inlet velocity when the Lun closure model was used.

Fig. 9 shows the contour plots obtained from the MFIX simulations and the OpenFOAM simulations with Agrawal and Lun models. Hardly any raceway was formed when the Lun closure model was used for the lowest inlet velocity; this confirms the result indicated in Fig. 8. The MFIX code results gave lower solid volume fractions in the raceway cavity than the OpenFOAM results. Furthermore, the contour plots indicate a gas jet next to the wall in the MFIX results.

One difference between the MFIX results and the OpenFOAM results is the more distinct raceway, meaning even lower phase fraction in the actual raceway; this could be related to the high near-wall gas velocity predicted by MFIX. Possibly the treatment of the boundary is different in the MFIX code when doing 2D simulation.

3.5. Raceway - Experimental Comparison

Mojamdar et al. (2018) experimentally studied the raceway formation in a pseudo-2D setup with the dimensions of 500 x 1000 x

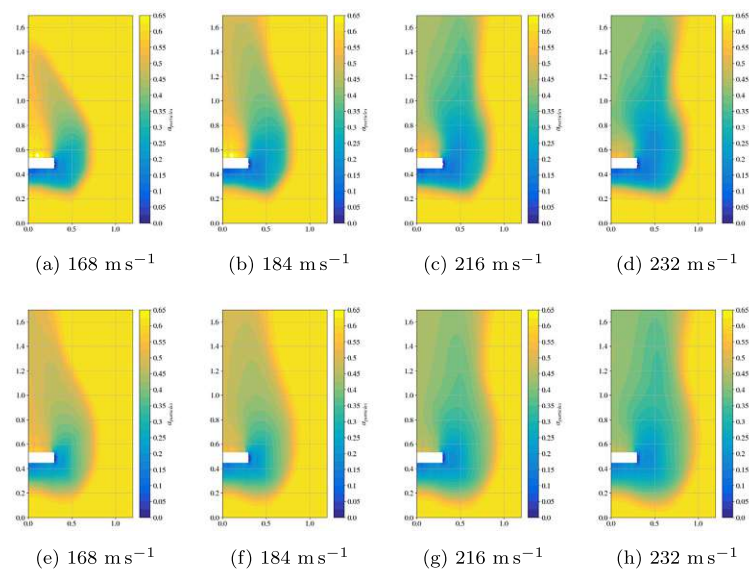


Fig. 7. Contour plots of the solid volume fraction obtained using the Agrawal model ((a)-(d)) and the Lun model ((e)-(h)).

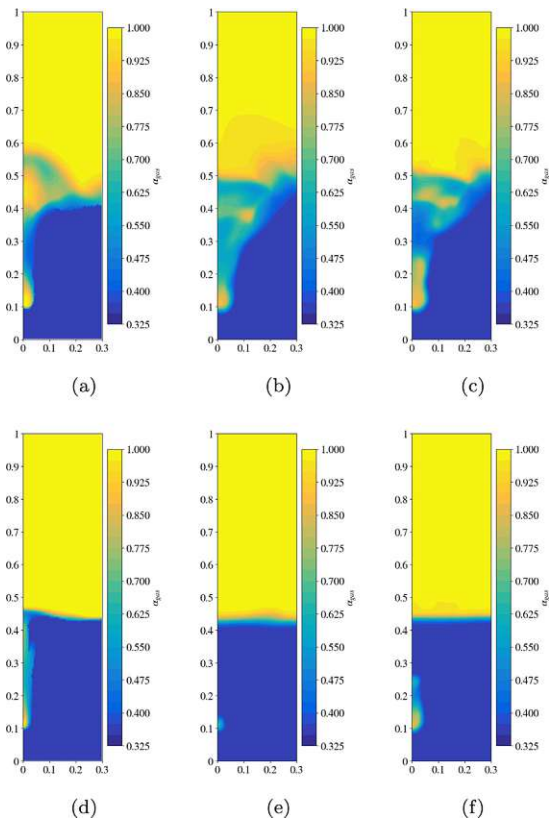


Fig. 9. Comparison between results for inlet velocity of 30 ms⁻¹ (a-c), and 20 ms⁻¹ (d-f) from MFX simulation (first column) with Lun model (second column) and Agrawal model (third column).

60 mm. The slot-type tuyere was positioned 160 mm above the bottom, reaching 50 mm into the bed. The domain was discretized by 21500 cells, approximately 90 in the horizontal and 240 in the vertical direction. Mojamdar et al. (2018) used cylindrical particles with a density of 940 kg m⁻³, a length-to-diameter ratio of 1.1, and equivalent diameter of 4 mm. The particles were approximated as spherical particles with the same diameter in the simulation. The approximation of cylindrical particles by spheres could be questionable, but the KTGF can only model spherical particles. Because the KTGF is often applied to depict industrial processes with non-spherical particles, we believe it is also valuable for comparing the TFM results with the experimental results here.

The inlet velocity was varied between 0.11 and 0.6 ms⁻¹ for the test cases and was given as the superficial bed velocity. The gas was modeled as a perfect gas at room temperature. The other parameters for the simulation setup are summarized in Table 4. The simulations were conducted for 4 s, since the raceway form stabilized after approximately 1 s.

Mojamdar et al. (2018) determined the raceway equivalent diameter in cold model experiments and investigated hysteresis effects. The raceway equivalent diameter is defined as the diameter of a circle with the same circumference as the raceway:

$$d_{RW} = \frac{U_{RW}}{\pi} \quad (30)$$

We conducted one transient simulation per set-point velocity, starting from a resting bed. Therefore, we compare the simulated raceway diameters to the experimental cases obtained at increasing

Table 4

Parameters used for the raceway simulation compared with experimental results by Mojamdar et al. (2018).

Description	Value	Unit
Initial bed porosity	0.6	-
Air viscosity	1.8 · 10 ⁻⁵	Pas
Particle diameter	0.004	m
Particle density	940	kg m ⁻³
Bed height	0.8	m
α_{min}	0.6	-
α_{max}	0.61	-
Virtual mass coeff.	0.5	-
Restitution coeff.	0.95	-
Maximum time step	10 ⁻³	s
Maximum Courant number	0.25	-

gas velocity. The porosity level, which defines the boundary of the raceway, is not clearly defined in the experiments. Therefore, we determined the raceway equivalent diameter for $\alpha_{particles} = 0.3$ and $\alpha_{particles} = 0.4$ as raceway boundaries. In general, the simulations reproduce the experimental trend given in Fig. 10.

Fig. 10 reveals that interstitial gas effects increase the predicted raceway size, for example, the Agrawal model gives larger raceway equivalent diameters than the Lun model.

We also compared the measured pressure distribution from Mojamdar et al. (2018) with the simulation results (Fig. 11). The pressure was reasonably predicted for most positions, but hardly any difference occurred between the Agrawal and Lun KTGF results. The peak pressure was underpredicted with both closure models, at higher gas velocity ($U = 0.5 \text{ ms}^{-1}$).

Fig. 12 compares the solid phase fraction contour plots for the OpenFOAM simulations and a superficial velocity of 0.5 ms⁻¹. The results indicate higher volume fraction gradients for the Agrawal closures compared with the Lun closure.

The shape of the raceway is circular and symmetrical. Sarkar et al. (2003) also conducted a similar study in a 2D cold model apparatus. The setup was nearly identical, and they concluded that the raceway shape was almost circular. This undermines the correct prediction of the raceway by the OpenFOAM simulation.

Fig. 13 displays the particle velocity vectors in the raceway zone. Two recirculating zones are shown, which agrees with the findings by Sarkar et al. (2003). The Agrawal model gave a higher

* Agrawal 0.3 ◊ Lun 0.3 × Experiment
● Agrawal 0.4 ◻ Lun 0.4

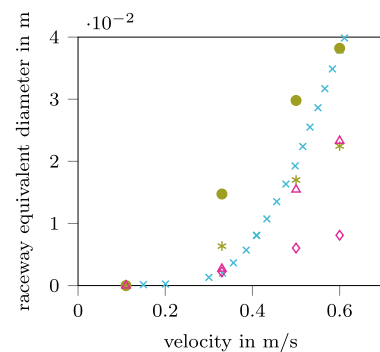


Fig. 10. Raceway equivalent diameter for experiments by Mojamdar et al. (2018) and simulation. Raceway boundary calculated with $\alpha_{particles} = 0.3$ and $\alpha_{particles} = 0.4$ in the simulation.

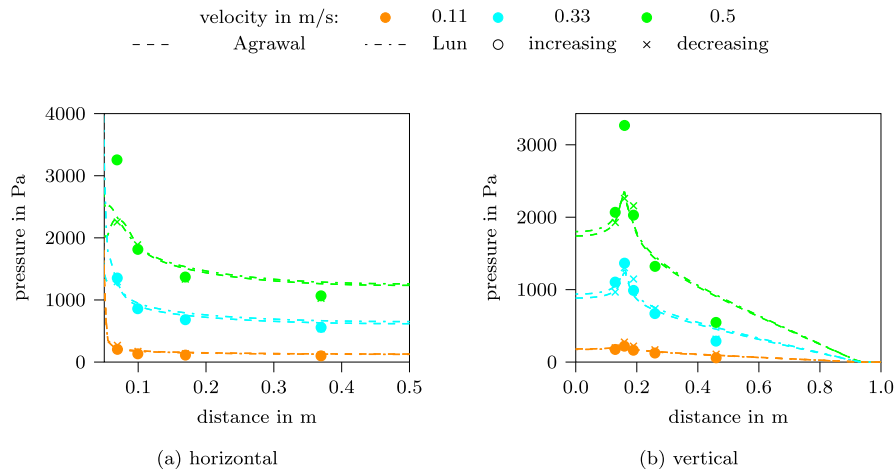


Fig. 11. Pressure along the horizontal and vertical lines in the 2D Raceway.

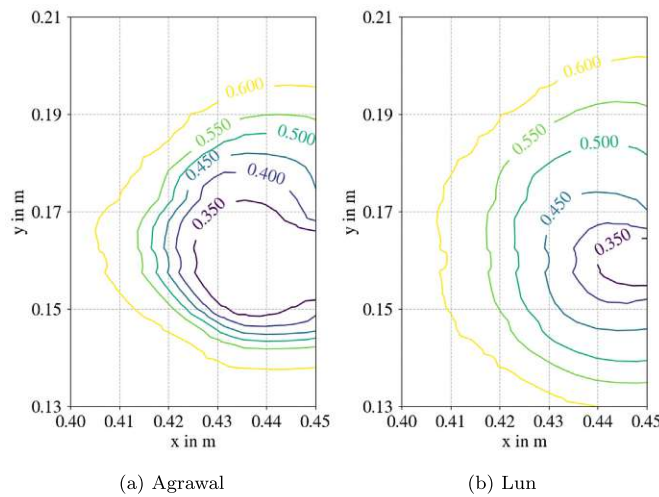


Fig. 12. Solid volume fraction isolines in the raceway zone for $U = 0.5 \text{ ms}^{-1}$.

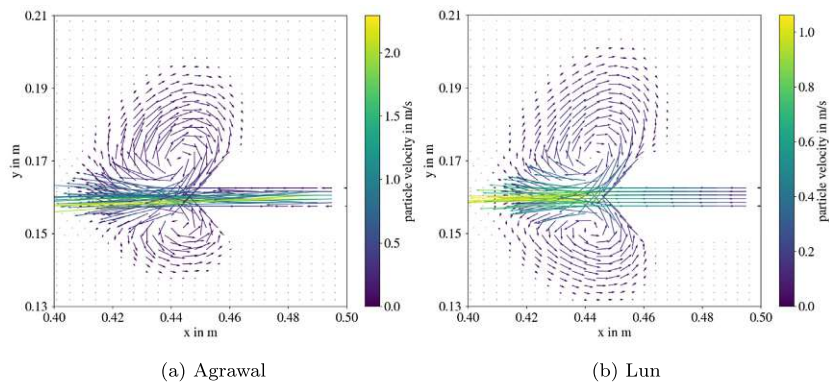


Fig. 13. Particle velocity in the raceway zone for $U = 0.5 \text{ ms}^{-1}$ inlet velocity.

particle velocity than the Lun model. This was caused by the larger raceway cavity predicted by the Agrawal model.

4. Conclusion

In this study, the KTGF closure models presented by Lun et al. (1984) and Agrawal et al. (2001) were systematically assessed. The difference between these models is that the Agrawal model considers the effect of the interstitial fluid by incorporating the drag correlation terms in the solid viscosity and solid conductivity models. We studied the difference between those formulations and compared the results with experimental data. In fluidized bed regimes, the effects of the interstitial fluid can possibly be neglected, since they do not affect the simulation results.

This study focuses on the prediction of raceway formation. The correct prediction of the raceway shape and formation is essential to understand the processes in ironmaking blast furnaces. For these cases, the influence of the chosen KTGF closure model is significant. The interstitial fluid effects become more dominant in the raceway regime, which can be attributed to the higher gas velocities and consequently higher contributions from the drag terms in the modified closure terms. The comparison of the simulation data with experimental data and DEM data reveals that the model by Agrawal et al. (2001) predicted the raceway shapes better than the Lun model (Lun et al., 1984).

We recommend the use of the Agrawal model, which incorporates the interstitial fluid effects when simulating raceway formation. The Agrawal model gives more accurate predictions in the raceway regime than the Lun model; nonetheless the results of both are almost identical in the fluidized bed regime.

Declaration of Competing Interest

The authors declare that they have no known competing financial interests or personal relationships that could have appeared to influence the work reported in this paper.

Acknowledgments

The authors gratefully acknowledge the funding support of K1-MET GmbH, metallurgical competence center. The research program of the competence center K1-MET is supported by COMET (Competence Center for Excellent Technologies), the Austrian program for competence centers. COMET is funded by the Federal Ministry for Transport, Innovation and Technology, the Federal Ministry for Science, Research and Economy, the provinces of Upper Austria, Tyrol, and Styria, and the Styrian Business Promotion Agency.

The authors acknowledge TU Wien Bibliothek for financial support for editing/proofreading and for financial support through its Open Access Funding Programme.

The computational results presented have been achieved in part using the Vienna Scientific Cluster (VSC).

References

Agrawal, K., Loezos, P.N., Syamlal, M., Sundaresan, S., 2001. The role of meso-scale structures in rapid gas-solid flows. *J. Fluid Mech.* 445, 151–185. <https://doi.org/10.1017/s0022112001005663>.

Almohammed, N., Alobaid, F., Breuer, M., Epple, B., 2014. A comparative study on the influence of the gas flow rate on the hydrodynamics of a gas-solid spouted fluidized bed using Euler-Euler and Euler-Lagrange/DEM models. *Powder Technol.* 264, 343–364. <https://doi.org/10.1016/j.powtec.2014.05.024>.

Balzer, G., Boelle, A., Simonin, A., 1995. Eulerian Gas-Solid Flow Modelling of Dense Fluidized Bed. Technical Report. Électricité de France.

Benyahia, S., Syamlal, M., O'Brien, T., 2012. Summary of MFIX Equations 2012–1. Technical Report. URL: <https://mfix.netl.doe.gov/documentation/MFIXEquations2012-1.pdf>.

Boelle, A., Balzer, G., Simonin, O., 1995. Second Order Prediction of the Particle-Phase Stress Tensor of Inelastic Spheres in Simple Shear Dense Suspensions. Technical Report.

Bösenhofer, M., 2020. On the modeling of multi-phase reactive flows: Thermochemical conversion in the raceway zone of blast furnaces. Ph.D. thesis. TU Wien. URL: <https://repositum.tuwien.at/handle/20.500.12708/16434>, doi:10.34726/HSS.2020.58548.

Bösenhofer, M., Wartha, E.M., Jordan, C., Harasek, M., Feilmayr, C., Hauzenberger, F., König, B., 2019. A raceway model based on open-source software, in: AISTech 2019, Pittsburgh, PA, USA, pp. 2641–2651. doi:10.1000/377.272.

Carnahan, N.F., Starling, K.E., 1969. Equation of state for nonattracting rigid spheres. *J. Chem. Phys.* 51, 635–636. <https://doi.org/10.1063/1.1672048>.

Chiesa, M., Mathiesen, V., Melheim, J.A., Halvorsen, B., 2005. Numerical simulation of particulate flow by the Eulerian-Lagrangian and the Eulerian-Eulerian approach with application to a fluidized bed. *Comput. Chem. Eng.* 29, 291–304. <https://doi.org/10.1016/j.compchemeng.2004.09.002>.

Feng, Y.Q., Pinson, D., Yu, A.B., Chew, S.J., Zulli, P., 2003. Numerical study of gas-solid flow in the raceway of a Blast Furnace. *Steel Res. Int.* 74, 523–530. <https://doi.org/10.1002/srin.200300229>.

Garzó, V., Tenneti, S., Subramaniam, S., Hrenya, C.M., 2012. Enskog kinetic theory for monodisperse gas-solid flows. *J. Fluid Mech.* 712, 129–168. <https://doi.org/10.1017/jfm.2012.404>.

Gidaspow, D., 1994. *Multiphase Flow and Fluidization - Continuum and Kinetic Theory Descriptions*. Academic Press Inc.

Johnson, P., Jackson, R., 1987. Frictional-collisional constitutive relations for granular materials, with application to plane shearing. *J. Fluid Mech.* 176, 67–93.

Johnson, P., Nott, P., Jackson, R., 1990. Frictional-collisional equations of motion for particulate flows and their application to chutes. *J. Fluid Mech.* 210, 501–535.

Koch, D.L., Sangani, A.S., 1999. Particle pressure and marginal stability limits for a homogeneous monodisperse gas-fluidized bed: kinetic theory and numerical simulations. *J. Fluid Mech.* 400, 229–263. <https://doi.org/10.1017/S0022112099006485>.

Kuang, S., Li, Z., Yu, A., 2018. Review on modeling and simulation of Blast Furnace. *Steel Res. Int.* 89, 1–25. <https://doi.org/10.1002/srin.201700071>.

Kuipers, J., Prins, W., van Swaaij, W., 1991. Theoretical and experimental bubble formation at a single orifice in a two-dimensional gas-fluidized bed. *Chem. Eng. Sci.* 46, 2881–2894.

Lichtenegger, T., Pirker, S., 2018. CFD-DEM modeling of strongly polydisperse particulate systems. *Powder Technol.* 325, 698–711. <https://doi.org/10.1016/j.powtec.2017.11.058>.

Liu, Y., Hinrichsen, O., 2014. CFD modeling of bubbling fluidized beds using OpenFOAM®: Model validation and comparison of TVD differencing schemes. *Comput. Chem. Eng.* 69, 75–88. <https://doi.org/10.1016/j.compchemeng.2014.07.002>.

Lu, Y., Liu, S., Zhang, X., Jiang, Z., E, D., 2020. A Probabilistic Statistical Method for the Determination of Void Morphology with CFD-DEM Approach. *Energies* 13. doi:10.3390/en13164041.

Lun, C.K., Savage, S.B., 1986. The Effects of an Impact Velocity Dependent Coefficient of Restitution on Stresses Developed by Sheared Granular Materials. *Acta Mech.* 63, 15–44. <https://doi.org/10.1007/BF01182538>.

Lun, C.K., Savage, S.B., Jeffrey, D.J., Chepurny, N., 1984. Kinetic theories for granular flow: inelastic particles in Couette flow and slightly inelastic particles in a general flowfield. *J. Fluid Mech.* 140, 223–256. <https://doi.org/10.1017/S0022112084000586>.

Ma, D., Ahmadi, G., 1988. A kinetic model for rapid granular flows of nearly elastic particles including interstitial fluid effects. *Powder Technol.* 56, 191–207. [https://doi.org/10.1016/0032-5910\(88\)80030-5](https://doi.org/10.1016/0032-5910(88)80030-5).

Mojamdar, V., Gupta, G.S., Puthukkudi, A., 2018. Raceway Formation in a Moving Bed. *ISIJ Int.* 58, 1396–1401. <https://doi.org/10.2355/isijinternational.ISIJINT-2017-698>.

Passalacqua, A., Fox, R.O., 2011. Implementation of an iterative solution procedure for multi-fluid gas-particle flow models on unstructured grids. *Powder Technol.* 213, 174–187. <https://doi.org/10.1016/j.powtec.2011.07.030>.

Passalacqua, A., Marmo, L., 2009. A critical comparison of frictional stress models applied to the simulation of bubbling fluidized beds. *Chem. Eng. Sci.* 160, 2795–2806. <https://doi.org/10.1016/j.ces.2009.03.005>.

Patil, D.J., Van Sint Annaland, M., Kuipers, J.A., 2005. Critical comparison of hydrodynamic models for gas-solid fluidized beds - Part I: Bubbling gas-solid fluidized beds operated with a jet. *Chem. Eng. Sci.* 60, 57–72. <https://doi.org/10.1016/j.ces.2004.07.059>.

Sarkar, S., Gupta, G.S., Litster, J.D., Rudolph, V., White, E.T., Choudhary, S.K., 2003. A cold model study of raceway hysteresis. *Metallurgical and Materials Transactions B* 34B, 183–191. <https://doi.org/10.1007/s11663-003-0005-1>.

Savage, S.B., 1998. Analyses of slow high-concentration flows of granular materials. *J. Fluid Mech.* 377, 1–26. <https://doi.org/10.1017/S0022112098002936>.

Schaeffer, D.G., 1987. Instability in the Evolution Equations Describing Incompressible Granular Flow. *Journal of Differential Equations* 66, 19–50. [https://doi.org/10.1016/0022-0396\(87\)90038-6](https://doi.org/10.1016/0022-0396(87)90038-6).

Schneiderbauer, S., Aigner, A., Pirker, S., 2012. A comprehensive frictional-kinetic model for gas-particle flows: Analysis of fluidized and moving bed regimes. *Chem. Eng. Sci.* 80, 279–292. <https://doi.org/10.1016/j.ces.2012.06.041>.

Eva-Maria Wartha, M. Bösenhofer and M. Harasek

Chemical Engineering Science 247 (2022) 117026

- Snider, D.M., Rourke, P.J.O., Andrews, M.J., 1998. Sediment flow in inclined vessels calculated using a multiphase particle-in-cell model for dense particle flows. *Int. J. Multiph. Flow* 24, 1359–1382.
- Srivastava, A., Sundaresan, S., 2003. Analysis of a frictional-kinetic model for gas-particle flow. *Powder Technol.* 129, 72–85. [https://doi.org/10.1016/S0032-5910\(02\)00132-8](https://doi.org/10.1016/S0032-5910(02)00132-8).
- Syamlal, M., Rogers, W., O'Brien, T.J., 1993. MFIx Documentation Theory Guide. Technical Report. <https://doi.org/10.2478/v10296-012-0006-z>.
- Tacconi, Z., 2018. Feasibility analysis of a two-fluid solver for cavitation and interface capturing as implemented in OpenFOAM. Tesi di laurea, Politecnico Di Milano.
- van Wachem, B.G.M., 2000. Derivation, Implementation, and Validation of Computer Simulation Models for Gas-Solid Fluidized Beds Ph.D. thesis. Delft University of Technology.
- Venier, C.M., Marquez Damian, S., Nigro, N.M., 2018. Assessment of gas-particle flow models for pseudo-2D fluidized bed applications. *Chem. Eng. Commun.* 205, 456–478. <https://doi.org/10.1080/00986445.2017.1403907>.
- Wartha, E.M., Bösenhofer, M., Harasek, M., 2020. Combining an implicit solution with an explicit corrector step for the solution of the continuity equations in a two-fluid solver. In: *14th International Conference on CFD in Oil & Gas, Metallurgical and Process Industries*, Trondheim, Norway.
- Weller, H., 2005. Derivation, Modelling and Solution of the Conditionally Averaged Two-Phase Flow Equations. Technical Report.
- Weller, H., Tabor, G., Jasak, H., Fureby, C., 1998. A tensorial approach to computational continuum mechanics using object-oriented techniques. *Computers in Physics* 12, 620–631. <https://doi.org/10.1063/1.168744>.
- Zhao, J., Liu, G., Li, W., Yin, X., Wu, Y., Wang, C., Lu, H., 2020. A comprehensive stress model for gas-particle flows in dense and dilute regimes. *Chem. Eng. Sci.* 226, 115833. <https://doi.org/10.1016/j.ces.2020.115833>.

Paper 3

Enhanced kinetic model identification for gas–solid reactions through Computational Fluid Dynamics

published in *Chemical Engineering Journal* in collaboration with Felix Birkelbach, Markus Bösenhofer and Michael Harasek.

My contribution: Implementation of the CFD models. Significant contribution to conceptualization and writing the original draft. Carrying out the simulations and analyzing the results.

E. M. Wartha, F. Birkelbach, M. Bösenhofer, and M. Harasek (2022a). “Enhanced kinetic model identification for gas–solid reactions through Computational Fluid Dynamics”. In: *Chemical Engineering Journal* 430.P2, p. 132850. ISSN: 13858947. DOI: 10.1016/j.cej.2021.132850



Contents lists available at ScienceDirect

Chemical Engineering Journal

journal homepage: www.elsevier.com/locate/cej

Enhanced kinetic model identification for gas–solid reactions through Computational Fluid Dynamics

Eva-Maria Wartha^{a,*}, Felix Birkelbach^b, Markus Bösenhofer^{a,c}, Michael Harasek^a

^a TU Wien, Institute of Chemical, Environmental and Bioscience Engineering, Getreidemarkt 9/166, 1060 Vienna, Austria

^b TU Wien, Institute for Energy Systems and Thermodynamics, Getreidemarkt 9/BA, 1060 Vienna, Austria

^c K1-Met GmbH, Area 4 - Simulation and Analyses, Stahlstrasse 14, BG 88, 4020 Linz, Austria

ARTICLE INFO

Keywords:

Kinetic modeling
Gas–solid reactions
Virtual experiment
Enhanced data
Computational Fluid Dynamics

ABSTRACT

Gas–solid reactions often play key roles in chemical engineering applications. To understand and design processes featuring such heterogeneous reactions, kinetic models are crucial. One way to identify kinetic models is via thermal analysis experiments. Even if those experiments are carried out meticulously, there will be some deviation between nominal reaction conditions and the actual reaction conditions directly at the reaction site. For situations, where these deviations are not negligible, we propose a new approach to compute the reaction conditions directly at the sample, based on the experimental data. A key feature of our approach is that no kinetic model is required for the simulation. For this reason, the enhanced data can be used for kinetic model identification. Though, a kinetic modeling method that can process arbitrary data is required, because the enhanced kinetic data will not obey the idealized assumptions of constant temperature or constant heating rate.

To showcase our approach, we applied it to the reaction system CuO/Cu₂O. Kinetic models with nominal and simulated values are derived with the TensorNPK method, showing the influence of the enhanced kinetic data on the identified reaction kinetics.

1. Introduction

Interest in kinetic models is two-fold: On the one hand, kinetic models allow us to predict the reaction rate for given reaction conditions. This information is indispensable for reactor design and operation. On the other hand, they provide us with a frame to interpret kinetic data and to gain insights into the reaction mechanism. Regardless of the model purpose, the starting point is always a kinetic data set that contains reaction rate values at various reaction conditions. The quality of the kinetic data set directly determines the quality of the kinetic model. For this reason, collecting kinetic data is a critical step in the modeling process. From the viewpoint of kinetic modeling there are – generally speaking – two main types of experimental error: Error in the reaction rate values and error in the reaction conditions. In this paper, we will focus on the latter.

The most widely used method for measuring the kinetics of gas–solid reactions is thermal analysis (TA). A sample is exposed to controlled reaction conditions (temperature and partial pressure of the reactant gas) and the reaction progress is measured.

To obtain reliable kinetic data, the reaction conditions in TA devices have to be controlled very precisely. This is challenging for three

main reasons: First, there are various other processes occurring simultaneously with the chemical reaction under consideration, which are interfering with the control of the reaction conditions. Typical examples are self-heating/cooling, depletion/accumulation of reactant gas or limited gas diffusion. Second, temperature and partial pressure can usually not be measured directly at the sample. The distance between the sample and the sensor leads to a deviation of the measured value from the actual value at the sample. Third, the reaction conditions may not be the same across the whole sample. These effects are the hardest to quantify. Nevertheless, it has been shown in various studies that these inhomogeneities can significantly affect the measurements [1–3].

Most of these measurement errors can be eliminated or at least minimized by conducting the experiments carefully. To guide researchers in this task and establish a reference of best-practices, the ICTAC [1,4] has published a set of recommendations on how to conduct kinetic experiments. Nevertheless, measurement errors cannot be eliminated completely. The effect of mass transfer limitations in TA devices on kinetic analysis was studied by various authors [5–8]. Also deviations of the measured temperature and the temperature of the sample due to thermal lag or due to self-heating/self-cooling have been observed

* Corresponding author.

E-mail address: eva-maria.wartha@tuwien.ac.at (E.-M. Wartha).

<https://doi.org/10.1016/j.cej.2021.132850>

Received 15 July 2021; Received in revised form 29 September 2021; Accepted 1 October 2021

Available online 12 October 2021

1385-8947/© 2021 The Authors. Published by Elsevier B.V. This is an open access article under the CC BY license (<http://creativecommons.org/licenses/by/4.0/>).

in many experimental studies [9–12]. When those deviations cannot be eliminated completely by adjusting the experimental procedure, computational methods can help to make kinetic data more precise.

The temperature distribution in a TA device has been studied by several authors [2,13–20] using Computational Fluid Dynamics (CFD). Even though it is commonly assumed that the temperature is uniform in the TA device, all of these studies revealed deviations between the assumed or set – further referred to as nominal – temperature assumption, and the actual temperature at the probe. Additionally, Benedetti et al. [21] showed that the gas consumption of the reaction itself leads to reduced concentrations and partial pressures at the reaction site compared to the nominal values. Despite these numerous detailed studies on non-idealities in a TA device, only one work suggested an approach for dealing with these deviations and for deriving more accurate kinetic models: An et al. [22] used a CFD model of a reacting particle in a drop tube furnace to adjust the kinetic rate devolatilization parameters by an iterative procedure, in which they fitted the computational results to the experimental values.

A feature that all the above studies have in common is that they use a reaction model to incorporate the effect of the reaction in the simulation and compute the temperature distribution in the TA device.

If we wanted to use the simulation results for kinetic model identification, we run into a chicken-and-egg situation: in order to do the CFD simulation, a model for the reaction kinetics is needed – but to get enhanced kinetic data for kinetic model identification, the results of the CFD simulation are needed. In this paper we propose an approach that bypasses the need for a kinetic model in the CFD simulation.

The next section discusses the methods that our study is based on. In Section 3 our virtual experimentation approach is introduced. We describe how the experimental data is fed into the simulation model, and we discuss the expected impact on kinetic models. To demonstrate our approach, we chose a kinetic study of the reaction system $\text{Cu}_2\text{O}/\text{CuO}$ (cuprous oxide/cupric oxide). The experimental setup and the experiments conducted in that study are described in Section 4. There, we also describe in detail the simulation model that we employed to recreate the experiments from the study. In Section 5, we first discuss the simulation results and then compare the kinetic model derived from the enhanced data from the virtual experiment with the kinetic model derived based on nominal values for the reaction conditions. We show that dynamic effects in the TA device can affect the kinetic modeling result despite adhering to quality standards for kinetic experiments.

2. Methods

This paper presents an enhanced kinetic modeling approach. For this novel approach, two established methods are employed: CFD for the virtual experimentation and the TensorNPK method for kinetic model identification. This section discusses the basic principles of these methods.

2.1. Computational fluid dynamics

A finite-volume method is used to model the gas–solid reaction process in the experimental setup. We use the open-source object-oriented library OpenFOAM [23], version 7.

The gas phase is modeled as an Eulerian phase, which is described by the continuity equation Eq. (1) and the momentum equations Eq. (2), where ρ_g is the density, \mathbf{U}_g the velocity, $\boldsymbol{\tau}_g$ the deviatoric stress of the gas phase. Additionally, the mass source term S_m resulting from reaction and the momentum source term S_u resulting from interaction with the solid phase are used in the equations.

$$\frac{\partial \rho_g}{\partial t} + \nabla \cdot (\rho_g \mathbf{U}_g) = S_m \quad (1)$$

$$\frac{\partial (\rho_g \mathbf{U}_g)}{\partial t} + \nabla \cdot (\rho_g \mathbf{U}_g \mathbf{U}_g) - \nabla \cdot (\boldsymbol{\tau}_g) = -\nabla p + \rho_g \mathbf{g} + S_u \quad (2)$$

Besides the continuity and momentum equation, the energy equation Eq. (3) and the species equation Eq. (4) are also needed to describe the multi-component gas flow:

$$\frac{\partial (\rho_g (h + K))}{\partial t} + \nabla \cdot (\rho_g \mathbf{U}_g (h + K)) - \nabla \cdot (\alpha_{\text{eff}} \nabla h) = \nabla p + \rho_g \mathbf{U}_g \cdot \mathbf{g} + S_h \quad (3)$$

$$\frac{\partial \rho_g Y_i}{\partial t} + \nabla \cdot (\rho_g \mathbf{U}_g Y_i) - \nabla \cdot \left(\frac{\mu_{\text{eff}}}{\text{Sc}} \nabla (\rho_g Y_i) \right) = S_i \quad (4)$$

where h is the enthalpy, K the kinetic energy, α_{eff} the effective thermal diffusivity, Y_i the mass fraction of species i , μ_{eff} the effective viscosity, Sc the Schmidt number and S_h and S_i the energy and species source terms, respectively.

Eq. (1) to Eq. (4) describe the gas phase. The coupling with the solid phase is realized by the source terms S . To compute the species and heat source term S_i and S_h the reaction kinetics are needed which are usually obtained from a kinetic model. In our new approach, we use the experimental data directly to avoid the need of a kinetic model (see Section 3). The solid phase is described within the Lagrangian framework. The particles are regarded as point centers of mass and Newton's law of motion is used to describe their movement:

$$\frac{d}{dt} (m_p u_p) = F \quad (5)$$

where m_p is the particle mass, u_p is the particle velocity, and F is the sum of the forces acting on the particle.

We use a two way coupling approach, which means the velocity of the Eulerian phase directly impacts the Lagrangian particles and vice versa [24]. For the momentum source term, the drag is calculated according to the Gidaspow model [25].

The coupling of the energy equations is done using the Nusselt correlation developed by Ranz and Marshall [26]:

$$\text{Nu} = 2 + 0.6 \text{Pr}^{1/3} \text{Re}^{1/2} \quad (6)$$

2.2. Kinetic modeling

For the kinetic modeling in this paper we employed the TensorNPK method [27,28]. It is a data-driven method that is based on the General Kinetic Equation (GKE)

$$\frac{d\alpha}{dt} = f(\alpha) k(T) h(p, p_{\text{eq}}), \quad (7)$$

where $f(\alpha)$ is the effect of the conversion α , $k(T)$ the effect of temperature T and $h(p, p_{\text{eq}})$ the effect of the driving force, usually expressed as a function of the partial pressure p and the equilibrium pressure p_{eq} . The GKE is by far the most commonly applied formula to model gas–solid reactions [4]. Essentially, it is a synthesis of solid-state and homogeneous reaction rate models. $f(\alpha)$ models effects in the solid, $k(T)$ an Arrhenius-like temperature effect and $h(p, p_{\text{eq}})$ concentration and equilibrium effects.

The parameter of the $h(p, p_{\text{eq}})$ term depends on the rate limiting step [29]. In [28] we showed that equilibrium effects in gas–solid reactions are best modeled based on the partial molar Gibbs enthalpy of the reaction $G_z(T, p)$. It is defined as the stoichiometric sum of the chemical potentials of the reacting substances. For simple gas–solid reactions, such as the oxidation of Cu_2O in our use case, the partial molar Gibbs enthalpy can also be expressed as a function of the partial pressure and the equilibrium partial pressure. The partial molar Gibbs enthalpy is the driving force of the chemical reaction. It is zero at the equilibrium and increases with distance from the equilibrium. For the kinetic models in this paper, we use the reduced Gibbs enthalpy as a measure for the equilibrium distance.

$$\Delta^{\text{eq}} = \frac{G_z}{v_g RT} = \ln \frac{p}{p_{\text{eq}}} \quad (8)$$

Here, v_g is the stoichiometric coefficient of the gaseous reactant.

The TensorNPK method extracts the effect of each variable (i.e. conversion, temperature and equilibrium distance) on the reaction rate

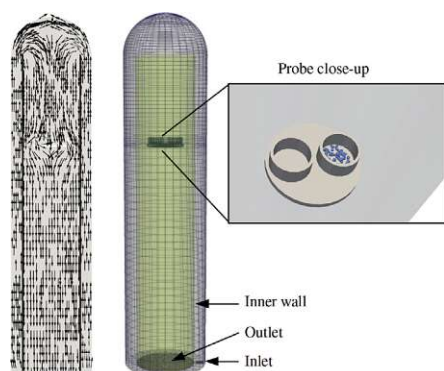


Fig. 1. Flow pattern through the TA device, the mesh and a close-up of the crucible holding the probe (from left to right).

from experimental data. The output of the TensorNPK method are vectors that describe the effect of each variable. These output vectors can be used to predict the reaction rate at given reaction conditions, further analyzed to get more insight into the kinetics or be used to fit reaction models. In this paper, we use the $k(T)$ vector to fit the Arrhenius equation and determine the apparent activation energy E_a . Also, we approximate the $h(\Delta^{eq})$ vector with a second order polynomial to describe the effect.

3. Virtual experiment

Modern thermal analysis (TA) devices use sophisticated strategies to control the reaction conditions as precisely as possible. The sample is placed in a crucible with thin walls made of a material with high thermal conductivity. The temperature sensor measures the temperature directly at the crucible to get a temperature reading as close to the sample as possible. This temperature is controlled to achieve the required temperature profile (isothermal or constant heating rate, usually). Though, the reaction itself will interfere with this temperature control: While the reaction progresses, the heat of reaction has to be compensated by the temperature control. Due to the heat of reaction and thermal lag, the temperature below the crucible can differ from the local temperature in the sample [11].

The reactant partial pressure is usually set by mixing the reactant gas with an inert gas, because most TA devices operate at ambient pressure. The gas flow is controlled with mass flow meters and (ideal) plug flow is assumed. Though, local concentration in the crucible may deviate from the bulk gas flow, because of mixing effects and diffusion effects of the reactant in the inert gas. If the reaction consumes the reactant faster than it can be replenished from the bulk gas flow, the local concentration will drop. Similarly, for reactions that produce gas, reactant gas can accumulate in the crucible.

The experimental procedures have to be carefully designed to reduce or eliminate those deviations. Though, for some reaction systems this might not be possible.

What can be done, when the limits of meticulous experimentation are reached, but the reaction conditions still do not meet the requirements of idealized experimental conditions? For these situations, we propose to couple the experimental analysis with a simulation to quantify the deviations and get accurate estimates of the actual reaction conditions in the sample.

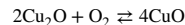
A spatially resolved 3D model of the TGA is generated to recreate the experiment with a CFD simulation — this simulation procedure will be referred to as the virtual experiment. To model the motion of gas and solid phase, and its interaction with the solid reactant, we use established physical CFD models (Section 2.1). When it comes

to modeling the reaction, we are confronted with a chicken-and-egg problem: we need a kinetic model for the simulation, but we also need the simulation to derive the kinetic model. This obstacle is overcome by applying the conversion rates obtained from the experiments directly in the simulation. Then, no kinetic model is needed. The measured conversion rates are set as fixed conversion rates in the CFD simulation. The only assumption required is that all particles react uniformly. This is inherently ensured within TA experiments, where uniform reaction progress needs to be ensured by choosing a sufficiently small sample mass [1,30], since the conversion rate is determined by one measurement only.

Regarding kinetic model identification, a caveat of our approach is that the simulated reaction conditions will generally deviate from idealized reaction conditions such as “isothermal” or “constant heating rate”. Consequently, most established kinetic modeling methods cannot be used with the presented approach, because they are based on exactly these idealized assumptions. To take advantage of the simulated reaction conditions from the virtual experiment for kinetic model identification, the kinetic modeling method needs the capability to process arbitrarily distributed data points. The TensorNPK method [27,28] meets these requirements. Another option would have been to use direct model fitting methods [31], but they require an a-priori selection of the model terms, which could conceal important information. For this reason, we chose the data-driven approach with the TensorNPK to process the data from the virtual experiments. The only requirement for the TensorNPK, is that the reaction obeys the GKE.

4. Use case

In general, the proposed approach can be applied to any gas–solid reaction system. To demonstrate the suggested approach and make the effects on kinetic model identification palpable, we use a set of kinetic measurements for the reaction system cuprous oxide/cupric oxide



that were conducted by Setoodeh Jahromy et al. [32]. This reaction system is of interest, because it is a promising candidate for thermochemical energy storage systems [33,34]. The experiments were recreated using OpenFOAM. In this section we will first describe the experimental setup that was used for the measurements, and then we will describe the simulation setup that was used to recreate these measurements.

4.1. Experimental setup

The reaction $\text{Cu}_2\text{O}/\text{CuO}$ was studied via simultaneous TA measurements on a NETZSCH STA 449 C JUPITER. The apparatus has a combined TGA-DSC (thermogravimetric analysis — differential scanning calorimetry) sample holder. For the measurements aluminum oxide crucibles were used. Experiments were conducted at ambient pressure. The total gas flow (N_2 and O_2) was set to 100 mL/min always, using red-y smart series mass-flow controllers by Voegtlin. The reaction was initiated by switching from pure N_2 to a mix of O_2 and N_2 . The mixing ratio was adjusted to achieve the studied oxygen partial pressures. The sample temperature was measured right below the crucible and controlled by the TA software.

To rule out inhomogeneous reaction conditions within the probe, the sample mass was adjusted so that no effect on the reaction progress could be observed. A sufficiently small sample mass should ensure that there are no concentration or temperature gradients within the probe; this means that the conversion progress is not influenced by the mass itself. This was experimentally confirmed for the experiments in our use case [32].

The experiments were conducted with a Cu_2O sample mass of 8.26 mg and for a combination of nominal temperatures (800, 830, 880 and 930 °C) and nominal oxygen partial pressures (0.1, 0.2, 0.5 and 1 bar).

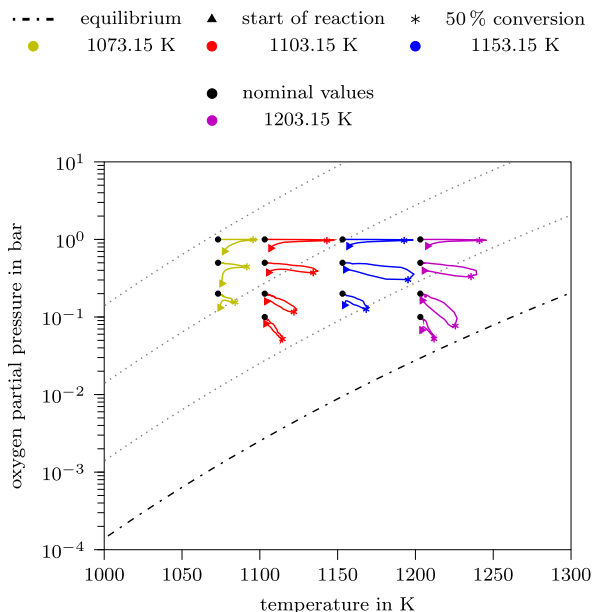


Fig. 2. Temperature and partial pressure at the probe. Nominal values (black dots) and simulated trajectories (in color — color-coded with the nominal temperature). Reaction equilibrium (dash-dotted) and equidistant lines (dotted) are marked.

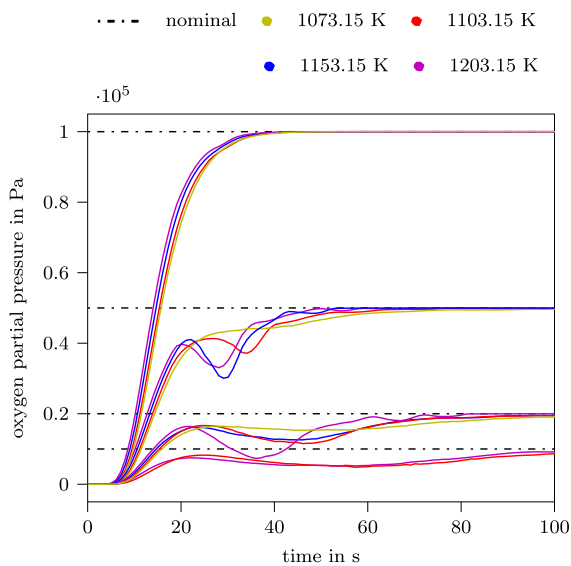


Fig. 3. Comparison between the nominal partial pressure and the actual partial pressure at the probe.

4.2. CFD setup

The TA apparatus was discretized with 30 600 hexahedral cells, displayed in Fig. 1. The solid walls were excluded in the simulation, and the wall temperature was fixed to the nominal-temperature, because this is controlled in the TA device. The mass flow and composition at the inlet were fixed according to the experimental setup. The sample was initialized as Cu₂O at the beginning of the experiment. The solid reactant was modeled by 209 Lagrangian parcels, with 10⁵ particles per parcel with a particle diameter of 5 μm. The experimental particle size

Table 1 Thermodynamic properties of the solid reactants.

	<i>W</i> g mol ⁻¹	<i>H_f</i> J mol ⁻¹	<i>c_p</i> J kg ⁻¹ K ⁻¹	<i>ρ</i> kg m ⁻³	<i>κ</i> W m ⁻¹ K ⁻¹
Cu ₂ O	143.091	-1 192 248	609	6000	0.78
CuO	79.545	-1 958 639	600	6480	0.78

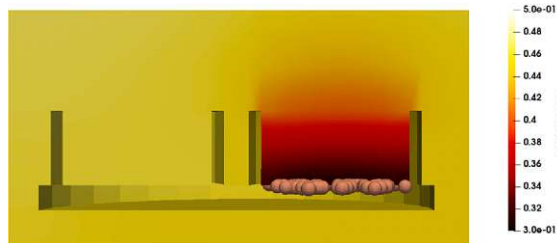


Fig. 4. Oxygen partial pressure of the virtual experiment at 1153.15 K and 0.5 bar oxygen partial pressure (nominal conditions) after 27 s experimental time, at 25% conversion.

distribution obtained with a Mastersizer 2000 [32] showed a bi-modal distribution. For this reason, the median diameter of the experimental particle size distribution was used.

The gas phase is modeled as perfect gas, the viscosity is calculated based on the Sutherland model, with the Sutherland coefficients (*A_s* = 1.512e - 6 and *T_s* = 120) from [35]. The heat capacity *c_p* is calculated from JANAF polynomials from [35], see Table 2.

For the solid species the thermal conductivity *κ*, density *ρ* and heat capacity *c_p* are assumed constant. They are given in Table 1 along with the heat of formation *H_f* and the molecular weight.

5. Results and discussion

In the previous sections we introduced the virtual experiment and explained how it is coupled with the real experiment to make use of the enhanced data. Now, we will showcase the method by applying it to the use case of Cu₂O oxidation. First, we discuss the deviations between nominal values and the values from the virtual experiment as well as the causes for these deviations. Then, we examine the effect on the identified kinetic model.

Fig. 2 shows the change of the reaction conditions during the virtual experiment in relation to the nominal values. Even though a very small sample mass has been used in the experiments (8.26 mg), the distance to the equilibrium reduces drastically compared to nominal values due to self-heating of the probe and a drop of the partial pressure. The temperature at the start of the reaction corresponds to the nominal temperature, but during the experiment the temperature increases due to the rapid release of reaction heat that cannot be dissipated instantly. This temperature increase also reduces the distance to equilibrium and consequently the driving force of the reaction. The drop in the oxygen partial pressure also contributes to the reduction of the equilibrium distance.

Fig. 3 shows the oxygen partial pressure in more detail. Initially, the partial pressure is zero, because the TA device is flooded with N₂ before the experiment. When the gas flow is switched to the O₂/N₂ mixture, the partial pressure quickly rises. Though, it does not do so immediately. This deviation from ideal plug-flow can be attributed to back mixing and diffusion. Once the reaction starts, there is an obvious drop in the partial pressure that is caused by the reactant depletion in close vicinity of the sample. Comparing the partial pressure drops in Fig. 3, it can be seen that the drop is more pronounced the faster the reaction proceeds, but in pure O₂ atmosphere, where the reaction is fastest, there is no drop in the partial pressure. This observation

suggests that the drop in partial pressure is caused by limited O_2 diffusion in N_2 atmosphere. This is in accordance with similar findings for gasification processes [36,37].

To visualize the reactant depletion at the sample, we chose the experiment with the nominal values 1153.15 K and 0.5 bar oxygen partial pressure, where the effect of reactant depletion is especially pronounced. Fig. 4 gives a close look on this effect inside the TA device. The partial pressure near the solid reactant is drastically reduced and the partial pressure gradient is clearly visible. Similar effects have been observed by [2,16,17].

The deviations between the idealized assumptions of constant temperature or partial pressure have been studied extensively, for example by [2,15–18]. A central take-away point of our study is, that it is possible to quantify these effects by setting up a CFD simulation and performing a virtual experiment. The results from the virtual experiment can be used to estimate the sample temperature and partial pressure in situations, when it is not feasible to improve the experimental design to the point where unwanted effects are eliminated completely and no deviations between the measured or nominal conditions and the actual conditions at the probe occur. Though, this approach is not meant to replace careful experimentation.

To make the impact on the kinetic model palpable, we used both the nominal values and the simulated values to derive kinetic models for the oxidation of Cu_2O with the TensorNPK method. Fig. 5 shows the contributions of conversion, temperature and distance to equilibrium according to the GKE. The simulated temperature and partial pressure affects the estimation of the $k(T)$ and $h(\Delta^{eq})$ terms in the GKE. With simulated values, the temperature sensitivity is considerably lower than with nominal values. This is, because high reaction rates are attributed to higher temperatures when self-heating is taken into consideration (Fig. 2). A similar observation can be made for the effect of the equilibrium distance: With simulated values it is less steep in close proximity to the equilibrium, because high reaction rates are attributed to smaller distances to the equilibrium.

This larger temperature sensitivity can also be seen in the activation energies that are derived from the $k(T)$ values: With nominal values the apparent activation energy is 218.9 kJ/mol; with simulated values it is 197.5 kJ/mol.

The estimation of the contributions to the GKE and the effect on the fitted models – such as the Arrhenius equation – show a significant impact of self-heating and reactant depletion. If these effects are not taken into account when deriving a kinetic model, this can have a practical meaning for chemical engineering applications. To illustrate this, we plotted the effective temperature dependency in Fig. 6. It shows the predicted reaction rate as a function of temperature at fixed oxygen partial pressures and $\alpha = 0.5$. These curves have been generated with the Arrhenius function and the second order polynomial fit to the effect of the equilibrium distance (solid lines in Fig. 5). Note, that the temperature input values to the kinetic models were in the range from 1070 K to 1200 K. The effective temperature dependency beyond these values is extrapolated. Even though the diagram should not be overinterpreted for this reason, it is a good illustration of the impact of self-heating and reactant depletion on the kinetic model nonetheless.

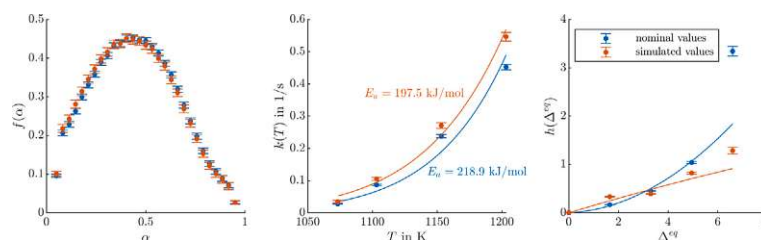


Fig. 5. Output of the TensorNPK method using the nominal reaction conditions and the simulated values as input.

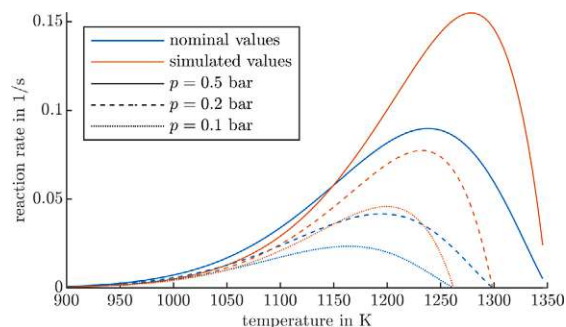


Fig. 6. Effective temperature dependency based on the two kinetic models in Fig. 5. The models were evaluated at $\alpha = 0.5$ and three partial pressures.

Table 2

Coefficients for the heat capacity calculated based on JANAF polynomials taken from [35].

N_2	3.531 01	-0.000 123 661	$-5.029 99 \cdot 10^{-7}$	$2.435 31 \cdot 10^{-9}$
	$-1.40881 \cdot 10^{-12}$	-1046.98	2.967 47	
O_2	3.782 46	-0.002 996 73	$9.8473 \cdot 10^{-6}$	$-9.6813 \cdot 10^{-9}$
	$3.243 73 \cdot 10^{-12}$	-1063.94	3.657 68	

The most striking difference between the two predictions is that the model based on enhanced kinetic data shows a much higher reaction rate peak. In general, the rate is dominated by the exponential Arrhenius function far away from the equilibrium, and then drops sharply towards the equilibrium. Thus, the later the drop, the higher the peak. The position of the drop depends mainly on the steepness at which the equilibrium dependency $h(\Delta^{eq})$ approaches zero. Fig. 5 shows that the model derived from simulated values is much steeper and, thus, it features higher peaks in the effective temperature dependency. The reason for this difference in steepness is, that the simulation showed that the experimental conversion rates need to be attributed to temperatures and partial pressures much closer to the equilibrium than the nominal values suggested.

This change of the peak has practical implications: It means that optimal (in the sense of highest rate) reaction conditions can be achieved much closer to the equilibrium than the nominal model would suggest. In fact, the peak reaction rate can be achieved at about 40 K above the prediction with nominal values. For applications in thermochemical energy storage, for example, this is good news. If the storage material can be operated at higher temperatures, the thermal efficiency can be expected to be considerably higher.

The observations on the CuO/Cu_2O reaction system demonstrated the possible effects of incorporating enhanced data in kinetic model identification, which could be done in the proposed way for any gas–solid reaction system. Although careful experimentation is still indispensable, the suggested approach to couple a virtual experiment with kinetic model identification paves the way towards more precise analysis of gas–solid reactions.

6. Conclusion

Accurate readings of the actual reaction conditions of the sample are essential for deriving reliable kinetic models. Even if experiments are conducted meticulously, nominal temperature and partial pressure values are known to be deviating from the actual conditions at the sample due to effects such as self-heating and reactant depletion.

These effects are inherent to gas–solid reactions and can never be eliminated completely. Though, with the presented method, the deviations can be quantified through a virtual experiment and the kinetic data can be enhanced. In the virtual experiment the temperature and partial pressure at the probe-site are determined with a CFD simulation which also takes into account the effect of the chemical reaction itself. The key novelty of our approach is that no kinetic model is required for the simulation. Instead, the reaction is modeled by using the experimentally determined conversion rates as direct input into the CFD simulation. In this way, the result of the virtual experiment can be used for kinetic model identification.

Since the enhanced data does not necessarily obey any simplified reaction conditions, e.g. isothermal or constant heating rate, a method to process arbitrary data for kinetic model identification is necessary.

To demonstrate our approach, we applied our approach to the oxidation of Cu_2O and used the TensorNPK method to derive two kinetic models: one using the classical approach with nominal values, and one using the reaction conditions directly at the sample calculated in the virtual experiment. The difference in the derived models can be critical for chemical engineering applications such as reactor design.

The results show that virtual experiments are a versatile tool to enhance experimental results when measured values are expected to be affected by effects such as self-heating/cooling and reactant depletion/accumulation. However, it is not meant to replace precise experimentation. Carefully planning, preparing and conducting experiments should still have highest priority. Our approach allows to quantify non-idealities in the virtual experiment and incorporate them in the kinetic model identification.

List of acronyms

CFD	Computational Fluid Dynamics
DSC	Differential Scanning Calorimetry
GKE	General Kinetic Equation
NPK	Non-parametric Kinetics
TA	Thermal Analysis
TGA	Thermogravimetric Analysis

List of symbols

symbol	name	unit
c_p	heat capacity	$\text{J kg}^{-1} \text{K}^{-1}$
\mathbf{g}	gravitational acceleration	m s^{-2}
h	enthalpy	J kg^{-1}
H_f	heat of formation	J kg^{-1}
K	kinetic energy	$\text{m}^2 \text{s}^{-2}$
p	pressure	Pa
S_h	energy source term	$\text{J m}^{-3} \text{s}^{-1}$
S_m	mass source term	$\text{kg m}^{-3} \text{s}^{-1}$
S_u	momentum source term	$\text{N m}^{-3} \text{s}^{-1}$
t	time	s
\mathbf{U}	velocity vector	m s^{-1}
W	molecular weight	g mol^{-1}
Y_i	mass fraction of species i	kg kg^{-1}
α_{eff}	effective thermal diffusivity	$\text{m}^2 \text{s}^{-1}$
κ	thermal conductivity	$\text{W m}^{-1} \text{K}^{-1}$
μ_{eff}	effective viscosity	Pa s
ρ	density	kg m^{-3}
$\boldsymbol{\tau}$	deviatoric stress tensor	N m^{-2}

Declaration of competing interest

The authors declare that they have no known competing financial interests or personal relationships that could have appeared to influence the work reported in this paper.

Acknowledgments

The authors gratefully acknowledge the funding support of K1-MET GmbH, Austria, metallurgical competence center. The research program of the competence center K1-MET is supported by COMET (Competence Center for Excellent Technologies), the Austrian program for competence centers. COMET is funded by the Federal Ministry for Transport, Innovation and Technology, the Federal Ministry for Science, Research and Economy, the provinces of Upper Austria, Tyrol, and Styria, and the Styrian Business Promotion Agency. The authors acknowledge TU Wien Bibliothek for financial support through its Open Access Funding Programme.

References

- [1] S. Vyazovkin, K. Chrissafis, M.L. Di Lorenzo, N. Koga, M. Pijolat, B. Roduit, N. Sbirrazzuoli, J.J. Suñol, ICTAC kinetics committee recommendations for collecting experimental thermal analysis data for kinetic computations, *Thermochimica Acta* 590 (2014) 1–23, <http://dx.doi.org/10.1016/j.tca.2014.05.036>.
- [2] S. Schulze, P. Nikrityuk, Z. Abosteif, S. Guhl, A. Richter, B. Meyer, Heat and mass transfer within thermogravimetric analyser: From simulation to improved estimation of kinetic data for char gasification, *Fuel* 187 (2017) 338–348, <http://dx.doi.org/10.1016/j.fuel.2016.09.048>.
- [3] A. Gomez, N. Mahinpey, Kinetic study of coal steam and CO₂ gasification: A new method to reduce interparticle diffusion, *Fuel* 148 (2015) 160–167, <http://dx.doi.org/10.1016/j.fuel.2015.01.071>.
- [4] S. Vyazovkin, A.K. Burnham, J.M. Criado, L.A. Pérez-Maqueda, C. Popescu, N. Sbirrazzuoli, ICTAC kinetics committee recommendations for performing kinetic computations on thermal analysis data, *Thermochimica Acta* 520 (2011) 1–19, <http://dx.doi.org/10.1016/j.tca.2011.03.034>.
- [5] B. Nowak, O. Karlström, P. Backman, A. Brink, M. Zevenhoven, S. Voglsam, F. Winter, M. Hupa, Mass transfer limitation in thermogravimetry of biomass gasification, *J. Therm. Anal. Calorim.* 111 (1) (2013) 183–192, <http://dx.doi.org/10.1007/s10973-012-2400-9>.
- [6] A. Jess, A.K. Andresen, Influence of mass transfer on thermogravimetric analysis of combustion and gasification reactivity of coke, *Fuel* 89 (7) (2010) 1541–1548, <http://dx.doi.org/10.1016/j.fuel.2009.09.002>.
- [7] P. Geng, Y. Zhang, Y. Zheng, Experimental estimate of CO₂ concentration distribution in the stagnant gas layer inside the thermogravimetric analysis (TGA) crucible, *Fuel* 224 (2018) 250–254, <http://dx.doi.org/10.1016/j.fuel.2018.03.057>.
- [8] M. Malekshahian, A. De Visscher, J.M. Hill, A non-equimolar mass transfer model for carbon dioxide gasification studies by thermogravimetric analysis, *Fuel Process. Technol.* 124 (2014) 1–10, <http://dx.doi.org/10.1016/j.fuproc.2014.02.009>.
- [9] R. Narayan, M.J. Antal, Thermal lag, fusion, and the compensation effect during biomass pyrolysis, *Ind. Eng. Chem. Res.* 35 (5) (1996) 1711–1721, <http://dx.doi.org/10.1021/ie950368i>.
- [10] M.J. Antal, G. Várhegyi, Impact of systematic errors on the determination of cellulose pyrolysis kinetics, *Energy Fuels* 11 (6) (1997) 1309–1310, <http://dx.doi.org/10.1021/ef970030w>.
- [11] O. Vekemans, J.P. Lavolette, J. Chaouki, Thermal behavior of an engineered fuel and its constituents for a large range of heating rates with emphasis on heat transfer limitations, *Thermochim. Acta* 601 (2015) 54–62, <http://dx.doi.org/10.1016/j.tca.2014.12.007>.
- [12] C. Branca, C. Di Blasi, Self-heating effects in the thermogravimetric analysis of wood char oxidation, *Fuel* 276 (April) (2020) 118012, <http://dx.doi.org/10.1016/j.fuel.2020.118012>.
- [13] R. Comesaña, *Contribuciones al modelado CFD de la Pirólisis de Biomasa Sólida Mediante la Simulación, Mejora y contraste experimental de un TG-FTIR*, (Thesis doctoral), Universidade de Vigo, 2011.
- [14] R. Comesaña, M.A. Gómez, M.A. Álvarez, P. Eguía, Thermal lag analysis on a simulated TGA-DSC device, *Thermochim. Acta* 547 (2012) 13–21, <http://dx.doi.org/10.1016/j.tca.2012.08.008>.
- [15] R. Comesaña, M.A. Gómez, M.A.A. Feijoo, P. Eguía, CFD simulation of a TG – DSC furnace during the indium phase change process, *Appl. Energy* 102 (2013) 293–298, <http://dx.doi.org/10.1016/j.apenergy.2012.07.019>.
- [16] R. Buczyński, G. Czernski, K. Zubek, R. Weber, P. Grzywacz, Evaluation of carbon dioxide gasification kinetics on the basis of non-isothermal measurements and CFD modelling of the thermogravimetric analyser, *Fuel* 228 (2018) 50–61, <http://dx.doi.org/10.1016/j.fuel.2018.04.134>.

- [17] S. Lan, M. Gaeni, H. Zondag, A.V. Steenhoven, C. Rindt, Direct numerical simulation of the thermal dehydration reaction in a TGA experiment, *Appl. Therm. Eng.* 128 (2018) 1175–1185, <http://dx.doi.org/10.1016/j.applthermaleng.2017.08.073>.
- [18] D. De La Cuesta, M.A. Gómez, J. Portteiro, L. Febrero, E. Granada, E. Arce, CFD analysis of a TG – DSC apparatus, *J. Therm. Anal. Calorim.* 118 (2014) 641–650, <http://dx.doi.org/10.1007/s10973-014-3734-2>.
- [19] L. Favergeon, J. Morandini, M. Pijolat, M. Soustelle, A general approach for kinetic modeling of solid-gas reactions at reactor scale : Application to kaolinite dehydroxylation, *Oil Gas Sci. Technol. Rev. IFP Energies Nouvelles* 68 (6) (2013) 1039–1048, <http://dx.doi.org/10.2516/ogst/2012018>.
- [20] V. Furtado de Moura, *Análise térmica computacional via cfd openfoam*, (Doctoral thesis), Universidade Federal do Espírito Santo, 2018.
- [21] A. Benedetti, M. Modesti, M. Strumendo, Cfd analysis of the CaO-CO₂ reaction in a thermo- gravimetric apparatus, *Chem. Eng. Trans.* 43 (2015) 1039–1044, <http://dx.doi.org/10.3303/CET1543174>.
- [22] F. An, F. Küster, R. Ackermann, S. Guhl, A. Richter, Heat and mass transfer analysis of a high-pressure TGA with defined gas flow for single-particle studies, *Chem. Eng. J.* 411 (January) (2021) 128503, <http://dx.doi.org/10.1016/j.cej.2021.128503>.
- [23] H. Weller, G. Tabor, H. Jasak, C. Fureby, A tensorial approach to computational continuum mechanics using object-oriented techniques, *Comput. Phys.* 12 (6) (1998) 620–631, <http://dx.doi.org/10.1063/1.168744>.
- [24] H.A. Jakobsen, *Chemical Reactor Modeling : Multiphase Reactive Flows*, Springer, Berlin [u.a.], 2008.
- [25] D. Gidaspow, *Multiphase Flow and Fluidization. – Continuum and Kinetic Theory Descriptions*, Academic Press Inc., 1994.
- [26] W.E. Ranz, W.R.J. Marshall, *Evaporation from drops Part I*, *Chem. Eng. Progress* 48 (3) (1952) 141–146.
- [27] F. Birkelbach, M. Deutsch, S. Flegkas, F. Winter, A. Werner, NPK 2.0: Introducing tensor decompositions to the kinetic analysis of gas-solid reactions, *Int. J. Chem. Kinetics* 51 (4) (2019) 280–290, <http://dx.doi.org/10.1002/kin.21251>.
- [28] F. Birkelbach, M. Deutsch, A. Werner, The effect of the reaction equilibrium on the kinetics of gas-solid reactions — A non-parametric modeling study, *Renew. Energy* 152 (2020) 300–307, <http://dx.doi.org/10.1016/j.renene.2020.01.033>.
- [29] L.-C. Söğütoğlu, F. Birkelbach, A. Werner, H. Fischer, H. Huinink, O. Adan, Hydration of salts as a two-step process: Water adsorption and hydrate formation, *Thermochim. Acta* 695 (2021) 178819, <http://dx.doi.org/10.1016/j.tca.2020.178819>.
- [30] N. Saadatkah, A. Carillo Garcia, S. Ackermann, P. Leclerc, M. Latifi, S. Samih, G.S. Patience, J. Chaouki, Experimental methods in chemical engineering: Thermogravimetric analysis—TGA, *Canadian J. Chem. Eng.* 98 (1) (2020) 34–43, <http://dx.doi.org/10.1002/cjce.23673>.
- [31] J. Opfermann, Kinetic analysis using multivariate non-linear regression. I. Basic concepts, *J. Therm. Anal. Calorim.* 60 (2) (2000) 641–658, <http://dx.doi.org/10.1023/A:1010167626551>.
- [32] S. Setoodeh Jahromy, F. Birkelbach, C. Jordan, C. Huber, M. Harasek, A. Werner, F. Winter, Impact of partial pressure, conversion, and temperature on the oxidation reaction kinetics of Cu₂O to CuO in thermochemical energy storage, *Energies* 12 (3) (2019) 508, <http://dx.doi.org/10.3390/en12030508>.
- [33] M. Deutsch, F. Horvath, C. Knoll, D. Lager, C. Gierl-Mayer, P. Weinberger, F. Winter, High-temperature energy storage: Kinetic investigations of the CuO/Cu₂O reaction cycle, *Energy Fuels* 31 (3) (2017) 2324–2334, <http://dx.doi.org/10.1021/acs.energyfuels.6b02343>.
- [34] E. Alonso, C. Pérez-Rábago, J. Licurgo, E. Fuentealba, C.A. Estrada, First experimental studies of solar redox reactions of copper oxides for thermochemical energy storage, *Sol. Energy* 115 (2015) 297–305, <http://dx.doi.org/10.1016/j.solener.2015.03.005>.
- [35] G.P. Smith, D.M. Golden, M. Frenklach, N.W. Moriarty, B. Eiteneer, M. Goldenberg, C.T. Bowman, R.K. Hanson, S. Song, W.C.J. Gardiner, V.V. Lissianski, Z. Qin, *GRI-MECH 3.0*, 2017, URL <http://www.me.berkeley.edu/gri-mech/>.
- [36] Y. Zhang, P. Geng, Y. Zheng, Exploration and practice to improve the kinetic analysis of char-CO₂ gasification via thermogravimetric analysis, *Chem. Eng. J.* 359 (2019) 298–304, <http://dx.doi.org/10.1016/j.cej.2018.11.122>.
- [37] A. Gómez-Barea, P. Ollero, R. Arjona, Reaction-diffusion model of TGA gasification experiments for estimating diffusional effects, *Fuel* 84 (12–13) (2005) 1695–1704, <http://dx.doi.org/10.1016/j.fuel.2005.02.003>.

Paper 4

The Effect of Turbulence on the Conversion of Coal under Blast Furnace Raceway Conditions

submitted to Fuel in collaboration with Nils Erland Haugen, Ewa Karchniwy, Markus Bösenhofer, Michael Harasek and Terese Løvås.

My contribution: Implementation of the model in OpenFOAM. Simulation and analyzes of the results. Conceptualization and writing the original draft.

The Effect of Turbulence on the Conversion of Coal under Blast Furnace Raceway Conditions

Eva-Maria Wartha^{a,*}, Nils Erland Haugen^{b,c}, Ewa Karchniwy^b, Markus Bösenhofer^{a,d}, Michael Harasek^a,
Terese Løvås^e

^aTU Wien, Institute of Chemical, Environmental and Bioscience Engineering, Getreidemarkt 9/166, 1060 Vienna, Austria

^bSINTEF Energi A.S., Sem Saelands vei 11, 7034 Trondheim, Norway

^cEnergy Engineering, Div. Energy Science, Luleå University of Technology, 97187 Luleå, Sweden

^dK1-Met GmbH, Area 4 - Simulation and Analyses, Stahlstrasse 14, BG 88, 4020 Linz, Austria

^eDepartment of Energy and Process Engineering, Norwegian University of Science and Technology, Kolbjørn Hejes vei 1B,
7034 Trondheim, Norway

Abstract

The main production route for steel in Europe is still via the blast furnace. Computational fluid dynamics (CFD) can be used to analyze the process virtually and thus improve its performance. Different reducing agents can be used to (partially) substitute the coke and consequently reduce overall emissions. To analyze different reducing agents effectively using CFD, their conversion process has to be modeled accurately. Under certain conditions, coal particles can cluster as the result of turbulence effects, which further reduces the mass transfer to the coal surface and consequently the conversion rate. We analyze the effect of turbulence under blast furnace raceway conditions on the conversion of coal particles and on the overall burnout. The model is applied in RANS to polydisperse particle systems and this is then compared to the simplified monodisperse assumption. Additionally, the model is extended to gasification reactions. Overall, we find that the turbulent effects on coal conversion are significant under blast furnace raceway conditions and should be considered in further simulations. Furthermore, we show that an a-priori assessment is difficult because the analysis via averaged quantities is impractical and the effects of turbulence need to be correlated to the regions of conversion.

Keywords: coal combustion, blast furnace, turbulence effects, kinetic-diffusion limited, computational fluid dynamics

1. Introduction

1 Blast furnaces together with basic oxygen furnaces account for around 60 % of current steel production
2 in Europe [1]. Due to its very large energy consumption and high CO₂ emissions, the process is subject
3 to ongoing improvements. Computational fluid dynamics (CFD) can help to better understand the process
4

*Corresponding author

Email address: eva-maria.wartha@tuwien.ac.at (Eva-Maria Wartha)

Preprint submitted to Fuel

June 3, 2022

Nomenclature

Acronyms

CFD Computational Fluid Dynamics
 DNS Direct Numerical Simulation
 EDC Eddy Dissipation Concept
 RANS Reynolds Averaged Navier-Stokes

Greek symbols

α mass transfer rate
 $\tilde{\alpha}$ correction factor
 ϵ turbulent dissipation rate, $\text{m}^2 \text{s}^{-3}$
 ν viscosity, $\text{m}^2 \text{s}^{-1}$
 ρ density, kg m^{-3}
 τ time scale, s

Roman symbols

$A_{1/2}$ parameters in the cluster model
 A surface area, m^2
 $A_{r,1/2}$ pre-exponential factor
 A_{sr} parameter for the CO/CO₂ ratio
 C concentration, kmol m^{-3}
 c_p specific heat capacity, $\text{J kg}^{-1} \text{K}^{-1}$
 Da Damköhler number
 D Diffusion coefficient, $\text{m}^2 \text{s}^{-1}$
 d diameter, m
 $\bar{d}_{p,1}$ average diameter on number basis, m
 $\bar{d}_{p,3}$ average diameter on mass basis, m
 $E_{a/1/2}$ activation energy
 e emissivity
 f scattering factor
 h retention coefficient
 $I(\tilde{\alpha})$ Index as a function of the correction factor
 k turbulent kinetic energy, $\text{m}^2 \text{s}^{-2}$
 L length, m

m number of particles
 n parameter in Rosin-Rammler dist.
 n_p particle number density
 p pressure, Pa
 Re Reynolds number
 R ideal gas constant, $\text{J mol}^{-1} \text{K}^{-1}$
 $RR(\tilde{\alpha})$ cumulative conversion rate
 Sc Schmidt number
 Sh Sherwood number
 St Stokes number
 T_A E_a/R , K
 T_{sr} parameter for the CO/CO₂ ratio
 T temperature, K
 v stoichiometric coefficient
 W molecular weight, kJ kmol^{-1}

Sub- & superscripts

0 initial condition / at time 0
 b bulk
 chem chemical
 cl cluster
 daf dry ash free
 f fluid
 g gas
 hom homogeneous
 i iteration index
 L integral
 p particles
 q quiescent
 rel relative
 s surface
 t turbulent

5 and obtain detailed information about the process conditions inside the blast furnace. Reducing agents can
 6 be supplied in the blast furnace raceway zone to reduce coke consumption [2, 3]. Fig. 1 shows a schematic
 7 blast furnace with its in- and outflows and the raceway zone highlighted. The raceway is the cavity formed
 8 in the vicinity of the tuyere.

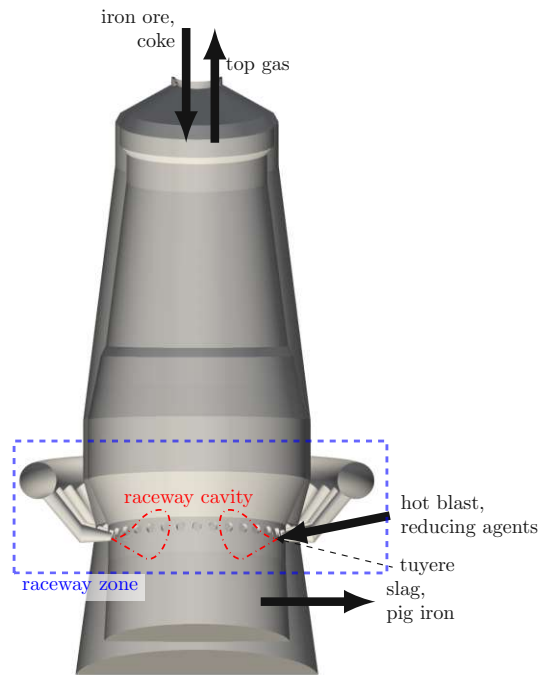


Figure 1: Schematic description of the blast furnace with in- and outflows marked by arrows. Raceway zone is marked by dashed rectangle, two raceway cavities by dashdotted lines and tuyere position by dashed arrow.

9 A commonly used reducing agent is pulverized coal. Pulverized coal particles have high heating rates,
 10 a short residence time in the raceway zone, and can withstand highly turbulent conditions. Because the
 11 experimental reconstruction of the raceway conditions is difficult [4], CFD can be used to test the conversion
 12 of different coals in the raceway zone virtually. Shen and Yu [5], Liu and Shen [6] and Liu et al. [7] presented
 13 studies modeling the coal as Lagrangian particles in the raceway zone. To gain useful insight in blast furnace
 14 operation through CFD, suitable models covering the essential effects of conversion need to be applied.

15 Many approaches to model the turbulent effects on homogeneous reactions, for example combustion
 16 reactions [8], exist. They can be applied to model the homogeneous reactions in the blast furnace and have
 17 been reviewed by [9]. On the contrary, the work on turbulent effects on heterogeneous reactions is relatively
 18 sparse. First attempts to study those effects have been made by Krüger et al. [10] and Haugen et al. [11].
 19 In direct numerical simulations (DNSs) they showed that turbulence can significantly influence the mass

20 transport to small particles and consequently reduce their conversion rate. They published a correction
21 factor to model this effect based on the turbulent flow conditions. Later on, the work has been extended to
22 polydisperse particle systems by Karchniwy et al. [12] and first unresolved simulation studies for industrial
23 scale applications have been presented by Karchniwy et al. [13]. Therefore, the question arises whether the
24 conditions in the raceway are such, that the influence of turbulent clustering should be taken into account
25 when modeling reducing agent conversion. Providing insight on these objectives is the main focus of this
26 paper.

27 To ground the ensuing discussion, the necessary models to describe the thermochemical conversion
28 process of Lagrangian particles in the blast furnace are introduced. This is followed by a recap of the
29 correlation for the turbulent effects on the conversion by Krüger et al. [10], Haugen et al. [11]. To obtain a
30 better understanding of the effects, their influence is illustrated in the theoretical considerations in Section 2.
31 We first studied the effect of the clustering in an injection rig. The particle diameter size was varied
32 and, additionally, the importance of the gasification reactions were also investigated. Following this, the
33 turbulent clustering effect was studied in a model of a real blast furnace, reported on in Section 3. Finally,
34 in Section 4, we summarize our results and present concluding remarks on the importance of clustering for
35 the coal conversion under blast furnace conditions.

36 2. Models and Implementation

37 We used a finite volume approach to simulate the flow and the combustion in the domain of interest.
38 The software OpenFOAM [14] - version 9 - was used as a basis, adding the necessary gasification and
39 devolatilization models and the model for the influence of turbulence on the mass transfer to the particles.
40 The model details are discussed in the following and the code amendments for the clustering model can be
41 found in [15].

42 2.1. Gas phase

43 Industrial processes, such as the blast furnace, are usually large in size. Therefore, the spatial resolution
44 used in CFD is limited and the turbulence scales are not resolved on the numerical mesh. In this study, we
45 used a Reynolds Averaged Navier Stokes Equation (RANS)-approach to model the fluid flow in the domain
46 of interest. A two-equation turbulence model was chosen - the $k-\epsilon$ model [16, 17], which is widely applied
47 in blast furnace simulations [9].

48 The gaseous phase is a multi-component mixture, which reacts with the solid particles. The volatile
49 components are released from the solid combust in the gas phase. The turbulent combustion process needs
50 to be modeled by a turbulence-chemistry interaction model. We used the Eddy Dissipation Concept (EDC)
51 from Magnussen [18], with the simplification of treating the fine structures as plug flow reactors (PFR)

52 instead of partially stirred reactors (PSR) due to its reduced computational cost. The implications of this
 53 modeling choice have been thoroughly discussed by Ertesvåg [19] and Bösenhofer et al. [20].

54 2.2. Solid particles

55 The combustible particles were treated as Lagrangian particles – modeled according to Newton’s laws
 56 of motion. The interaction between the solid and gas phase was modeled by a drag model for the momen-
 57 tum (spherical drag model) and a heat transfer model [21, 22] for the energy. The species and momentum
 58 equations were coupled through the source terms from the thermo-chemical conversion. The coal conver-
 59 sion was treated as a consecutive process consisting of: drying of the moist coal (vaporization of water),
 60 devolatilization, and char conversion. The modeling details of each conversion step are described in the
 61 following subsections.

62 2.2.1. Drying

63 The drying process of the coal was modeled according to:

$$\frac{dm_{\text{H}_2\text{O}}}{dt} = \text{Sh} \frac{D_{\text{H}_2\text{O}}}{d_p} (C_{\text{H}_2\text{O},s} - C_{\text{H}_2\text{O},b}) \pi d_p^2 W_{\text{H}_2\text{O}} \quad (1)$$

64 where the Sherwood correlation according to Eq. (9) was used - with the standard relative velocity u_{rel} for
 65 the particle Reynolds number, Eq (11). $D_{\text{H}_2\text{O}}$ is the diffusion coefficient for water, d_p the particle diameter,
 66 $W_{\text{H}_2\text{O}}$ the molecular weight of water, and $C_{\text{H}_2\text{O},s}$ and $C_{\text{H}_2\text{O},b}$ the vapor concentration at the surface and
 67 in the bulk, respectively, calculated by the ideal gas law at film temperature. For the calculation of the
 68 concentrations $C_{\text{H}_2\text{O},s}$ and $C_{\text{H}_2\text{O},b}$ the saturation pressure and bulk pressure, and the mass fraction at the
 69 surface and in the bulk were used.

70 2.2.2. Devolatilization

71 A two-step kinetic model was used to model the devolatilization process above a temperature of 400 K.
 72 In this model, the release rate of volatiles for a given particle is given by:

$$\frac{dm_{vol}}{dt} = \left[\alpha_1 A_{r,1} \exp \frac{E_1}{RT} + \alpha_2 A_{r,2} \exp \frac{E_2}{RT} \right] m_{vol,0} \quad (2)$$

73 where $m_{vol,0}$ is the initial volatile content of the particle, and $A_{r,1}$, $A_{r,2}$, E_1 , E_2 are the kinetic parameters
 74 taken from Shen et al. [23], see Table A.3. Shen et al. [23] compared different devolatilization models for coal
 75 combustion under blast furnace conditions and concluded that this two competing step model is sufficiently
 76 accurate. The parameters α_1 and α_2 were calculated based on the volatiles content:

$$\alpha_1 = Y_{vol,daf} \quad \alpha_2 = 1.25\alpha_1^2 + 0.92\alpha_1. \quad (3)$$

77 The volatiles were modeled as one pseudo-species according to the elemental analysis for the coal. The
 78 thermophysical properties of that volatile species were modeled as for CH_4 and the heat balance was closed
 79 by adjusting the latent heat of devolatilization L_{devol} . The same approach was used e.g. by Petersen and
 80 Werther [24] in combination with a gasification model.

81 2.2.3. Char conversion

82 The remaining char after drying and devolatilization was modeled as carbon and ash. The carbon reacts
 83 according to the shrinking particle model [25], taking boundary diffusion limitation and kinetic limitation
 84 into account, while neglecting any pore diffusion effects, such that the conversion of char is given by:

$$\frac{dm_{char}}{dt} = \eta A_p p_i \frac{k_{kin} k_{dif}}{k_{kin} + k_{dif}} \quad (4)$$

85 with the particle surface area A_p , the partial pressure of the reactant p_i , the effectiveness factor η - a model
 86 parameter - and the reaction contributions, taken as a resistance model between the kinetic reaction rate
 87 k_{kin} and the diffusion rate k_{dif} .

88 The kinetic reaction rate was modeled according to an Arrhenius expression:

$$k_{kin} = A_r \exp \frac{E_a}{RT} \quad (5)$$

89 where A_r is the pre-exponential factor, E_a the activation energy, R the ideal gas constant and T the
 90 temperature, see Table A.4. The diffusion rate determined through mass transfer to the boundary was
 91 modeled as:

$$k_{dif} = \frac{C}{d_p} \left(\frac{T_p + T_f}{2} \right)^{0.75} \quad (6)$$

92 where C is a diffusion constant (Table A.4), d_p the particle diameter, and T_p and T_f the particle and fluid
 93 temperatures, respectively.

94 2.3. Turbulence effect

95 The models presented for the thermochemical conversion process of a coal particle are based on single
 96 particle models. Krüger et al. [10] and Haugen et al. [11] showed that small particles cluster in turbulent
 97 eddies. Consequently, since particles consume oxygen, the local oxygen concentration in the particle sur-
 98 roundings is typically significantly lower than the average oxygen concentration in the larger control volume.
 99 This leads to reduced mass transfer to the particle surface and consequently to reduced conversion rates.

100 For the derivation of the turbulence effect, several dimensionless numbers were used, which are introduced
 101 here. First, the Damköhler number, which relates the integral time scale:

$$\tau_L = \frac{2k}{3\epsilon} \quad (7)$$

102 to the chemical time scale τ_{chem} :

$$\text{Da} = \frac{\tau_L}{\tau_{\text{chem}}} = \tau_L \alpha_{\text{hom,q}}. \quad (8)$$

103 The chemical timescale was approximated as the inverse of the reaction rate in a homogeneous quiescent
104 flow $\alpha_{\text{hom,q}}$. Furthermore, the Sherwood number was used, which represents the rate of convective mass
105 transfer to diffusive mass transfer. It can be expressed in analogy to the Nusselt number for heat transfer
106 by the following correlation:

$$\text{Sh} = 2 + 0.69\text{Re}^{1/2}\text{Sc}^{1/3} \quad (9)$$

107 where the Schmidt number (Sc) is defined as the ratio of the viscous (dynamic viscosity ν) to the mass
108 diffusion rate (diffusion coefficient D):

$$\text{Sc} = \frac{\nu}{D}. \quad (10)$$

109 Special care needs to be taken for the particle Reynolds number, because no true relative velocity exists
110 between the velocity fluctuations of the turbulent fluid and the Lagrangian particles [11]:

$$\text{Re} = \frac{u_{\text{rel}} d_p}{\nu}. \quad (11)$$

111 The true relative velocity velocity was approximated according to Haugen et al. [11]:

$$u_{\text{rel}} = \min \left(0.41 \sqrt{\frac{2}{3}} k, 0.41 \sqrt{\frac{2}{3}} k \left[\frac{\text{St} k_L^{-2/3} - k_\eta^{-2/3}}{k_L^{-2/3} - k_\eta^{-2/3}} \right] \right) \quad (12)$$

112 including the turbulent kinetic energy k , the wave number of the integral scale

$$k_L = 2\pi\epsilon \left(\frac{3}{2k} \right)^{3/2} \quad (13)$$

113 and the Kolmogorov scale

$$k_\eta = 2\pi \frac{\epsilon^{0.25}}{\nu^{0.75}}. \quad (14)$$

114 The Stokes number

$$\text{St} = \frac{\tau_P}{\tau_L} \quad (15)$$

115 is the ratio of the integral to the particle time scale, where

$$\tau_P = \frac{\rho_p d_p^2}{18\mu}. \quad (16)$$

116 Let us now turn to the actual turbulence effect on the mass transfer rate to the particles. Krüger et al.
117 [10] proposed a correction factor to define the relationship between the reaction rate in turbulence-induced
118 clusters, α , in relation to the reaction rate in a homogeneous quiescent flow, $\alpha_{\text{hom,q}}$:

$$\tilde{\alpha} = \frac{\alpha}{\alpha_{\text{hom,q}}}. \quad (17)$$

119 The reaction rate in homogeneous, quiescent flow, based on pure diffusion limitation is given as:

$$\alpha_{\text{hom,q}} = An_p k_{\text{eff}} = An_p k_{\text{diff}} \quad (18)$$

120 where A is the mean external surface area of the particles, n_p the particle number density and k_{eff} the
121 effective reaction rate, which in case of diffusion limitation is equal to the diffusion rate k_{diff} .

122 To investigate the effect of turbulent clusters, two cases can be considered: First, for small Damköhler
123 numbers (Eq. (8)), referred to as the individual particle combustion regime, the oxygen consumption rate
124 scales linearly with the particle number density and is enhanced by the turbulence, scaling with the Sherwood
125 number (Eq. (9)) as:

$$\alpha_{\text{hom,t}} = \alpha_{\text{hom,q}} \frac{\text{Sh}}{2}. \quad (19)$$

126 Second, for large Damköhler numbers, referred to as sheath combustion, the conversion is independent
127 of the particle number density:

$$\alpha_{\text{cl}} = \frac{(A_1 A_2) \text{Sh}}{\tau_L \text{St}}. \quad (20)$$

128 The correlation for $A_1 A_2$ was derived by Haugen et al. [11] as $A_1 A_2 = 0.08 + \frac{\text{St}}{3}$, where St is the Stokes
129 number (Eq. (15)) and τ_L is the integral time scale (Eq.(7)). The regimes for high and low Damköhler
130 numbers were connected by taking the harmonic mean:

$$\alpha = \frac{\alpha_{\text{cl}} \alpha_{\text{hom,t}}}{\alpha_{\text{cl}} + \alpha_{\text{hom,t}}}. \quad (21)$$

131 Combining Eq. (17), Eq. (19), Eq. (21), and Eq. (8) yields the correction factor, which was also obtained
132 by Krüger et al. [10], as:

$$\tilde{\alpha} = \frac{\alpha_{\text{cl}}}{\alpha_{\text{cl}} + \text{DaSh}/(2\tau_L)} \frac{\text{Sh}}{2}. \quad (22)$$

133 The models shown were derived based on the assumption of isotropic turbulence. This was expected to
134 be a relatively good approximation for the char conversion phase and the correlation for the clustering could
135 be applied to RANS. Karchniwy et al. [13] presented the application of the model in RANS simulations.
136 However, since the correlation was only applied for single particle diameters in different cases and for
137 polydisperse particles in RANS, some clarification should be made. The Sherwood and Stokes numbers can
138 be calculated on a particle or parcel basis, as for a single diameter. However, we suggest using averaged
139 values on a cell basis for the Damköhler number and for the theoretical combustion in a quiescent flow.
140 This strategy seems justifiable because Karchniwy et al. [12] showed that polydisperse particles cluster in
141 the same regions and in a similar way. Furthermore, the Damköhler number is an average measure for the
142 overall conversion process of the particle cloud without clustering.

143 2.4. Theoretical considerations

144 If a blended reaction model as in Eq. (4) is used, the clustering only influences the mass transport to the
 145 particles and therefore only the diffusion reaction rate and not the intrinsic kinetics, Karchniwy et al. [13]
 146 showed, that even if the turbulence correction factor $\tilde{\alpha}$ is low in some cases, the clustering is less influential
 147 if the conversion is mainly controlled by kinetics. To illustrate the two regimes, Fig. 2 shows the diffusion
 148 reaction rate, the kinetic reaction rate and the effective reaction rate as a function of temperature for the
 149 char oxidation parameters used in this study (see Table A.4).

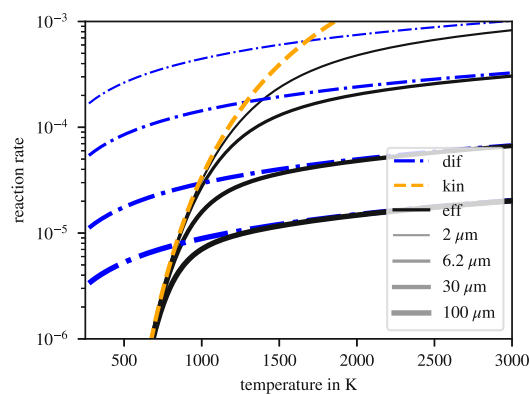


Figure 2: Reaction rates - kinetic effect (orange), diffusional effect (blue) and effective (black) - over temperature for different particle sizes (varying line width)

150 As can be seen from Fig. 2, the regime change is not only influenced by temperature, but also by the
 151 particle diameter. This is because the kinetic reaction rate is not influenced by the diameter but the diffusion
 152 rate varies with $1/d_p$. Therefore, the thermochemical conversion of smaller particles is usually less diffusion
 153 controlled. Although, specific parameters were used for Fig. 2, a kinetic-diffusion limited reaction model
 154 will always show similar characteristics.

155 Fig. 3 shows the correction factor $\tilde{\alpha}$ as a function of the particle diameter for a range of turbulent kinetic
 156 energy and particle number density values. The temperature was fixed to 2500K and the particle density to
 157 1300kg m^{-3} , because only minor effects of those parameters were observed. The most influential parameter
 158 seems to be the particle number density. The reason for this is that for large particle number densities the
 159 chemical timescale becomes comparable and eventually also larger than the life time of the particle clusters.
 160 The volume occupied by the cluster will therefore be void of oxygen, while the surrounding volumes will
 161 contain much oxygen.

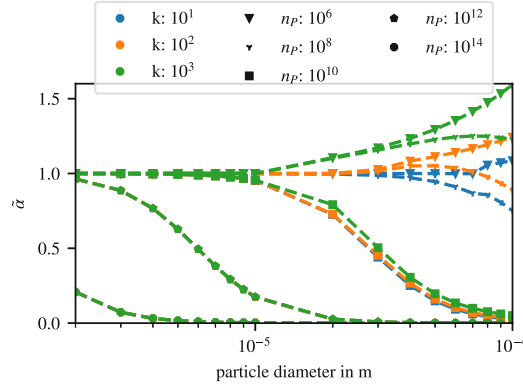


Figure 3: Correction factor as a function of particle diameter, computed for $\rho = 1300\text{kg m}^{-3}$, $T = 2500\text{ K}$, $p = 1\text{ bar}$

162 **3. Results**

163 *3.1. Injection Rig*

164 To study the turbulent clustering effects on coal under raceway conditions an injection rig was first
 165 investigated. The setup was designed to resemble blast furnace conditions from Mathieson et al. [26]. A
 166 preheated coflow was injected to mimic the blast, and coal was injected through a lance inclined by 6° to
 167 resemble the injection lance in a blast furnace, see Fig. 4. The walls around the combustion chamber were
 168 insulated.

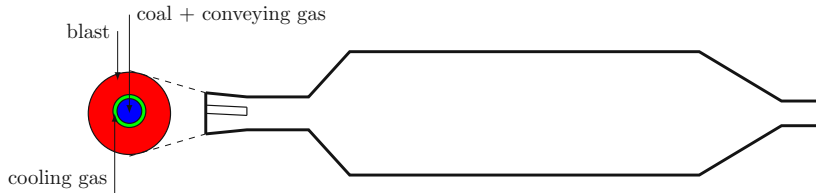


Figure 4: Schematic drawing based on the experimental setup from Mathieson et al. [26] and publications from Shen et al. [23, 27, 28]

169 For the CFD simulation, the domain was discretized by approximately half a million, mainly hexahedral,
 170 cells using snappyHexMesh from OpenFOAM-9 [29]. The boundary conditions were set according to the
 171 experiment and are summarized in Table 1. The case setup can be found in the following repository [15]. At
 172 the outlet, the pressure was set to 1 bar and Neumann boundary conditions used for the other quantities.
 173 For the turbulent kinetic energy, a 5% turbulence intensity inlet condition was used and for the dissipation
 174 rate a turbulent mixing length model with wall function models at the wall boundaries.

175 The coal with the lowest volatile content from Shen et al. [27] was chosen to investigate the turbulence

Table 1: Boundary conditions for the injection rig simulations

	temperature	inflow	type
	K	Nm ³ /h	
blast	1473	300	air
conveying gas	298	2	N ₂
cooling gas	298	3.2	air
chamber walls	1800	-	-

176 effects on char combustion. The mass flow rate of the coal is 31.6 kg h⁻¹. The particles were injected with
 177 an inlet velocity of 20 ms⁻¹ and an initial temperature of 300 K. The proximate and ultimate analysis
 178 of the coal are given in Table A.4. The particles are reflected at the wall boundaries and the velocity is
 179 multiplied by a restitution coefficient, which was set to 0.9. Additional constant particle parameters are
 180 given in Table A.4.

181 Different cases were investigated to study the effect of clustering on coal conversion in the injection rig.
 182 In Section 3.1.1, we study the effect with a fixed particle diameter, equal to the mean diameter on mass
 183 basis ($\bar{d}_{p,3} = 30\mu\text{m}$) or the mean diameter on number basis ($\bar{d}_{p,1} = 6.2\mu\text{m}$). In Section 3.1.2, the case is
 184 then extended by employing a diameter distribution of the particles to compare it to the single diameter
 185 approximation. Finally, the effect of turbulence on additional gasification reactions is shown in Section 3.1.3.

186 3.1.1. Injection rig - fixed diameter

187 Fig. 5 shows the conversion averaged over the downstream position for the two different particle diameters.
 188 For both cases the result is plotted with the standard conversion model (“standard”) and the model including
 189 the turbulent clustering effects (“clustering”). For the larger particles $\bar{d}_{p,3}$, we see a slight reduction in
 190 conversion caused by turbulence. This is especially pronounced in the downstream part of the rig. The
 191 results agree with the average turbulence correction factor, shown in Fig. 6, which is below one until $z=1.2$ m
 192 of the domain. At the beginning, we have lower correction factors for this case, but the coal still dries and
 193 devolatilizes and, therefore, no influence on the char conversion can be seen. The char conversion for the $\bar{d}_{p,3}$
 194 particles is mainly diffusion controlled, because the particles are already heated up above 1200 K when char
 195 conversion begins, as shown in Fig. 2.

196 For the small particles ($\bar{d}_{p,1} = 6.2\mu\text{m}$), we observe a reduction in conversion at the first section (up to
 197 0.2 m), followed by no influence of turbulence at approximately 0.4 to 0.6 m downstream. Fig. 6 shows the
 198 average turbulence correction factor, which is below 1 for the small particles in the whole domain. This
 199 confounds the observation from Fig. 5, where the conversion seems not to have been influenced or even
 200 enhanced by the turbulence for the small particles between 0.45 and 0.6 m.

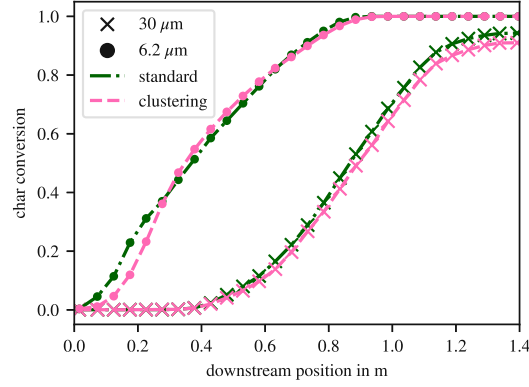


Figure 5: Char conversion in the injection rig averaged over the downstream position for the case with particle diameter $\bar{d}_{p,3} = 30\mu\text{m}$ and $\bar{d}_{p,1} = 6.2\mu\text{m}$.

201 Therefore, in Fig. 7 we take a closer look at the combination of the turbulence correction factor and the
 202 CO source term in the cross section of the rig. In the first part of the rig (up to 0.2 m), the turbulence
 203 correction factor is virtually everywhere well below unity, corresponding to a reduction in the conversion.
 204 Further downstream, $\tilde{\alpha}$ is still well below unity in the jet center, but approaches unity in the outer parts.
 205 This shows that for this particular case, the regions where most of the char conversion occurs are correlated
 206 with the regions where the correction factor is approaching unity. Furthermore, the overall conversion of
 207 the smaller particles is less diffusion controlled than for the larger particles, see Fig. 2, which leads overall
 208 to few turbulence effects.

209 To quantitatively evaluate the effect of clustering, let us organize all particles in increasing order with
 210 respect to their correction factor $\tilde{\alpha}$. The particle with the lowest correction factor is identified by the index
 211 $i = 0$ and the particle with the highest correction factor with $i = m$, where m is the total number of
 212 particles. We now define the index $I(\tilde{\alpha})$ as the index of the particle with the highest correction factor that
 213 is still below $\tilde{\alpha}$. The cumulative conversion rate $RR(\tilde{\alpha})$ to quantitatively evaluate the turbulence effect is
 214 then given by:

$$RR(\tilde{\alpha}) = \left(\sum_{i=0}^{i=I(\tilde{\alpha})} \frac{dm_{\text{char},i}}{dt} \right) / \left(\sum_{i=0}^{i=m} \frac{dm_{\text{char},i}}{dt} \right) \quad (23)$$

215 In Fig. 8 this cumulative conversion rate is plotted over the correction factor. The point for $RR(\tilde{\alpha}) = 50\%$
 216 is marked by circles. This evaluation gives a better estimate of the overall turbulence influence than the
 217 average calculation of $\tilde{\alpha}$ as a function of the downstream position in Fig. 6. However, whether the conversion
 218 is diffusion or kinetic controlled will also influence the overall turbulence effect. Fig 8 suggests that the
 219 reduction in mass transfer is stronger for the $\bar{d}_{p,1} = 6.2\mu\text{m}$ particles than for the $\bar{d}_{p,3} = 30\mu\text{m}$ particles,
 220 but it is less according to Fig. 5 because the conversion of the $\bar{d}_{p,1}$ particles is less diffusion controlled than

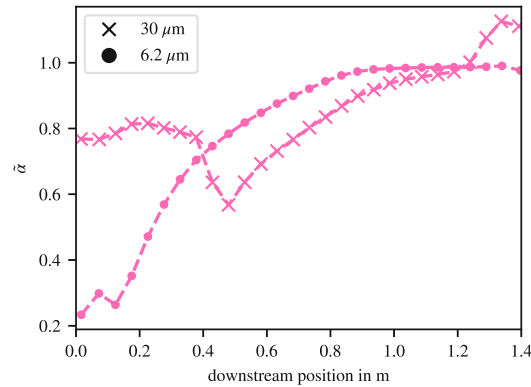


Figure 6: Turbulence correction factor in the injection rig averaged over the downstream position for the case with particle diameter $\bar{d}_{p,3} = 30\mu\text{m}$ and $\bar{d}_{p,1} = 6.2\mu\text{m}$.

221 for the $\bar{d}_{p,3}$ particles (see Fig. 2). Overall, the relation shown in Fig. 8 gives a quantitative estimate of the
 222 possible influence of turbulence, but is still dependent on the conversion regime.

223 3.1.2. Injection rig – diameter distribution

224 We now look at the effect of the particle size distribution for the same setup as studied in Section 3.1.1. In
 225 real applications, and in the experiments by Shen et al. [27], coal particles are present in certain size ranges.
 226 Karchniwy et al. [12] showed that polydisperse particles experience the effects of clustering in the same way
 227 as monodisperse systems do. Therefore, the turbulence correction factor for monodispersed particles was
 228 applied directly to all the particles here.

229 Fig. 9 shows the overall char conversion as a function of downstream position for different size groups
 230 – comparing the standard model and the model with turbulent clustering effects. Similarly, as for the
 231 $\bar{d}_{p,3}$ particles, the char conversion is effectively reduced through the reduced mass transfer to the clusters.
 232 Compared to the char conversion for the $\bar{d}_{p,3}$ particles ($30\mu\text{m}$) as shown in Fig. 5, the char conversion starts
 233 earlier and overall is slightly reduced. This is related to the difference in the char conversion rate for the
 234 differently sized particles. The reduction in the average conversion at approximately 1.2 m downstream
 235 might seem unreasonable at first. However, this is related to the averaging of all the particles and the fact
 236 that particles of different size hit the wall at different positions where the injection rig’s cross-section is
 237 reducing. This is also undermined by the conversion rates of the grouped particles in Fig 9. They have
 238 been grouped by size and their average conversion has been plotted. The smallest particles are converted
 239 quite fast, with only a minor influence of turbulence – similar to the $\bar{d}_{p,1}$ particles before. The influence
 240 of clustering becomes more pronounced for the larger particles. The largest particles are only converted
 241 slightly before they reach the end of the injection rig. Overall, the conversion behavior and influence of

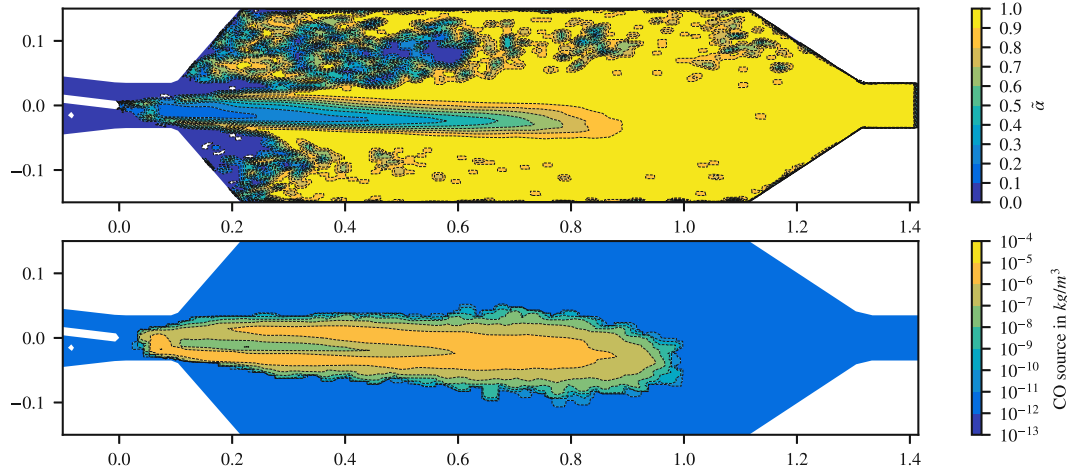


Figure 7: The turbulence correction factor $\bar{\alpha}$ (top) and the CO source term from char oxidation (bottom) for the simulation with $\bar{d}_{p,1} = 6.2\mu\text{m}$

242 clustering is similar to the conversion of the $\bar{d}_{p,3}$ particles, but also the effects of smaller and larger particles,
 243 contributing to the average char conversion marked by the green average lines in Fig. 9.

244 3.1.3. Injection rig – oxidation & gasification

245 In the blast furnace, besides char oxidation, gasification reactions play an important role. According to
 246 Maier [30] a kinetic-diffusion approach can be chosen to model the gasification reactions using the kinetic
 247 parameters given in Table A.4. For the effect of turbulence, the same relation, as derived by Krüger
 248 et al. [10], was used for the gasification reactions. This is justifiable since the derivation was not limited
 249 to oxidation reactions. For the H_2O and CO_2 gasification reactions, the assumption of diffusion limited
 250 reactions is reasonable for high temperature, since these reactants also need to be transported to the char
 251 surface. However, for lower temperatures and in the presence of O_2 , the assumption of the model does not
 252 hold, since for these conditions CO_2 can be present right at the surface due to char oxidation. Nevertheless,
 253 for the blast furnace application the temperatures are high and, in general, the gasification reactions are
 254 mainly kinetically limited for low temperatures.

255 Fig. 10 shows the conversion as a function of downstream position for the diameter distribution with
 256 oxidation and oxidation and gasification reactions. Naturally, the overall conversion is higher if gasification
 257 is considered. The overall trend is similar for both cases, but the effect of turbulence is slightly higher when
 258 gasification reactions are included. This is related to the fact that oxygen depletion plays only a minor role
 259 for the gasification reactions. This means that reactions also occur in the regions with lower turbulence
 260 correction factors. Additionally, temperatures are quite high, and therefore the gasification reactions are

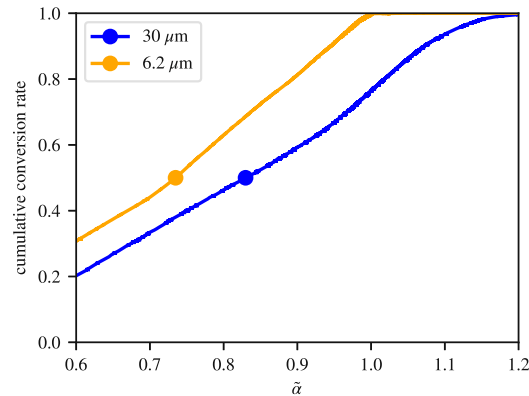


Figure 8: Cumulative reaction rate over turbulence correction factor $\tilde{\alpha}$

261 also partly diffusion controlled.

262 For simplicity, the same relation used to compute the diffusion parameter for the Schmidt number
 263 was employed for the turbulence effect for oxidation and gasification reactions. The diffusion parameter
 264 was approximated by a third order polynomial depending on temperature, based on the diffusion model
 265 for oxygen in nitrogen. The diffusional parameter is slightly different for CO_2 and H_2O . However, the
 266 differences are negligible, especially in the regimes where mass transfer is reduced by turbulence. However, if
 267 the model were applied to H_2 gasification, the differences might be significant and an independent Sherwood
 268 number should be calculated.

269 3.2. Blast Furnace Raceway

270 To study the effect of turbulence under real blast furnace conditions, the raceway zone of a blast furnace
 271 was simulated with pulverized coal injection. A description of the simulated blast furnace and the boundary
 272 conditions is given by Maier [30]. In the raceway zone, not only are the blast and the reducing agents present,
 273 but also the coke supplied from the top and the liquid iron and slag. Because the coke also reacts with the
 274 blast, it is also modeled as an Eulerian phase in the raceway zone. The conversion of coke is modeled by
 275 oxidation, and H_2O , H_2 and CO_2 gasification reactions. The coke bed has a porosity of 0.5 and is assumed
 276 stationary, with a prefixed raceway shape and size, because the focus is on the reducing agents. Details on
 277 the chosen coke conversion models can be found in [31].

278 To study the turbulence effect on the coal conversion, 680 kg/h of the same coal as in the lab scale
 279 simulation were injected into the blast furnace. Fig. 11 shows the gas phase temperature profile in the
 280 central plane of the simulated raceway zone. The projected position of the coal particles is marked by points
 281 and scaled by their mass. The Lagrangian coal particles are deleted when they hit the stationary coke bed.
 282 This simplification is made because a lot of coal is converted before hitting the coke bed and there is a lack

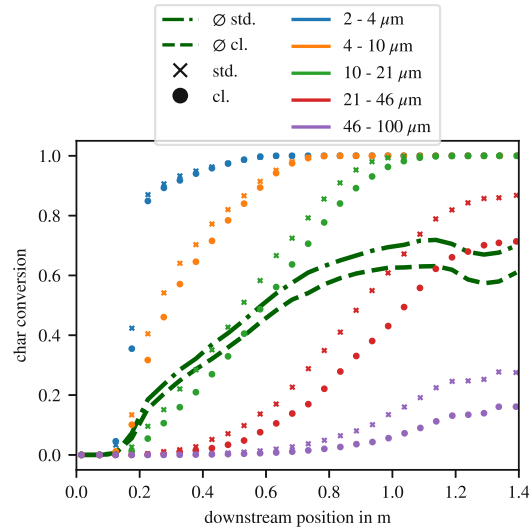


Figure 9: Char conversion of polydisperse coal particles averaged over downstream position. The average (\emptyset) conversion in dashed (with clustering) and dash-dotted lines (without clustering). The conversion for different size groups are marked by circles and crosses for the standard model and model with clustering effects, respectively.

283 of validated interaction models for coke and reducing agents, therefore the interaction is often neglected,
 284 e.g. by [32].

285 The temperature in the beginning of the coal plume decreases first due to drying and devolatilization.
 286 In the raceway zone around the coal jet, the temperature increases due to volatile combustion and oxidation
 287 reactions. Predicting the thermal state of the lower blast furnace influenced by the pulverized coal helps to
 288 understand the influence of different coal flow rates and types on blast furnace operation [3]. According to
 289 Babich [3] the full burnout of pulverized coal within the raceway zone is hardly possible for high coal flow
 290 rates. However, an accurate prediction of the burnout helps to gain insight on the maximal possible coal
 291 rate for coke substitution.

292 The average char conversion of the dried and devolatilized coal particles is plotted in Fig. 12. Similar to
 293 the char conversion in the injection rig for the polydisperse particles, we see a clear reduction in conversion
 294 of the coal particles when the clustering effect is considered.

295 4. Conclusion

296 The presented results show that the reduction in mass transfer rate to small particles plays a crucial
 297 role under blast furnace raceway conditions. The highly turbulent flow leads to strong clustering, which
 298 is determined by the calculated correction factor $\tilde{\alpha}$. Additionally, the high temperatures lead to high

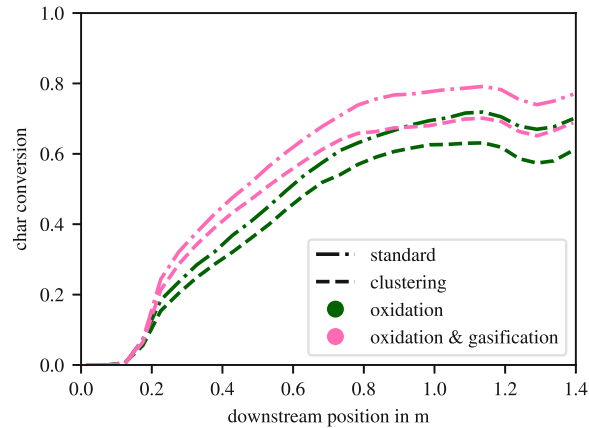


Figure 10: Char conversion as a function of the downstream position using oxidation (green), and oxidation and gasification (pink) reactions. The results from the standard model are shown by dash-dotted lines and from the model including clustering effects with dashed lines.

299 kinetic rates and consequently to diffusion controlled conversion regimes. The incorporation of the model
 300 significantly influenced the overall predicted char conversion of pulverized coal particles in the raceway zone.

301 The correct estimation of coal conversion is important to predict the maximum possible coal flow rate
 302 and consequently the coke substitution rate. Furthermore, an accurate prediction of the coal burnout helps
 303 to estimate the thermal state of the blast furnace raceway zone which is beneficial to support process
 304 control. Additionally, further studies to substitute the coal by renewable reducing agents, such as biochar,
 305 will benefit by the inclusion of the turbulent effects on conversion. In the future, an improvement of the
 306 model by including the interactions between reducing agents and the coke bed, and a moving coke bed
 307 could be beneficial. From a general perspective, the results indicate that an a-priori estimation through
 308 the calculation of average correction factors is impractical because the regions of correction factors have
 309 to be correlated to regions of actual reaction. Additionally, the simplified representation of small particles
 310 by particles with a mean diameter strongly influences the prediction of the correction factors and should
 311 therefore be avoided.

312 Finally, we would like to emphasize that the models used to account for the effect of turbulence used
 313 here, which were developed by Krüger et al. [10] and Haugen et al. [11], are based on the assumption of
 314 isotropic turbulence. This is expected to be a relatively good approximation for the char conversion phase,
 315 but care should nevertheless be taken.

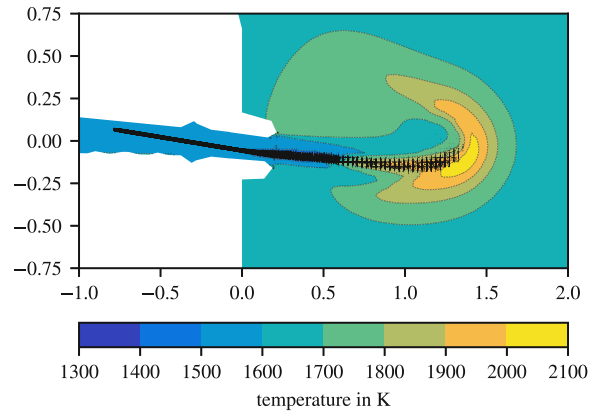


Figure 11: Raceway with temperature distribution and pulverized coal particles

316 **5. Acknowledgements**

317 The authors gratefully acknowledge the funding support of K1-MET GmbH, metallurgical competence
 318 center. The research program of the competence center K1-MET is supported by COMET (Competence
 319 Center for Excellent Technologies), the Austrian program for competence centers. COMET is funded by the
 320 Federal Ministry for Transport, Innovation and Technology, the Federal Ministry for Science, Research and
 321 Economy, the provinces of Upper Austria, Tyrol, and Styria, and the Styrian Business Promotion Agency.
 322 The computational results presented were achieved in part using the Vienna Scientific Cluster (VSC). The
 323 authors acknowledge TU Wien Bibliothek for financial support for editing/proofreading. With the support
 324 of the Erasmus+ programme of the European Union. The European Commission support for the production
 325 of this publication does not constitute an endorsement of the contents which reflects the views only of the
 326 authors, and the Commission cannot be held responsible for any use which may be made of the information
 327 contained therein.

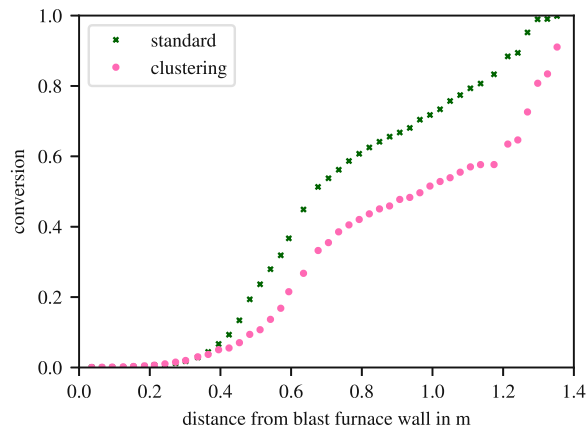


Figure 12: Raceway with average conversion over x for standard model and with clustering effect

328 **Appendix A. Parameters**

329 The reaction rate parameters used in the different cases presented in this paper and details about the
 330 modeled coal are summarized here. The gas phase reactions are shown in Table A.2 based on the work from
 331 Westbrook and Dryer [33]. The parameters for the devolatilization model (Eq. (2)) are given in Table A.3.

Table A.2: Gas-phase reactions: Reaction rate parameters taken from Westbrook and Dryer [33] - first reaction modeled same as methane combustion

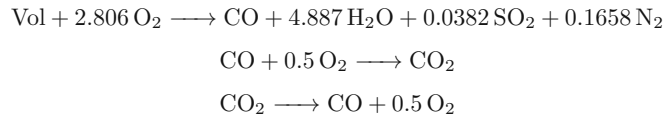


Table A.3: Devolatilization reaction: Kinetic parameters for the two-competing step devolatilization model according to [23]

	A_1	A_2	E_1	E_2
unit	s^{-1}		J kmol^{-1}	
value	3.7e5	1.46e13	1800	30189

332 For the coal particles studied in this paper, the proximate analysis, the ultimate analysis from Shen
 333 et al. [27] and the conversion rate parameters are summarized in Table A.4. The conversion rate parameters
 334 are given according to Eq. (4). Kinetic parameters for oxidation are from Silaen and Wang [34] and for
 335 gasification from Maier [30]. The diffusion parameter set as by Karchniwy et al. [13] and the effectiveness
 336 factors as by Maier [30]. The stoichiometric coefficients for the char oxidation products ($v_{\text{CO}} = 2\frac{\phi-1}{\phi}$ and
 337 $v_{\text{CO}_2} = \frac{2-\phi}{\phi}$) are calculated as suggest by Shen et al. [27]:

$$\phi = \frac{2A_{sr} \exp\left(\frac{T_{sr}}{T_f}\right) + 2}{2 + A_{sr} \exp\left(\frac{T_{sr}}{T_f}\right)} \quad (\text{A.1})$$

338 using $A_{sr} = 2500$ and $T_{sr} = 6240$.

Table A.4: Proximate analysis, ultimate analysis, particle parameters and reaction rate parameters.

moisture	vol.	ash	fixed c.	HCV
%	%	%	%	MJ kg ⁻¹
0.9	12.4	8	78.7	32.98
elemental analysis in %				
C	H	N	S	O
91.3	4	1.9	0.5	2.3
constant particle parameters				
epsilon	f	h	ρ_p	c_p
-	-	-	kg m ⁻³	J kg ⁻¹ K ⁻¹
0.9	0.5	0.3	1300	1500
reaction rate parameters				
	A_r	E_a	C	η
	s m ⁻¹	J kmol ⁻¹	s K ^{-$\frac{3}{4}$}	-
oxid.	0.052	$6.1 \cdot 10^7$	$5 \cdot 10^{-12}$	0.6
CO ₂ gasif.	20230	$3.304 \cdot 10^8$	$5 \cdot 10^{-12}$	0.7
H ₂ O gasif.	606.9	$2.697 \cdot 10^8$	$5 \cdot 10^{-12}$	0.6

339 **References**

- 340 [1] Commission of the European Communities, . Commission Staff Working Document: Towards competitive and clean
341 European steel. Tech. Rep.; Commission of the Eueropean Communities; 2021.
- 342 [2] Babich, A., Senk, D.. Coal use in iron and steel metallurgy. In: The Coal Handbook: Towards Cleaner Production;
343 vol. 2. Woodhead Publishing Limited. ISBN 9781782421177; 2013, p. 267–311. doi:10.1533/9781782421177.3.267.
- 344 [3] Babich, A.. Blast furnace injection for minimizing the coke rate and CO2 emissions. *Ironmaking and Steelmaking*
345 2021;0(0):1–14. URL: <https://doi.org/10.1080/03019233.2021.1900037>. doi:10.1080/03019233.2021.1900037.
- 346 [4] Bösenhofer, M., Wartha, E.M., Jordan, C., Feilmayr, C., Stocker, H., Hauzenberger, F., et al. Suitability of pulverised
347 coal testing facilities for blast furnace applications. *Ironmaking and Steelmaking* 2020;47(5). doi:10.1080/03019233.2019.
348 1565152.
- 349 [5] Shen, Y., Yu, A.. Characterization of Coal Burnout in the Raceway of an Ironmaking Blast Furnace. *Steel Research*
350 *International* 2015;86(6):604–611. doi:10.1002/srin.201400333.
- 351 [6] Liu, Y., Shen, Y.. Combined Experimental and Numerical Study of Charcoal Injection in a Blast Furnace: Effect of
352 Biomass Pretreatment. *Energy and Fuels* 2020;34(1):827–841. doi:10.1021/acs.energyfuels.9b02949.
- 353 [7] Liu, L., Kuang, S., Jiao, L., Guo, B., Yu, A.. Optimization of pulverized coal injection (PCI) rate in an ironmaking
354 blast furnace by an integrated process model. *Fuel* 2021;(October):122832. URL: <https://doi.org/10.1016/j.fuel.2021.122832>. doi:10.1016/j.fuel.2021.122832.
- 355 [8] Veynante, D., Vervisch, L.. Turbulent combustion modeling. *Progress in Energy and Combustion Science* 2002;28(3):193–
356 266. doi:10.1016/S0360-1285(01)00017-X.
- 357 [9] Tabet, F., Gökalp, I.. Review on CFD based models for co-firing coal and biomass. *Renewable and Sustainable Energy*
358 *Reviews* 2015;51:1101–1114. doi:10.1016/j.rser.2015.07.045.
- 359 [10] Krüger, J., Haugen, N.E.L., Løvås, T.. Correlation effects between turbulence and the conversion rate of pulverized
360 char particles. *Combustion and Flame* 2017;185:160–172. doi:10.1016/j.combustflame.2017.07.008.
- 361 [11] Haugen, N.E.L., Krüger, J., Mitra, D., Løvås, T.. The effect of turbulence on mass transfer rates of small inertial
362 particles with surface reactions. *Journal of Fluid Mechanics* 2018;836:932–951. doi:10.1017/jfm.2017.820.
- 363 [12] Karchniwy, E., Klimanek, A., Haugen, N.E.L.. The effect of turbulence on mass transfer rates between inertial
364 polydisperse particles and fluid. *Journal of Fluid Mechanics* 2019;874(x):1147–1168. doi:10.1017/jfm.2019.493.
- 365 [13] Karchniwy, E., Haugen, N.E.L., Klimanek, A., Langørgen, Ø., Sladek, S.. The effect of turbulence on mass transfer in
366 solid fuel combustion: RANS model. *Combustion and Flame* 2021;227:65–78. doi:10.1016/j.combustflame.2020.12.040.
- 367 [14] Weller, H., Tabor, G., Jasak, H., Fureby, C.. A tensorial approach to computational continuum mechanics using
368 object-oriented techniques. *Computers in Physics* 1998;12(6):620–631. doi:10.1063/1.168744.
- 369 [15] clusterCloud. 2022. doi:<https://zenodo.org/record/6579850#.Yo381j1BxH4>.
- 370 [16] Jones, W.P., Launder, B.E.. The prediction of laminarization with a two-equation model of turbulence. *International*
371 *Journal of Heat and Mass Transfer* 1972;15:301–314.
- 372 [17] Launder, B.E., Spalding, D.B.. The numerical computation of turbulent flows. *Computer Methods in Applied Mechanics*
373 *and Engineering* 1974;3:269–289. doi:[https://doi.org/10.1016/0045-7825\(74\)90029-2](https://doi.org/10.1016/0045-7825(74)90029-2).
- 374 [18] Magnussen, B.. The Eddy Dissipation Concept a Bridge between science and technology. In: ECCOMAS Thematic
375 Conference on Computational Combustion. 2005.,
- 376 [19] Ertesvåg, I.S.. Analysis of Some Recently Proposed Modifications to the Eddy Dissipation Concept (EDC). *Combustion*
377 *Science and Technology* 2020;192(6):1108–1136. doi:10.1080/00102202.2019.1611565.
- 378 [20] Bösenhofer, M., Wartha, E.M., Jordan, C., Harasek, M.. The eddy dissipation concept-analysis of different fine structure
379 treatments for classical combustion. *Energies* 2018;11(7). doi:10.3390/en11071902.
- 380 [21] Ranz, W.E., Marshall, W.R.J.. Evaporation from drops Part I. *Chemical Engineering Progress* 1952;48(3):141–146.

- 382 [22] Ranz, W.E., Marshall, W.R.J. Evaporation from drops: Part II. *Chemical Engineering Progress* 1952;48(4):173–180.
- 383 [23] Shen, Y.S., Guo, B., Yu, A., Maldonado, D., Austin, P., Zulli, P. Three-dimensional modelling of coal combustion
384 in blast furnace. *ISIJ International* 2008;48(6):777–786. doi:10.2355/isijinternational.48.777.
- 385 [24] Petersen, I., Werther, J.. Experimental investigation and modeling of gasification of sewage sludge in the circulating
386 fluidized bed. *Chemical Engineering and Processing: Process Intensification* 2005;44(7):717–736. doi:10.1016/j.cep.
387 2004.09.001.
- 388 [25] Yagi, B.S., Kunii, D.. Combustion of Solids. *Symposium (International) on Combustion* 1955;5(1):231–244. doi:https:
389 //doi.org/10.1016/S0082-0784(55)80033-1.
- 390 [26] Mathieson, J.G., Truelove, J.S., Rogers, H.. Toward an understanding of coal combustion in blast furnace tuyere
391 injection. *Fuel* 2005;84(10):1229–1237. doi:10.1016/j.fuel.2004.06.036.
- 392 [27] Shen, Y.S., Maldonado, D., Guo, B.Y., Yu, A.B., Austin, P., Zulli, P.. Computational fluid dynamics study of
393 pulverized coal combustion in blast furnace raceway. *Industrial and Engineering Chemistry Research* 2009;48(23):10314–
394 10323. doi:10.1021/ie900853d.
- 395 [28] Shen, Y.S., Guo, B.Y., Yu, A.B., Zulli, P.. A three-dimensional numerical study of the combustion of coal blends
396 in blast furnace. *Fuel* 2009;88(2):255–263. URL: <http://dx.doi.org/10.1016/j.fuel.2008.08.013>. doi:10.1016/j.fuel.
397 2008.08.013.
- 398 [29] OpenFOAM Foundation, . *OpenFOAM-9*. 2021. URL: <https://github.com/OpenFOAM/OpenFOAM-9>.
- 399 [30] Maier, C.. *Numerical Modeling of the Blast Furnace Process Injection of Auxiliary Reducing Agents Into the Raceway*.
400 *Dissertation; Technische Universität Wien*; 2015. doi:10.34726/hss.2015.14843.
- 401 [31] Wartha, E.M., Bösenhofer, M., Hauzenberger, F., Stocker, H., Feilmayr, C., Harasek, M.. Influence of Raceway Shape
402 on Species Concentration. In: *AISTech - Iron and Steel Technology Conference Proceedings*. Pittsburgh; 2022,.
- 403 [32] Shen, Y.S., Guo, B.Y., Yu, A.B., Austin, P.R., Zulli, P.. Three-dimensional modelling of in-furnace coal/coke
404 combustion in a blast furnace. *Fuel* 2011;90(2):728–738. doi:10.1016/j.fuel.2010.08.030.
- 405 [33] Westbrook, C.K., Dryer, F.L.. Simplified Reaction Mechanisms for the Oxidation of Hydrocarbon Fuels in Flames.
406 *Combustion Science and Technology* 1981;27(1-2):31–43. doi:10.1080/00102208108946970.
- 407 [34] Silaen, A., Wang, T.. Comparison of Instantaneous, Equilibrium, and Finite-Rate Gasification Models in an Entrained-
408 Flow Coal Gasifier. In: *Proceedings of the 26th International Pittsburgh Coal Conference*. 2009,.

Conference Publications

Conference Paper I

Computational Improvements for the Eddy Dissipation Concept by Operator Splitting and Tabulation

by Eva-Maria Wartha, Markus Bösenhofer and Michael Harasek; oral presentation at 28th European Symposium on Computer Aided Process Engineering in Graz and published in the proceedings

My contribution: Conceptualization of the paper. Writing the original draft. Simulation of the flame, analysis of the results and visualization.

E. M. Wartha, M. Bösenhofer, and M. Harasek (2018). "Computational Improvements for the Eddy Dissipation Concept by Operator Splitting and Tabulation". In: *Proceedings of the 28th European Symposium on Computer Aided Process Engineering*. Vol. 43. 2010, pp. 1687–1692. ISBN: 9780444642356. DOI: 10.1016/B978-0-444-64235-6.50294-1

"Reprinted from Proceedings of the 28th European Symposium on Computer Aided Process Engineering, Vol 43, E. M. Wartha, M. Bösenhofer, and M. Harasek, Computational Improvements for the Eddy Dissipation Concept by Operator Splitting and Tabulation, 1678-1692, Copyright (2018), with permission from Elsevier."

Anton Friedl, Jiří J. Klemeš, Stefan Radl, Petar S. Varbanov, Thomas Wallek (Eds.)
Proceedings of the 28th European Symposium on Computer Aided Process Engineering
June 10th to 13th, 2018, Graz, Austria. © 2018 Elsevier B.V. All rights reserved.
<http://dx.doi.org/10.1016/B978-0-444-64235-6.50294-1>

Computational Improvements for the Eddy Dissipation Concept by Operator Splitting and Tabulation

Eva-Maria Wartha^{a*}, Markus Bösenhofer^{a,b} and Michael Harasek^a

^aTechnische Universität Wien, Getreidemarkt 9/166, 1060 Vienna, Austria

^bK1-MET GmbH, Stahlstraße 14, Betriebsgebäude (BG) 88, 4020 Linz, Austria
eva-maria.wartha@tuwien.ac.at

Abstract

The Eddy Dissipation Concept (EDC) is a well working concept for turbulent reacting flows, which depicts the influence of chemical reactions as well as turbulence. The problem when using detailed chemical mechanisms - necessary for more information about radical species and pollutants - is the vastly increased computational demand. Operator splitting and in situ adaptive tabulation (ISAT) can be a way to reduce the computational effort and improve the application of detailed chemical mechanisms with the EDC. Two operator splitting mechanisms are presented and used for the simulation of Sandia Flame D. The computational time can be decreased and the results fit well to the experimental results.

Keywords: turbulent combustion, OpenFOAM, Eddy Dissipation Concept (EDC), operator splitting, in situ adaptive tabulation (ISAT)

1. Introduction

Simulation can be a great tool to improve the understanding of complex processes and consequently enhance efficiency and reduce emissions. In many systems, such as biomass combustion, pulverized coal combustion or blast furnaces, gas phase combustion occurs and needs to be modeled.

The Eddy Dissipation Concept (EDC) (Magnussen, 1981) is a widely used combustion model, which couples the effect of chemical reactions and the effect of turbulence. It has been widely used for many applications, e.g. by Zahirović et al. (2010), Stefanidis et al. (2006) and Rehm (2010). When using detailed chemical mechanisms the computational demand increases significantly compared to global or skeletal mechanisms. Therefore, computational improvements for the EDC are necessary to make use of detailed chemical mechanisms possible to enable additional insight on radical species or NO_x formation.

In situ adaptive tabulation (ISAT) has been proposed by Pope (1997) to decrease the computational time for reactive flow calculations. Originally, it has been used in combination with PDF methods, but it can also be used in conjunction with the EDC. In the EDC the species concentration in the reacting structures can be described by an ordinary differential equation (ODE)-system. Mixing and chemical reactions are taken into account there. ISAT can only be used for the chemical part of the equations, since taking both into account would distort the table and make a look-up inefficient, (Pope, 1997) and (Rehm, 2010). Therefore, operator splitting has to be used to split the ODE and enable ISAT.

Rehm (2010) presented two operator splitting methods for the EDC. The computational

time could not be reduced there, but also no results with regard to the accuracy were presented.

In the following the EDC and operator splitting methods are explained. These methods are then used to simulate Sandia Flame D in OpenFOAM, a turbulent methane-air jet flame. Experimental flame data from Barlow and Frank (1998) and Schneider et al. (2003) is used to validate the simulation results. Moreover, operator splitting and direct integration results are compared.

2. Model Description

2.1. Eddy Dissipation Concept

The EDC models the interaction between turbulence and chemical reactions. It assumes that the fluid consists of surroundings and fine structures, whose size is in the order of the Kolmogorov length scale (Magnussen, 1981). Since educts need to be mixed on a molecular scale to react, reactions only occur in the fine structures.

Magnussen (1981) derived the description of the fine structures based on an energy cascade model. The fine structure fraction γ^* is expressed by the turbulent kinetic energy k , the dissipation rate ε , the kinematic viscosity ν and a constant $C_\gamma = 2.13$, Eq.(1). The mass transfer between the fine structures and the surroundings per unit of mass of the fine structures and time can also be expressed by ν , ε and $C_\tau = 0.41$, Eq.(2). The residence time in the fine structures τ^* is the reciprocal of \dot{m}^* . The mass transfer per unit of fluid \dot{m} can be calculated by the mass transfer per unit of mass of the fine structures and the fine structure fraction, Eq.(2).

$$\gamma^* = C_\gamma^3 \left(\frac{\nu \varepsilon}{k^2} \right)^{\frac{3}{4}} \quad (1)$$

$$\dot{m}^* = \frac{1}{C_\tau} \left(\frac{\varepsilon}{\nu} \right)^{\frac{1}{2}} = \frac{1}{\tau^*} = \gamma^* \frac{1}{\dot{m}} \quad (2)$$

To obtain the mass transfer rate for one species R_i^* per unit volume of the reacting fine structure fraction χ , the species concentration in the fine structures and the surroundings is required, Eq. (3). The concentration and the density in the fine structures and the surroundings are also taken into account. When using the detailed chemistry approach, the fraction of the reacting fine structures χ is usually set to one, as suggested by Gran and Magnussen (1996). The relation between some property Ψ in the surroundings (\circ), the fine structures ($*$) and the fluid average ($\bar{}$) is given in Eq.(4).

$$R_i^* = \frac{\dot{m}^* \rho^*}{1 - \gamma^* \chi} \left(\bar{c}_i - \frac{c_i^*}{\rho^*} \right) \quad (3)$$

$$\bar{\Psi} = \gamma^* \chi \Psi^* + (1 - \gamma^* \chi) \Psi^\circ \quad (4)$$

Different concepts exist to model the chemical reactions in the fine structures: the fast chemistry approach (Magnussen, 1981), the local extinction approach (Byggstoyl and Magnussen, 1983) or the detailed chemistry approach (Gran and Magnussen, 1996). To use a detailed chemical mechanism, the latter has to be used. There, the fine structures are treated as adiabatic and isobaric perfectly stirred reactors (PSRs). This leads to the following set of ODEs, Eq.(5). Where h^* is the enthalpy, p^* the pressure and Y_i^* the

mass fraction of species i in the fine structures. $\hat{\omega}_i$ denotes the reaction rate and Y_i° the concentration of species i in the surroundings.

$$\frac{dh^*}{dt} = 0 \quad \frac{dp^*}{dt} = 0 \quad \frac{dY_i^*}{dt} = \hat{\omega}_i + \frac{1}{\tau^*} (Y_i^\circ - Y_i^*) \quad (5)$$

2.2. Operator Splitting

Operator splitting splits the species conservation equation in Eq.(5) into a chemical and a mixing part, solves them separately and combines the solutions to get a solution of the original ODE. Two second order operator splitting methods, Strang splitting and Staggered splitting, which are used for the simulation in OpenFOAM are presented here.

2.2.1. Strang Splitting

The chemical subproblem is denoted by A and the mixing one by B. Strang splitting (Strang, 1963), shown in Figure 1, provides a solution of the original ODE by first solving subproblem A on a time interval $\Delta t/2$, Eq.(6). Then subproblem B is solved on a time interval Δt with the solution from A as its initial condition, Eq.(7). The final solution, marked by a circle, Eq.(9) is obtained by solving subproblem A again on the remaining time interval $\Delta t/2$, Eq.(8).

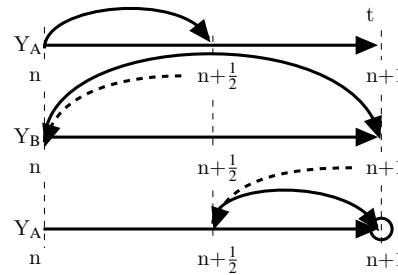


Figure 1: Strang splitting scheme

$$\frac{d(Y_i^*)_A}{dt} = \hat{\omega}_i \quad \text{with } (Y_i^*)_A(t=0) = Y_i^*(t=0) \quad (6)$$

$$\frac{d(Y_i^*)_B}{dt} = \frac{1}{\tau^*} (Y_i^\circ - Y_i^*) \quad \text{with } (Y_i^*)_B(t=0) = (Y_i^*)_A(t = \Delta t/2) \quad (7)$$

$$\frac{d(Y_i^*)_A}{dt} = \hat{\omega}_i \quad \text{with } (Y_i^*)_A(t = \Delta t/2) = (Y_i^*)_B(t = \Delta t) \quad (8)$$

$$Y_i^*(t = \Delta t) = (Y_i^*)_A(\Delta t) \quad (9)$$

2.2.2. Staggered Splitting

Figure 2 shows the solution procedure of the Staggered splitting scheme. Subproblem A is solved for a time step Δt from n to $n+1$ and subproblem B is solved from $n+\frac{1}{2}$ to $n+\frac{3}{2}$, taking the solution from subproblem A as initial condition. The solution is approximated by the mean of the solutions of subproblem A and B marked by circles in Figure 2, Eq.(10). The initial time step, needs special treatment: the mixing subproblem is solved on a time interval $\Delta t/2$ to obtain the initial conditions for subproblem A.

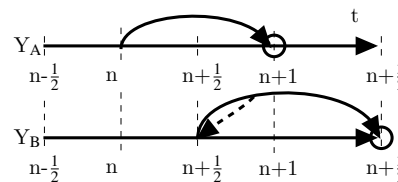


Figure 2: Staggered splitting, adapted from Ren and Pope (2008)

$$Y_i^*(t=n) = \frac{1}{2} \left((Y_i^*)_A(t=n+1) + (Y_i^*)_B \left(t = n + \frac{3}{2} \right) \right) \quad (10)$$

3. Simulation Details

Sandia Flame D was simulated in OpenFOAM using the in-house solver rhoEdcFoam. A 2D-wedge was simulated with a grid of 4329 cells (4218 hexahedras and 111 prisms). A transient simulation was conducted for 0.5 seconds to achieve a description of the steady-state of the flame. Radiation was neglected due to studies showing, that radiation has a minor impact on the results (Li et al., 2017).

For the chemical reactions the detailed chemical mechanism GRI-3.0 from Smith et al. (2017), including 53 species and 325 reactions, was used. The simulations have been conducted with direct integration and the presented operator splitting methods in conjunction with ISAT. The retrieval tolerance for ISAT was set to 10^{-4} . The results from a simulation using a global mechanism are also added for comparison.

The presented operator splitting methods are second order methods, i.e. the error is proportional to $\mathcal{O}(\Delta t^2)$. To improve the predictions and limit the error done by operator splitting, a maximum operator splitting time step size of $\Delta t = 10^{-3}$ s and $\Delta t = 10^{-4}$ s was tested.

4. Results and Discussion

Figure 3(a) to Figure 3(c) show the centerline profiles of temperature, CO₂ and NO mass concentration for the different simulations (x/d represents the axial position normalized by the jet diameter $d=7.2$ mm). The results from direct integration fit best to the experimental results for temperature and CO₂ mass concentration. The profiles show, that operator splitting approximates the solution well, but is a bit less accurate. For the NO mass concentration the solution from Staggered splitting fits even better to the experimental results than the direct integration.

To quantify the accuracy of the predictions, the sum of squared errors (SSE) was calculated for all available data points and for different quantities (temperature T, velocity u, and different species concentrations). The SSE was normalized to the SSE of direct integration to compare the different simulation settings (Figure 3(d)). Staggered splitting seems to be even more accurate than direct integration. The improved predictions could result from increased stability or be due to error compensation resulting from taking the mean in Eq. (10). Strang splitting gives in general better predictions than the global mechanism but gives less accurate predictions than the other simulations.

Figure 3(e) to Figure 3(h) show results from Staggered splitting and Strang splitting with and without limited time step size. The time step size was limited to 10^{-3} s and 10^{-4} s for Staggered splitting. The profiles of the temperature at the centerline (Figure 3(e) and Figure 3(g)), show that the limited splitting schemes give a bit improved, especially smoother, predictions. The SSE was calculated and normalized to the simulations without time step limitation. For Staggered splitting, the limited case gives improved predictions for all quantities, except methane. The smaller limit for the time step, i.e. 10^{-4} s, did not lead to a significant improvement. Therefore, the time step limit was only set to 10^{-3} s for Strang splitting.

For Strang splitting the improvement is not as big and also for methane no improvement is achieved through the limited time step size. In general the limited time step size gives a bit more accurate predictions, with only minimally increased computational demand.

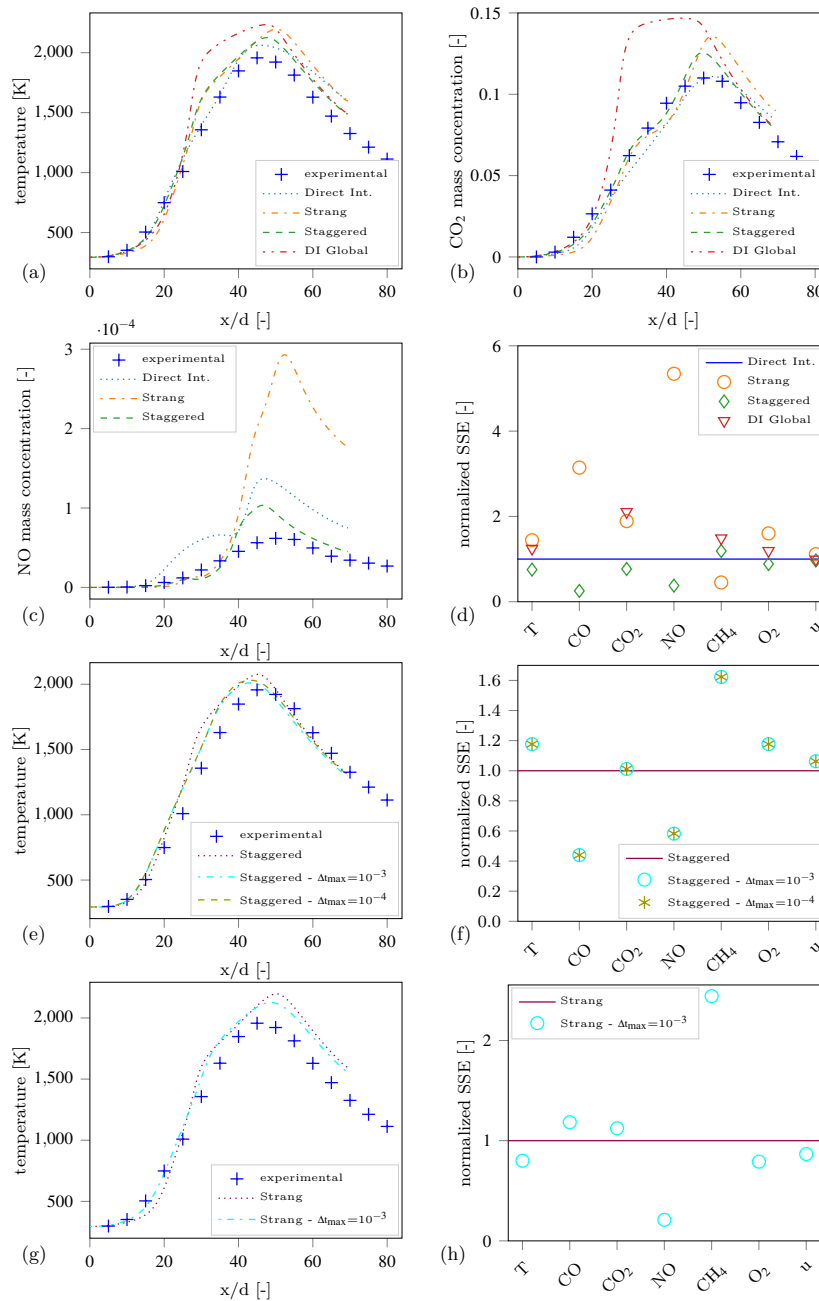


Figure 3: Comparison of simulation results and experimental data for (a) temperature (b) CO₂ and (c) NO mass concentration and (d) comparison of the normalized SSE for all data points; Results using limited time steps in (e) to (h)

Since the simulations were not carried out on the same computers, the computational time can only be roughly compared. Using Strang splitting with an ISAT-tolerance of 10^{-4} , the computational time could be reduced by approximately 23 % compared to direct integration. Further comparisons on the computational time with different ISAT settings and without ISAT are presented by Wartha (2017).

Staggered splitting is even faster than Strang splitting, since it needs less function calls for one operator splitting step. The reduction of computational time for Staggered splitting compared to Strang splitting is around 20 %.

5. Conclusion and Outlook

The use of a detailed chemical mechanism is important to predict species like radicals or pollutants, which are not present in global mechanisms. The presented operator splitting methods, Strang and Staggered splitting, work and can reduce the computational demand when detailed chemical mechanisms are used in conjunction with the EDC. Good predictions for temperature and concentrations have been achieved for Sandia Flame D. For some cases Staggered splitting gives even better results than direct integration. Furthermore, the computational demand is smallest for Staggered splitting. Therefore, Staggered splitting seems to be the best choice.

To substantiate those findings, further test cases with other flames should be conducted to ensure, that the presented findings are also valid for other combustion regimes.

References

- R. S. Barlow, J. H. Frank, 1998. Effects of turbulence on specific mass fractions in methane/air jet flames. Twenty-Seventh Symposium (International) on Combustion 27, 1087–1095.
- S. Byggstoyl, B. Magnussen, 1983. A model for flame extinction in turbulent flow. Fourth Symposium on Turbulent Shear Flows 4, 32–38.
- I. R. Gran, B. F. Magnussen, 1996. A Numerical Study of a Bluff-Body Stabilized Diffusion Flame. Part 2. Influence of Combustion Modeling And Finite-Rate Chemistry. Combustion Science and Technology 119, 191–217.
- Z. Li, A. Cuoci, A. Sadiki, A. Parente, 2017. Comprehensive numerical study of the Adelaide Jet in Hot-Coflow burner by means of RANS and detailed chemistry. Energy 139, 555–570.
- B. Magnussen, 1981. On the structure of turbulence and a generalized eddy dissipation concept for chemical reaction in turbulent flow. 19th American Institute of Aeronautics and Astronautics Aerospace Science Meeting, 1–6.
- S. B. Pope, 1997. Computationally efficient implementation of combustion chemistry using in situ adaptive tabulation. Combustion Theory and Modelling 7830 (1), 41–63.
- M. Rehm, 2010. Numerische Strömungssimulation der Hochdruckvergasung unter Berücksichtigung detaillierter Reaktionsmechanismen. Ph.D. thesis, Technische Universität Bergakademie Freiberg.
- Z. Ren, S. B. Pope, 2008. Second-order splitting schemes for a class of reactive systems. Journal of Computational Physics 227 (17), 8165–8176.
- C. Schneider, A. Dreizler, J. Janicka, E. P. Hassel, 2003. Flow field measurements of stable and locally extinguishing hydrocarbon-fuelled jet flames. Combustion and Flame 135 (1-2), 185–190.
- G. P. Smith, D. M. Golden, M. Frenklach, N. W. Moriarty, B. Eiteneer, M. Goldenberg, C. T. Bowman, R. K. Hanson, S. Song, W. C. J. Gardiner, V. V. Lissianski, Z. Qin, 2017. GRI-MECH 3.0. URL <http://www.me.berkeley.edu/gri-mech/>
- G. D. Stefanidis, B. Merci, G. J. Heynderickx, G. B. Marin, 2006. CFD simulations of steam cracking furnaces using detailed combustion mechanisms. Computers and Chemical Engineering 30 (4), 635–649.
- G. Strang, 1963. Accurate partial difference methods I: Linear cauchy problems. Archive for Rational Mechanics and Analysis 12 (1), 392–402.
- E.-M. Wartha, 2017. A Study on New Developments and Chemical Time Scale Definitions for the Eddy Dissipation Concept. Master's thesis, Technische Universität Wien.
- S. Zahirović, R. Scharler, P. Kilpinen, I. Obernberger, 2010. Validation of flow simulation and gas combustion sub-models for the CFD-based prediction of NO_x formation in biomass grate furnaces. Combustion Theory and Modelling 15, 61–87.

Conference Paper II

Mesh Partitioning of Reactive Flow Simulations – Speed-up and Other Side Effects

by Eva-Maria Wartha, Markus Bösenhofer, Christian Jordan and Michael Harasek; poster presentation at the 9th European Combustion Meeting in Lisboa and published in the proceedings

My contribution: Conceptualization of the paper. Writing the original draft. Carrying out the simulations and analyzing the results.

E.-M. Wartha, M. Bösenhofer, C. Jordan, and M. Harasek (2019). “Mesh Partitioning of Reactive Flow Simulations – Speed-up and Other Side Effects”. In: *9th European Combustion Meeting*. Lisboa

Mesh Partitioning of Reactive Flow Simulations – Speed-up and Other Side Effects

E.-M. Wartha^{*1}, M. Bösenhofer^{1,2}, C. Jordan¹, M. Harasek¹

¹ Technische Universität Wien, Getreidemarkt 9/166, 1060 Vienna, Austria

² K1-MET GmbH, Stahlstraße 14, Betriebsgebäude (BG) 88, 4020 Linz, Austria

Abstract

Despite continuously increasing computational power, an efficient use of the available resources remains important. Reactive flow simulations differ from other simulations due to their high complexity. For efficient use of computational resources for reactive flow simulations we conducted a case study in OpenFOAM[®], an open-source code for computational fluid dynamics. For coupling turbulence and chemistry the well-known Eddy Dissipation Concept was chosen. Guidelines on how to choose optimal partition size depending on reaction mechanism size were derived and interesting speed-up behavior for small meshes was observed. The influence of common speed-up techniques, such as tabulation are presented as well.

Introduction

Industrial processes often incorporate reactive flows, such as gasifiers, blast furnaces or rotary kilns. There, many physical phenomena occur at the same time, which influence the overall process. Computational fluid dynamics (CFD) has become increasingly important in designing and improving plants and apparatus in the chemical and process industry. Capturing the involved phenomena is essential when simulating these processes. This can lead to complex and computationally expensive calculations. Nowadays, huge clusters are available for parallelized CFD simulations. Nevertheless, computational time is still valuable and the computational resources need to be used wisely to ensure fast calculations.

For parallel calculations on multiple processors the computational domain is split into subdomains. Useful domain partitioning strategies for flow simulations have been presented in literature, f.ex. in [1], but computational routines for reacting flows differ fundamentally from flow simulations. The solution of the chemical reaction system is computationally more expensive and, therefore partitioning strategies might differ. Dynamic mesh partitioning strategies have also been suggested to enhance fast chemistry calculations, [2,3], but no guideline, besides some minor remarks by Harasek [4], has been found on how small a reactive flow calculation can be partitioned while still gaining essential speed-up.

Therefore, this paper focusses on efficient mesh partitioning strategies for reacting flows and partitioning sizes depending on the complexity of chemical reaction mechanisms and tabulation. The study was carried out using the open source CFD code OpenFOAM[®] [5]. The gas phase is modeled with the Eddy Dissipation concept (EDC), a method for coupling turbulence and chemical reactions.

In the following section a short overview on the EDC is given and strategies for speed-up and their influence on parallelization is discussed.

The results section compares speed-up and computational time for different test cases with different

mechanism size. Additionally, the influence of tabulation on the computational time and speed-up is discussed.

The Eddy Dissipation Concept

One of the most common methods for simulating reactive gas flows is the EDC. It provides a strategy for coupling chemical reactions and turbulence. The basic assumption is that reactions occur only in the fine structures (denoted by $*$), where the educts are mixed on a molecular scale. Based on the turbulence energy cascade, Magnussen [6] derived expressions for the fine structure fraction γ^* (and the dimensionless fine structure length scale γ_L), Eq. (1), and the mass transfer rate to the fine structures \dot{m}^* , Eq. (2), depending on the turbulent kinetic energy k , its dissipation rate ε , the kinematic viscosity ν and two constants C_γ and C_τ . The fine structure residence time τ^* is inversely proportionate to \dot{m}^* .

$$\gamma^* = C_\gamma \left(\frac{\varepsilon \nu}{k^2} \right)^{3/4} = \gamma_L^{1/3} \quad (1)$$

$$\dot{m}^* = \frac{1}{C_\tau} \left(\frac{\varepsilon}{\nu} \right)^{1/2} = \frac{1}{\tau^*} \quad (2)$$

The change of mass in the mean cell (denoted by $-$) for species i is given by Eq. (3), where Y_i denotes the mass fraction of specie i and χ the reacting fraction of the fine structures. Eq. (4) shows the relation between the fine structures, the surroundings (denoted by $^\circ$) and the mean cell for any quantity Ψ , such as temperature, mass fraction (Y) or density (ρ).

$$\bar{R}_i = \frac{\bar{\rho} \dot{m}^* \gamma_L^3 \chi}{(1 - \gamma_L^3 \chi)} (\bar{Y}_i - Y_i^*) \quad (3)$$

$$\bar{\Psi} = \gamma^* \chi \Psi^* + (1 - \gamma^* \chi) \Psi^\circ \quad (4)$$

In later publications Magnussen proposed different exponents for γ_L to account for the reaction space extending to surroundings [7,8].

Eq. (3) describes the mass transfer between the fine structure and the surroundings, but the chemistry in the

* Corresponding author: eva-maria.wartha@tuwien.ac.at
Proceedings of the European Combustion Meeting 2019

fine structure still needs to be modeled. There are various approaches: the fast chemistry approach, which assumes infinitely fast reactions [6], the local extinction approach, presented in [9], or the detailed chemistry approach [10], which is the most complex but probably the most common nowadays.

The fine structures are assumed to behave like perfectly stirred reactors (PSRs), Eq. (5). This leads to complex systems of Ordinary Differential Equations (ODEs), but arbitrary chemical mechanisms can be applied with this modeling approach.

$$\frac{dY_i^*}{dt} = \dot{\omega}_i + \frac{1}{\tau}(Y_i^\circ - Y_i^*) \quad (5)$$

Therefore, the PSR model is often simplified to a plug flow reactor (PFR) model and the mixing term in Eq. (5) is neglected to reduce the numerical effort. The commercial CFD code ANSYS Fluent[®] applies this approach. Although this simplification is often made, the difference in the formulation is apparent, for a more thorough discussion see [11].

The reacting fine structure fraction χ is usually set to one in conjunction with the detailed chemistry approach [10], which may only be valid in regions with high turbulence [12].

Tabulation and Operator Splitting

Reactive flow simulations are computationally expensive, but there are methods to reduce the calculation time, including mechanism reduction or tabulation. A common tabulation method is in situ adaptive tabulation (ISAT), which was introduced by Pope [13]. Here, in situ means, that the table is built up during the calculation. Thus, no table needs to be prepared beforehand and only the accessed region of the composition space is tabulated.

The ISAT table has the form of a binary tree. It is assumed that a tabulation point Φ^0 is enveloped by the so-called ellipsoid of accuracy (EOA). Given a query point Φ^p , the binary tree is searched and when a leaf is reached it is checked if the query point lies within the EOA. If this is true, the search results in a retrieve. Otherwise, the ODE is solved to obtain the new composition and it is checked if it is within the given tolerance. If it is, the EOA expands – a growth. Otherwise, an additional leaf is added to the table. For a more thorough discussion we refer to [13].

ISAT is only efficiently viable in conjunction with the PFR formulation, because tabulation including the mixing term and the reaction term, Eq. (5), would make a look-up inefficient and deteriorate the table [13,14]. Operator splitting can enable tabulation for the PSR formulation, but reduces the accuracy to some extent. Operator splitting methods have been presented and discussed in [15,16].

In the conducted simulations the staggered splitting scheme was used [15]. Operator splitting methods split the problem, Eq. (5), into two subproblems, the mixing

problem (subproblem A) and the chemical problem (subproblem B), Eq. (6) and Eq. (7).

$$\frac{d(Y_i^*)_A}{dt} = \dot{\omega}_i \quad (6)$$

$$\frac{d(Y_i^*)_B}{dt} = \frac{1}{\tau}(Y_i^\circ - Y_i^*) \quad (7)$$

The staggered splitting scheme works as follows: First, subproblem A is solved for Δt from n to $n+1$. Then, subproblem B is solved from $n+1/2$ to $n+3/2$ using the solution from subproblem A as initial condition, Figure 1. The solution after a given time step is taken as the mean of the two subproblem solutions.

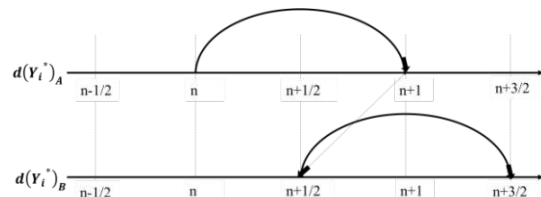


Figure 1: Staggered splitting scheme adapted from [15]

OpenFOAM[®]

OpenFOAM[®] is an open-source CFD-tool distributed under the General Public License. It is fully object-oriented and written in C++. For parallelization the public domain openMPI [17] is used, which is based on the concept of message passing interface (MPI).

This parallelization is realized with the halo layer principle in OpenFOAM[®]. The mesh is split into subdomains and data for cells next to the boundary is duplicated, see Figure 2.

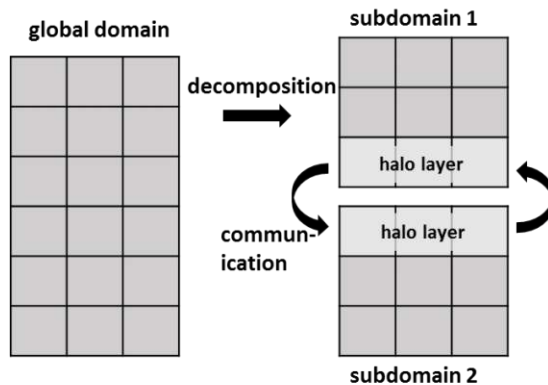


Figure 2: Parallelization in OpenFOAM[®] based on the halo layer principle, adapted from [1]

Only the information of the cells in the halo layer is passed between the processor cores with this approach. Therefore, each processor core creates its own ISAT table and the build-up time and the number of retrieves depends on the number of cells per processor.

Simulation Set-up / Test Cases

Sandia Flame D, a piloted methane-air jet flame, which is widely used for validation cases due to the

experimental data available from [18,19], was chosen as a test case. The flame is highly turbulent with a jet Reynolds number of 22 400, a jet diameter of 7.2 mm and a pilot diameter of 18.2 mm.

Two solvers have been used for the test cases. First, the reactingFoam solver from OpenFOAM® version (6.0). With this solver the PFR formulation is used and different versions of Eq. (3) can be chosen. Here we chose the formulation from [7], where the exponents of γ_L change to 2.

Second, the rhoEdeFoam [20] solver was used, which is an in-house code based on OpenFOAM®. There, the PSR formulation is available and the ISAT tabulation can be used in combination with the staggered splitting scheme [15].

Two different meshes were constructed. A 2D axisymmetric mesh and a full 3D mesh. The 2D mesh has been used when the full 3D simulation was not possible due to the high computational requirements and the 2D and 3D simulation have also been compared.

Four different chemical mechanisms for the combustion of methane flames have been used (Table 1): the GRI-3.0 [21], two reduced GRI-3.0 mechanisms and a one-step mechanism [22]. The first reduced GRI-3.0, hereafter referred to as “Reduced”, is distributed with OpenFOAM® (Version 6.0). In the code a reference to the original GRI-3.0 is made, but apparently it is the GRI-3.0 without NO_x reactions used by [23]. The second reduced mechanism is referred to as “DRGEP”, which is short for directed relation graph with error propagation, and was reduced based on the DRGEP method presented by Pepiot-Desjardins [24].

Table 1: Mechanisms used in the simulation for Sandia Flame D

	No. of species	No. of reactions
GRI-3.0	53	325
Reduced	36	219
DRGEP	19	48
One-Step	5	1

Results

Due to the open-MPI architecture of OpenFOAM® the ISAT table is built and stored per processor core. One might expect that simulations using ISAT are not as well parallelizable as simulations without tabulation. This is only partially correct. Using a small number of cores the speed-up with tabulation is even greater than without it. Only with a larger number of cores the tabulation overhead becomes an issue and the implementation without ISAT starts outperforming the one with ISAT.

Figure 3 shows simulations conducted with reactingFoam comparing tabulation and no tabulation with the different reaction mechanisms for the 3D mesh.

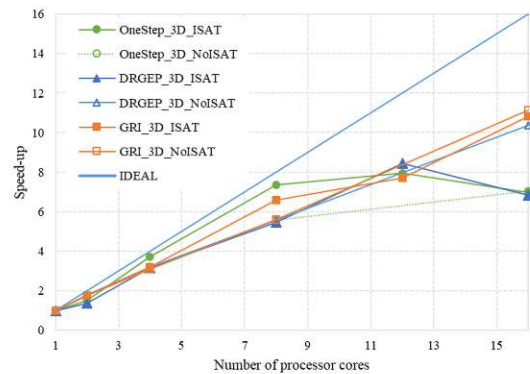


Figure 3 Speed-up of reactions with and without ISAT using reactingFoam

The same result can be observed for the 2D mesh and for rhoEdeFoam simulation in Figure 4. The speed-up is plotted against the number of processor cores to emphasize the difference between 2D and 3D mesh. Even when the number of cells per processor is already quite low (~5000 cells for 2D simulation) the speed-up with ISAT is quite high when distributed to only 2-4 cores.

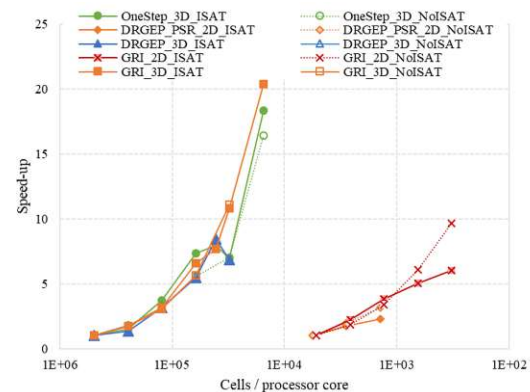


Figure 4 Speed-up of simulations with a 2D and 3D mesh using reactingFoam and rhoEdeFoam (labeled by PSR)

To analyse the effect of mechanism size, we compare reactingFoam simulations using ISAT in Figure 5. For the partitioning for up to 8 processor cores (this means ~60 000 cells), the speed-up is good for all mechanisms. For more processor cores the speed-up drops significantly for small mechanisms. For more complex mechanisms, such as GRI-3.0, more processors still improve the performance. This leads to the conclusion, that it is ok to partition reactive flow calculations well below ~50 000 cells per processor, if a complex reaction mechanism is used.

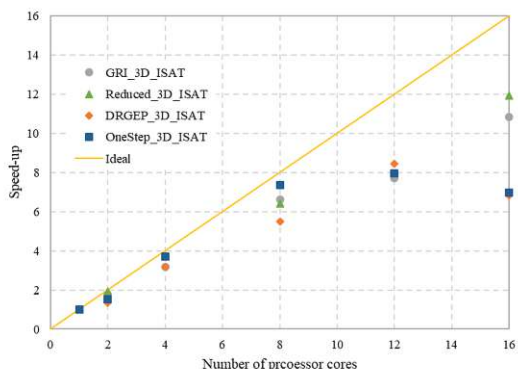


Figure 5 Speed-up of simulations with different reaction Mechanisms using reactingFoam and ISAT

Figure 6 shows the speed-up of the simulations with a 2D mesh, where the GRI-3.0 was used with reactingFoam and the DRGEP mechanism with rhoEdcFoam. The plot indicates that speed-up trends are similar for the PFR and PSR formulation. For the DRGEP with PSR formulation we see good speed-up for up to 2 processors (2 800 cells/processor core). For GRI-3.0 with PSR the speed-up was reasonably good for even fewer cores.

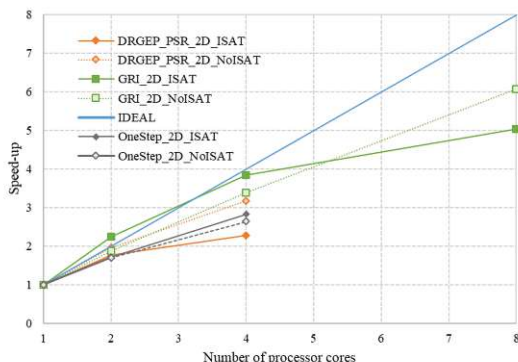


Figure 6 Comparison of PSR (rhoEdcFoam) and PFR (reactingFoam) formulation for the 2D mesh

Figure 7 shows the total CPU time versus cells per processor core for all simulations conducted with the reactingFoam solver with the 3D mesh. The speed-up gained by tabulation can be seen, which is significant for any mechanism size. The reduction in CPU time through tabulation is more pronounced for more complex reaction mechanisms.

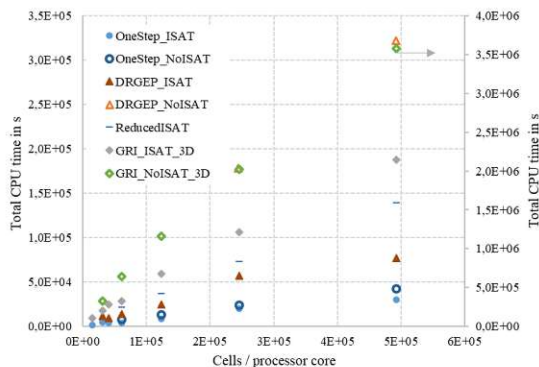


Figure 7 Total CPU time for all reactingFoam simulations – GRI_NoISAT_3D is plotted on the right y-axis

Figure 8 shows the CPU time per cell versus the cells per processor core for all simulations of Figure 7. Except of the GRI-3.0 without ISAT and the DRGEP without ISAT, the CPU time per cell stays constant for low numbers of cells per processor.

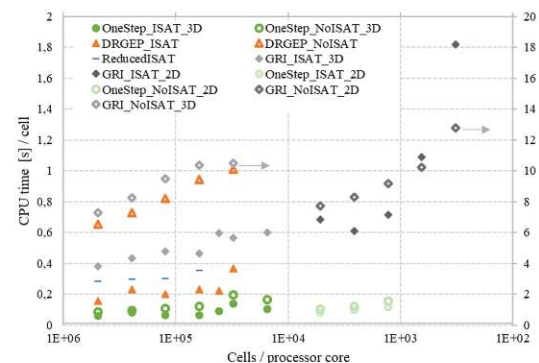


Figure 8 Comparison of CPU time per cell for all the simulations done with reactingFoam – GRI without ISAT is plotted on the left y-axis

Figure 9 also shows that the communication between the processor cores already consumes an evident part of the CPU time when distributed to more than 8 processor cores for the 3D simulations with the simplest reaction mechanism, having less than ~60 000 cells per processor core.

Interestingly, the CPU time per cell is decreasing for the GRI-3.0 without ISAT when switching from 3D to 2D simulation. Up until now the reason remains unclear.

Figure 9 shows the actual execution time for the test cases. The high execution time for complex mechanisms is still limiting to full-scale industrial reactive flow simulations. Faster calculation can be achieved by tabulation, but the size of the reaction mechanism has still the biggest influence.

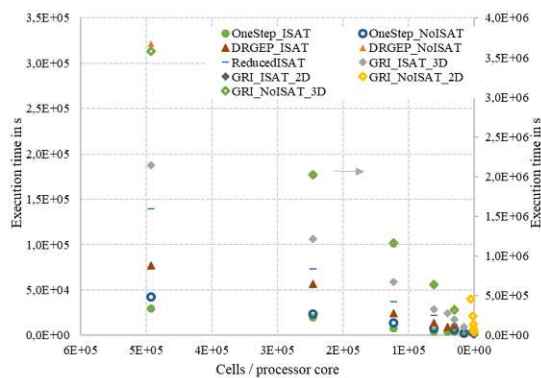


Figure 9 Total Execution time for the simulations with reactingFoam – GRI_NoISAT_3D plotted on the left y-axis

Conclusions

The influence of the mechanism on the total computation time of reactive flow simulations becomes evident in the presented results. Choosing the partitioning size accordingly can greatly improve the efficiency of the simulations. Thus, an elaborated partitioning strategy is needed. We showed that tabulation has a greater impact on simulations with complex reaction mechanisms than on simpler ones.

Our results suggest to split up reactive flow calculations to approximately 60 000 cells per processor. This agrees well with the suggestion in [1], who suggested to use between 50 000 and 100 000 cells per processor core and aim for the lower value for more complex simulations.

For more complex mechanisms, a noticeable speed-up can be achieved by reducing the number of cells as low as to 5 000 cells, as similarly suggested in [4].

When the mesh is already quite small, e.g. 5 000 cells, a partitioning is still useful up to 2 cores and speed-up can be gained, although the number of cells per processor gets very low.

Acknowledgments

The authors gratefully acknowledge the funding support of K1-MET GmbH, metallurgical competence center. The research program of the competence center K1-MET is supported by COMET (Competence Center for Excellent Technologies), the Austrian program for competence centers. COMET is funded by the Federal Ministry for Transport, Innovation and Technology, the Federal Ministry for Science, Research and Economy, the province of Upper Austria, Tyrol, and Styria, the Styrian Business Promotion Agency. Apart from funding, the project activities are financed by the industrial partners Primetals Technologies Austria, voestalpine Stahl and voestalpine Stahl Donawitz.

The computational results presented have been achieved in part using the Vienna Scientific Cluster (VSC).

References

- [1] B. Haddadi, C. Jordan, M. Harasek, Cost efficient CFD simulations: Proper selection of domain partitioning strategies, *Comput. Phys. Commun.* 219 (2017) 121–134.

- [2] L. Liang, J.G. Stevens, J.T. Farrell, A dynamic multi-zone partitioning scheme for solving detailed chemical kinetics in reactive flow computations, *Combust. Sci. Technol.* 181 (2009) 1345–1371. doi:10.1016/j.cpc.2017.05.014.
- [3] V. Hiremath, S.R. Lantz, H. Wang, S.B. Pope, Computationally-efficient and scalable parallel implementation of chemistry in simulations of turbulent combustion, *Combust. Flame.* 159 (2012) 3096–3109. doi:10.1080/00102200903190836.
- [4] M. Harasek, C. Jordan, C. Kuttner, C. Maier, S. Pohn, Steady-state RANS simulation of a swirling, non-premixed industrial methane-air burner using edcSimpleFoam, Report. (2011) 1–7. doi:10.1016/j.combustflame.2012.04.013.
- [5] H.G. Weller, G. Tabor, H. Jasak, C. Fureby, A tensorial approach to computational continuum mechanics using object-oriented techniques, *Comput. Phys.* 12 (1998).
- [6] B.F. Magnussen, On the structure of turbulence and a generalized eddy dissipation concept for chemical reaction in turbulent flow, (1981) 6.
- [7] B.F. Magnussen, The Eddy Dissipation Concept a Bridge between science and technology, in: *ECCOMAS Them. Conf. Comput. Combust.*, 2005.
- [8] B.F. Magnussen, Modeling of NO_x and Soot Formation by the Eddy Dissipation Concept, in: *Int. Flame Res. Found.*, 1989.
- [9] S. Byggstoyl, B.F. Magnussen, A model for flame extinction in turbulent flow, *Fourth Symp. Turbul. Shear Flows.* 4 (1983) 32–38. doi:10.1007/978-3-642-69996-2_31.
- [10] I.R. Gran, B.F. Magnussen, A Numerical Study of a Bluff-Body Stabilized Diffusion Flame. Part 2. Influence of Combustion Modeling And Finite-Rate Chemistry, *Combust. Sci. Technol.* 119 (1996) 191–217. doi:10.1080/00102209608951999.
- [11] M. Bösenhofer, E.-M. Wartha, C. Jordan, M. Harasek, The eddy dissipation concept-analysis of different fine structure treatments for classical combustion, *Energies.* 11 (2018). doi:10.3390/en11071902.
- [12] M.T. Lewandowski, I.S. Ertesvåg, Analysis of the Eddy Dissipation Concept formulation for MILD combustion modelling, *Fuel.* 224 (2018) 687–700. doi:10.1016/j.fuel.2018.03.110.
- [13] S.B. Pope, Computationally efficient implementation of combustion chemistry using in situ adaptive tabulation, *Combust. Theory Model.* 7830 (1997) 41–63. doi:10.1088/1364-7830/1/1/006.
- [14] M. Rehm, Numerische Strömungssimulation der Hochdruckvergasung unter Berücksichtigung detaillierter Reaktionsmechanismen, 2010.
- [15] Z. Ren, S.B. Pope, Second-order splitting

- schemes for a class of reactive systems, *J. Comput. Phys.* 227 (2008) 8165–8176.
doi:10.1016/j.jcp.2008.05.019.
- [16] E.-M. Wartha, M. Bösenhofer, M. Harasek, Computational Improvements for the Eddy Dissipation Concept by Operator Splitting and Tabulation, 2018. doi:10.1016/B978-0-444-64235-6.50294-1.
- [17] E. Gabriel, G.E. Fagg, G. Bosilca, T. Angskun, J.J. Dongarra, J.M. Squyres, V. Sahay, P. Kambadur, B. Barrett, A. Lumsdaine, R.H. Castain, D.J. Daniel, R.L. Graham, T.S. Wodall, Open MPI: Goals, Concept, and Design of a Next Generation MPI Implementation, in: 11th Eur. PVM/MPI Users' Gr. Meet., 2004: pp. 97–104.
- [18] R.S. Barlow, J.H. Frank, Effects of turbulence on specific mass fractions in methane/air jet flames, *Twenty-Seventh Symp. Combust.* 27 (1998) 1087–1095.
- [19] C. Schneider, A. Dreizler, J. Janicka, E.P. Hassel, Flow field measurements of stable and locally extinguishing hydrocarbon-fuelled jet flames, *Combust. Flame.* 135 (2003) 185–190. doi:10.1016/S0010-2180(03)00150-0.
- [20] M. Bösenhofer, C. Jordan, M. Harasek, A Flame D Modelling Study Employing Eddy Dissipation Concept Modifications, in: 8th Eur. Combust. Meet., 2017: pp. 1–6. doi:DOI: 10.13140/RG.2.2.11472.97285.
- [21] C.K. Westbrook, F.L. Dryer, Simplified Reaction Mechanisms for the Oxidation of Hydrocarbon Fuels in Flames, *Combust. Sci. Technol.* 27 (1981) 31–43. doi:10.1080/00102208108946970.
- [22] C.K. Westbrook, F.L. Dryer, Chemical kinetic modeling of hydrocarbon combustion, *Prog. Energy Combust. Sci.* 10 (1984) 1–57. doi:10.1016/0360-1285(84)90118-7.
- [23] A. Parente, C. Galletti, L. Tognotti, Effect of the combustion model and kinetic mechanism on the MILD combustion in an industrial burner fed with hydrogen enriched fuels, *Int. J. Hydrogen Energy.* 33 (2008) 7553–7564. doi:10.1016/j.ijhydene.2008.09.058.
- [24] P. Pepiot-Desjardins, H. Pitsch, An efficient error-propagation-based reduction method for large chemical kinetic mechanisms, *Combust. Flame.* 154 (2008) 67–81. doi:10.1016/j.combustflame.2007.10.020.

Conference Paper III

Combining and Implicit Solution with an Explicit Corrector Step for the Solution of the Continuity Equations in a Two-Fluid Solver

by Eva-Maria Wartha, Markus Bösenhofer and Michael Harasek; oral presentation at the 14th International Conference on CFD in Oil & Gas, Metallurgical and Process Industries in Trondheim and published in the proceedings

My contribution: Implementation of the algorithm in OpenFOAM. Setting up, simulating and analyzing the test cases. Conceptualization and writing the original draft of the paper.

E.-M. Wartha, M. Bösenhofer, and M. Harasek (2020b). “Combining an implicit solution with an explicit corrector step for the solution of the continuity equations in a two-fluid solver”. In: *14th International Conference on CFD in Oil & Gas, Metallurgical and Process Industries*. Trondheim, pp. 123–131

14th International Conference on CFD in Oil & Gas, Metallurgical and Process Industries
SINTEF, Trondheim, NORWAY
October 12-14, 2020

COMBINING AN IMPLICIT SOLUTION WITH AN EXPLICIT CORRECTOR STEP FOR THE SOLUTION OF THE CONTINUITY EQUATIONS IN A TWO-FLUID SOLVER

Eva-Maria WARTHA^{1*}, Markus BÖSENHOFER^{1,2}, Michael HARASEK¹

¹Technische Universität Wien - Institute of Chemical Environmental and Bioscience Engineering, 1060 Vienna, Austria

²K1-MET GmbH, Area 4 - Simulation and Analyses, Linz, Austria

* E-mail: eva-maria.wartha@tuwien.ac.at

ABSTRACT

To model two-phase flows in industrial applications, for example the raceway zone in a blast furnace, an Eulerian two-fluid model is usually the method of choice. It has proven to predict the behavior of gas-solid flows well and has a justifiable computational demand. Although, it is already widely used, there are still some deficiencies which arise from the averaged equations. Especially the continuity equation needs some special care compared to single phase flows. The consistency and boundedness need to be ensured, which is not straightforward. One widely used approach to target this problem is to use the relative velocities in the continuity equation. A drawback is, that this modified equation is non-linear in the phase fraction and therefore needs to be solved iteratively if solved implicitly. We propose to solve the discretized equation by combining an implicit solution step with (an) explicit corrector step(s). This new approach was implemented in the open source software OpenFOAM® and compared with the standard implementation. The new algorithm gives good prediction results for several test cases and this implicit approach could lead to larger time steps through better stability of the solution procedure.

Keywords: Two-Fluid Flow, Euler-Euler Approach, Raceway Simulation .

NOMENCLATURE

Greek Symbols

α	Phase fraction, [-]
η	Constant = 2 [-]
κ	Solid conductivity [kg/ms]
λ	Blending coefficient [-]
ξ	Coupling term, [s^{-1}]
ρ	Density, [kg/m^3]
τ	Stress tensor, [kg/ms^2]
ϕ	Angle of internal friction [°]
φ	Velocity, [m/s]

Latin Symbols

p	Pressure, [Pa].
t	Time, [s]
A	Diagonal contributions
F	Flux [m/s]
Fr	Constant = 0.05 [-]
K	Drag coefficient [kg/m^3s]
P	Constant = 5 [-]

S	Source term
V	Cell volume[-]
$(I_{2D})^{-1/2}$	2nd-order deviatoric shear stress tensor
g	Gravitational acceleration [m/s^2]
S	Surface normal vector [-]
U	Velocity, [m/s]

Sub/superscripts

e	Explicit
f	Face value
g	Gas
i	Implicit
n	Time step
p	Center value
r	Relative value
s	Solid
C	Convective
H	High order
L	Low order
$fric$	Frictional
$ktgf$	Kinetic theory of granular flows
min	Minimum for frictional effects
max	Maximum (packing) limit
*	Quantity enlarged with decoupling terms

INTRODUCTION

Industrial processes often incorporate two- or multi-phase flows, for example: fluidized beds for pyrolysis (Papadakis *et al.*, 2008) or the blast furnace for pig iron production (Abhale *et al.*, 2020). The simulation of such processes using computational fluid dynamics (CFD) helps to understand and improve them. To accurately and efficiently predict the phenomena dominating the operation, well calibrated models and numerical procedures are essential.

In general, the solid phase in a two-phase flow could be described by using Lagrangian or Eulerian models. The Lagrangian models offer more detail, since they are able to resolve particle interactions on a per particle basis (van der Hoef *et al.*, 2008; Agrawal *et al.*, 2001). Although, computer power is and has been increasing, the computational demand is still limiting. Therefore, this approach is usually only applied to small scales or low solid concentrations. For the many two-phase flows in industry, which incorporate dense solid flows, the Eulerian models are the way to go, (van der Hoef *et al.*, 2008). Here, both (gas and solid) phases are treated as interpenetrating continua. Particle interactions

can not be resolved using those models but the models have proven to correctly predict phenomena in two-phase flows. Compared to single-phase flows, the coupled equations are more difficult to solve and need special treatment, (Passalacqua and Fox, 2011; Weller, 2005). To further speed-up simulations the community is constantly trying to improve the algorithms to solve the equations. In this paper we suggest an alternative algorithm for the solution of the continuity equation in two-phase flows.

The algorithmic approach is described in the following section. The new approach was implemented in OpenFOAM® and tested on several test cases. The results are presented and provide promising results for the application of the new algorithm.

THEORY

Two-Fluid solvers are widely used for dense gas-solid systems. They treat both the phases as interpenetrating continua and use the Navier-Stokes equations for their description. Compared to a single-fluid system, the phase fraction is added to the descriptive equations. The phase-averaged equations for the solid phase are given in the following. Eq. 1 shows the continuity equation and Eq. 2 the momentum equation, where α_s is the solid phase volume fraction, \mathbf{U}_s the solid velocity and \mathbf{U}_g the gas velocity, ρ_s the solid density, τ_s the solid stress tensor, p the pressure, p_s the solid pressure, \mathbf{g} the gravitational acceleration and K_{sg} the drag interaction coefficient. The solid pressure p_s is modeled based on the Kinetic Theory of Granular Flows, which is shortly described in a following section.

$$\frac{\partial}{\partial t} (\alpha_s \rho_s) + \nabla \cdot (\alpha_s \rho_s \mathbf{U}_s) = 0 \quad (1)$$

$$\frac{\partial}{\partial t} (\alpha_s \rho_s \mathbf{U}_s) + \nabla \cdot (\alpha_s \rho_s \mathbf{U}_s \mathbf{U}_s) = \nabla \cdot (\alpha_s \bar{\tau}_s) - \alpha_s \nabla p - \nabla p_s + \alpha_s \rho_s \mathbf{g} + K_{sg} (\mathbf{U}_g - \mathbf{U}_s) \quad (2)$$

The equations for the gas phase are formulated similarly by using the quantities of the gas phase (gas volume fraction α_g , gas density ρ_g and gas stress tensor τ_g):

$$\frac{\partial}{\partial t} (\alpha_g \rho_g) + \nabla \cdot (\alpha_g \rho_g \mathbf{U}_g) = 0 \quad (3)$$

$$\frac{\partial}{\partial t} (\alpha_g \rho_g \mathbf{U}_g) + \nabla \cdot (\alpha_g \rho_g \mathbf{U}_g \mathbf{U}_g) = \nabla \cdot (\alpha_g \bar{\tau}_g) - \alpha_g \nabla p + \alpha_g \rho_g \mathbf{g} + K_{sg} (\mathbf{U}_s - \mathbf{U}_g) \quad (4)$$

The two phases are coupled through the momentum exchange terms. In Eq. 2 and Eq. 4 only the drag term is considered ($K_{sg} (\mathbf{U}_g - \mathbf{U}_s)$). Furthermore, the following condition links the phases:

$$\sum \alpha_i = \alpha_s + \alpha_g = 1 \quad (5)$$

With the phase-averaged equations, some problems arise in the solution procedure, because the conservativeness of the solution and the boundedness of the phase volume fraction need to be ensured. Rusche (2002) and Oliveira and Issa (2003) recap different approaches of the discretization of the continuity equation. Here (and in OpenFOAM®) we use an approach presented by (Weller, 2005) and (Passalacqua

and Fox, 2011) where the equation is reformulated in the following way:

$$\frac{\partial}{\partial t} (\alpha_s) + \nabla \cdot (\alpha_s \mathbf{U}) + \nabla \cdot (\alpha_g \alpha_s \mathbf{U}_r) = 0 \quad (6)$$

using the average phase velocity \mathbf{U}

$$\mathbf{U} = \alpha_s \mathbf{U}_s + \alpha_g \mathbf{U}_g \quad (7)$$

and the relative phase velocity \mathbf{U}_r

$$\mathbf{U}_r = \mathbf{U}_s - \mathbf{U}_g \quad (8)$$

The derivation of the coupling terms and the phase pressure yields the modified phase continuity equation, derived by (Passalacqua and Fox, 2011):

$$\frac{\partial \alpha_s}{\partial t} + \nabla \cdot (\alpha_{s,f} \varphi^*) + \nabla \cdot (\alpha_g \alpha_s \varphi_{r,s}^*) - \nabla \cdot \left[\alpha_{s,f} \xi_{s,f} \left(\frac{1}{\rho_s} \frac{\partial p_s}{\partial \alpha_s} \right) |f| |\mathbf{S}| \nabla^\perp \alpha_s \right] = 0 \quad (9)$$

Where \mathbf{S} is the surface normal vector and the averaged flux (φ) (Eq. 11) and the relative flux ($\varphi_{r,s}$) (Eq. 13) are used. The fluxes (φ^* and $\varphi_{r,s}^*$) are modified by a term resulting from the decoupling of the momentum equations:

$$\varphi^* = \varphi + \alpha_{s,f} \xi_{s,f} \left(\frac{1}{\rho_s} \frac{\partial p_s}{\partial \alpha_s} \right) |f| |\mathbf{S}| \nabla^\perp \alpha_s \quad (10)$$

$$\varphi = \alpha_s \varphi_s + \alpha_g \varphi_g \quad (11)$$

$$\varphi_{r,s}^* = \varphi_{r,s} + \xi_{s,f} \left(\frac{1}{\rho_s} \frac{\partial p_s}{\partial \alpha_s} \right) |f| |\mathbf{S}| \nabla^\perp \alpha_s \quad (12)$$

$$\varphi_{r,s} = \varphi_s - \varphi_g \quad (13)$$

$$\xi_{s,f} = \frac{1}{A_s + \frac{K_{sg}}{\rho_s}} \quad (14)$$

The partially implicit algorithm (explained by (Weller, 2005) and (Venier *et al.*, 2018)) is used for the decoupling. The term $\xi_{s,f}$ results from this decoupling of the momentum equations - in Eq. 14 only the drag term (K_{sg}) is mentioned, but also the implicit part of the virtual mass force term can be added to $\xi_{s,f}$. A_s is the coefficient matrix arising from the discretisation of the momentum equation.

Boundedness can only be ensured, if a fully implicit solution algorithm is chosen (Rusche, 2002; Passalacqua and Fox, 2011), but the non-linearity in α (Eq. 9) requires sub-iterations when using an implicit approach.

An upwind differencing scheme can also ensure the boundedness of the solution of Eq. 9. A drawback from the upwind schemes is numerical diffusion and consequently unsatisfying results. Therefore, an algorithm, called MULES (Multidimensional Universal Limiter with Explicit Solution) for blending high-order and upwind solution has been introduced in OpenFOAM®. The MULES algorithm is described in the next section.

Since this MULES algorithm requires quite small time stepping, ≤ 0.25 (Wardle and Weller, 2013), we wanted to suggest a new algorithm to possibly combine the benefits of a fully implicit and the MULES algorithm. This suggested and newly implemented algorithm, named ICMULES, is introduced afterwards and tested on several benchmark cases.

MULES Algorithm

MULES is the abbreviation for "Multidimensional Universal Limiter with Explicit Solution" and is an iterative algorithm to solve hyperbolic equations (Tacconi, 2018). The method explicitly integrates in time and uses a blending of first-order upwind and high-order schemes for the calculation of the fluxes. This ensures the boundedness while keeping the influence of numerical diffusion low.

In the OpenFOAM® Code the *MULES:explicitSolve* function is used to partly solve the modified continuity Eq. 9. The function solves Eq. 9 without the consideration of the last term, see Eq. 15. F_{Cf}^n denotes the convective fluxes, which correspond to the second and third term in Eq. 9. The fluxes are calculated with consideration of the lower ($\alpha = 0$) and upper (α_{max}) limits of the phase fraction. S_i and S_e represent the source terms of the continuity equation arising from f.ex. phase change or compression.

$$\frac{\alpha_{sp}^{n+1} - \alpha_p^n}{\Delta t} V_p + \sum_f F_{Cf}^n = \alpha_{sp}^{n+1} S_i + S_e \quad (15)$$

The fluxes are blended by fluxes calculated with a low order discretisation scheme F_C^L and fluxes calculated with a high order discretisation scheme F_C^H . The low order and an antidiffusive flux A are summed up, see Eq. 17. The antidiffusive flux is calculated as:

$$A = (F_C^H - F_C^L) \quad (16)$$

A limiter function λ , based on the limits of α_s and the neighboring cell values is computed, which determines the degree of blending.

$$\frac{\alpha_{sp}^{n+1} - \alpha_p^n}{\Delta t} V_p + \sum_f F_{Cf}^{n,L} + \sum_f \lambda_f A = \alpha_{sp}^{n+1} S_i + S_e \quad (17)$$

More details on the computation of the limiter λ are given in (Tacconi, 2018).

ICMULES Algorithm

The suggested new algorithm combines an implicit solution step with a corrector step using MULES. Therefore, it will be called ICMULES (Implicit Corrected by MULES) in the following. The implicit step solves Eq. 9. In the present paper the following discretization schemes are used: implicit Euler in time, limited linear for the convective term with the relative flux, pure upwind for the other flux, a linear scheme for the gradient and linear with correction for the laplacian term.

The MULES algorithm is used in the next step to calculate an antidiffusive flux A , as previously, to ensure the boundedness of the solution. This antidiffusive flux is used to correct alpha similarly to Eq. 17:

$$\frac{\alpha_{sp}^{corr} - \alpha_{sp}^i}{\Delta t} V_p + \sum_f \lambda_f A = \alpha_{sp}^{n+1} S_i + S_e \quad (18)$$

If the corrector step is used multiple times, an underrelaxation factor of 0.5 for all but the first iteration is introduced. It is usually applied three times in the following test cases.

Kinetic Theory Models

The solid phase fraction and its movement are modeled by the Kinetic Theory of Granular Flows (KTGF) (Gidaspow, 1994). A granular temperature Θ_s is used to model the solid phase viscosity and the particle pressure. Usually, a partial differential equation (PDE) for the granular temperature is constructed and solved (see (Gidaspow, 1994) or (Venier *et al.*, 2018) for further details).

If dissipation is assumed to be equal to production of the granular temperature, an algebraic equation is derived and solved instead of the PDE. (This is denoted in the OpenFOAM® settings by `equilibrium=on`).

For the solid viscosity $\mu_{s,ktgf}$ and the solid conductivity κ_s different models using the radial distribution function g_0 , the granular temperature Θ_s and the restitution coefficient e_s exist.

Different models were proposed in literature for the calculation of the granular pressure, the frictional stress and the radial distribution function. A short recap of the used models is given below:

Granular Pressure Models

(a) Lun

$$p_s = \rho_s \alpha_s \Theta_s + 2\rho_s \alpha_s^2 g_0 \Theta_s (1 + e_s) \quad (19)$$

For the granular pressure the relation presented by (Ding and Gidaspow, 1990) is used, which is derived based on Lun's velocity relations in a collision (Lun *et al.*, 1984).

Frictional Stress Models

The kinetic theory of granular flows does not model particle interactions with multiple neighboring particles near the packing limit, (Srivastava and Sundaresan, 2003; Venier *et al.*, 2018). Therefore, models to account for friction, frictional stress models, were introduced near the packing limit (when $\alpha_s > \alpha_{min}$). A frictional pressure and a frictional viscosity are added to the solid pressure and the solid viscosity:

$$p_s = p_{s,ktgf} + p_{s,fric} \quad (20)$$

$$\mu_s = \mu_{s,ktgf} + \mu_{s,fric} \quad (21)$$

Passalacqua and Fox (2011) and Venier *et al.* (2018) compare different frictional stress models and their influence on the simulation. Commonly used models are:

(a) Johnson Jackson (Johnson *et al.*, 1990)

$$p_{s,fric} = Fr \frac{(\alpha_s - \alpha_{min})^\eta}{(\alpha_{s,max} - \alpha_s)^P} \quad (22)$$

$$\mu_{s,fric} = 0.5 p_{s,fric} \sin(\phi) \quad (23)$$

(b) Schaeffer (Schaeffer, 1987)

$$p_{s,fric} = 10^{25} (\alpha_s - \alpha_{s,min})^{10} \quad (24)$$

$$\mu_{s,fric} = 0.5 p_{s,fric} (I_{2D})^{-1/2} \sin(\phi) \quad (25)$$

The angle of internal friction Φ was set to 28 for the Schaeffer model and to 28.5 for the Johnson Jackson model in the simulations.

Radial Models

Different models to calculate the radial distribution function g_0 used in the granular pressure formulation (Eq. 19) have been proposed: (a) Carnahan Starling (Carnahan and Starling, 1969)

$$g_0 = \frac{1}{1 - \alpha_s} + \frac{3\alpha_s}{2(1 - \alpha_s)^2} + \frac{\alpha_s^2}{2(1 - \alpha_s)^3} \quad (26)$$

(b) Lun Savage (Lun and Savage, 1986)

$$g_0 = \left(1 - \frac{\alpha_s}{\alpha_{max}}\right)^{-2.5\alpha_{max}} \quad (27)$$

(c) Sinclair Jackson (Lun and Savage, 1986; Sinclair and Jackson, 1989)

$$g_0 = \left(1 - \left(\frac{\alpha_s}{\alpha_{max}}\right)^{1/3}\right)^{-1} \quad (28)$$

It has to be noted, that the Carnahan Starling model does not take the maximum packing limit α_{max} into account, also emphasized by (Venier *et al.*, 2016). Therefore, the choice of the frictional stress model in conjunction with this model is essential, which will also be shown in the Results section.

RESULTS

Common test cases for two-fluid models are chosen to test the stability of the newly proposed algorithm. The results are compared to simulations with MULES. Furthermore, the influence of different frictional stress and radial models was tested to ensure the applicability of the ICMULES with different settings.

The test cases and the corresponding models used are summarized in Table 1. The abbreviations there correspond to the test cases: falling block=f.b., settling suspension=s.s., bubble growth=b.g. and raceway=r.w.. The letters (a)/(b)/(c) correspond to the models described in the section about the kinetic theory.

In the following subsections the chosen test cases are described and their results are presented.

Table 1: Models for the kinetic theory used for the different test cases and the chosen parameters

Model	f.b.	s.s.	b.g.	r.w.
equilibrium	off	off	off	off
viscosity	(a)	(b)	(b)	(b)
conductivity	(a)	(b)	(b)	(b)
granular pressure	(a)	(a)	(a)	(a)
frictional stress	(a)	(a)/(b)	(b)	(b)
radial	(a)	(c)	(a)/(b)	(c)
Parameters				
packing limit	0.63	0.60	0.63	0.63
α_{min}	0.60	0.55	varying	0.6
restitution coeff.	0.80	0.80	0.95	0.95

Falling Block (f.b.)

The falling block test case is chosen to check the stability of the algorithm. It was also used by (Passalacqua and Fox, 2011) and (Venier *et al.*, 2013). A block (dimensions: 0.026 m x 0.08 m) with a solid volume fraction of 0.58 is introduced at a height of 0.012 m in a 2D-domain with 0.05 m width and 0.2 m height. It falls down solely by gravity. A

hexahedral mesh with 10 x 40 cells is used for the simulation in OpenFOAM®.

The particles have a diameter of 0.4 mm and a density of 2000 kg/m³. The fluid phase viscosity is 1.84 · 10⁻⁵ Pa·s and a Prandtl Number of 0.7 is used. No virtual mass effects are taken into account and the drag is modeled as suggested by (Gidaspow, 1994), blending the Ergun and the Wen-Yu drag models.

The velocity boundary conditions are set as Dirichlet boundary conditions at the bottom and top for particle velocity and at the walls and the bottom for the air velocity. A Neumann boundary condition is set for the air velocity at the top and the particle velocity at the walls.

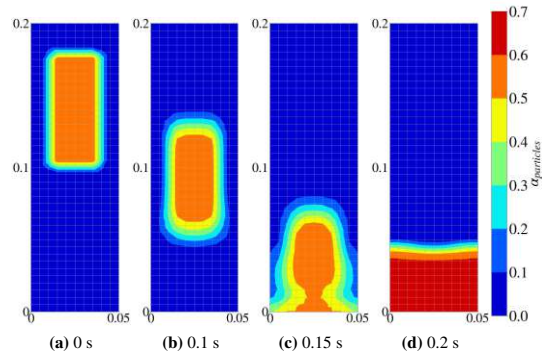


Figure 1: Falling block using MULES algorithm

The results using MULES and ICMULES are shown in Figure 1 and Figure 2, respectively. The results are very similar for the both algorithms. The particles are slightly denser packed when using the ICMULES algorithm. The snapshot at 0.2 s is not the finally settled bed.

The difference in the maximum packing could be related to the chosen radial and frictional stress model. The used radial model (Carnahan Starling) does not take the maximum packing limit into account. It is also discussed by (Schneiderbauer *et al.*, 2012), that the maximum packing limit is ensured by the divergence of the frictional stresses, when the Carnahan Starling or a similar model is used for the radial distribution function. The MULES algorithm is still enforcing the packing limit by accounting for it in the flux reconstruction. The correction step in the ICMULES is not enforcing this limit. The question remains if this property is related to a physical model or it is a "numerical" trick in the MULES algorithm. Probably, one should anyways aim to choose a physically valid combination of radial model and frictional stress model, which ensures the packing limit.

Settling Suspension (s.s.)

The settling suspension case uses also a 2D-setup with 0.05 m width and 0.3 m height and is discretized by 8 x 40 hexahedral cells. The whole column is initialized with a solid volume fraction of 0.3. Through gravity, the particles settle after time until they reach the packing limit ($\alpha_{max} = 0.6$). Passalacqua and Fox (2011) use this case to test an implicit solution. Venier *et al.* (2016) use it to compare partial elimination with partially implicit approach for the decoupling of the momentum equations.

The properties of the solid and fluid fraction are the same as for the falling block case, except that the Prandtl number was

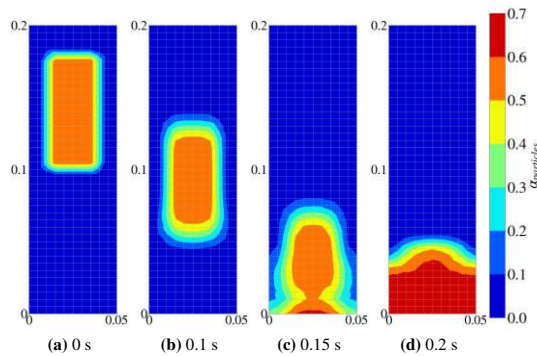


Figure 2: Falling block using ICMULES

set to unity for both phases. The boundary conditions as well as the virtual mass and drag effects are treated in the same way as for the falling block case.

The solid void fraction profiles after different settling times are shown in Figure 3. The two algorithms are compared to the literature data from (Passalacqua and Fox, 2011) and (Venier *et al.*, 2016). Here, two different frictional stress models, the Johnson and Jackson (a) and the Schaeffer (b) model were applied.

Figure 3 shows, that the MULES and ICMULES case agree very well at the later settling times. In the beginning, at $t = 0.1$ s, there is a difference at the top of the column. We are not entirely sure, what is causing those differences between the MULES and ICMULES results. Because the ICMULES algorithm fits better to the presented literature data the presented algorithm seems valid. One reason for the differences at the beginning of the column could be that numerical diffusion is more pronounced when applying the MULES algorithm.

At later times, the major difference between the solutions results from the different frictional stress models. The Schaeffer (b) model limits the phase fraction already to the α_{min} value. The results from the JohnsonJackson (a) model agree well with the results from literature and the results from ICMULES and MULES are virtually identical for the later time steps ($t = 0.6$ seconds).

Bubble Growth (b.g.)

The 2D bubble growth case checks the bubble growth in a fluidised bed with a central jet. Venier *et al.* (2018) studied the influence of the third dimension and did not find a significant impact, therefore, we only use the 2D case here. The geometry is 0.57 m wide and 1 m high and is discretized by 112 x 200 cells, which was determined to be the "best" mesh regarding the trade-off between calculation time and accuracy (Venier *et al.*, 2018).

First, the bubble formation with no frictional stress - or more precisely $\alpha_{min} > \alpha_{max}$ to avoid the contribution of frictional stresses was studied, see previous section about the frictional stress models. This was done to eliminate the influence of the chosen frictional stress model on the test results and solely study the influence of the radial model.

When using the ICMULES algorithm, the choice of the radial model determines if the packing limit is ensured, as discussed in the previous section. The ICMULES can enforce the packing limit when using the radial distribution models of Lun

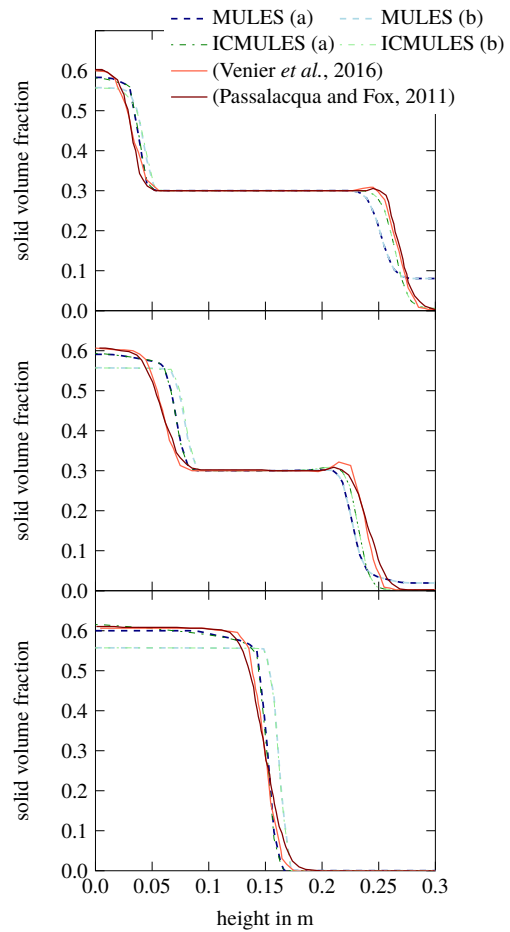


Figure 3: Solid volume fraction α_s after $t = 0.1, 0.15$ and 0.6 seconds settling time (from top to bottom), (a) and (b) refer to the frictional stress model

Savage or Sinclair Jackson, because there α_{max} is used in the formulations. The contribution of the radial function g_0 has a singularity at the packing limit and avoids overpacking in that way. When the Carnahan Starling model is used, the ICMULES cannot enforce the packing limit, see Figure 4 (d). The results in Figure 4 (d) show clearly, that the ICMULES is not applicable without a proper frictional stress model near the packing limit.

The MULES algorithm can always enforce the packing limit, because α_{max} is given as an input parameter for the flux calculation and ensures α values between 0 and α_{max} through the algorithmic implementation.

When the results without frictional stress with the Lun Savage radial model are compared, they are identical for the explicit and implicit algorithm, see Figure 4. The agreement with the experiments seems though to be best for the Carnahan Starling model using the explicit algorithm. Comparing the simulated and measured bubble detachment time, Table 2 indicates that the Lun Savage model agrees better with the experiments.

Table 2: Bubble detachment time in seconds. Experimental values from (Kuipers *et al.*, 1991). Simulations without frictional stress model

Exp.	MULES		ICMULES		radial model
	(a)	(b)	(a)	(b)	
0.17	0.19	0.15	0.31	0.15	

The simulations without frictional stress model were conducted to highlight the differences of the algorithmic approaches. For simulations near the packing limit it is usually not advised to ignore the frictional stresses, because the kinetic theory can not account for multiple particle interactions. Therefore, we also studied the bubble formation with a frictional stress model. We chose the Schaeffer frictional stress model, because it can be applied with the Carnahan Starling radial model. The results of the bubble formation at $t = 0.1, 0.14$ and 0.18 s are also shown in Figure 4. The minimum frictional packing was set to $\alpha_{min} = 0.6$.

Kuipers *et al.* (1991) presented also the bubble diameter ratio of the experiments. Figure 5 compares those ratios with the ones from the simulation without frictional stress. In the simulation the bubble was measured as the region with a void fraction below 0.2. The bubble shape with the Lun Savage radial model and no frictional stresses is predicted in line with the experiments for the first 0.15 seconds. Then, the vertical stretch is over and/or the longitudinal stretch under predicted. The same comparison was made for the bubble prediction using the Schaeffer frictional stress model, see Figure 6. Here the longitudinal stretch of the bubble seems way overpredicted. This is already visible in Figure 4. Nevertheless, the bubble diameter ratio shows, that the algorithm is not influencing the results. The deviations between simulation and experiments are most likely related to the models and settings chosen therein.

2D Raceway (r.w.)

The last studied test case in this paper is a 2D Raceway formation test case. The test case was first presented by (Feng *et al.*, 2003). They studied the raceway formation in a simple 2D-setup by DEM simulation. Here, we test the applicability of an Euler-Euler algorithm in the prediction of the raceway formation in comparison with those DEM results. Furthermore, we test the proposed algorithm ICMULES and study the simulation time in comparison with the original algorithm.

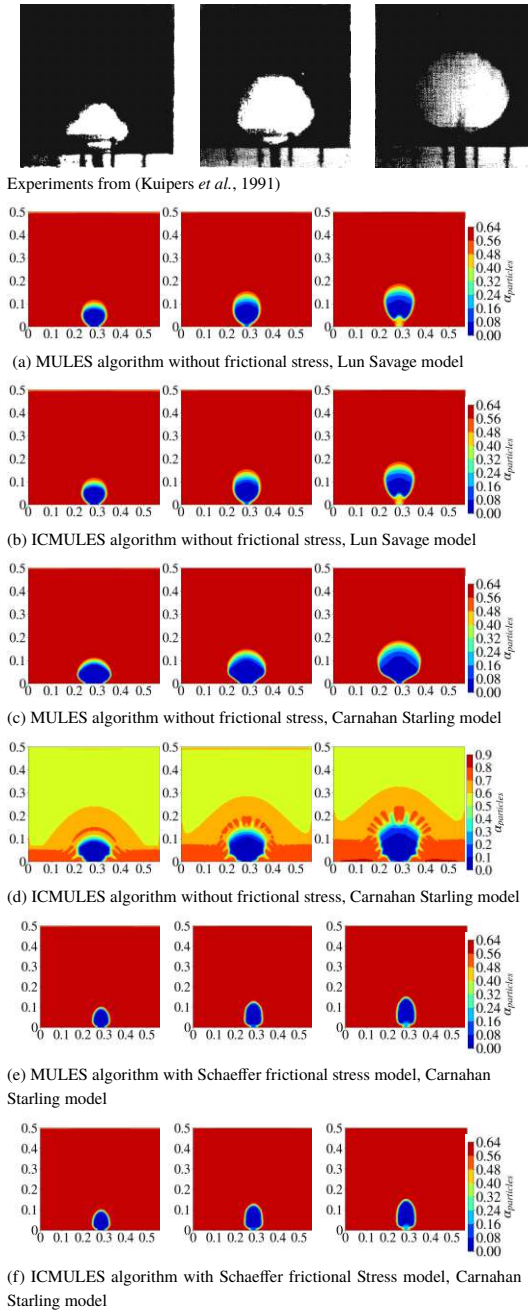


Figure 4: Single Bubble after 0.1, 0.14 and 0.18 seconds (column-wise).

Implicit Solution with an Explicit Corrector in a Two-Fluid Solver / CFD 2020

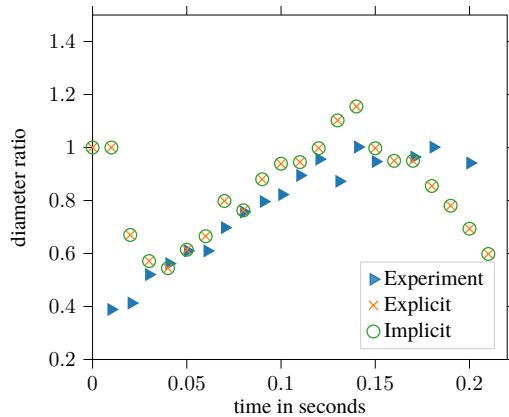


Figure 5: Comparison of the diameter ratio for the experiments from (Kuipers *et al.*, 1991) and the simulations using No Frictional Stress and Lun Savage radial model

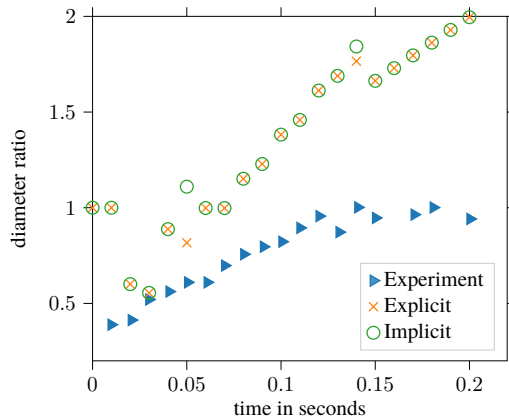


Figure 6: Comparison of the diameter ratio for the experiments from (Kuipers *et al.*, 1991) and the simulations using Schaeffer and Carnahan Starling model

The raceway is simulated as a 2D raceway, same as by (Feng *et al.*, 2003). The bed is 1 m high and 0.3 m wide. It was discretized by a uniform mesh using 200x60 cells. The jet inlet is positioned 0.1 m above the bottom of the bed and is 0.02 m wide. Table 3 lists the physical parameters for solid and gas phase used in the simulation.

Neumann boundary conditions for the air velocity are set at the walls and bottom. The inlet velocity is set to 20, 25 and 30 m/s for the different cases studied. At the top, the air pressure is fixed and no inflow is allowed. The particle velocity is set to zero at the inlet and outlet and a partial slip condition is used at the wall and bottom (Johnson and Jackson, 1987) with a specular coefficient of one. The specular coefficient defines the degree of frictional interaction between walls and particles (specular coefficient = 0 corresponds to frictionless walls). The velocity at the boundary is calculated based on this interaction coefficient. The granular temperature at the walls and bottom is also treated by the JohnsonJackson-

Table 3: simulation parameters for the raceway case

Solid phase		
diameter	m	0.004
density	kg/m ³	2500
Gas phase		
density	kg/m ³	1.205
viscosity	kg/(ms)	1.8·10 ⁻⁵

ParticleTheta conditions, described in (Johnson and Jackson, 1987), using the same specular coefficient and a restitution coefficient of 0.95.

As a result of the previous test cases, we decided to use the Schaeffer frictional stress model and the Carnahan Starling radial model for the simulations. The maximum packing limit was set to $\alpha_{max} = 0.63$ and the minimum frictional velocity to $\alpha_{min} = 0.6$.

Figure 7 and Figure 8 show the results from the raceway formation for two different inlet velocities: 25 and 30 m/s. For the 20 m/s practically no raceway is formed, which qualitatively agrees with the presented results in (Feng *et al.*, 2003). For the case with 25 m/s inlet velocity, the raceway is reaching a steady state after some time. For 30 m/s inlet velocity the bed performs more like a bubbly bed and the raceway does not seem to reach a steady state. The MULES and ICMULES algorithms give the same results for the raceway formation. For these cases a fixed time step of 10⁻⁵ s was used.

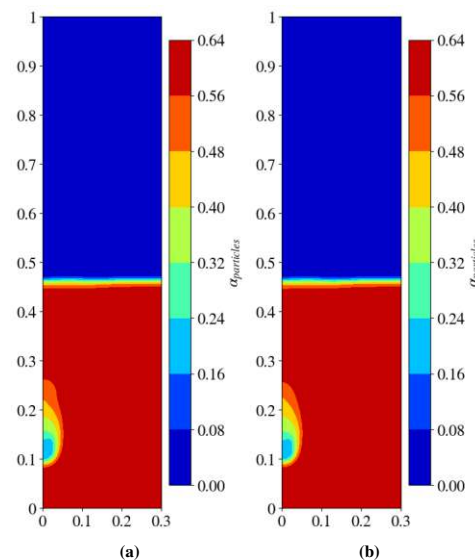


Figure 7: Raceway formation for 25 m/s inlet velocity after 1 s simulation time for the different algorithms: (a) MULES (b) ICMULES

We also compare the raceway penetration depths from (Feng *et al.*, 2003) and the simulations. It is not entirely clear, how the raceway penetration depth is defined by Feng *et al.* (2003). Here it was calculated as the distance from the air inlet to the region with a void fraction above 0.3. Table 4 shows the results from the simulation and literature. The penetration depth agrees well for the cases of high velocity (30 and 25 m/s). For 20 m/s no raceway is formed in the

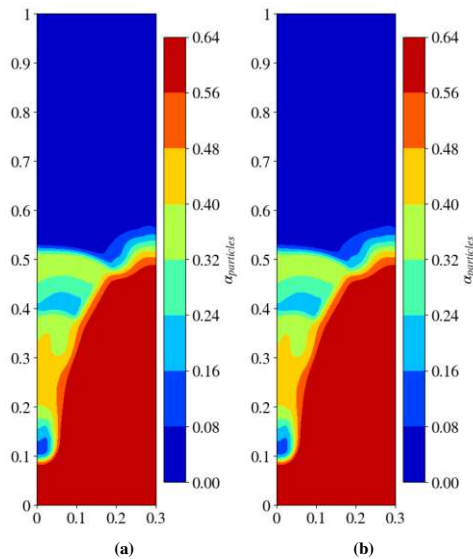


Figure 8: Raceway formation for 30 m/s inlet velocity after 1 s simulation time for the different algorithms: (a) MULES (b) ICMULES

OpenFOAM® simulations. Better agreement might be obtained, by also accounting for virtual mass effects, which were neglected here.

Table 4: Raceway penetration depth in mm in comparison

	paper	explicit	implicit
0.30 m/s	42	41	41
0.25 m/s	30	32	32
0.20 m/s	25	-	-

The above test cases were all tested with the same time step sizes for MULES and ICMULES and consequently resulted in approximately the same computational time. To give an indication on the possible computational improvements through the ICMULES, we also tested the Raceway case with variable time step using a maximum Courant number of 0.6. The computational time of the two cases yields 13805 s using MULES and 4008 s using ICMULES.

Figure 9 shows the results of the simulations with bigger time steps. This reveals, that the results from MULES with a bigger time step are not consistent with the results with lower time step. Contrary, the results from ICMULES agree well with the results in Figure 8.

CONCLUSION

In nearly all the test cases the newly introduced algorithm ICMULES gave similar results as the MULES algorithm. Only for certain model combinations, where the packing limit is not ensured through the radial or frictional stress model, the results differ significantly. There, the ICMULES algorithm fails to enforce the packing limit. This might be a limitation of the newly proposed algorithm. On the contrary, the question remains, if the packing limit should be enforced purely by numerical treatment, if the frictional or the radial model does not depict this packing limitation.

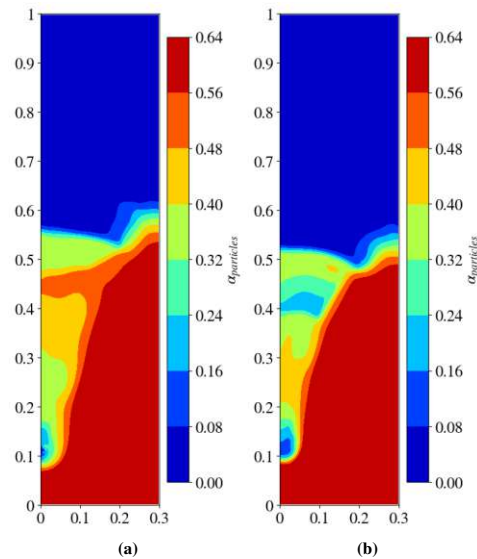


Figure 9: Raceway formation for 30 m/s inlet velocity after 1 s simulation time for the different algorithms using variable time stepping with maxCo = 0.6: (a) MULES (b) ICMULES

First results were presented, showing that the ICMULES enables considerable speed-up, since it produces consistent results also for higher Courant numbers, i.e. time steps.

In conclusion, the introduced algorithm can be used for the simulation of gas-solid systems, also near the packing limit, if suitable frictional and radial models are chosen.

ACKNOWLEDGMENT

The authors gratefully acknowledge the funding support of K1-MET GmbH, metallurgical competence center. The research program of the competence center K1-MET is supported by COMET (Competence Center for Excellent Technologies), the Austrian program for competence centers. COMET is funded by the Federal Ministry for Transport, Innovation and Technology, the Federal Ministry for Digital and Economic Affairs, the province of Upper Austria, Tyrol, and Styria. Apart from funding, the project activities are financed by the industrial partners Primetals Technologies Austria, voestalpine Stahl and voestalpine Stahl Donawitz.

REFERENCES

ABHALE, P.B., VISWANATHAN, N.N. and SAXEN, H. (2020). “Numerical Modelling of blast furnace – Evolution and recent trends”. *Mineral processing and Extractive Metallurgy*, **129(2)**, 166–183.

AGRAWAL, K., LOEZOS, P.N., SYAMLAL, M. and SUNDARESAN, S. (2001). “The role of meso-scale structures in rapid gas–solid flows”. *J. Fluid Mech.*, **445**, 151–185.

CARNAHAN, N.F. and STARLING, K.E. (1969). “Equation of state for nonattracting rigid spheres”. *The Journal of Chemical Physics*, **51(2)**, 635–636.

DING, J. and GIDASPOW, D. (1990). “A bubbling fluidization model using kinetic theory of granular flow”. *AIChE Journal*, **36(4)**, 523–538.

- FENG, Y.Q., PINSON, D., YU, A.B. and ZULLI, P. (2003). "Numerical Study of Gas-Solid Flow in the Raceway of a Blast Furnace". *Steel research*, **74(9)**, 523–530.
- GIDASPOW, D. (1994). *Multiphase Flow and Fluidization - Continuum and Kinetic Theory Descriptions*. Academic Press, Inc.
- JOHNSON, P. and JACKSON, R. (1987). "Frictional-collisional constitutive relations for granular materials, with application to plane shearing". *J. Fluid Mech.*, **179**, 67–93.
- JOHNSON, P., NOTT, P. and JACKSON, R. (1990). "Frictional-Collisional Equations of Motion for Granular Materials and Their Application to chutes". *Journal of Fluid Mechanics*, **210**, 501–535.
- KUIPERS, J., PRINS, W. and VAN SWAAIJ, W. (1991). "Theoretical and Experimental Bubble Formation at a Single Orifice in a Two-Dimensional Gas-Fluidized Bed". *Chemical Engineering Science*, **46(11)**, 2881–2894.
- LUN, C.K. and SAVAGE, S.B. (1986). "The effects of an impact velocity dependent coefficient of restitution on stresses developed by sheared granular materials". *Acta Mechanica*, **63(1-4)**, 15–44.
- LUN, C.K., SAVAGE, S.B., JEFFREY, D.J. and CHEPURNIY, N. (1984). "Kinetic theories for granular flow: Inelastic particles in Couette flow and slightly inelastic particles in a general flowfield". *Journal of Fluid Mechanics*, **140**, 223–256.
- OLIVEIRA, P.J. and ISSA, R.I. (2003). "Numerical aspects of an algorithm for the Eulerian simulation of two-phase flows". *International Journal for Numerical Methods in Fluids*, **43(10-11)**, 1177–1198.
- PAPADIKIS, K., BRIDGWATER, A. and GU, S. (2008). "CFD modelling of the fast pyrolysis of biomass in fluidised bed reactors, Part A: Eulerian computation of momentum transport in bubbling fluidised beds". *Chemical Engineering Science*, **63**, 4218–4227.
- PASSALACQUA, A. and FOX, R.O. (2011). "Implementation of an iterative solution procedure for multi-fluid gas-particle flow models on unstructured grids". *Powder Technology*, **213**, 174–187.
- RUSCHE, H. (2002). *Computational Fluid Dynamics of Dispersed Two-Phase Flows at High Phase Fractions*. Ph.D. thesis, Imperial College of Science, Technology & Medicine.
- SCHAEFFER, D.G. (1987). "Instability in the evolution equations describing incompressible granular flow". *Journal of Differential Equations*, **66(1)**, 19–50.
- SCHNEIDERBAUER, S., AIGNER, A. and PIRKER, S. (2012). "A comprehensive frictional-kinetic model for gas-particle flows: Analysis of fluidized and moving bed regimes". *Chemical Engineering Science*, 279–292.
- SINCLAIR, J.L. and JACKSON, R. (1989). "Gas particle flow in a vertical pipe with particle interactions". *AIChE Journal*, **35(9)**, 1473–1486.
- SRIVASTAVA, A. and SUNDARESAN, S. (2003). "Analysis of a frictional-kinetic model for gas-particle flow". *Powder Technology*, **129**, 72–85.
- TACCONI, Z. (2018). *Feasibility analysis of a two-fluid solver for cavitation and interface capturing as implemented in OpenFOAM*. Tesi di laurea, Politecnico Di Milano.
- VAN DER HOEF, M., VAN SINT ANNALAND, M., DEEN, N. and KUIPERS, J. (2008). "Numerical Simulation of Dense Gas-Solid Fluidized Beds: A Multiscale Modeling Strategy". *Annu. Rev. Fluid Mech.*, **40**, 47–70.
- VENIER, C., DAMIAN, S.M., RAMAJO, D. and NIGRO, N. (2013). "Numerical analysis of Multiphase Solid-Gas Flow with Eulerian Models and Kinetic Theory Closure". *Mecánica Computacional*, **XXXII**, 1849–1862.
- VENIER, C.M., MARQUEZ, S. and NIGRO, N.M. (2016). "Numerical aspects of Eulerian gas – particles flow formulations". *Computers and Fluids*, **133**, 151–169.
- VENIER, C.M., Marquez Damian, S. and NIGRO, N.M. (2018). "Assessment of gas-particle flow models for pseudo-2D fluidized bed applications". *Chemical Engineering Communications*, **205(4)**, 456–478.
- WARDLE, K.E. and WELLER, H.G. (2013). "Hybrid Multiphase CFD Solver for Coupled Dispersed/Segregated Flows in Liquid-Liquid Extraction". *International Journal of Chemical Engineering*, 1–13.
- WELLER, H. (2005). "Derivation, Modelling and Solution of the Conditionally Averaged Two-Phase Flow Equations". Tech. rep.

Conference Paper IV

Artificial Neural Networks to Substitute the ODE Solver in Reactive Flow Simulations

by Eva-Maria Wartha, Marlon Danilo Cabrera Ormaza, Markus Bösenhofer and Michael Harasek; oral presentation at the 10th European Combustion Meeting in Naples and published in the proceedings

E.-M. Wartha, M. D. Cabrera Ormaza, M. Bösenhofer, and M. Harasek (2021). “Artificial Neural Networks for the Application to Reactive Flow Simulations”. In: *10th European Combustion Meeting*. 4, pp. 266–271

Artificial Neural Networks to Substitute the ODE Solver in Reactive Flow Simulations

E.-M. Wartha^{1*}, M. D. Cabrera Ormaza¹, M. Bösenhofer^{1,2}, M. Harasek¹

¹Technische Universität Wien, Institute of Chemical, Environmental and Bioscience Engineering, Getreidemarkt 9/166, 1060 Wien

²K1-Met GmbH, Area 4 -Simulation and Analyses, Stahlstraße 14, BG 88, 4020 Linz

Abstract

The Eddy Dissipation Concept is often applied to couple turbulence and chemistry in computational fluid dynamics, because it can be coupled with any chemical mechanism. The solution of a system of ordinary differential equations is required to calculate the mass fraction changes. We present an approach to substitute the ODE-Solver by multiple artificial neural networks for speed-up. The training and validation results from plug flow reactor simulations are very promising in terms of accuracy and speed-up, but the results from Flame D show, that a network with arbitrary time step is necessary for speed-up and a variable for characterization of the solution space seems to be required.

Introduction

First theories building the foundation for artificial neural networks (ANNs) have been developed in the 40s but has lost attention around the millennial [1]. Due to better available hardware and datasets research on ANNs has gained attention in the past 15 years. The advancement in ANNs paved their way into many applications. Besides well-known application fields, such as image or speech recognition, ANNs can also be applied for chemical problems [2], f.ex. search for reaction components [3] or in combination with computational fluid dynamics (CFD), f.ex.: [4,5].

CFD is a widely used tool in chemical engineering and many processes can be investigated by CFD simulations. Many simulations are numerically too expensive despite the ever increasing computational power. Solving detailed chemistry is the most expensive part of such CFD simulations. Consequently, speed-up of the chemistry solution is an important objective and we aim to achieve the required speed-up through the use of artificial intelligence.

ANNs have been applied in combination with the flamelet model [6,7], the probability density function [8], or for tabulation [5].

An alternative model for combustion simulations, which describes the interaction between is the Eddy Dissipation Concept (EDC). Its benefit is that it can be used with any chemical reaction mechanism, but the solution of the system of ordinary differential equations (ODEs) describing the species mass fraction changes can become computationally very expensive. This system of ODEs is often considered stiff and therefore requires small time stepping in the solution and sophisticated ODE-solvers.

The substitution of the ODE-Solver by one or multiple ANNs to approximate the solution of the chemistry system could speed-up the simulation and has been already proposed in literature [9,8,10].

Theory

Turbulence-chemistry interactions are modeled by the Eddy Dissipation Concept (EDC) [11,12]. The EDC divides the fluid into fine structures (*) and surroundings (°). Because the educts only mix on a molecular scale in the fine structures, they react only there. Based on the turbulence energy cascade, the fine structure mass fraction γ^* can be described by:

$$\gamma^* = 4.6 \left(\frac{\nu \varepsilon}{k^2} \right)^{\frac{1}{2}} \quad (1)$$

where ε is the turbulent dissipation rate, ν the kinematic viscosity and k the turbulent kinetic energy. The residence time in the fine structure τ^* is modeled by:

$$\tau^* = 0.41 \left(\frac{\nu}{\varepsilon} \right)^{\frac{1}{2}} \quad (2)$$

The mean mass transfer between the fine structures and the surroundings is defined as:

$$\bar{R}_i = \frac{\rho \gamma^*}{\tau^* (1 - \gamma^*)} (\bar{Y}_i - Y_i^*) \quad (3)$$

Where ρ is the density in the computational cell and Y_i is the mass fraction in the fine structure, surroundings or the mean cell (-). The reaction of species in the fine structures is modelled by a perfectly stirred reactor (PSR) [12]. Because the additional mixing term significantly increases the numerical effort the model is often simplified to a plug flow reactor (PFR). Discussion about this simplification can be found in [13,14]. Within this paper we use the PFR simplification.

Eq.(4) describes the concentration evolution of species i in the fine structures, where $\dot{\omega}_i$ describes the chemical reaction rate of species i . The reaction rate is determined by the chemical mechanism, more precisely the reactions therein.

$$\frac{dY_i^*}{dt} = \dot{\omega}_i \quad (4)$$

The set of ODEs, as described in Eq.(4), can be computationally expensive to solve because it can be

* Corresponding author: eva-maria.wartha@tuwien.ac.at
Proceedings of the European Combustion Meeting 2021

stiff. Therefore, we aim to substitute the solution obtained with an ODE-solver by an ANN.

Although, we use the PFR model for the fine structures here, the concept could be used in the same manner for application to the chemical subproblem when using the PSR model. The ODE equation for the PSR is typically solved by operator splitting approaches, see f.ex.: [15–17].

Methods

An ANN can in general approximate the solution to any continuous multivariate function with a certain architecture and specific activation function [18]. In this work we apply a feedforward neural network with multiple layers. The input parameters are species mass fractions and the temperature, the output parameters are the species mass fractions after a fixed time step, see Figure 1.

The calculation of one output is given as:

$$y^l = \sigma(x^l(w^l)^T + b^l) \quad (5)$$

where x^l is the input to layer l , w^l is the matrix of weights, b^l is the vector of biases, σ is the activation function and y^l is the output of layer l .

Therefore, different ANNs are trained for different time steps. This was done similarly to the work in [9] because it reduces the size of the dataset and allows for faster training.

To train an ANN one needs a representative training and validation data set. Here we can easily generate an arbitrarily large data set by solving the chemical system, Eq.(4), for arbitrary initial conditions. In any case, we need to ensure that the data is representative for the solution space, where the ANN shall be used.

Therefore, we decided to follow an approach suggested by [9]. Laubscher uses the Bilger’s mixture fraction, Eq.(6), described in [19], where Z denotes the elemental mass concentration of c =carbon, o =oxygen, h =hydrogen and W denotes the elemental mass of the respective element. The initial conditions are constructed based on uniformly distributed mixture fractions over a mixture fraction range between 0.1 and 1. The calculation of the mixture fractions relies on an underdetermined system. For 50% of the mixture fraction calculations we use the least-squares algorithm and for the other 50% the non-negative least squares algorithm. This is done to ensure uniformly distributed mass fractions, but also obtain zero mass fractions. For a more detailed discussion and explanation of the data generation see [20].

$$Z = \frac{2(Z_c - Z_{c,ox})/W_c + (Z_H - Z_{H,ox})/2W_H + 2(Z_O - Z_{O,ox})/W_O}{2(Z_{c,fu} - Z_{c,ox})/W_c + (Z_{H,fu} - Z_{H,ox})/2W_H + 2(Z_{O,fu} - Z_{O,ox})/W_O} \quad (6)$$

Additionally, the temperature is also uniformly distributed in a range between T_{min} and T_{max} . Here they were chosen as 300 and 3000 K respectively. These initial conditions are then used for integration (until steady state or a maximum integration time) where each

time-step pair represents an input-output pair. The obtained data set is split into a training and validation set (split factor = 0.9). For a more detailed explanation of the used procedure see [20].

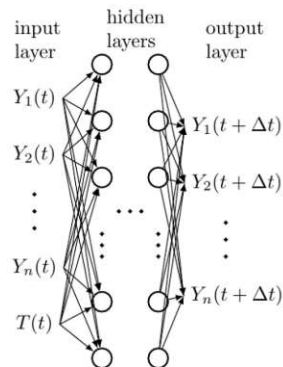


Figure 1: Schematic representation of the used architecture including input and output parameters

To evaluate the training of the network, the quality of the approximation is estimated by the loss function. We use the mean squared error, Eq.(7) as a loss function here. Where n_s is the number of species, Y_i^{ODE} the mass fraction of species i calculated by the ODE-Solver and Y_i^{ANN} the mass fraction of species i calculated by the ANN.

$$\sum_{n_s} \frac{(Y_i^{ANN} - Y_i^{ODE})^2}{n_s} \quad (7)$$

In the training of the ANN the weights and biases are adjusted in a way to minimize this loss function. In this work, the adaptive moment estimation algorithm (ADAM) [21] is used to adjust the parameters of the ANN.

A common choice as activation function is tanh. When applying tanh it is especially important to scale the input values between -1 and 1. Since the tanh is quite expensive in its evaluation and suffers from the vanishing gradient problem [22], the Rectifier Linear Unit (ReLU) has become more popular to use as activation function:

$$ReLU(x_i) = \begin{cases} x_i & \text{if } x_i \geq 0 \\ 0 & \text{otherwise} \end{cases} \quad (8)$$

A nice property of ReLU is, that it enforces the non-negativity constraint for the mass fractions. Therefore, it will be applied as activation function in the last layer.

Unfortunately, the “dying ReLU” is a problem which arises when using ReLU as activation function [23]. Therefore, the LeakyReLU was used as activation function in all layers in the training, see Eq.(9). The

LeakyReLU ensures a small gradient when $x_i < 0$. The parameter α was set to 0.01 in this work.

$$\text{LeakyReLU}(x_i) = \begin{cases} x_i & \text{if } x_i \geq 0 \\ \alpha x_i & \text{otherwise} \end{cases} \quad (9)$$

The ANN shall be applied in conjunction with the EDC to speed up reactive flow simulations. For the CFD simulation we use the open-source Code OpenFOAM® [24] in combination with an in-house ANN chemistry library. The customized chemistry model reads the previously trained weights and biases of the network(s) and uses them instead of the ODE-Solver to approximate the PFR-model for the fine structures.

The integration time of the ODE, Eq.(4), is defined by the fine structure residence time, Eq.(3). Since we only train ANNs for fixed time step sizes, we approximate the integration time by combining multiple of those steps.

Besides the validation in python using the validation data set, we also apply the ANNs for combustion simulation. As a test case Sandia Flame D [25,26], a piloted methane-air jet flame, was chosen.

We use the reaction mechanism from [27] for the flame simulation, which is based on the well-known Jones-Lindstedt mechanism [28]. It consists of 4 reactions and 7 species.

The computational grid consists of 5170 cells. The P1 radiation approximation was used. ANN and the ODE-Solver are only applied in cells, where the temperature is greater than a threshold reaction temperature. Additionally, the ANN is only applied in cells with a mixture fraction above 0.1.

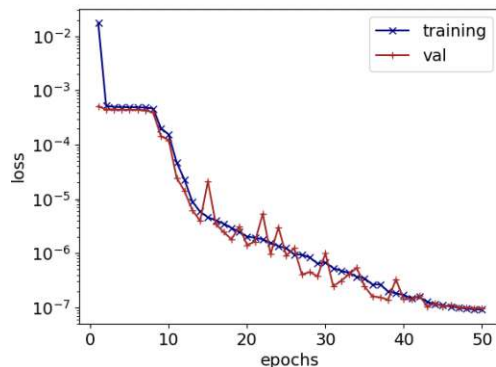


Figure 2: Training and validation loss for the training of the ANN with time step size 1e-4 s

The data generation and training of the ANNs was done using python-3.8 [29]. To handle the reaction mechanisms cantera was used [30]. The pytorch [31] package was used, for the machine learning part. Other packages used were pandas [32] for reading, writing and handling in- and output data and scipy [33].

The ANN training was done on an AMD FX(tm)-8350 (8 cores) with 30 GB RAM and a NVIDIA GeForce GT710.

Results and Discussion

Based on the findings from [20] we trained three networks with 4 layers and 64 neurons in each layer for time step sizes of 1e-3, 1e-4 and 1e-5 seconds.

Figure 2 shows the evolution of the loss for training and validation over the epochs of training. The training and the validation losses decrease in the same manner, which indicates that overfitting is not an issue.

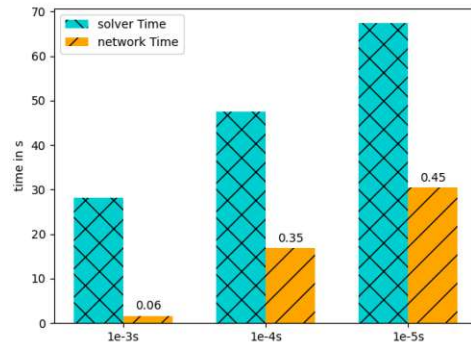


Figure 3: Solver time and solution of the network in comparison (Python)

The execution time was tested with the neural network and compared to python's VODE solver. The solver is provided via the scipy package [33]. It uses a stiff ODE-solver based on the backward differentiation formula (BDF). For the ANN trained for the different time steps the result is shown in Figure 3. The execution time was tested for plug flow reactor simulations. As expected the improvements increase for larger time steps because the matrix multiplication is executed less often.

The reason, why the solver time is also increasing drastically for smaller time steps is probably related to the type of the solver. The first internal time step after restart is small while they increase for subsequent iterations, compare f.ex. [34].

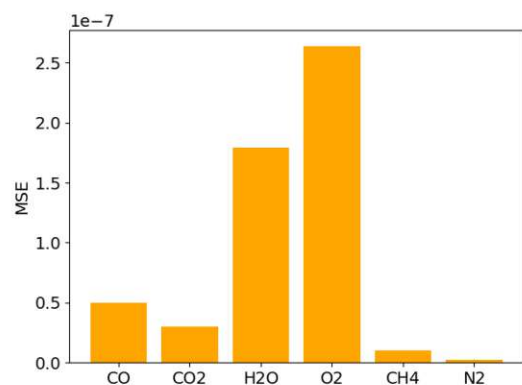


Figure 4: Error between the simulation using the standard ODE solver and the one with the approximated integration time

The integration time of the fine structures, defined by the fine structure residence time, can only be approximated by the ANNs with fixed time steps. To verify, that this approximation of the integration time

does not influence the solution (too much), we simulated Flame D with the ODE solver using the same approximation for the integration time. To quantify the difference, we calculated the Mean Squared Error between the standard ODE solver and this approximation for the species concentrations on the axial profiles ($r/d = 1, 2, 3, 7.5, 15, 30, 45, 60$). Figure 4 **Errore. L'origine riferimento non è stata trovata.** shows the errors associated with this integration time approximation. They are very small for all species. Therefore, we concluded that the approximation error of the residence time is negligible.

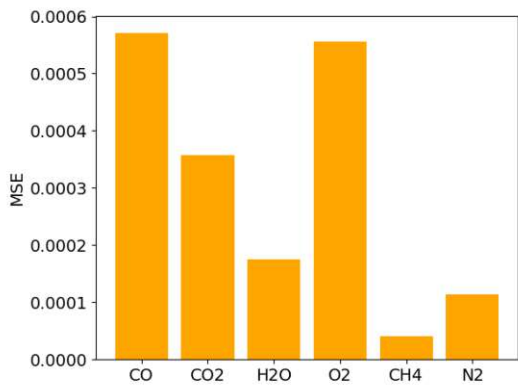


Figure 5: Error between the simulation with ODE solver and the simulation using the trained ANNs based on mixture fraction training data

The trained ANNs were used to simulate Flame D. We also calculated the MSE for the different species on the axial profiles, Figure 5 **Errore. L'origine riferimento non è stata trovata.** The MSE is orders of magnitude larger than for the comparison between the standard ODE-Solver and the “time-clipped” ODE-Solver. Especially, the CO production and O₂

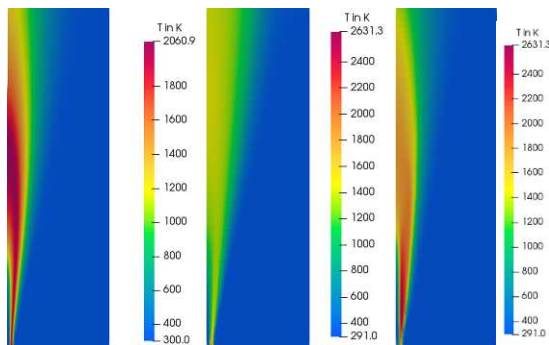


Figure 6: Temperature distribution of the simulation (from left to right) using the ODE solver, the ANN based on mixture fraction data and the ANN based on simulation data

consumption rate seems to be off.

Figure 7 also shows the temperature distribution in the Flame for the simulation with the ODE-Solver and with the ANN approximator. The difference here can be clearly seen, although the training and validation gave

very good results and the errors for the ANN were minimal.

Comparing Laubscher’s [9] work, we see that also his ANN approximation was off, when the start initial conditions and the temperature field was not obtained from the ODE-Solver. This indicates, that a one-time step prediction by the ANN works well, but the error accumulates over multiple time steps. This accumulation is not considered in the training, because the loss function takes only into account the error between one input and one output.

Besides this circumstance, a difference between the training data space and the actual solution space could also be a reason for the deviations. To test this assumption, we trained three additional neural networks, using Flame D data from a previous simulation as initial conditions to generate the training data.

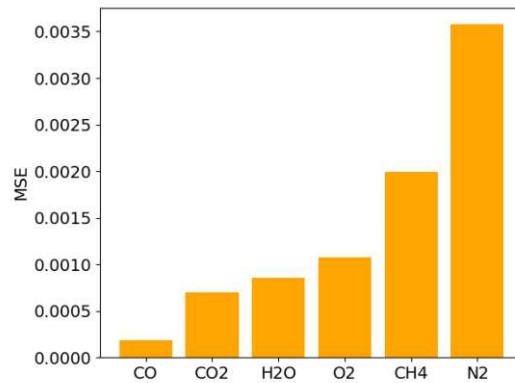


Figure 7: Error between the simulation with ODE solver and with ANN trained with simulation data

The predicted temperature field seems to be more accurate than the one obtained with the other ANN, see Figure 7. Calculating the mean squared errors for the species at the axial profiles results in higher errors than for the ANNs trained based on the generated data, Figure 7. The error could be again related to the error propagation. Based on the temperature distribution this network seems to be better, but no final conclusion can be drawn here.

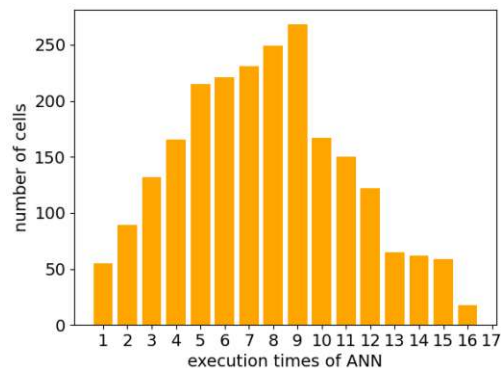


Figure 8: Number of times the ANN is used per cell count

The reason for this investigation was to speed-up reactive flow simulations. We showed the speed-up through the ANN in python. Similar results were shown in [9], who showed a significant speed-up through the usage of ANNs. The current implementation does not bring any speed-up in the OpenFOAM® simulations. One reason could be the efficiency of the seulex solver in OpenFOAM®, which is supposed to be more efficient than solvers based on BDF [34].

Another reason could be the inefficient approximation of the integration time. Laubscher [9] only approximated the integration time by the closest ANN, but we applied the ANNs multiple times to approximate the integration time better. This leads to a lot of applications of the ANN and consequently to a lot of matrix multiplications Figure 8 shows the distribution of the number of executions over the number of cells.

Conclusions

We presented a framework to generate and train a neural network to substitute the ODE-Solver in reactive flow simulations.

The tests on the sole approximation of the chemistry part brought significant speed-up compared to the ODE-Solver. Unfortunately, this speed-up could not be transferred to the combustion simulations, because the fixed-time step networks need to be applied multiple times to approximate the integration time in the simulation.

One approach to overcome this issue would be to train a network, with the time step as input parameter. It has to be investigated, if a similar network architecture can be capable to fulfill this task, or if either the network complexity has to be increased or some kind of progress variable needs to be introduced to measure the advancement of the reaction and distinguish between reaction pathways.

An alternative to generate training data, was for example presented by [35,36], who used DNS data for the training of their neural networks and later on used those in LES combustion simulations.

Acknowledgments

The authors gratefully acknowledge the funding support of K1-MET GmbH, metallurgical competence center. The research program of the competence center K1-MET is supported by COMET (Competence Center for Excellent Technologies), the Austrian program for competence centers. COMET is funded by the Federal Ministry for Transport, Innovation and Technology, the Federal Ministry for Digital and Economic Affairs, the province of Upper Austria, Tyrol, and Styria. Apart from funding, the project activities are financed by the industrial partners Primetals Technologies Austria, voestalpine Stahl and voestalpine Stahl Donawitz.

References

- [1] L. Hardesty, Explained: Neural networks, (2014). <https://news.mit.edu/2017/explained-neural-networks-deep-learning-0414> (accessed February 22, 2021).

- [2] H. Cartwright, Development and Use of artificial Intelligence in Chemistry, in: *Rev. Comput. Chem.*, 2007: pp. 349–389.
- [3] P. Plehiers, L.A. Vandewalle, G.B. Marin, C. V Stevens, K.M. Van Geem, Accelerating reactive CFD simulations with detailed pyrolysis chemistry using artificial neural networks, 2019 AIChE Annu. Meet. (2019).
- [4] J.A. Blasco, N. Fueyo, C. Dopazo, J. Ballester, Modelling the temporal evolution of a reduced combustion chemical system with an artificial neural network, *Combust. Flame.* 113 (1998)
- [5] L.L.C. Franke, A.K. Chatzopoulos, S. Rigopoulos, Tabulation of combustion chemistry via Artificial Neural Networks (ANNs): Methodology and application to LES-PDF simulation of Sydney flame L, *Combust. Flame.* 185 (2017) 245–260.
- [6] A. Kempf, F. Flemming, J. Janicka, Investigation of lengthscales, scalar dissipation, and flame orientation in a piloted diffusion flame by les, *Proc. Combust. Inst.* 30 (2005) 557–565. <https://doi.org/10.1016/j.proci.2004.08.182>.
- [7] O. Owoyele, P. Kundu, M.M. Ameen, T. Echekeki, S. Som, Application of deep artificial neural networks to multi-dimensional flamelet libraries and spray flames, *Int. J. Engine Res.* 21 (2020) 151–168.
- [8] F.C. Christo, A.R. Masri, E.M. Nebot, Artificial Neural Network Implementation of Chemistry with pdf Simulation of H₂ / C O₂ Flames, *Combust. Flame.* 106 (1996) 406–427.
- [9] R. Laubscher, Utilization of artificial neural networks to resolve chemical kinetics in turbulent fine structures of an advanced CFD combustion model, Stellenbosch University, 2017.
- [10] F.C. Christo, A.R. Masri, E.M. Nebot, S.B. Pope, An integrated PDF/neural network approach for simulating turbulent reacting systems, *Symp. Combust.* 26 (1996) 43–48.
- [11] B.F. Magnussen, Modeling of NO_x and Soot Formation by the Eddy Dissipation Concept, in: *Int. Flame Res. Found.*, 1989.
- [12] B.F. Magnussen, On the structure of turbulence and a generalized eddy dissipation concept for chemical reaction in turbulent flow, (1981) 6.
- [13] M. Bösenhofer, E.-M. Wartha, C. Jordan, M. Harasek, The eddy dissipation concept-analysis of different fine structure treatments for classical combustion, *Energies.* 11 (2018).
- [14] S. Tomasch, I.S. Ertesvåg, The influence of the reactor model on EDC's mean reaction rate - A study on the relevance of choice, in: *Proc. 9th Eur. Combust. Meet.* 2019, 2019.
- [15] S.B. Pope, Computationally efficient implementation of combustion chemistry using in situ adaptive tabulation, *Combust. Theory*

- Model. 7830 (1997) 41–63..
- [16] M. Rehm, Numerische Strömungssimulation der Hochdruckvergasung unter Berücksichtigung detaillierter Reaktionsmechanismen, 2010.
- [17] E.M. Wartha, M. Bösenhofer, M. Harasek, Computational Improvements for the Eddy Dissipation Concept by Operator Splitting and Tabulation, in: *Comput. Aided Chem. Eng.*, 2018: pp. 1687–1692.
- [18] V.E. Ismailov, On the approximation by neural networks with bounded number of neurons in hidden layers, *J. Math. Anal. Appl.* 417 (2014) 963–969. <https://doi.org/10.1016/j.jmaa.2014.03.092>.
- [19] H. K. Versteeg, W. Malalasekera, Introduction: Computational Fluid Dynamics The Finite Volume Method, 2006. <https://doi.org/10.2514/1.22547>.
- [20] M.D. Cabrera Ormazá, Artificial Neural Networks for the Application to Reactive Flow Simulations, Technische Universität Wien, 2021. <https://doi.org/10.34726/hss.2021.58068>.
- [21] D.P. Kingma, J.L. Ba, Adam: A method for stochastic optimization, 3rd Int. Conf. Learn. Represent. ICLR 2015 - Conf. Track Proc. (2015) 1–15.
- [22] S. Hochreiter, Untersuchungen zu dynamischen neuronalen Netzen. Diploma. Technische Universität München, Technische Universität München, 1991.
- [23] L. Lu, Y. Shin, Y. Su, G.E. Karniadakis, Dying ReLU and initialization: Theory and numerical examples, *Commun. Comput. Phys.* 28 (2020) 1671–1706.
- [24] H.G. Weller, G. Tabor, H. Jasak, C. Fureby, A tensorial approach to computational continuum mechanics using object-oriented techniques, *Comput. Phys.* 12 (1998) 620–631.
- [25] C. Schneider, A. Dreizler, J. Janicka, E.P. Hassel, Flow field measurements of stable and locally extinguishing hydrocarbon-fuelled jet flames, *Combust. Flame.* 135 (2003) 185–190.
- [26] R.S. Barlow, J.H. Frank, A.N. Karpetis, J.Y. Chen, Piloted methane/air jet flames: Transport effects and aspects of scalar structure, *Combust. Flame.* 143 (2005) 433–449.
- [27] J. Andersen, C.L. Rasmussen, T. Giselsson, P. Glarborg, Global combustion mechanisms for use in CFD modeling under oxy-fuel conditions, *Energy and Fuels.* 23 (2009) 1379–1389.
- [28] W.P. Jones, R.P. Lindstedt, Global Reaction Schemes for Hydrocarbon Combustion, *Combust. Flame.* 78 (1988) 233–249.
- [29] G. Van Rossum, F.L. Drake, Python 3 Reference Manual, CreateSpace, 2009. <https://doi.org/10.5555/1593511>.
- [30] D.G. Goodwin, R.L. Speth, H.K. Moffat, B.W. Weber, Cantera: An Object-oriented Software Toolkit for Chemical Kinetics, Thermodynamics, and Transport Processes, (2018). <https://doi.org/10.5281/zenodo.1174508>.
- [31] A. Paszke, S. Gross, F. Massa, A. Lerer, J. Bradbury, G. Chanan, T. Killeen, Z. Lin, N. Gimelshein, L. Antiga, A. Desmaison, A. Kopf, E. Yang, Z. DeVito, M. Raison, A. Tejani, S. Chilamkurthy, B. Steiner, L. Fang, J. Bai, S. Chintala, PyTorch: An Imperative Style, High-Performance Deep Learning Library, in: H. Wallach, H. Larochelle, A. Beygelzimer, F. d\$'Alché-Buc, E. Fox, R. Garnett (Eds.), *Adv. Neural Inf. Process. Syst.* 32, Curran Associates, Inc., 2019: pp. 8024–8035. <http://papers.neurips.cc/paper/9015-pytorch-an-imperative-style-high-performance-deep-learning-library.pdf>.
- [32] T. development team, pandas-dev/pandas: Pandas, (2020). <https://doi.org/10.5281/zenodo.3509134>.
- [33] P. Virtanen, R. Gommers, T.E. Oliphant, M. Haberland, T. Reddy, D. Cournapeau, E. Burovski, P. Peterson, W. Weckesser, J. Bright, S.J. van der Walt, M. Brett, J. Wilson, K.J. Millman, N. Mayorov, A.R.J. Nelson, E. Jones, R. Kern, E. Larson, C.J. Carey, I.Ihan Polat, Y. Feng, E.W. Moore, J. VanderPlas, D. Laxalde, J. Perktold, R. Cimrman, I. Henriksen, E.A. Quintero, C.R. Harris, A.M. Archibald, A.H. Ribeiro, F. Pedregosa, P. van Mulbregt, SciPy 1.0 Contributors, {SciPy} 1.0: Fundamental Algorithms for Scientific Computing in Python, *Nat. Methods.* 17 (2020) 261–272. <https://doi.org/10.1038/s41592-019-0686-2>.
- [34] A. Imren, D.C. Haworth, On the merits of extrapolation-based stiff ODE solvers for combustion CFD, *Combust. Flame.* 174 (2016) 1–15.
- [35] B.A. Sen, E.R. Hawkes, S. Menon, Large eddy simulation of extinction and reignition with artificial neural networks based chemical kinetics, *Combust. Flame.* 157 (2010) 566–578.
- [36] B.A. Sen, S. Menon, Linear eddy mixing based tabulation and artificial neural networks for large eddy simulations of turbulent flames, *Combust. Flame.* 157 (2010) 62–74.

Conference Paper V

Influence of Raceway Shape on Species Concentrations

by Eva-Maria Wartha, Markus Bösenhofer, Franz Hauzenberger, Hugo Stocker, Christoph Feilmayr and Michael Harasek; oral presentation (from Markus Bösenhofer) at AISTech and published in the proceedings

My contribution: Simulation and analyzes of the results. Conceptualization and writing the original draft.

E.-M. Wartha, M. Bösenhofer, F. Hauzenberger, H. Stocker, C. Feilmayr, and M. Harasek (2022c). “Influence of Raceway Shape on Species Concentration”. In: *AISTech - Iron and Steel Technology Conference Proceedings*. Pittsburgh

"Reprinted from AISTech Proceedings, with permission from Amanda Blyth, AIST Manager Publications."

Influence of Raceway Shape on Species Concentration

Wartha Eva-Maria¹, Bösenhofer Markus^{1,2}, Hauzenberger Franz³, Stocker Hugo⁴, Feilmayr Christoph⁵, Harasek Michael¹

¹TU Wien, Institute of Chemical, Environmental and Bioscience Engineering
Getreidemarkt 9/166, Vienna, Austria, 1060
Phone: +43-1-58801-166 270
Email: eva-maria.wartha@tuwien.ac.at

²K1-Met GmbH, Area 4 – Simulation and Analyses
Stahlstrasse 14, BG 88, Linz, Austria, 4020

³Primetals Technologies Austria GmbH
Turmstraße 44, Linz, Austria, 4031

⁴voestalpine Stahl Donawitz GmbH
Kerpelystraße 199, Leoben, Austria, 8700

⁵voestalpine Stahl GmbH
voestalpine-Straße 3, Postfach 3, Linz, Austria, 4020

Keywords: Blast furnace, Computational fluid dynamics, Raceway shape,

INTRODUCTION

The main steel production route is the blast furnace route, which accounts for ~60% of the overall steel production in Europe [1]. Although being used for centuries, the process is still under intensive investigation. The large energy consumption and the high carbon emissions in the blast furnace process increase the need for process optimization and offer possibilities for improvements. The heart of the blast furnace is the raceway zone, where the hot blast enters, forming the raceway cavity. The blast oxidizes the coke and the auxiliary reducing agents providing the necessary heat and creating reducing gases to reduce the iron oxides.

Due to the high temperatures, detailed measurements inside or near the raceway zone are practically impossible. Therefore, computational modeling techniques can be an excellent opportunity to study the processes in the raceway zone and gain insight into the processes occurring.

However, the large scale of the plant, its high temperatures and reactions, and the interaction between solid and gas flow also pose challenges in modeling and computational cost. Therefore, a sensitive choice of models, balancing the computational cost and the needed accuracy, is essential for profound predictions. In the following, we will demonstrate a strategy that can be applied to large-scale applications, i.e., the blast furnace raceway. The model setup is validated based on comparison with experimental data, and we exemplify the importance of the model choice for predicting the raceway shape and consequently the species concentrations.

MODELING THEORY

The discrete-element-method (DEM) is probably the most detailed way to model solid particle movement, and their interaction is the discrete-element-method (DEM). Because the particle-particle interactions are resolved there, the description is very accurate but leads to high computational demand. Therefore, the application of DEM to large-scale applications, such as the blast furnace, is still hindered by its high computational cost [2,3].

An Eulerian description of the solid flow reduces detail but can describe dense solid flows on large scales. The sub-models used to model solid movement in such a framework need to be carefully chosen to maintain reasonable prediction accuracy. In this paper, we exemplify the influence of such model choices on the prediction of solid's movement and distribution and how it also influences the species concentration prediction in the gas phase.

In the Eulerian framework, all phases are modeled as interpenetrating continua. The momentum equations of both phases are coupled with interaction terms, e.g., drag.

Since the model under investigation aims to be applied to industrial scale plants, the gas phase is modeled with Reynolds-Averaged-Navier-Stokes (RANS) equations. The model is closed by modeling the turbulence with the $k-\epsilon$ model [4].

To close the phase-averaged momentum equation for the solid flow, the kinetic theory of granular flows (KTGF) [5–7] is the method of choice. Based on the resemblance between a dense gas and a dense solid flow, the KTGF was derived with the

knowledge of the kinetic theory of dense gases. A granular temperature is introduced, which describes the particle velocity fluctuations. The equation for the granular temperature needs to be closed by modeling terms. Different concepts to close those model terms exist, see, e.g. [8] for an in-depth summary. We focus on two approaches introduced by [5] and [9], which can be distinguished by not considering or considering the interstitial fluid effects, respectively. In a previous study based on cold model experiments, the difference in those two approaches significantly impacts the shape of the predicted raceway form [10]. In the following, we study the impact of these models and the raceway shape on the reactions and consequently the species distribution in the raceway zone.

In addition to the forces accounted for in the KTGF models, frictional effects come into play when the solid fraction becomes large. Those effects are modeled above a specified volume fraction α_{min} by adding the frictional pressure and frictional viscosity to the solid pressure and solid viscosity, respectively. In the presented work, we apply the models from [11]. For a detailed discussion on this modeling choice we refer to [12,13] or our previous work [14]. The radial distribution function was modeled according to [15].

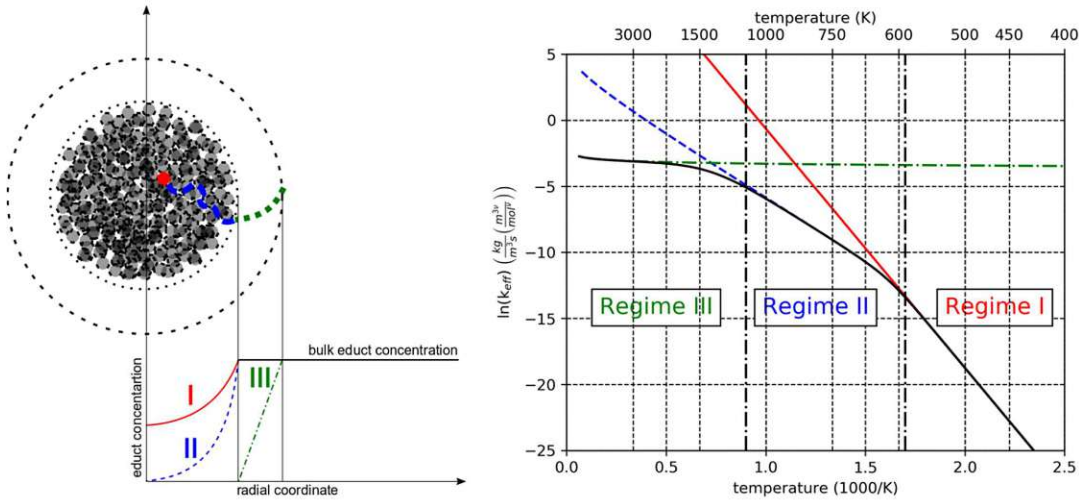


Figure 1: Schematic representation of the gas-solid reaction model and its different regimes from [25]

To model the gas-solid reactions a mechanistic model for porous media, accounting for the intrinsic reaction rate, mass transfer through the boundary layer, and the mass transfer through the porous structure is chosen. Figure 1 shows a qualitative representation of the three different regimes contributing to the effective reaction rate for coke conversion. The effective reaction rate is modeled as follows:

$$k_{eff} = \frac{1}{\frac{1}{\beta c^{1-v}} + \frac{1}{\eta k_{kin}}} c^v \quad (1)$$

Where k_{kin} refers to the kinetic reaction rate, which is reduced by the effectiveness factor η to account for the mass transfer through the pores to the actual reaction sites. The mass transfer limitation through the boundary layer is expressed through β and c is the concentration of the gaseous reactant with its coefficient v . The kinetic reaction rate is modeled based on an Arrhenius approach:

$$k_{kin} = A \cdot \exp\left(\frac{-E_a}{RT_p}\right) \quad (2)$$

where A is the pre-exponential factor, E_a the activation energy, R the specific gas constant and T_p the particle temperature. The effectiveness factor to account for pore diffusion is modeled according to [16]:

$$\eta = \frac{1}{\Phi} \left(\frac{1}{\tanh(\Phi)} - \frac{1}{\Phi} \right) \quad (3)$$

where Φ is the Thiele modulus, which was derived by [17] for the relation of catalytic activity and the size of particles. It is given as:

$$\Phi = \frac{d_p}{2} \sqrt{\frac{1 + \nu k_{kin} \rho_p c^{v-1}}{2 D_{eff}}} \quad (4)$$

with d_p being the particle diameter, ρ_p the particle density and D_{eff} the effective diffusion coefficient, which is computed from the pore Diffusion coefficient based on Knudsen diffusion [18] D_{kn} , porosity ϵ and tortuosity τ :

$$D_{eff} = \frac{1}{\left(\frac{1}{D_{kn}} + \frac{1}{D_{gas}}\right) \tau} \epsilon \quad (5)$$

The mass transfer through the boundary layer is modeled as follows:

$$\beta = \frac{Sh D_{gas}}{d_p} A_{sp} \quad (6)$$

with the diffusion coefficient D_{gas} computed based on the model from [19], the particle diameter, the surface area calculated as $\frac{6}{d_p \rho_s}$ and the Sherwood correlation according to [20]:

$$Sh = \frac{0.375}{1 - \alpha_s} (Re)^{0.641} (Sc)^{1/3} \quad (7)$$

Additionally, the gas phase reactions need to be modeled to obtain a reasonable estimate of the gas phase concentration. In turbulent flows, the turbulence-chemistry interaction needs to be taken into account. This is done by employing the Eddy Dissipation Concept [21]. The fine structures where the actual reaction occurs are assumed to behave as perfectly stirred reactors (PSRs). To reduce the computational demand, we choose a plug flow reactor (PFR) model instead, which has been discussed by [22] and is also employed in this way in many commercial CFD codes, e.g., Fluent [23].

Implementation details

The simulations were conducted in OpenFOAM. The framework has been presented by [24]. In addition to the standard functionalities in OpenFOAM, a generic multiphase chemistry framework has been implemented [25], which has been used to model the aforementioned gas-solid reactions.

The solution of the continuity equations in multi-fluid Euler-Euler-simulations poses a special challenge. In [14] we proposed a different algorithm to solve the continuity equation of a two-fluid system. This has computational improvements compared to the original version. Therefore, we use this algorithm to predict the raceway shape for the three-dimensional cases in the following and solve for the chemistry in the stationary bed. For the two-dimensional cases, the standard algorithm in OpenFOAM, version 9, has been used, where the algorithm was generalized to treat multiple Eulerian phases.

Model Cases

Nogami et al. [26] studied the raceway formation in a coke bed under high temperature conditions. They reported the experimental results from this small-scale apparatus, which resembles the raceway conditions in the blast furnace. Since the species concentration profiles have been measured in this setup, this case will be used to validate our simulation cases. The comparison between the experimental case is first made in the full-scale 3D geometry, see Figure 2 (a). The mesh was refined near the tuyere inlet to save computational cost.

Additionally, the 3D model is abstracted to 2D, as similarly done by [27], see Figure 2 (b). Often, 2D models are used to investigate real processes. Therefore, it is crucial that our 2D simplifications predict the process accurately enough.

According to the experiment, the blast temperature and mass flow rate were set at 800°C and 710 Nm³/h with oxygen enriched air (10Nm³/h pure oxygen). The coke inflow from the top was set to be equivalent to the coke consumption to maintain a constant bed height, as done in the experiment.

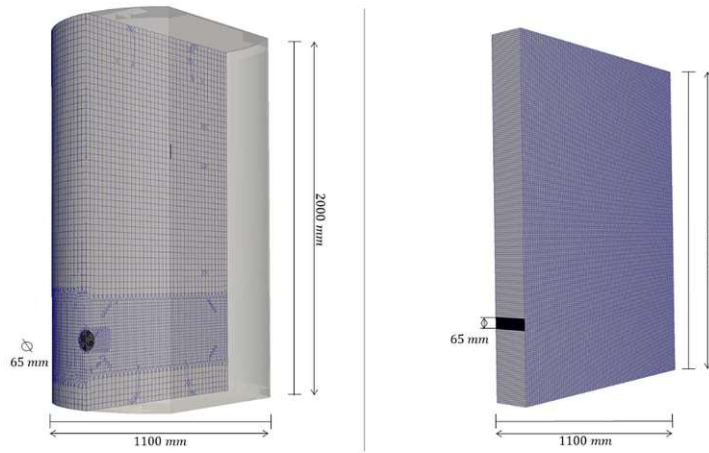


Figure 2: Left: 3D representation, Right: 2D representation of the setup under investigation

Table I: Parameters for the modeled coke

Name	Value	Unit
pore diameter	200e-9	m
tortuosity	3.7	-
particle diameter	0.03	m
particle density	1081	kg/m ³
heat capacity	$200 + 2 \cdot T - 0.001 \cdot T^2 + 1.7 \cdot 10^{-7} \cdot T^3$	J/(kgK)
heat transfer coefficient	$-0.76 + 6.3 \cdot 10^{-3} \cdot T + 10^{-3} \cdot T^2$	W/(m ² K)
heat of formation coke	-609393	J/kg

The considered heterogeneous reactions in the simulations are given in Table II, where the kinetic parameters for the oxidation and CO₂ gasification are taken from [28] and the gasification with H₂O from [29]. The gas-phase reactions considered are shown in Table III and are based on the work from [30]

Table II: Reactions and their parameters for the heterogeneous reactions. A is the pre-exponential factor in m^{3ν}/(kg s mol^{ν-1}) and T_A is the activation energy divided by the specific gas constant in K, and ν is the power for the gas phase species concentration in the reaction rate expression.

reaction	A	T _A	ν
$coke + 1.0475O_2 \rightarrow CO_2 + 0.146H_2O$	4.8e9	16731	0.59
$coke + 0.949H_2O \rightarrow CO + 1.095H_2$	3.42	15600	1
$coke + CO_2 \rightarrow 2CO + 0.051H_2O + 0.095H_2$	2.7e5	18520	0.13

Table III: Reaction rate parameters for the gas phase reactions. A is the pre-exponential factor in mol/m³ and T_A defined as for the heterogeneous reaction. The power of the species concentration is given if not equal to the stoichiometric coefficient.

reaction	A	T _A	ν
$CO + 0.5 O_2 \rightarrow CO_2$	1.25908e10	20446	O ₂ : 0.25, H ₂ O: 0.5
$CO_2 \rightarrow CO + 0.5 O_2$	5e8	20446	
$H_2 + 0.5O_2 \rightarrow H_2O$	9.87e5	3728	O ₂ : 1

RESULTS

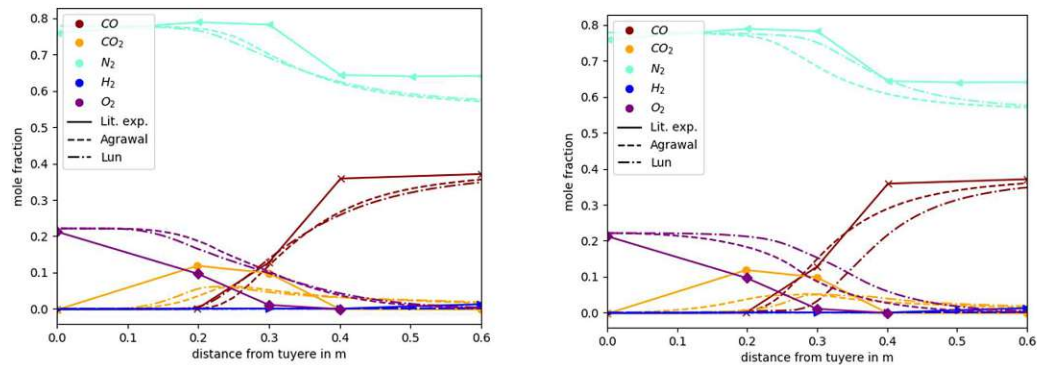


Figure 3: Species concentration profiles from [26] and simulation results, left from 3D setup and right from the 2D setup

Figure 3 shows the species concentration profiles of the conducted simulations. On the left side of the figure, the results of the 3D simulations are compared to the experimental results from [19]. Interestingly, the modeling choice of the closure terms of the KTGF does not significantly affect the raceway shape or the species concentrations. In all the cold model studies presented in [10], the choice of the closure terms had a significant influence on the raceway shape. Probably, the change to a full 3D representation of the geometry makes the difference. In general, the simulation results agree very well with the experimental results. The drop of the oxygen concentration is slightly underpredicted, and consequently, also the peak of the CO_2 concentration. This could also be related to a deficiency of the reaction model chosen for the coal (Table II). These were taken from [28] because no details about the type of coal were given in [19]. The results might be even more accurate if the reaction parameters are specifically derived for the used coke.

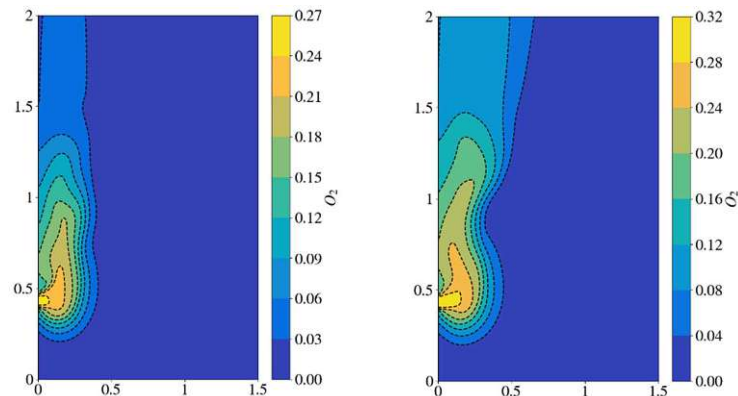


Figure 4: Species mass fraction O_2 contours for the base case (left) and the case with oxygen enrichment in the blast (right)

On the right-hand side of Figure 3, the results from the 2D case are shown. Here, the modeling choice for the KTGF closure models has a significant influence on the raceway shape and the species concentrations. Only the closure terms proposed by [9] predict the raceway shape and consequently the species concentrations reasonably well. This is in agreement with the results from the cold model experiments presented in [10]. These results suggest that for 2D simulations using the KTGF, one should use the closure models proposed by [8]. Therefore, we study the influence of further oxygen enrichment of the blast with this setup.

The oxygen enrichment of the blast was increased to 27 vol-%. Figure 4 shows the resulting oxygen mass fractions for the base case and the one with additional oxygen enrichment. Naturally, the oxygen concentration is increased in the overall domain.

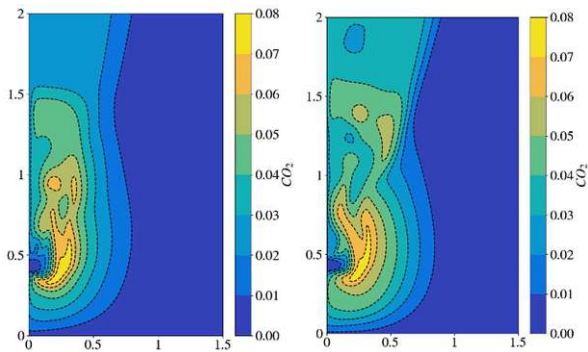


Figure 5: Species mass fraction CO₂ contours for the base case (left) and the case with oxygen enrichment in the blast (right)

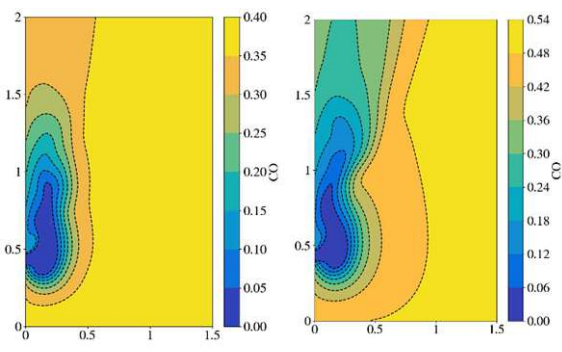


Figure 5: Species mass fraction CO contours for the base case (left) and the case with oxygen enrichment in the blast (right)

The CO and CO₂ mass fractions show the same trend because the increased amount of oxygen leads naturally to an increased reaction. The zone of CO₂ around the raceway broadens, see Figure 5, which depicts a widened reaction zone of the coke. Interestingly, the peak concentration of CO₂ does not significantly increase.

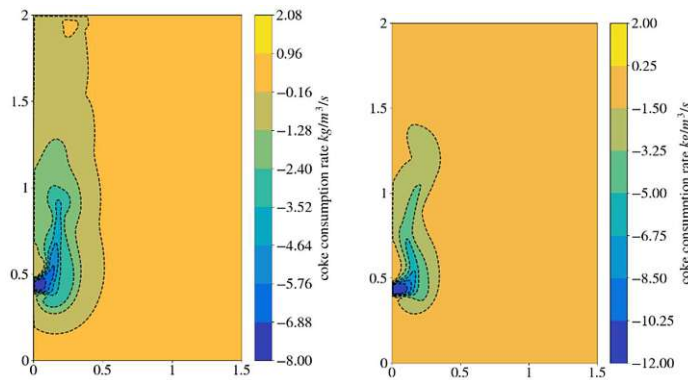


Figure 7: Coke consumption rate for the base case (left) and the case with increased oxygen enrichment (right)

Figure 7 shows the coke consumption rate in the studied cases. It might seem as the reaction zone was broadened on the right side in the figure, but this is mainly due to the different scaling. Overall, the coke consumption rate is increased in the case with increased oxygen enrichment, which is in alignment with the shown species mass fractions in Figure 55 and Figure 5.

CONCLUSIONS

We presented a modeling framework to be applied to large-scale blast furnace geometries. The use of an Eulerian description of the solid phase allows for larger geometries but poses additional challenges on the chosen model. Based on a comparison with experimental results, we could show that our modeling choice is sufficiently accurate and that choosing the closure terms in the KTGF is especially important when a simplified two-dimensional representation is chosen.

With the simplified model, the influence of oxygen enrichment in the blast was studied. The presented models can easily be applied to larger scale to study process variations in an existing blast furnace.

ACKNOWLEDGEMENTS

The authors gratefully acknowledge the funding support of K1-MET GmbH, metallurgical competence center. The research program of the competence center K1-MET is supported by COMET (Competence Center for Excellent Technologies), the Austrian program for competence centers. COMET is funded by the Federal Ministry for Transport, Innovation and

Technology, the Federal Ministry for Science, Research and Economy, the provinces of Upper Austria, Tyrol, and Styria, and the Styrian Business Promotion Agency.

The computational results presented have been achieved in part using the Vienna Scientific Cluster (VSC).

REFERENCES

- [1] Remus R, Aguado Monsonet MA, Roudier S, Sancho LD. Best Available Techniques (BAT) Reference Document for Iron and Steel Production. 2013.
- [2] Lichtenegger T, Pirker S. CFD-DEM modeling of strongly polydisperse particulate systems. *Powder Technology* 2018;325:698–711. <https://doi.org/10.1016/j.powtec.2017.11.058>.
- [3] Chiesa M, Mathiesen V, Melheim JA, Halvorsen B. Numerical simulation of particulate flow by the Eulerian-Lagrangian and the Eulerian-Eulerian approach with application to a fluidized bed. *Computers and Chemical Engineering* 2005;29:291–304. <https://doi.org/10.1016/j.compchemeng.2004.09.002>.
- [4] Jones WP, Launder BE. The prediction of laminarization with a two-equation model of turbulence. *Int J Heat Mass Transfer* 1972;15:301–14.
- [5] Lun CKK, Savage SB, Jeffrey DJ, Chepuriniy N. Kinetic theories for granular flow: Inelastic particles in Couette flow and slightly inelastic particles in a general flowfield. *Journal of Fluid Mechanics* 1984;140:223–56. <https://doi.org/10.1017/S0022112084000586>.
- [6] Savage SB. Analyses of slow high-concentration flows of granular materials. *Journal of Fluid Mechanics* 1998;377:1–26. <https://doi.org/10.1017/S0022112098002936>.
- [7] Gidaspow D. *Multiphase Flow and Fluidization . - Continuum and Kinetic Theory Descriptions*. Academic Press, Inc.; 1994.
- [8] van Wachem BGM. *Derivation, Implementation, and Validation of Computer Simulation Models for Gas-Solid Fluidized Beds*. 2000.
- [9] Agrawal K, Loezos PN, Syamlal M, Sundaresan S. The role of meso-scale structures in rapid gas–solid flows. *Journal of Fluid Mechanics* 2001;445:151–85. <https://doi.org/10.1017/s0022112001005663>.
- [10] Wartha EM, Bösenhofer M, Harasek M. Importance of considering interstitial fluid effects in the kinetic theory of granular flow for raceway formation prediction. *Chemical Engineering Science* 2022;247:117026. <https://doi.org/10.1016/j.ces.2021.117026>.
- [11] Schaeffer DG. Instability in the evolution equations describing incompressible granular flow. *Journal of Differential Equations* 1987;66:19–50. [https://doi.org/10.1016/0022-0396\(87\)90038-6](https://doi.org/10.1016/0022-0396(87)90038-6).
- [12] Venier CM, Marquez Damian S, Nigro NM. Assessment of gas-particle flow models for pseudo-2D fluidized bed applications. *Chemical Engineering Communications* 2018;205:456–78. <https://doi.org/10.1080/00986445.2017.1403907>.
- [13] Passalacqua A, Marmo L. A critical comparison of frictional stress models applied to the simulation of bubbling fluidized beds. *Chemical Engineering Science* 2009;64:2795–806. <https://doi.org/10.1016/j.ces.2009.03.005>.
- [14] Wartha E-M, Bösenhofer M, Harasek M. Combining an implicit solution with an explicit corrector step for the solution of the continuity equations in a two-fluid solver. 14th International Conference on CFD in Oil & Gas, Metallurgical and Process Industries, Trondheim: 2020.
- [15] Carnahan NF, Starling KE. Equation of state for nonattracting rigid spheres. *The Journal of Chemical Physics* 1969;51:635–6. <https://doi.org/10.1063/1.1672048>.

- [16] Liu GS, Niksa S. Coal conversion submodels for design applications at elevated pressures. Part II. Char gasification. *Progress in Energy and Combustion Science* 2004;30:679–717. <https://doi.org/10.1016/j.peccs.2004.08.001>.
- [17] Thiele EW. Relation between Catalytic Activity and Size of Particle. *Industrial and Engineering Chemistry* 1939;31:916–20. <https://doi.org/10.1021/ie50355a027>.
- [18] Szekely J, Evans JW, Sohn HY. *GAS-SOLID REACTIONS*. 1976.
- [19] Hishida M, Hayashif AK. Numerical Simulation of Pulsed Jet Plume Combustion. *Dynamics of Heterogeneous Combustion and Reacting Systems* 1993:343–61. <https://doi.org/10.2514/5.9781600866258.0343.0361>.
- [20] Petrovic LJ, Thodos G. Mass Transfer in Flow of Gases through Packed Beds. Low Reynolds Number Region. *Industrial & Engineering Chemistry Fundamentals* 1968;7:274–80.
- [21] Magnussen BF. The Eddy Dissipation Concept a Bridge between science and technology. *ECCOMAS Thematic Conference on Computational Combustion*, 2005.
- [22] Bösenhofer M, Wartha E-M, Jordan C, Harasek M. The eddy dissipation concept-analysis of different fine structure treatments for classical combustion. *Energies* 2018;11. <https://doi.org/10.3390/en11071902>.
- [23] ANSYS. *ANSYS Fluent - CFD Software | ANSYS* 2016.
- [24] Bösenhofer M, Wartha EM, Jordan C, Harasek M, Feilmayr C, Hauzenberger F, et al. A raceway model based on open-source software. *AISTech - Iron and Steel Technology Conference Proceedings*, vol. 2019- May, 2019. <https://doi.org/10.33313/377/272>.
- [25] Bösenhofer M. On the modeling of multi-phase reactive flows: Thermo-chemical conversion in the raceway zone of blast furnaces. *Doctoral thesis*. 2020.
- [26] Nogami H, Yamaoka H, Takatani K. Raceway design for the innovative blast furnace. *ISIJ International* 2004;44:2150–8. <https://doi.org/10.2355/isijinternational.44.2150>.
- [27] E D, Zhou P, Guo S, Zeng J, Xu Q, Guo L, et al. Particle-scale study of coke combustion in the raceway of an ironmaking blast furnace. *Fuel* 2021:122490. <https://doi.org/10.1016/j.fuel.2021.122490>.
- [28] Rumpel S. *Die autotherme Wirbelschichtpyrolyse zur Erzeugung heizwertreicher Stützbrennstoffe*. 2000.
- [29] Tepper H. *Zur Vergasung von Rest- und Abfallholz in Wirbelschichtreaktoren für dezentrale Energieversorgungsanlagen*. 2005.
- [30] Westbrook CK, Dryer FL. Simplified Reaction Mechanisms for the Oxidation of Hydrocarbon Fuels in Flames. *Combustion Science and Technology* 1981;27:31–43. <https://doi.org/10.1080/00102208108946970>.

Co-Author Publications

Co-Author Paper A

The eddy dissipation concept – analysis of different fine structure treatments for classical combustion

by Markus Bösenhofer, Eva-Maria Wartha, Christian Jordan and Michael Harasek; published in *energies*.

Abstract

The Eddy Dissipation Concept (EDC) is common in modeling turbulent combustion. Several model improvements have been proposed in literature; recent modifications aim to extend its validity to Moderate or Intense Low oxygen Dilution (MILD) conditions. In general, the EDC divides a fluid into a reacting and a non-reacting part. The reacting part is modeled as perfectly stirred reactor (PSR) or plug flow reactor (PFR). EDC theory suggests PSR treatment, while PFR treatment provides numerical advantages. Literature lacks a thorough evaluation of the consequences of employing the PFR fine structure treatment. Therefore, these consequences were evaluated by employing tests to isolate the effects of the EDC variations and fine structure treatment and by conducting a Sandia Flame D modeling study. Species concentration as well as EDC species consumption/production rates were evaluated. The isolated tests revealed an influence of the EDC improvements on the EDC rates, which is prominent at low shares of the reacting fluid. In contrast, PSR and PFR differences increase at large fine fraction shares. The modeling study revealed significant differences in the EDC rates of intermediate species. Summarizing, the PFR fine structure treatment might be chosen for schematic investigations, but for detailed investigations a careful evaluation is necessary.

My contribution: Conceptualization, Software, Validation, Resources, Writing—Review and Editing

M. Bösenhofer, E.-M. Wartha, C. Jordan, and M. Harasek (2018b). “The eddy dissipation concept-analysis of different fine structure treatments for classical combustion”. In: *Energies* 11.7. ISSN: 19961073. DOI: 10.3390/en11071902

Co-Author Paper B

Pulverized Coal Conversion in Blast Furnaces – Analysis of Involved Scales

by Markus Bösenhofer, Eva-Maria Wartha, F. Hauzenberger Christian Jordan, Franz Hauzenberger, Christoph Feilmayr, Hugo Stocker, Johannes Rieger, Bern-

hard König and Michael Harasek; published in AISTech - Iron and Steel Technology Conference Proceedings

Abstract

Pulverized coal conversion is a process involving scales range from nanometers for the particle pores to meters for the blast furnace. For an ideal coke replacement ratio, the coal has to be converted within the oxygen rich zone in the vicinity of the tuyeres. The time of flight before leaving this zone is 20 – 40 ms. Analysis of involved scales gives valuable information for optimization. After discussing the theoretical foundation, we present a reference case of pulverized coal injection. Based on this case, we discuss the involved scales and analyze the coal conversion process in the raceway zone.

My contribution: Conceptualization. Writing - Review and Editing.

M. Bösenhofer, E.-M. Wartha, C. Jordan, F. Hauzenberger, C. Feilmayr, H. Stocker, J. Rieger, B. König, and M. Harasek (2020b). “Pulverized Coal Conversion in Blast Furnaces – Analysis of Involved Scales”. In: *AISTech - Iron and Steel Technology Conference Proceedings*

Co-Author Paper C
Characterization of Gas Phase Reaction Regime in the Raceway Zone

by Markus Bösenhofer, Eva-Maria Wartha, Christian Jordan, Michael Harasek, Christoph Feilmayr and Franz Hauzenberger; published in AISTech - Iron and Steel Technology Conference Proceedings

Abstract

My contribution: Conceptualization. Writing - Review and Editing.

M. Bösenhofer, E. Wartha, C. Jordan, M. Harasek, C. Feilmayr, and F. Hauzenberger (2018a). “Characterization of gas phase reaction regime in the raceway zone”. In: *AISTech - Iron and Steel Technology Conference Proceedings*, pp. 441–454. ISBN: 978-193511772-8

Curriculum Vitae - Eva-Maria Wartha

date of birth 07/07/1994

place of birth Vienna

ORCID  <https://orcid.org/0000-0002-5564-8440>

Education

11/2017 – now **TU Wien** – Doctoral programme in engineering sciences

field: Chemical and Process Engineering

08/2021 – 02/2022 **NTNU** – Research stay with combustion kinetics group

topic: Turbulence influence on solid conversion in the blast furnace

11/2015 – 11/2017 **TU Wien** – Master studies in chemical engineering

08/2016 – 12/2016 **NTNU** – Erasmus semester in Trondheim, Norway

09/2012 – 11/2015 **TU Wien** – Bachelor studies in chemical engineering

bachelor thesis: Conceptualization of a high temperature heat pump with water

09/2004 – 06/2012 **BG/BRG/BORG Kurzwiese** – Eisenstadt

08/2010 – 01/2011 **Ilmajoen lukio** – Finland

Work Experience

04/2018 – now **TU Wien** – Vienna, Austria

project ass. Institute of chemical, environmental and bioscience engineering

07/2015 – 08/2015 **Berndorf Band GmbH** – Berndorf, Austria

internship Technical production and processing

07/2014 – 08/2014 **Leobersdorfer Maschinenfabrik** – Leobersdorf, Austria

internship Bachelor thesis

07/2013 **Mars Austria OG** – Breitenbrunn, Austria

internship Production